



**Rockwell International**

**Rocketdyne Division  
6633 Canoga Avenue  
Canoga Park, California 91304**

RI/RD79-321



**LSES MODEL TEST PROGRAM**

**ENGINEERING DESIGN AND ANALYSIS REPORT**

29 November 1979

Contract N00024-78-C-2370

**PREPARED BY**

LSES Project Engineering  
Canoga Park, California

**APPROVED BY**

J. R. Lauffer

Director

Waterjet Programs

*FRANK  
MIDN*

## ACKNOWLEDGEMENT

Grateful acknowledgement is made to the following Rocketdyne personnel for their efforts and technical contribution to the LSES model program: Dr. E. D. Jackson and the Hydrodynamics unit for the analytical design of the model pump and for evaluating and analyzing the experimental results; Mr. R. L. McMillion and his staff in the Engineering Development Laboratory for conducting the tests and performing the necessary facility modifications; Mr. R. J. McClelland and his staff for providing design support during the entire program; and Mr. F. Lee and the Stress unit for providing technical support in the area of structural analysis.

## INTRODUCTION

This report summarizes the LSES Model Test Program conducted under contract N00024-78-C-2370 and is submitted to fulfill Contract Data Item A002. The tests discussed in this report were performed at Rocketdyne's Canoga Park, California Pump Test Facility. A hydrodynamic scale model of the 3K SES Propulsor (PJ-46) was designed, fabricated and tested during the 18-month program. Figure 1 shows the program schedule and task outline. All effort is complete.



## SUMMARY AND CONCLUSIONS

In March 1979, Rocketdyne began an ambitious program in which an exact hydrodynamic model of the 3K SES Propulsor (PJ-46, Fig. 2) was to be designed, fabricated, and tested. This program was structured to give test verification to the PJ-46 propulsor designed under a previous contract. The model geometry was proportionally scaled (by a factor of 1:6.3329) from the full-scale design. A tip speed of 200 ft/sec. was maintained resulting in the same mechanical stresses and fluid pressures (static and dynamic) for both the model and full-scale propulsor.

In addition to being geometrically similar, the model hydrodynamic components were fabricated from the same material e.g., an aluminum inlet elbow and titanium inducer, stator, rotor, straightening vanes, and other housings. A design which allowed complete yaw probe surveys of inlet and discharge conditions for every component, as well as visual observation of the inducer and rotor (while operating), was fabricated.

Tests were performed to establish the head rise, efficiency, suction capability, and cavitation endurance of the model pump. Surveys of the flowfield (radial and circumferential) were performed using fixed position kiel (total pressure) probes and a motorized yaw probe equipped with either a wedge (early) or cobra head (later in the program). Turbine speed matching and discharge separation problems were solved by minor design changes which were incorporated in the model pump hardware.

Test results have verified that the 3K SES propulsor design exceeds all ship operating requirements. At hump conditions (40,000 hp, 40.8 ft TIH), the thrust margin is 3.8% (149,830 lbf versus 144,400 lbf specification minimum). The flowrate is 132,710 gpm and the turbine speed is 4,073 rpm. The projected thrust versus TIH curve for the full-scale propulsor is shown in Fig. 3. Cavitation endurance tests have shown that after 42 hours (73 on inducer) at hump conditions, the pump performance has not been degraded.

Facility malfunctions caused the termination of endurance testing at 42 hours (100 previously planned). All other program goals were successfully met.

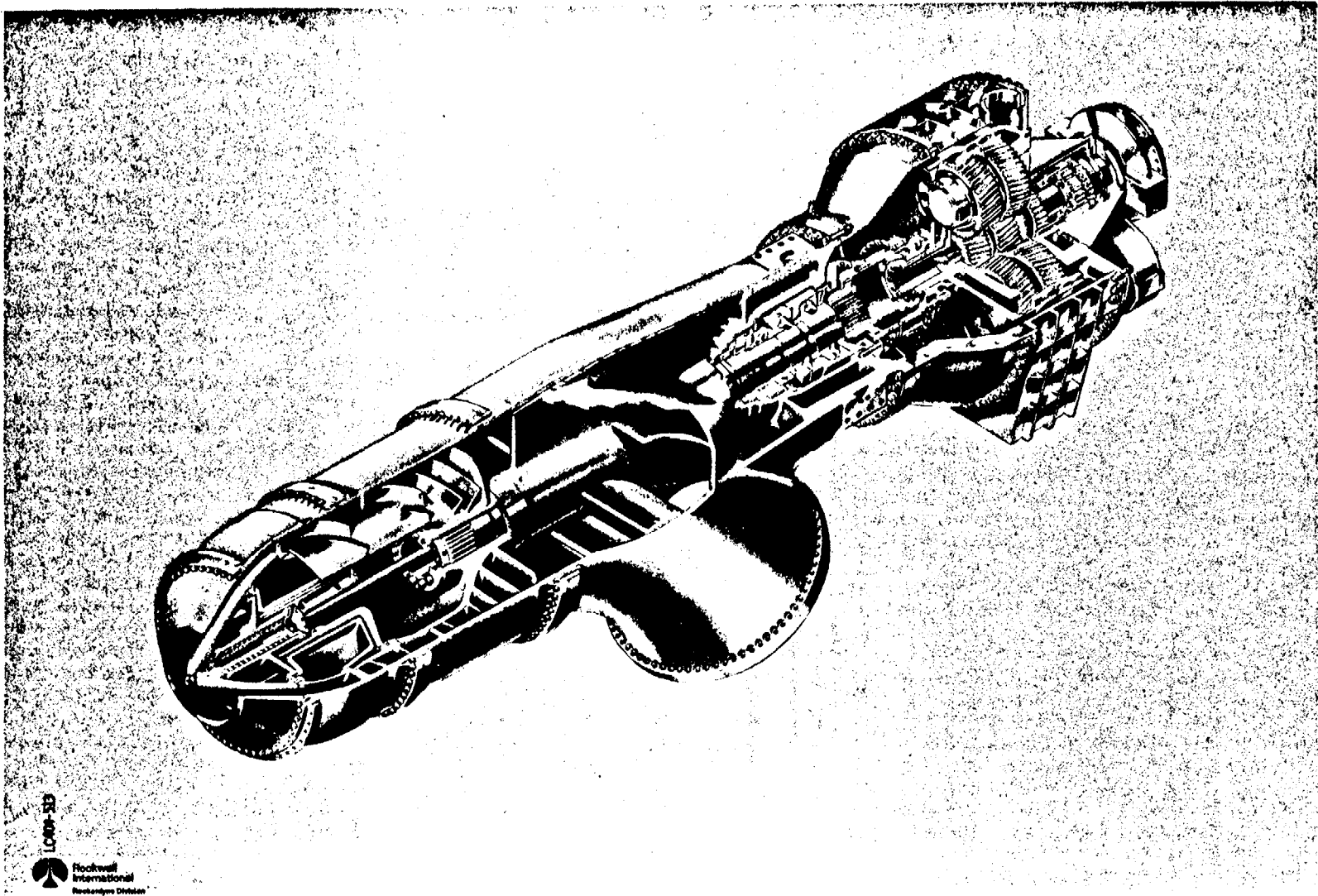


Figure 2. 3K SES Propulsor Assembly

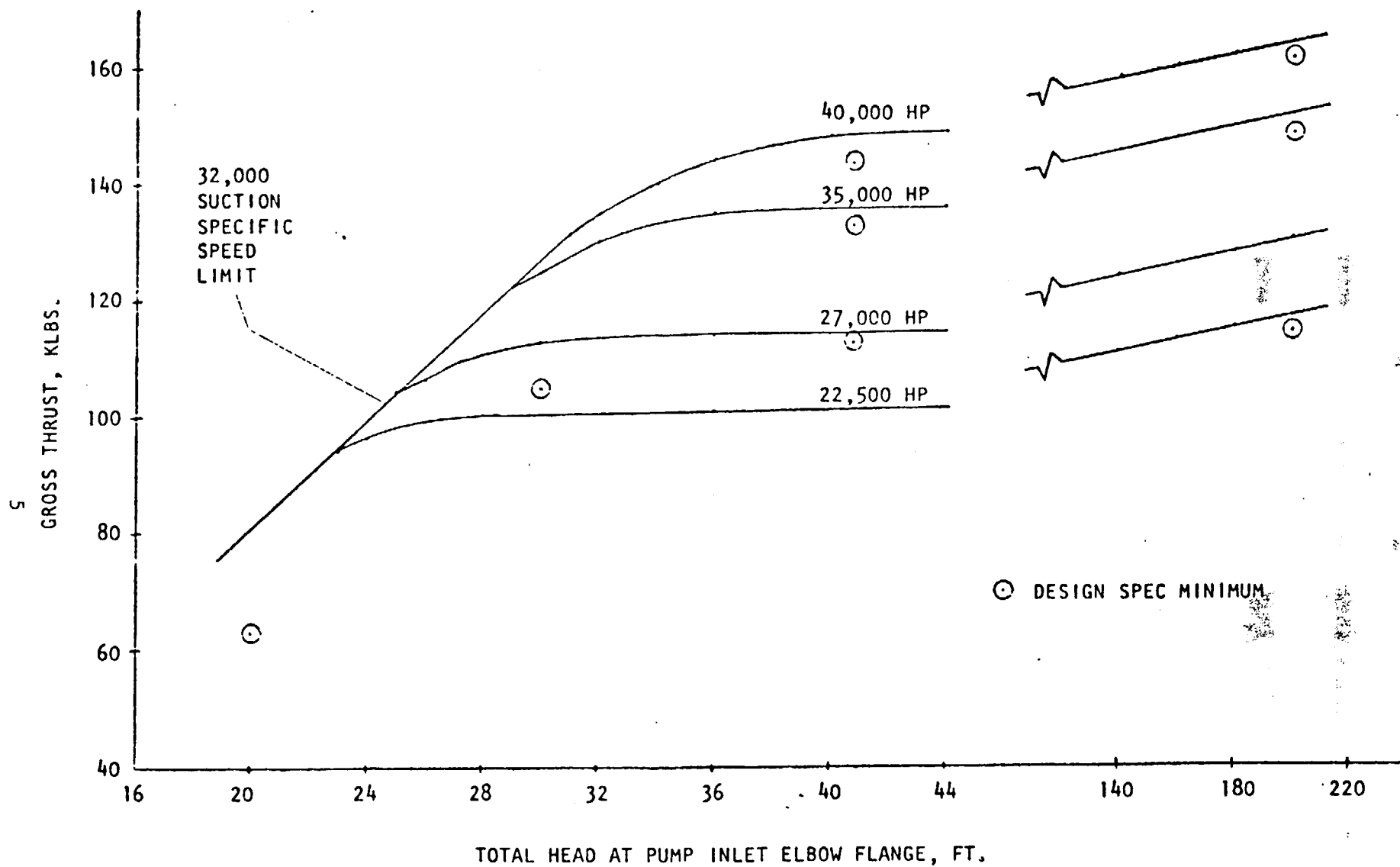


Figure 3. Thrust Versus Total Inlet Head

The model test program has shown the value of model testing. Inexpensive (compared to full-scale) testing is possible ahead of full-scale development testing. This gives advanced warning of problems and allows time to perfect designs, measurement devices, and test techniques. The model pump is scheduled for additional testing under contract to Rohr Marine. Strain gage, distortion, broaching, and increased endurance tests are planned.

## RECOMMENDATIONS

Based on the excellent test results of this program, it is recommended that all of the design changes made to the model be incorporated into the 3K SES design currently being fabricated. Furthermore, it is recommended that continued model testing be performed on all aspects of propulsor operation such as; steering and reversing, lower power operation, foreign object ingestion, noise measurements, instrumentation and test procedure checkout, and model testing for improved performance.

## CONTENTS

Introduction . . . . .	1
Summary and Conclusions . . . . .	3
Recommendations . . . . .	7/8
<u>Discussion</u> . . . . .	11/12
Design and Analysis (SOW Task 3.1) . . . . .	11/12
Mechanical Design . . . . .	11/12
Hydrodynamic Design . . . . .	46
Facility Modification Design . . . . .	106
Fabrication and Facility Modification (SOW Task 3.2) . . . . .	111
Pump Fabrication . . . . .	111
Model Test Results (SOW Task 3.3) . . . . .	115
Test Procedures and Techniques . . . . .	115
Problems Encountered . . . . .	129
Test Results . . . . .	133
Comparison of Results to Required Performance . . . . .	210
List of Illustrations . . . . .	213
List of Tables . . . . .	217

DISCUSSION  
DESIGN AND ANALYSIS (SOW TASK 3-1)

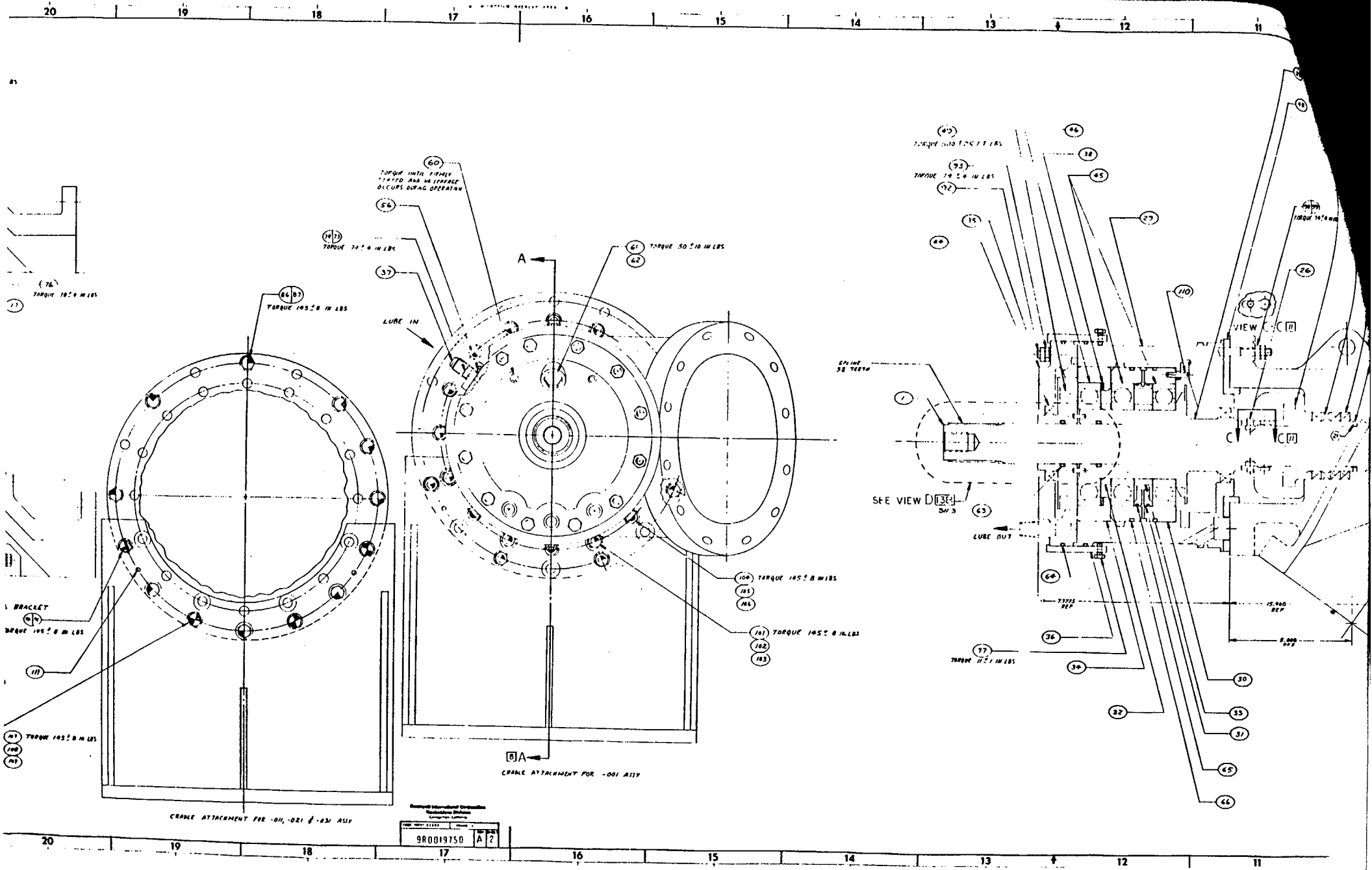
MECHANICAL DESIGN

Model Pump

Hydrodynamic Components. The LSES propulsor pump is a scale model of the full-size 3K SES propulsor pump. The outside diameter of the rotating parts is 7.232 inches, compared to a full-size diameter of 45.8 inches. Thus, a scale factor of 6.3329 is used to scale the model pump down from full-size dimensions. All model part dimensions and blade clearances are scaled down from nominal full-size dimensions. In addition, operating conditions used during LSES model testing are scaled to properly simulate full-size pump operation.

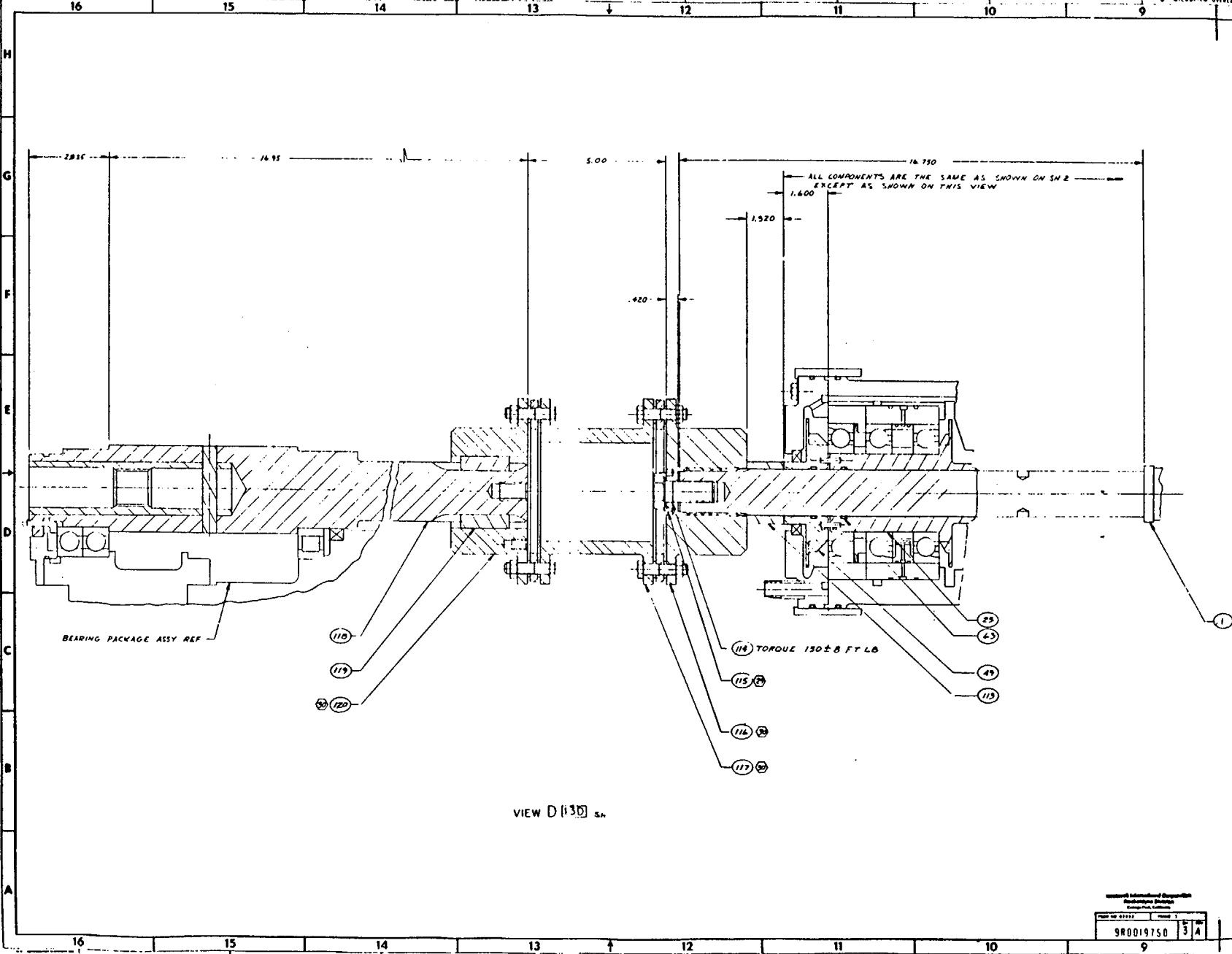
The model pump includes the aluminum inlet elbow, which houses the forward bearings and water seal, the stator housing, the discharge housing, the nozzle and movable pintle, the aft bearing assembly, and the major rotating elements consisting of the main shaft, inducer, and rotor. The direction of rotation of the rotating components is clockwise when looking aft at the face of the inducer. The model pump assembly drawing is included as Fig. 4, 5, and 6.

As the main shaft and inducer rotate, water enters the inlet where it passes around either side of the splitter vane mounted in the inlet. The water then passes between, and is turned by, the guide vanes mounted in the inlet elbow perpendicular to the splitter. The water then accelerates through the inducer and into the first stator section, which directs the flow into the single-row axial rotor. At the exit of the rotor, some of the flow is tapped off to supply the water that cools and lubricates the aft rubber bearing. The water leaving the rubber bearing passes forward through the water tube into the inside of the main shaft where it is ducted through holes in the shaft back into the main flow stream at the low-pressure area just ahead of the inducer. The main flow of water leaving the axial rotor flows into the discharge housing where straightening vanes are used both to remove whirl and to drop the static pressure at the downstream end of the rotor drum for axial force control. The straightening vane exit flow passes through a pseudo nozzle, which accelerates the fluid to high velocity.



980019150  
 A 2





BEARING PACKAGE ASSY REF

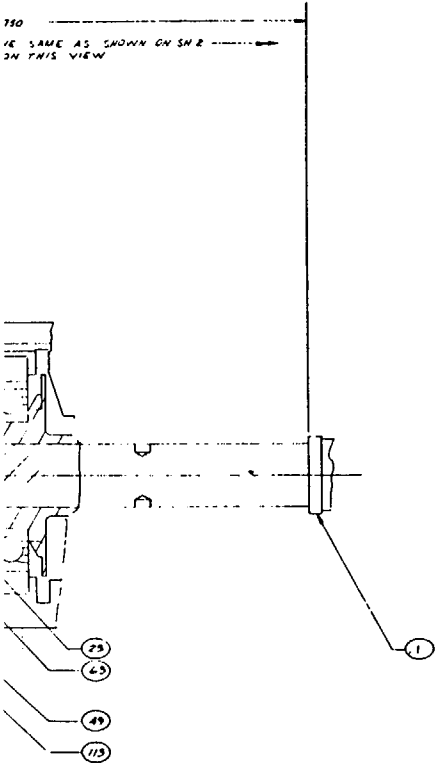
ALL COMPONENTS ARE THE SAME AS SHOWN ON SH 2 EXCEPT AS SHOWN ON THIS VIEW

114 TORQUE 150 ± 8 FT LB

VIEW D (13) s

General International Corporation	
Aerospac Division	
Cincinnati, Ohio	
Part No. 980019750	Rev. 1
980019750	3 A

1. NOT BE REVISIONS 2. CHECK BY REVISIONS 3. DATE OF REVISIONS 4. NAME OF REVISIONS 5. NAME OF REVISIONS		DATE 10/1/75
THIS IS A ADDLO		10/1/75



FOR INFORMATION

Figure 5. LSES Model Pump Drive Train Drawing

15/16

National Aeronautics and Space Administration Langley Research Center Hampton, Virginia 23060-2199	
Project No. 81131	Revision 3
9R0019750	A

TITLE MODEL PUMP DRIVE TRAIN	DATE 10/1/75	DRAWN BY J. OZGUR	CHECKED BY J. OZGUR
PROJECT NO. 81131	REVISION 3	DRAWING NO. 9R0019750	SHEET NO. 15/16



**FOR INFORMATION**

1. REV. STATUS OF  
 "A" BLOCK, 3 SW MADE BY  
 1) ITEM 1: 9001971-005  
 WAS 9001971-003  
 2) ITEM 43: MS 29518-223  
 WAS MS 29715-27  
 3) ITEM 54: 3 R200 WAS 1 R200  
 4) ITEM 55: 2 R200 WAS 3 R200  
 5) ITEM 59: 2 R200 WAS 3 R200  
 6) SELECTED ITEMS # 18 & 100  
 7) ADDED ITEMS # 18 & 100  
 8) REVISED MISC # 18  
 9) REVISED MISC # 100  
 10) ITEM 7: 9001971-001  
 WAS 9001971-001  
 EFFECT ON ITEMS 1 THRU 10  
 HEAT PARTS MADE

ITEM NO	PART NO OR IDENTIFYING NO	NAME/DESCRIPTION	MATERIAL	SPECIFICATION	ZONE - SW	ITEM NO	PART NO OR IDENTIFYING NO	NAME/DESCRIPTION	MATERIAL	SPECIFICATION	ZONE - SW
120	KEOR944087	HUB		15 - 3		10	PS0061474	RETAINER			10
119	KEOR944086-07	KEY		15 - 3		11	PS0061444	RETAINER			11
118	KEOR944085	SHAFT		15 - 3		12	PS0061374	FLANGE, INSULATOR			12
117	NO 742 REINORD	COUPLING		11 - 3		13	PS0061367	BURRL BEARING			13
116	KEOR944098	HUB		11 - 3		14	2MM214WJ	BEARING			14
115	MS5381-17	LOCKWASHER		11 - 3		15	2MM214WJ-DUL	BEARING PAIR			15
114	MUM-1010-4724	BOLT		11 - 3		16	6341471	SEAL			16
113	9KUC1992R 603	SPACER		10 - 3		17	9P0019891-003	SHIM			17
112	MS28715-247	PACKING		8 - 2		18	9P0019745-011	CABLE, ASSY OF			18
111	MS131597	SPRING PIN		20 - 2		19	9P0019745-001	CABLE, ASSY OF			19
110	MS111590	SPRING PIN		12 - 2		20	9P0019921-003	SPACER, PATER			20
109	MS4191-E	NUT		20 - 2		21	9P0019874-003	SPACER, INDUCER			21
108	MS19120-11	WASHER		20 - 2		22	9P0019874-003	SPRING			22
107	MS1565-69	BOLT		20 - 2		23	9P0019835-003	FITTING OIL, MET			23
106	MS19120-11	WASHER		18 - 2		24	9P0019824-003	SEITE, PLANGE HOUSING			24
105	MS1565-69	NUT		18 - 2		25	9P0019824-001	PLATE			25
104	MS19120-11	WASHER		18 - 2		26	9P0019824-001	SPACER, PEARING			26
103	MS19120-11	WASHER		18 - 2		27	9P0019824-001	SPACER, PEARING			27
102	MS1565-69	NUT		18 - 2		28	9P0019824-001	SPACER, PEARING			28
101	MS1565-69	BOLT		18 - 2		29	9P0019824-001	SPACER, PEARING			29
100				18 - 2		30	9P0019824-001	SPACER, PEARING			30
99				18 - 2		31	9P0019824-001	SPACER, PEARING			31
98				18 - 2		32	9P0019824-001	SPACER, PEARING			32
97				18 - 2		33	9P0019824-001	SPACER, PEARING			33
96				18 - 2		34	9P0019824-001	SPACER, PEARING			34
95				18 - 2		35	9P0019824-001	SPACER, PEARING			35
94				18 - 2		36	9P0019824-001	SPACER, PEARING			36
93				18 - 2		37	9P0019824-001	SPACER, PEARING			37
92				18 - 2		38	9P0019824-001	SPACER, PEARING			38
91				18 - 2		39	9P0019824-001	SPACER, PEARING			39
90				18 - 2		40	9P0019824-001	SPACER, PEARING			40
89				18 - 2		41	9P0019824-001	SPACER, PEARING			41
88				18 - 2		42	9P0019824-001	SPACER, PEARING			42
87				18 - 2		43	9P0019824-001	SPACER, PEARING			43
86				18 - 2		44	9P0019824-001	SPACER, PEARING			44
85				18 - 2		45	9P0019824-001	SPACER, PEARING			45
84				18 - 2		46	9P0019824-001	SPACER, PEARING			46
83				18 - 2		47	9P0019824-001	SPACER, PEARING			47
82				18 - 2		48	9P0019824-001	SPACER, PEARING			48
81				18 - 2		49	9P0019824-001	SPACER, PEARING			49
80				18 - 2		50	9P0019824-001	SPACER, PEARING			50
79				18 - 2		51	9P0019824-001	SPACER, PEARING			51
78				18 - 2		52	9P0019824-001	SPACER, PEARING			52
77				18 - 2		53	9P0019824-001	SPACER, PEARING			53
76				18 - 2		54	9P0019824-001	SPACER, PEARING			54
75				18 - 2		55	9P0019824-001	SPACER, PEARING			55
74				18 - 2		56	9P0019824-001	SPACER, PEARING			56
73				18 - 2		57	9P0019824-001	SPACER, PEARING			57
72				18 - 2		58	9P0019824-001	SPACER, PEARING			58
71				18 - 2		59	9P0019824-001	SPACER, PEARING			59
70				18 - 2		60	9P0019824-001	SPACER, PEARING			60
69				18 - 2		61	9P0019824-001	SPACER, PEARING			61
68				18 - 2		62	9P0019824-001	SPACER, PEARING			62
67				18 - 2		63	9P0019824-001	SPACER, PEARING			63
66				18 - 2		64	9P0019824-001	SPACER, PEARING			64
65				18 - 2		65	9P0019824-001	SPACER, PEARING			65
64				18 - 2		66	9P0019824-001	SPACER, PEARING			66
63				18 - 2		67	9P0019824-001	SPACER, PEARING			67
62				18 - 2		68	9P0019824-001	SPACER, PEARING			68
61				18 - 2		69	9P0019824-001	SPACER, PEARING			69
60				18 - 2		70	9P0019824-001	SPACER, PEARING			70
59				18 - 2		71	9P0019824-001	SPACER, PEARING			71
58				18 - 2		72	9P0019824-001	SPACER, PEARING			72
57				18 - 2		73	9P0019824-001	SPACER, PEARING			73
56				18 - 2		74	9P0019824-001	SPACER, PEARING			74
55				18 - 2		75	9P0019824-001	SPACER, PEARING			75
54				18 - 2		76	9P0019824-001	SPACER, PEARING			76
53				18 - 2		77	9P0019824-001	SPACER, PEARING			77
52				18 - 2		78	9P0019824-001	SPACER, PEARING			78
51				18 - 2		79	9P0019824-001	SPACER, PEARING			79
50				18 - 2		80	9P0019824-001	SPACER, PEARING			80
49				18 - 2		81	9P0019824-001	SPACER, PEARING			81
48				18 - 2		82	9P0019824-001	SPACER, PEARING			82
47				18 - 2		83	9P0019824-001	SPACER, PEARING			83
46				18 - 2		84	9P0019824-001	SPACER, PEARING			84
45				18 - 2		85	9P0019824-001	SPACER, PEARING			85
44				18 - 2		86	9P0019824-001	SPACER, PEARING			86
43				18 - 2		87	9P0019824-001	SPACER, PEARING			87
42				18 - 2		88	9P0019824-001	SPACER, PEARING			88
41				18 - 2		89	9P0019824-001	SPACER, PEARING			89
40				18 - 2		90	9P0019824-001	SPACER, PEARING			90
39				18 - 2		91	9P0019824-001	SPACER, PEARING			91
38				18 - 2		92	9P0019824-001	SPACER, PEARING			92
37				18 - 2		93	9P0019824-001	SPACER, PEARING			93
36				18 - 2		94	9P0019824-001	SPACER, PEARING			94
35				18 - 2		95	9P0019824-001	SPACER, PEARING			95
34				18 - 2		96	9P0019824-001	SPACER, PEARING			96
33				18 - 2		97	9P0019824-001	SPACER, PEARING			97
32				18 - 2		98	9P0019824-001	SPACER, PEARING			98
31				18 - 2		99	9P0019824-001	SPACER, PEARING			99
30				18 - 2		100	9P0019824-001	SPACER, PEARING			100

Figure 6. LSES Model Pump Parts List

REVISION STATUS OF SHEETS

A	A	A
SW3	SW2	SW1

WATERJET ASSEMBLY

02602 90019750

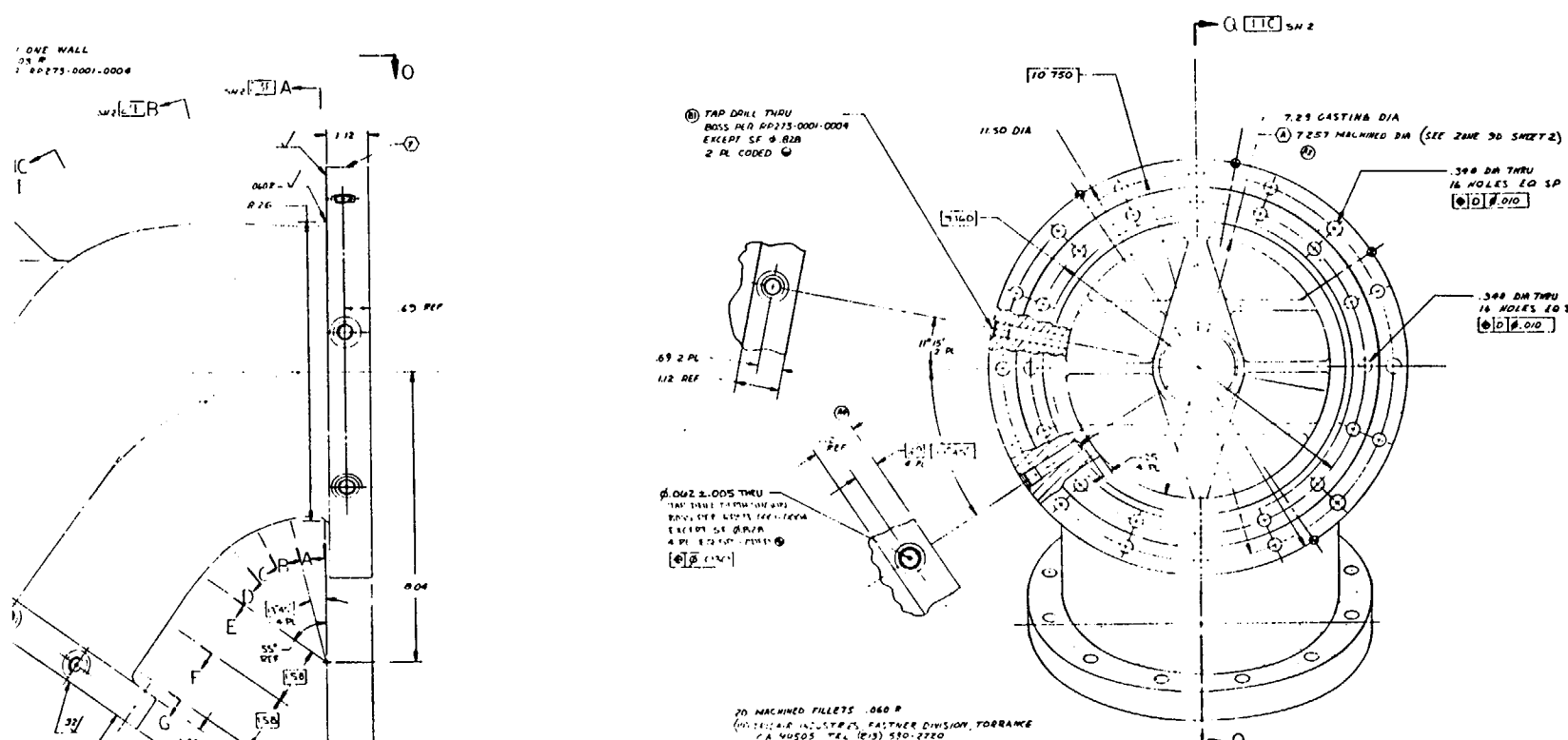
9P0019750 1A

Inlet Housing. The inlet housing is an A-357-T6 aluminum casting. An overall view of the inlet housing showing instrumentation locations is shown in Fig. 7, and Fig. 8 shows the important dimensions and several cross-sectional views of the inlet elbow. As shown in Fig. 7, the instrumentation bosses are machined in the inlet and discharge flanges. Instrumentation locations on the inlet housing consist of four static pressure ports located at 90 degrees from each other and two kiel-yaw probe ports positioned as shown. The housing forms an angled duct with the inlet set at a 55-degree angle to the run of the duct so that the inlet flow is turned 55 degrees before reaching the inducer. A splitter vane in the inlet, with guide vanes at right angles to it, forms a housing that encloses the shaft. The flow is guided around the shaft by the splitter vane, and the three integrally cast turning vanes direct the flow into the inducer section and also reduce any possible flow distortion. The flow area in the inlet housing is maintained nearly constant to reduce losses.

Inducer. Figure 9 presents a drawing and tabulation of blade coordinates of the LSES model pump inducer, and photographs of the inducer front row and kicker sections are shown in Fig. 10 and 11. The inducer front row and kicker sections are made from two commercially pure titanium forgings joined together by seven pins. The pins allow for potential studies of kicker clocking. The inducer has 4 full blades, 4 partial blades, and 16 kicker blades, and the design tolerances on these hydrodynamic surfaces are +0.010 inch and -0.00 inch all around. Four cylindrical surfaces describe the hydrodynamic surface on the full and partial blades. The cylindrical coordinates are shown in tabulated form in Fig. 9 with the full and partial blades described at radii of 1.700, 2.330, 2.960, and 3.590 inches. The hub is defined by their Z (axial) and R (radial) coordinates in the table in the lower left-hand corner of Fig. . The leading edge and trailing edge trim coordinates for the full and partial blades are shown in the tables in zone B9 of Fig. 9. Also, the leading edges for the full blade are defined by sections N-N, P-P, Q-Q, and R-R. The inducer has elliptical fillets on the full and partial blades as shown by view L in zone No. 20 of Fig. 9. The kicker fillet radius is 0.080 inch. The inducer is positioned concentrically on the shaft, with an interference fit on the forward and aft



ONE WALL  
ON R  
2 RP275-0001-0006



(B) TAP DRILL THRU  
BOSS HOLE 00175-0001-0004  
EXCEPT SEE 8 R2B  
2 R.L. CODED

0.002 ± 0.005 THRU  
TAP THREE TAP DRILL THRU BOSS  
HOLE WITH 0.010 DIA  
EXCEPT SEE 8 R2B  
4 PL. R.L. CODED

- 20 MACHINED FILLETS .060 R
- (A) MIL-STD-113, PARTNER DIVISION, TORRANCE  
P.A. NUSSO TEL (913) 550-2720
- (B) REFER TO ASSEMBLY INSTRUCTIONS FOR TAP DRILLS  
WITH NET WELD 0585 ZINC CHROMATE PRIMER C  
INSTALL WHILE WET.
- (C) TO ACT ANODIZE
- (D) PERFORM LEAK TEST PER MIL-2-6844
- 15 PRESSURE TEST WITH WATER AT 810 ± 20 PSIG  
FOR 15 MINUTES, NO VISUAL EVIDENCE OF  
DAMAGE OR LEAKAGE ALLOWED
- 16 RADIOGRAPHIC INSPECT PER MIL-A-1810C,  
TABLE III, GRADE C ALL AREAS
- 17 TWO TENSILE SPECIMENS SHALL BE INTEGRALLY  
CAST WITH CASTING AND FILED PER PARTS  
OF MIL-A-1810C, TABLE III, GRADE C
- 18 ALL CAST WALLS SHALL HAVE THE FOLLOWING MINIMUM  
WELD BEHIND DIMENSION 0.001 ± 0.0005  
VIBROFINISH (SEE DETAIL 1) TO 25% MIN  
RECOGNITION (IN DIA) TO 0.125 MIN
- 11. MACHINE PER RADIOS-016

- 10 CAST WALLS AND WELDS 38% Zn.
- (A) CAST FILLET RADIUS 1/16 ± 0.04
- (B) CAST CORNER RADIUS 1/16 ± 0.04
- (C) IMPRESSION STAMP IDENTIFY
- (D) THIS IS A MODEL IN THE FULL SIZE LSES  
INLET HOUSING
- (E) THESE DIMENSIONS APPLY AFTER ANODIZING
- (F) ANODIZE PER MIL-A-1352 TYPE III, EXCEPT 0.001 ± 0.0005  
THICK, SODIUM DICHROMATE SEAL
- (G) ALL INTERIOR CAST SURFACES, DEFINED BY BASIC DIM  
SHALL HAVE A FINISH SURFACE TEXTURE EQUIV TO 32  
OR BETTER PER MIL-STD-113
- (H) WELD BEHIND OF FILLETS IS PERMITTED PRIOR TO  
HEAT TREATMENT, USE 587 AL FILLER.
- (I) CASTING SHALL BE REWORKABLE IN T-6 CONDITION.  
WITH 100% PROTECTIVE COATING

NO.	DESCRIPTION	DATE	BY	CHKD
1	ISSUED FOR LSES MODEL			
2	RELOCATED FROM STATUS BLOCK			
3	1) 15.400 ± 0.005 WAS 15.400			
4	2) 7.257 WAS 7.240			
5	3) RADIOS-016 WAS RADIOS-002			
6	ADDED WTE 20			
7	ADDED 17.75 0001-0004			
8	INSTRUMENTATION PARTS			
9	EFFECT ON ITEMS 1 & 2			
10	LSES MODEL			
11	EFFECT ON ITEM 4			
12	LSES MODEL			
13	1) RELOCATED PARTS 0001-0004			
14	2) IN VIEW R.P. ADDED RADIOS-0004			
15	PART 2 PLACES			
16	1) IN VIEW R.P. ADDED RADIOS-0004			
17	PART 4 PLACES			
18	EFFECT ON ITEM 1			
19	LSES MODEL			
20	EFFECT ON ITEMS 2 & 3			
21	LSES MODEL			

A	B
SPR	SHI

REVISION STATUS OF SHEETS

FOR INFORMATION  
Figure 7. LSES Model Inlet Housing

21/22

NO.	MATERIAL	SIZE	SPECIFICATION	TOLER.
005	MAKE FROM 005			
009	ASSY IN AL CTSO		MIL-A-21180	9E

NO.	DESCRIPTION	DATE	BY	CHKD
1	ISSUED FOR LSES MODEL			
2	RELOCATED FROM STATUS BLOCK			
3	1) 15.400 ± 0.005 WAS 15.400			
4	2) 7.257 WAS 7.240			
5	3) RADIOS-016 WAS RADIOS-002			
6	ADDED WTE 20			
7	ADDED 17.75 0001-0004			
8	INSTRUMENTATION PARTS			
9	EFFECT ON ITEMS 1 & 2			
10	LSES MODEL			
11	EFFECT ON ITEM 4			
12	LSES MODEL			
13	1) RELOCATED PARTS 0001-0004			
14	2) IN VIEW R.P. ADDED RADIOS-0004			
15	PART 2 PLACES			
16	1) IN VIEW R.P. ADDED RADIOS-0004			
17	PART 4 PLACES			
18	EFFECT ON ITEM 1			
19	LSES MODEL			
20	EFFECT ON ITEMS 2 & 3			
21	LSES MODEL			

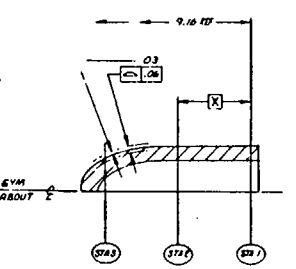
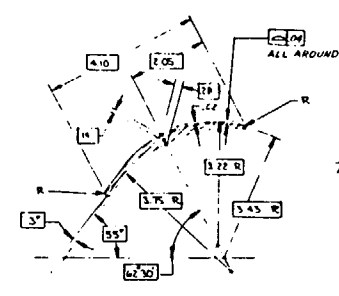
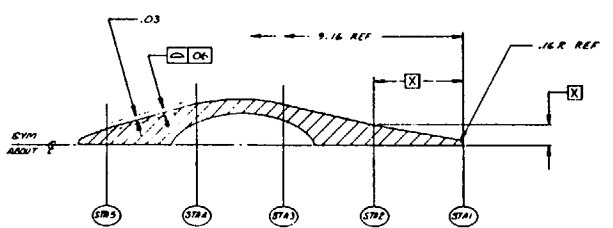
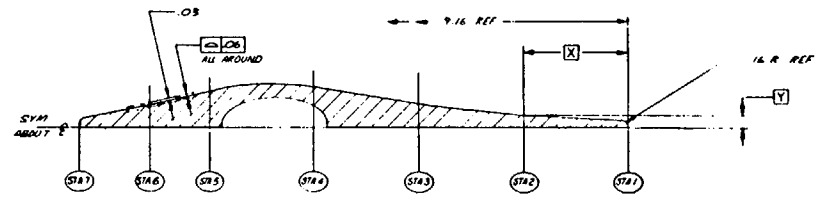
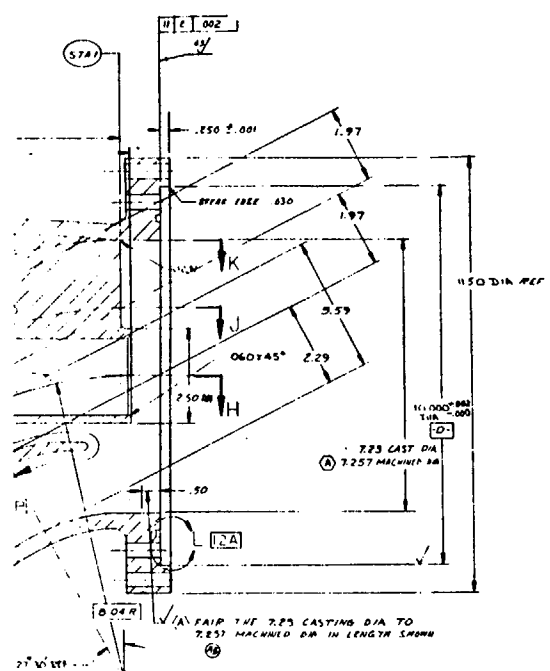
NOTED

NO.	DESCRIPTION	DATE	BY	CHKD
1	ISSUED FOR LSES MODEL			
2	RELOCATED FROM STATUS BLOCK			
3	1) 15.400 ± 0.005 WAS 15.400			
4	2) 7.257 WAS 7.240			
5	3) RADIOS-016 WAS RADIOS-002			
6	ADDED WTE 20			
7	ADDED 17.75 0001-0004			
8	INSTRUMENTATION PARTS			
9	EFFECT ON ITEMS 1 & 2			
10	LSES MODEL			
11	EFFECT ON ITEM 4			
12	LSES MODEL			
13	1) RELOCATED PARTS 0001-0004			
14	2) IN VIEW R.P. ADDED RADIOS-0004			
15	PART 2 PLACES			
16	1) IN VIEW R.P. ADDED RADIOS-0004			
17	PART 4 PLACES			
18	EFFECT ON ITEM 1			
19	LSES MODEL			
20	EFFECT ON ITEMS 2 & 3			
21	LSES MODEL			

HOUSING, INLET  
LSES MODEL  
1 02602 566019742

1970-1974





SECTION K-K		SECTION J-J		SECTION H-H	
X	Y	X	Y	X	Y
2.74	25	2.34	.51	1.93	L25
5.49	59	4.67	1.05	3.86	R6
8.25	107	7.01	1.05		
10.97	92	9.34	.41		
12.55	80				

REVISIONS

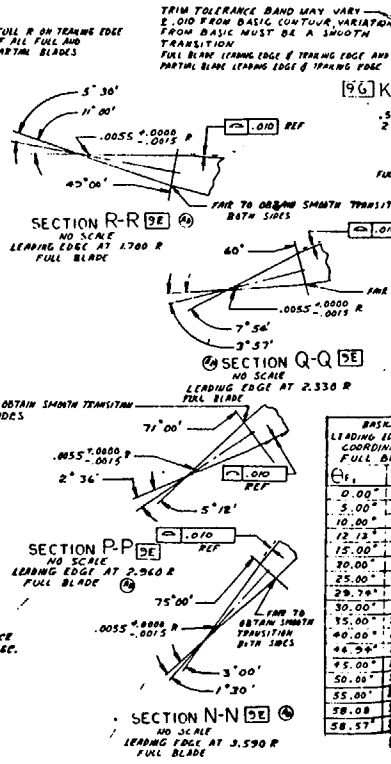
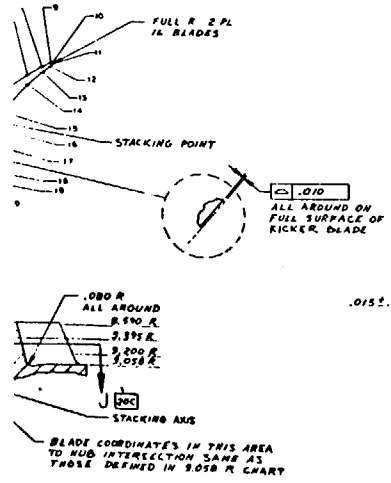
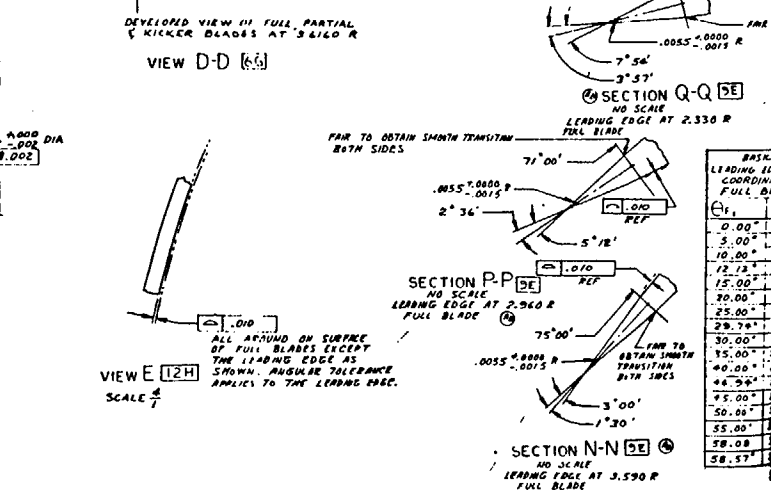
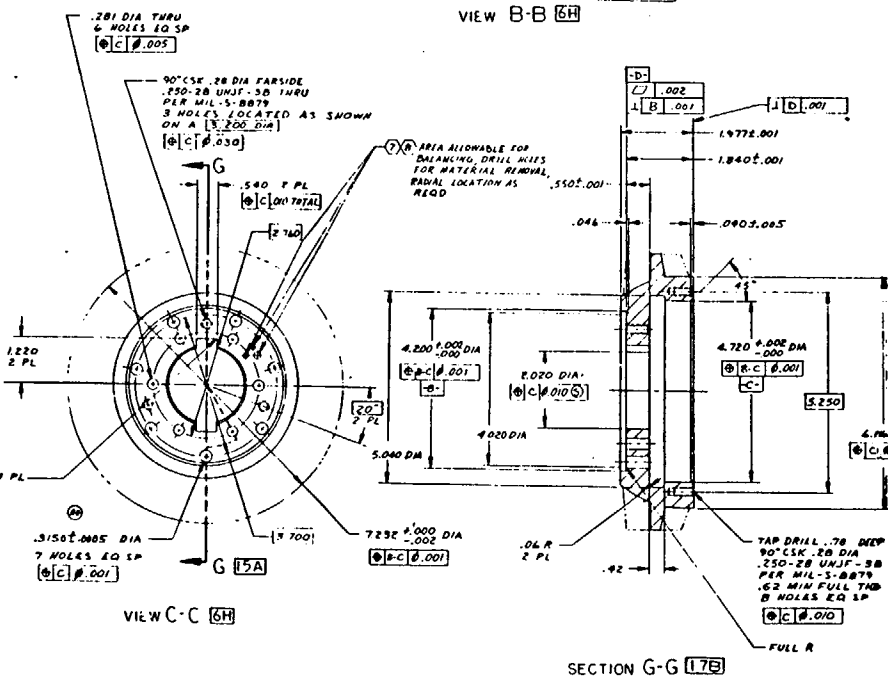
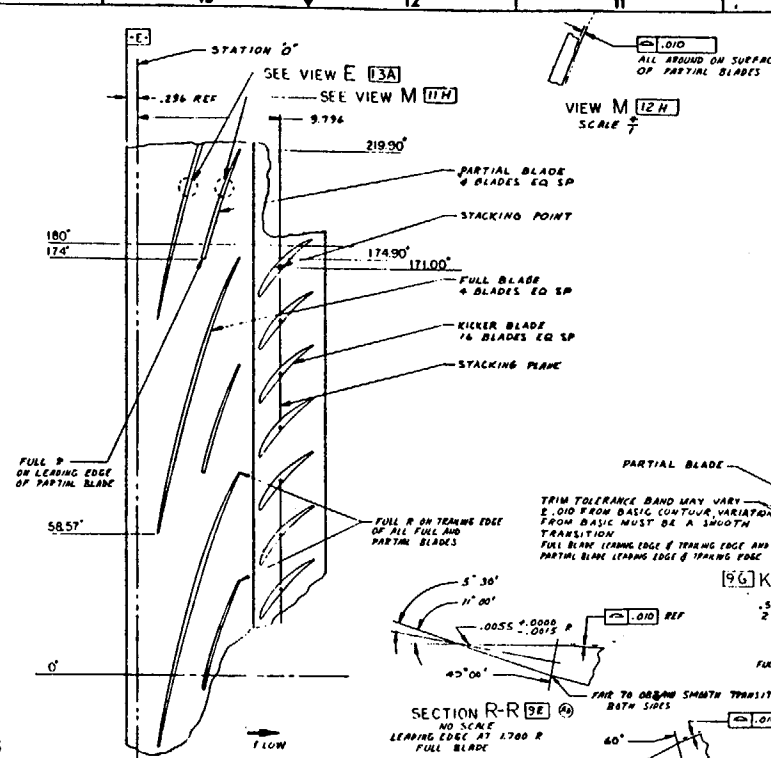
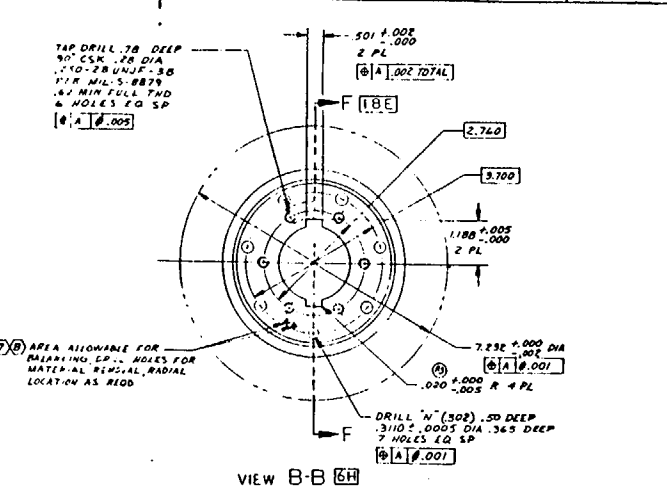
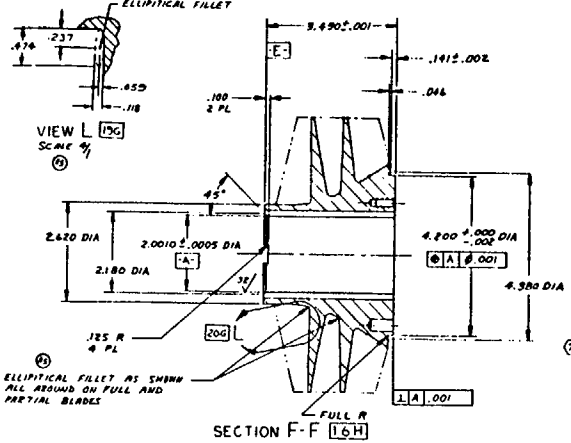
NO	DATE	DESCRIPTION
1		FOR INFORMATION
2		REVISED PICTURE OF SECTION H-H, SECTION J-J & SECTION K-K
3		REVISED PICTURE OF SECTION H-H, SECTION J-J & SECTION K-K
4		REVISED PICTURE OF SECTION H-H, SECTION J-J & SECTION K-K
5		REVISED PICTURE OF SECTION H-H, SECTION J-J & SECTION K-K
6		REVISED PICTURE OF SECTION H-H, SECTION J-J & SECTION K-K
7		REVISED PICTURE OF SECTION H-H, SECTION J-J & SECTION K-K
8		REVISED PICTURE OF SECTION H-H, SECTION J-J & SECTION K-K
9		REVISED PICTURE OF SECTION H-H, SECTION J-J & SECTION K-K
10		REVISED PICTURE OF SECTION H-H, SECTION J-J & SECTION K-K
11		REVISED PICTURE OF SECTION H-H, SECTION J-J & SECTION K-K
12		REVISED PICTURE OF SECTION H-H, SECTION J-J & SECTION K-K
13		REVISED PICTURE OF SECTION H-H, SECTION J-J & SECTION K-K

FOR INFORMATION  
 Figure 8. LSES Model Inlet Elbow  
 23/24

980019742

NO	DATE	DESCRIPTION
1		FOR INFORMATION
2		REVISED PICTURE OF SECTION H-H, SECTION J-J & SECTION K-K
3		REVISED PICTURE OF SECTION H-H, SECTION J-J & SECTION K-K
4		REVISED PICTURE OF SECTION H-H, SECTION J-J & SECTION K-K
5		REVISED PICTURE OF SECTION H-H, SECTION J-J & SECTION K-K
6		REVISED PICTURE OF SECTION H-H, SECTION J-J & SECTION K-K
7		REVISED PICTURE OF SECTION H-H, SECTION J-J & SECTION K-K
8		REVISED PICTURE OF SECTION H-H, SECTION J-J & SECTION K-K
9		REVISED PICTURE OF SECTION H-H, SECTION J-J & SECTION K-K
10		REVISED PICTURE OF SECTION H-H, SECTION J-J & SECTION K-K
11		REVISED PICTURE OF SECTION H-H, SECTION J-J & SECTION K-K
12		REVISED PICTURE OF SECTION H-H, SECTION J-J & SECTION K-K
13		REVISED PICTURE OF SECTION H-H, SECTION J-J & SECTION K-K

1	2.950
2	2.920
3	2.890
4	2.860
5	2.830
6	2.800
7	2.770
8	2.740
9	2.710
10	2.680
11	2.650
12	2.620
13	2.590
14	2.560
15	2.530
16	2.500
17	2.470
18	2.440
19	2.410
20	2.380

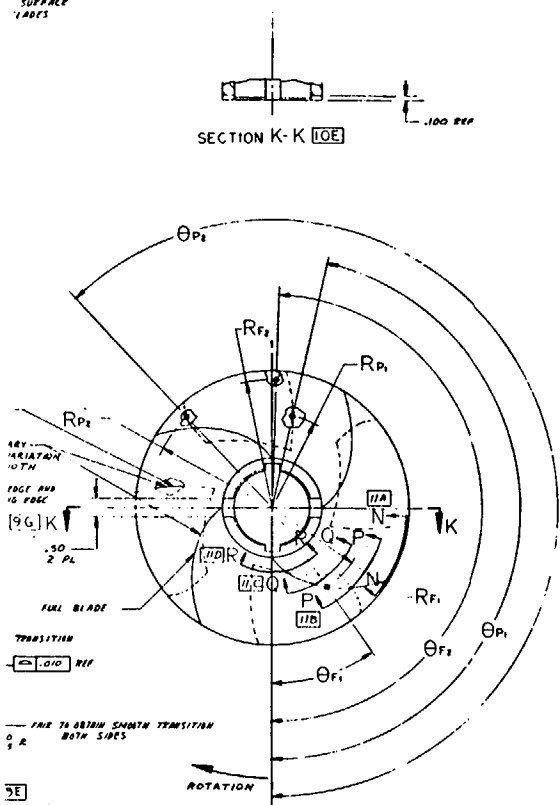


9R0019743	A
-----------	---

57

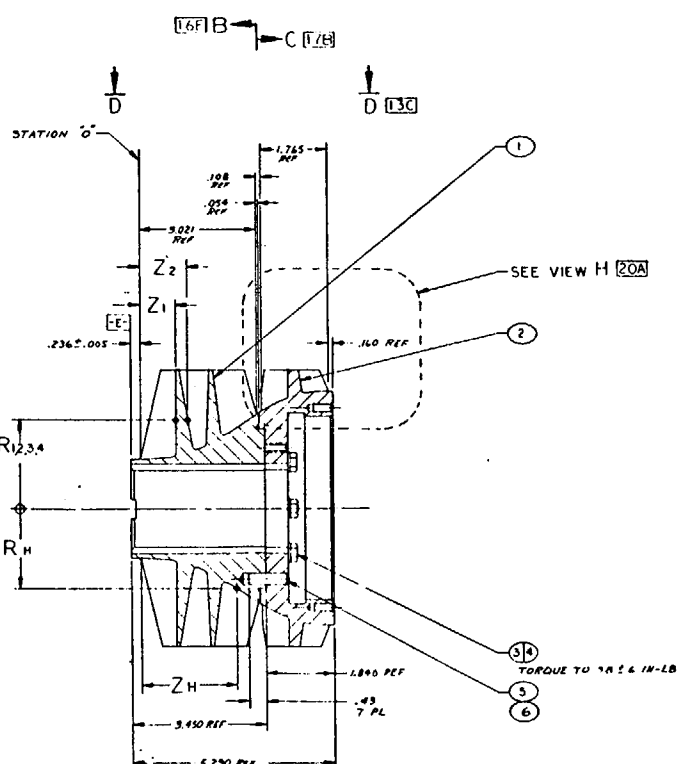
19	18	17	16	15	14	13	12	11
----	----	----	----	----	----	----	----	----

SURFACE  
TRADES



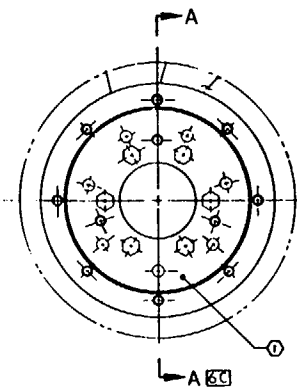
BASIC LEADING EDGE TRIM COORDINATES FULL BLADE		BASIC TRAILING EDGE TRIM COORDINATES FULL BLADE	
$\theta$	$R_{F1}$	$\theta$	$R_{F2}$
0.00	1.3098	167.9	1.3740
5.00	1.4665	162.9	1.7500
10.00	1.6289	163.9	1.9821
15.00	1.7972	168.9	2.1724
20.00	1.9708	165.9	2.3287
25.00	2.1500	164.9	2.4497
29.74	2.3300	168.9	2.6347
30.00	2.4180	169.9	2.8157
35.00	2.5180	170.9	2.9637
40.00	2.5847	171.9	3.1747
44.96	2.6600	172.9	3.4000
49.00	2.7424	173.9	3.6028
50.00	2.7974	174.0	3.6740
55.00	3.4320		
58.08	3.5900		
58.57	3.6740		

ROCKWELL INTERNATIONAL CORPORATION  
980019743 A



SECTION A-A [3D]

- ① BOLTS & WASHERS ARE MANUFACTURING UNS ONLY
- ② CALL ENGINEER BEFORE DRILLING HOLES AS TO SIZE, DEPTH & SPECIFIC LOCATION
- ③ BLANKS TO WITHIN .2 GRAM-INCH BY REMOVING MATERIAL IN AREA INDICATED. MATCH MAKE BALANCED PARTS.



- C. MACHINED FILETS .050 R
- 5. PENETRANT INSPECT PER MIL-18860 NO LIQUID INDICATIONS PERMITTED
- A. CAUTION: DO NOT USE CHLORINATED SOLVENTS OR METHYL ALCOHOL
- ④ MATERIAL SHALL MEET REQUIREMENTS OF AMS 4321 EXCEPT AS NOTED:
  - ① DRILLING 8.00 OD x 6.50 LONG
  - ② OXYGEN CONTENT 20% BY WEIGHT MAX
  - ③ ALUMINUM SOL. IN 1500'S 1.00% FOR 2 HOURS & 15 MINUTES AT TEMPERATURE AND AIR COOL
- MACHINE ALL PAIR ④
- ULTRASONIC INSPECT PER MIL-18850 CLASS A MECHANICAL REQUIREMENTS:
  - ULTIMATE STRENGTH: 75,000 PSI MIN
  - YIELD STRENGTH: 55,000 PSI MIN
- ⑤ MACHINE PER RADIOS-016
- ⑥ ELECTROCHEMICAL ETCH IDENTIFY PER RADIOS-008.

LIMITED RIGHTS LEGEND  
Contract No. W00024-18-C-2120  
Contractor: ROCKWELL INTERNATIONAL CORPORATION  
Explanation of Limited Rights Data Indication Use: Limited rights data is identified as being the industry design set forth in this drawing. Those portions of this technical data indicated as limited rights data shall not, without the written permission of the above Contractor, be either (a) used, released or disclosed in whole or in part outside the Government, or (b) used by a party other than the Government except for: (1) emergency repair or overhaul work only, by or for the Government, where the item or process concerned is not otherwise reasonably available to enable timely performance of the work, provided that the release or disclosure hereof outside the Government shall be made subject to a prohibition against further use, release, or disclosure, or (2) release to a foreign government, as the interest of the United States may require, only for information or evaluation within such government or for emergency repair or overhaul work by or for such government under the conditions of (1) above. This legend, together with the indications of the positions of this data which are subject to such limitations shall be included on any reproduction hereof which includes any part of the portion subject to such limitations.

FOR INFORMATION

Figure 9. LSES Model Inducer Assembly

25/26

REV	QTY	ITEM	PART OR IDENTIFYING NO	NOMENCLATURE OR DESCRIPTION	MATERIAL	SPECIFICATION	ZONE
7	—	6	RD122-383-1928	DOWEL PIN			
—	7	5	RD122-383-1928	DOWEL PIN			SD
④	REF	4	EDS1-001-0005	WASHER			SD
②	REF	3	RD111-1010-3614	BOLT			SD
③	1	1	—	KEY HALF	COIL PURE TITANIUM F088	AMS 4921	EF
③	1	1	—	FRONT HALF	COIL PURE TITANIUM F088	AMS 4921	EF
④-1	④-1	—	BR019743	INDUCER ASSY			
REV	QTY	ITEM	PART OR IDENTIFYING NO	NOMENCLATURE OR DESCRIPTION	MATERIAL	SPECIFICATION	ZONE

④ NONE

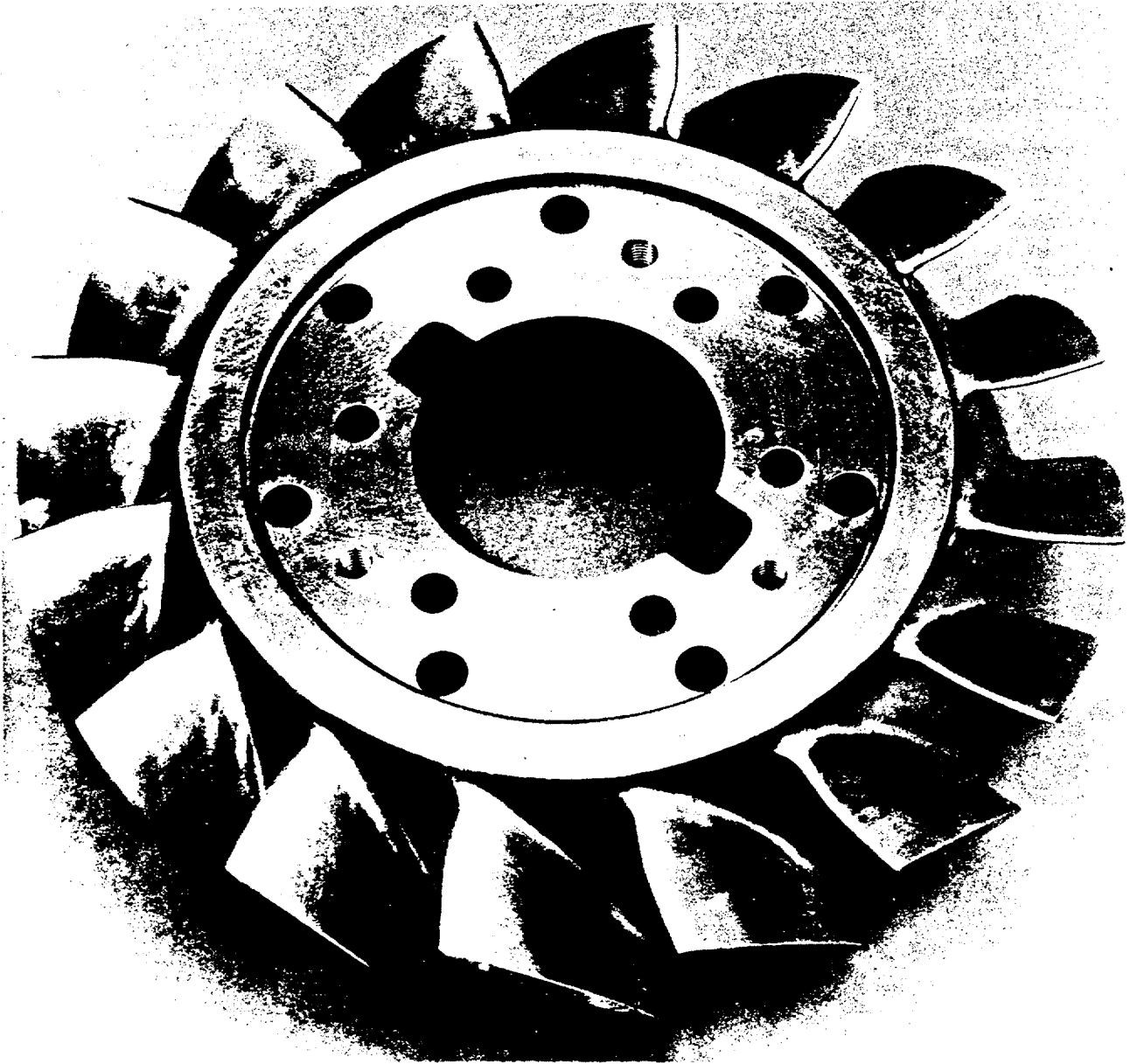
⑤ NOTED

⑥ 076002 980019743



4MS45-10/19/79-1-C4E

Figure 10. Inducer (Front Row)



4MS45-10/19/79-1-C4A

Figure 11. Kicker -005

pilot diameters and bears against the shaft shoulder to transmit the axial thrust through the shaft to the forward thrust bearings. The torque is transmitted from the shaft to the inducer by a keyway machined in the inducer.

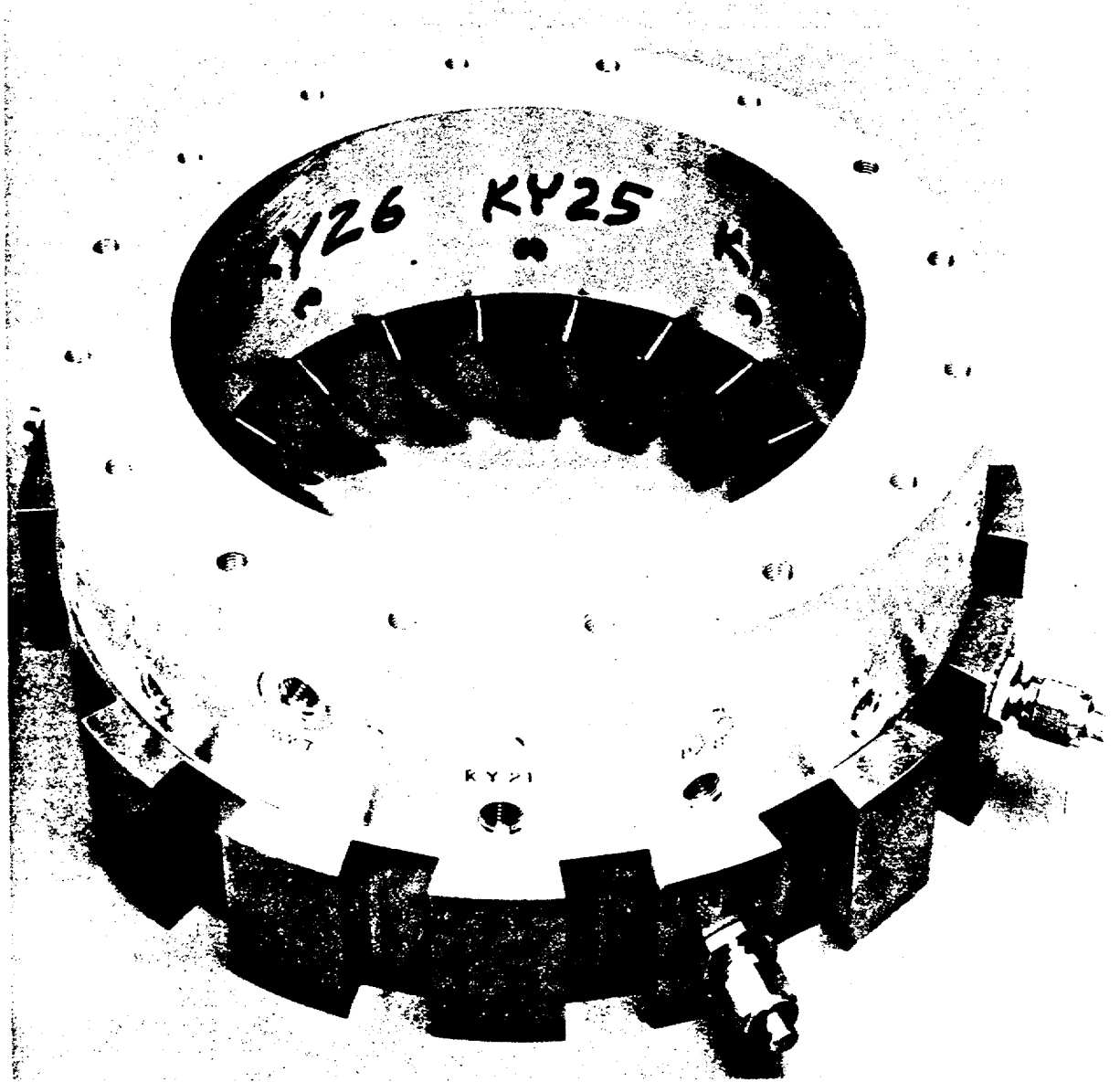
Stator Housing. The LSES stator housing is shown in Fig. 12 and 13. Figure 13 is a photograph showing both the stator and aluminum tunnel with eight kiel-yaw probe ports. The small holes shown in the figure are used for static pressure measurements. Commercially pure titanium is used for all parts of the stator housing to provide the required cavitation and corrosion resistance. The stator housing contains 19 stationary stator vanes that direct the flow coming from the kicker stage of the inducer to the blades of the axial rotor. The stator housing has five static pressure ports located at mid-passage between vanes and spaced axially as indicated in Fig. 12. Four planar cuts and four cylindrical cuts at radii of 3.058, 3.286, 3.505, and 3.616 inches completely define the 19 stator vanes. The fillet radius is 0.039 inch, and the tolerances are +0.010 inch and -0.00 inch all around. The notches on the outside of the stator housing are machined for thrust rods to pass through the housing when the plastic tunnel is in place.

Rotor. The LSES model rotor is a one-piece, commercially pure titanium forging with 17 blades. The model rotor drawing is presented in Fig. 14, and it should be noted that part number 9R0019746-007 is the final configuration of the rotor. A photograph of the axial rotor is shown in Fig. 15. Six planar cuts at radii of 3.0580, 3.2390, 3.3357, 3.4443, 3.6160, and 3.5923 inches describe the geometry of the rotor blades. A complete tabulation of blade coordinates is shown in Fig. 14, and section D-D shows the points at which the coordinates are defined and their location on the blade. The tolerances on the rotor are +0.010 inch and -0.00 inch all around. The direction of rotation is counter-clockwise looking fwd, as shown in the drawing (Fig. 14). The rotor is located concentric to the inducer and rubber bearing sleeve by interference-fit pilot diameters.

Discharge Housing. The LSES model propulsor discharge housing is made from a commercially pure titanium forging. It is attached to the stator and houses



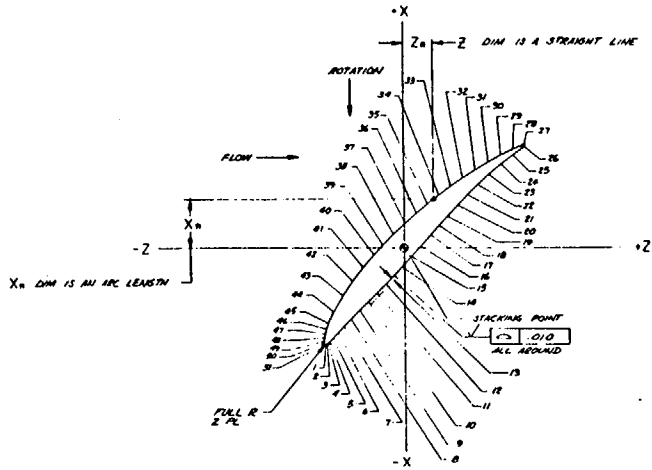




4MS62-5/4/79-C1E

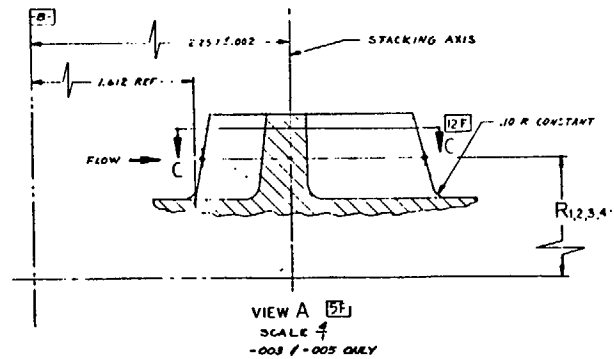
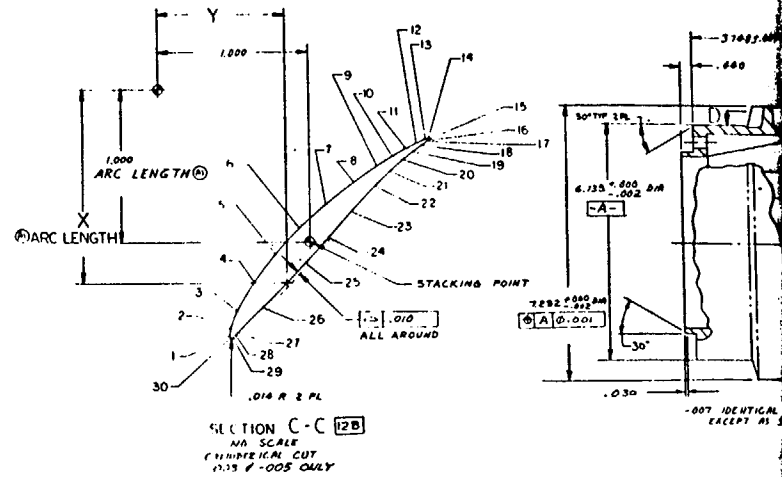
Figure 13. Stator

1.600  
 1.491  
 1.385  
 1.272  
 1.150  
 1.022  
 .899  
 .774  
 .646  
 .516  
 .384  
 .251  
 .117  
 .000  
 .117  
 .251  
 .384  
 .516  
 .646  
 .774  
 .899  
 1.022  
 1.150  
 1.272  
 1.385  
 1.491  
 1.600

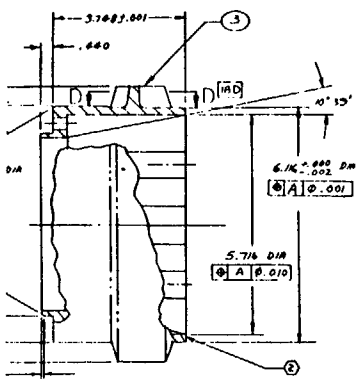


ALL DIMENSIONS ARE BASIC FOR -003 & -005

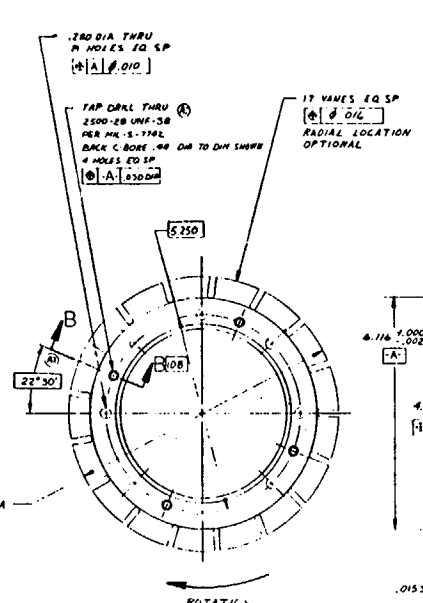
	R <sub>1</sub> : 3.058		R <sub>2</sub> : 3.200		R <sub>3</sub> : 3.335		R <sub>4</sub> : 3.550		R <sub>5</sub> : 3.616	
	X	Y	X	Y	X	Y	X	Y	X	Y
1	1.522	.353	1.498	.371	1.471	.389	1.440	.408	1.405	.429
2	1.476	.365	1.503	.371	1.538	.426	1.576	.460	1.579	.465
3	1.361	.420	1.397	.449	1.432	.478	1.433	.507	1.462	.510
4	1.191	.520	1.215	.543	1.243	.601	1.272	.649	1.276	.622
5	1.031	.552	1.045	.574	1.065	.607	1.085	.666	1.088	.767
6	.893	.566	.899	.600	.907	.624	.916	.678	.915	.928
7	.780	.557	.775	.644	.768	.760	.760	.707	.759	1.025
8	.689	.532	.671	.715	.644	1.025	.672	1.210	.618	1.294
9	.627	.533	.598	.757	.558	1.041	.577	1.454	.512	1.651
10	.596	.644	.557	1.039	.506	1.598	.454	1.557	.449	1.552
11	.577	.722	.527	1.719	.444	1.693	.406	1.648	.338	1.642
12	.559	1.053	.529	1.817	.440	1.767	.371	1.718	.362	1.712
13	.557	1.328	.501	1.930	.423	1.837	.346	1.785	.335	1.770
14	.558	1.445	.500	1.907	.420	1.856	.341	1.801	.330	1.794
15	.564	1.511	.507	1.913	.420	1.861	.349	1.809	.338	1.802
16	.570	1.549	.512	1.911	.421	1.859	.352	1.808	.340	1.801
17	.575	1.644	.515	1.907	.421	1.855	.356	1.804	.345	1.797
18	.582	1.687	.519	1.854	.416	1.804	.353	1.757	.345	1.750
19	.603	1.815	.555	1.783	.449	1.740	.424	1.697	.418	1.691
20	.635	1.733	.593	1.705	.515	1.573	.477	1.629	.470	1.624
21	.669	1.627	.643	1.604	.601	1.373	.553	1.542	.547	1.537
22	.750	1.506	.723	1.487	.685	1.163	.648	1.140	.643	1.137
23	.870	1.308	.855	1.307	.838	1.090	.815	1.079	.810	1.070
24	.996	1.070	.986	1.021	.987	1.022	.981	1.023	.980	1.023
25	1.124	.933	1.131	.941	1.137	.953	1.049	.969	1.045	.966
26	1.268	.799	1.286	.819	1.311	.848	1.038	.876	1.041	.879
27	1.425	.633	1.450	.670	1.485	.676	1.020	.699	1.024	.698
28	1.538	.512	1.563	.559	1.598	.536	1.033	.472	1.037	.477
29	1.539	.341	1.544	.368	1.549	.424	1.033	.461	1.038	.466
30	1.533	.356	1.538	.382	1.542	.419	1.026	.456	1.031	.460



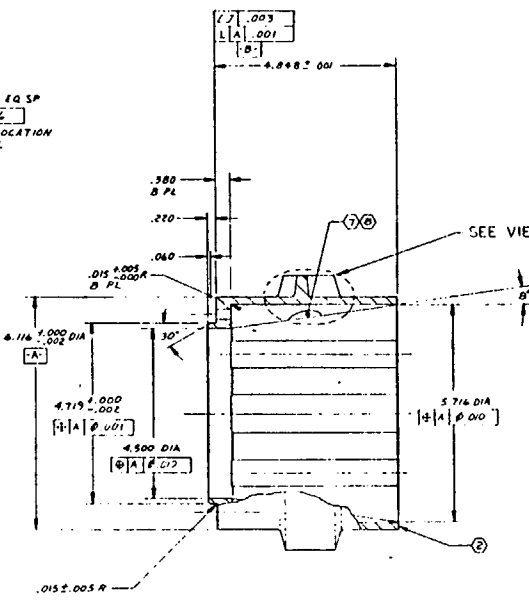
Standard International Organization  
 Specifications (Metric)  
 Engineering Unit System  
 9R0019746



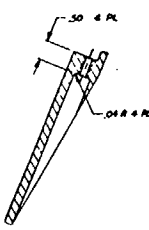
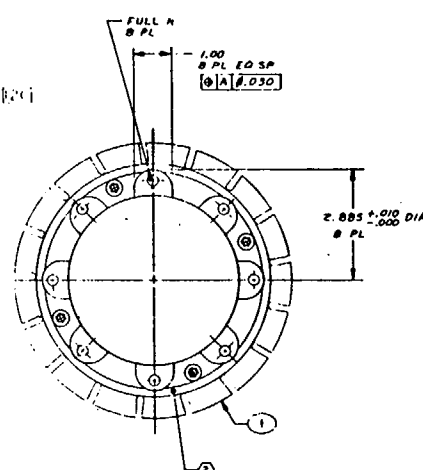
007 IDENTICAL TO 002 EXCEPT AS SHOWN



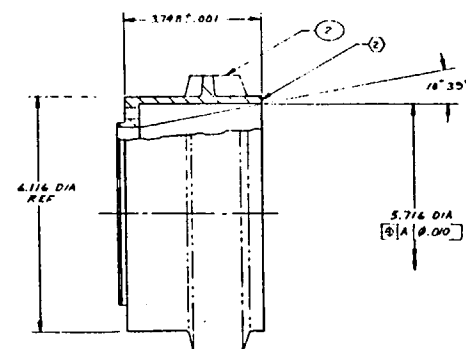
ROTATIONAL



SEE VIEW A



SECTION B-B



005 IDENTICAL TO 003 EXCEPT AS SHOWN

- ① IS THE ANGLE SUBTENDED BY THE ARC LENGTH AS AT THE GIVEN RADIUS
- ② BALANCE TO WITHIN 1 GRAM-INCH.
- ③ MATERIAL REMOVAL AREA ALLOWABLE FOR BALANCING CALL ENGINEERING BEFORE MATERIAL REMOVAL
- ④ MODEL MADE TO .1579 OF ACTUAL SIZE OF LSES ROTOR
- ⑤ PERMANENT INSPECT PER MIL-I-8866 NO LINEAR IND. ARTICLES PERMITTED
- ⑥ CAUTION: DO NOT USE CHLORINATED SOLVENTS OR METHYL ALCOHOL
- ⑦ MATERIAL SHALL MEET REQUIREMENTS OF AMS 4921 EXCEPT AS NOTED:
  - FORMING H.L. JD'S & DD LONG
  - DISTEN. CONTENT .25% BY WEIGHT MAX.
  - ANNEAL 1.5-2.0 HRS AT 1300°F FOR 2 HOURS
  - 2 IS MIL-S-13000 AT TEMPERATURE AND AIR COOL.
  - MACHINING ALL OVER (U)
  - ULTRACLEAN INSPECT PER MIL-I-8850 CLASS A.
  - MICHAICAL PROPERTIES:
    - ULTIMATE STRENGTH — 75000 PSI MIN
    - YIELD STRENGTH — 51500 PSI MIN
- ⑧ ELECTROCHEMICAL ETCH IDENTIFY PER RAD10A-008
- ⑨ MACHINE PER RAD103-010.

REV	DESCRIPTION	DATE
1	ISSUED AS DRAWING	11/11/50
2	REVISION	
3	REVISION	
4	REVISION	
5	REVISION	
6	REVISION	
7	REVISION	
8	REVISION	
9	REVISION	
10	REVISION	
11	REVISION	
12	REVISION	
13	REVISION	
14	REVISION	
15	REVISION	
16	REVISION	
17	REVISION	
18	REVISION	
19	REVISION	
20	REVISION	

FOR INFORMATION

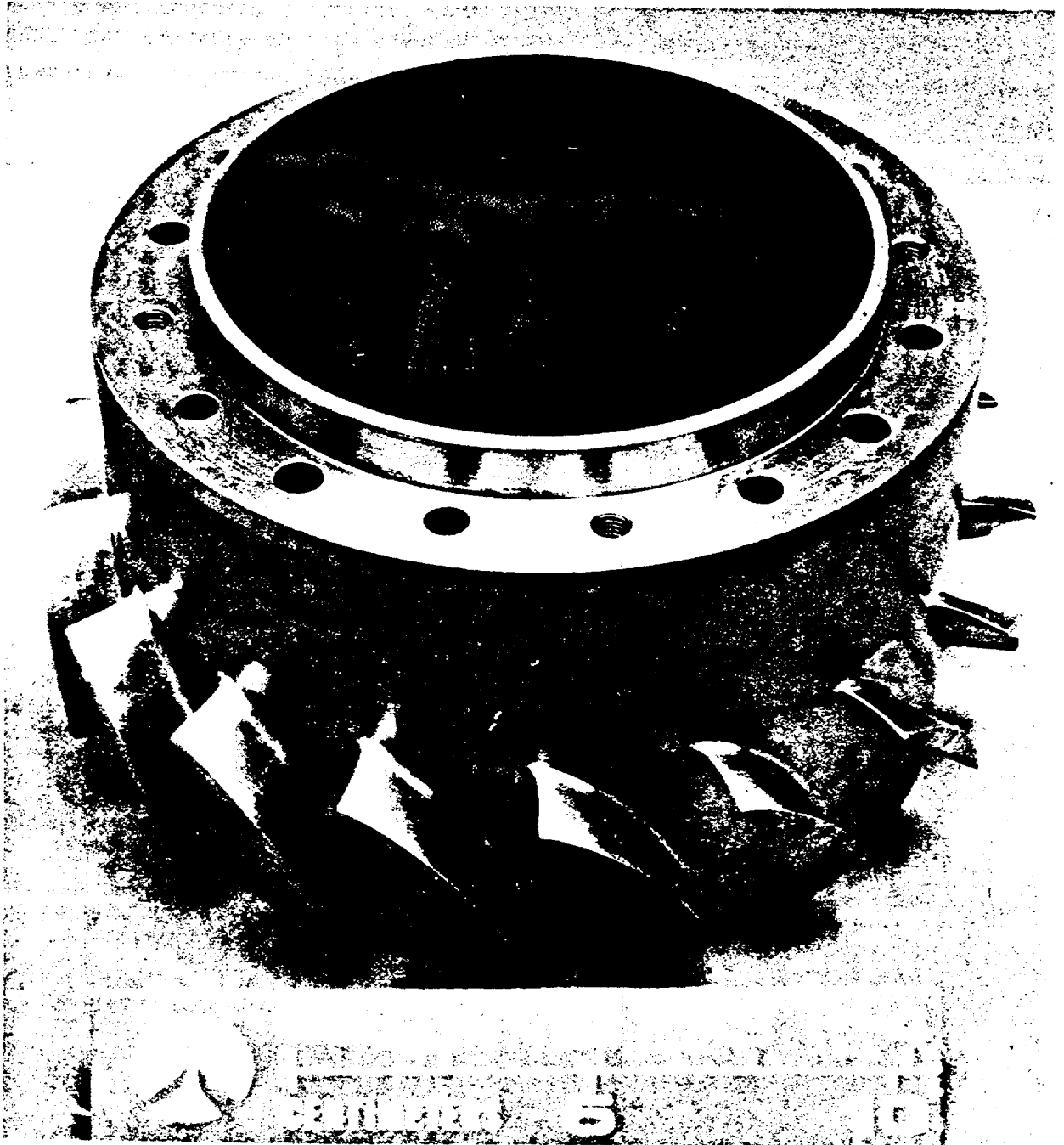
Figure 14. LSES Model Rotor

35/36

ITEM NO	PART OR IDENTIFYING NO	DESCRIPTION	MATERIAL	SPECIFICATION
3	990019746-007	ROTOR	CHML FILE TITANIUM FORG	AMS 4921
2	990019746-005	RETAINING NUT	MAK P8UM -003	
1	990019746-001	NUT CH	KOML PURE TITANIUM FORG	AMS 4921

REV	DESCRIPTION	DATE
1	ISSUED AS DRAWING	11/11/50
2	REVISION	
3	REVISION	
4	REVISION	
5	REVISION	
6	REVISION	
7	REVISION	
8	REVISION	
9	REVISION	
10	REVISION	
11	REVISION	
12	REVISION	
13	REVISION	
14	REVISION	
15	REVISION	
16	REVISION	
17	REVISION	
18	REVISION	
19	REVISION	
20	REVISION	

REV	DESCRIPTION	DATE
1	ISSUED AS DRAWING	11/11/50
2	REVISION	
3	REVISION	
4	REVISION	
5	REVISION	
6	REVISION	
7	REVISION	
8	REVISION	
9	REVISION	
10	REVISION	
11	REVISION	
12	REVISION	
13	REVISION	
14	REVISION	
15	REVISION	
16	REVISION	
17	REVISION	
18	REVISION	
19	REVISION	
20	REVISION	

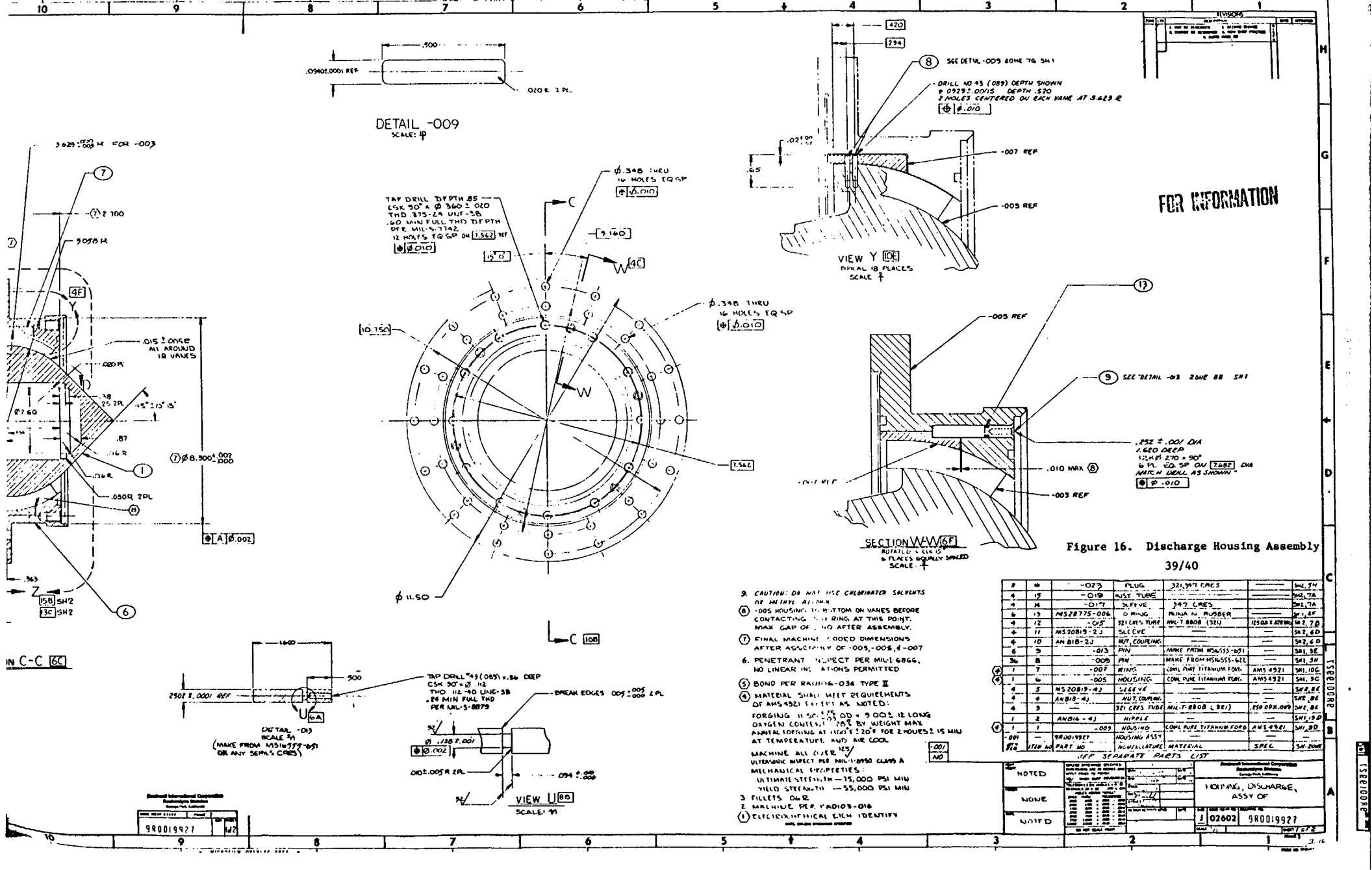


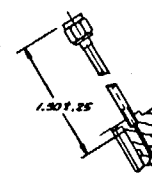
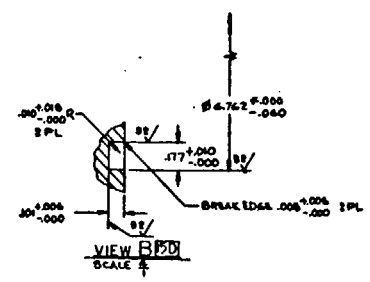
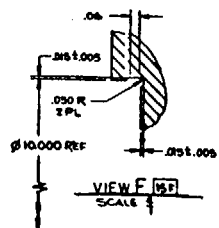
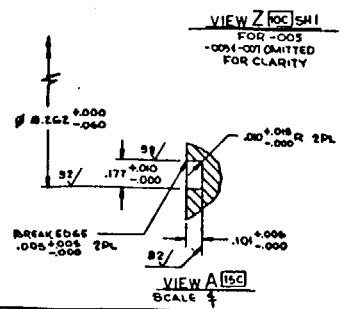
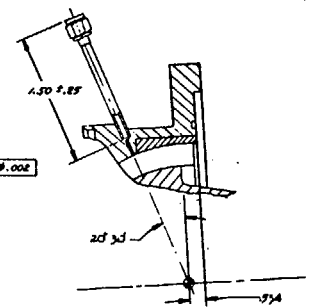
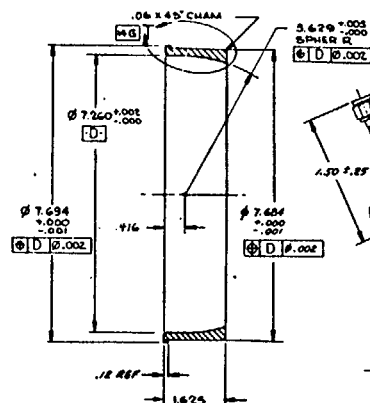
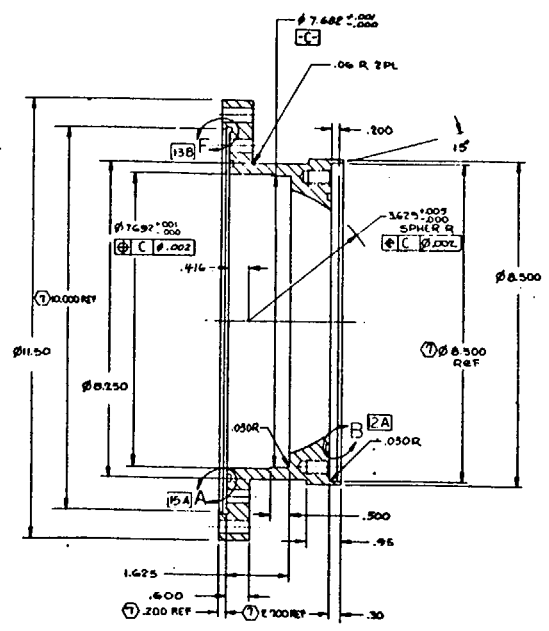
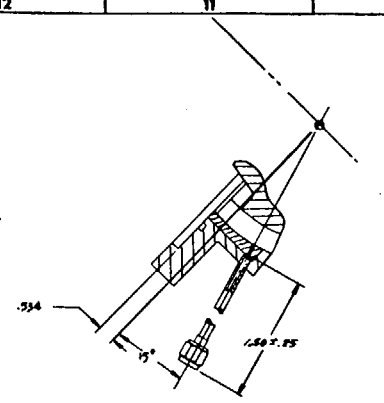
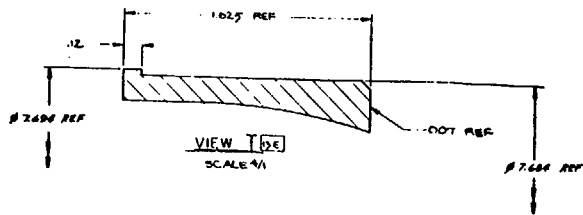
4MS45-10/19/79-C1H

Figure 15. Rotor -007

18 straightening vanes to ensure an even axial flow distribution to the nozzle. It also provides support to the aft end of the rotating assembly via the rubber bearing and support for the pintle assembly and nozzle. Drawings of the LSES discharge housing are shown in Fig. 16, which represents an overall view of the blade geometry, and in Fig. 17, which presents several sectional views and instrumentation locations. Figure 18 is a photograph of the discharge housing which shows the discharge housing, straightening vanes, and rubber bearing. Two spherical cuts at the hub and tip radii of 3.1976 and 3.5529 inches define the geometry of the straightening vanes. The table of spherical coordinates is given in Fig. 16. The fillet radius of the vanes is 0.060 inch, and the tolerances are +0.010 inch and -0.00 inch all around. The pintle is an integrally machined, 45-degree pintle made from commercially pure titanium, and it forms the inner surface of the nozzle flow passage. There are five static pressure ports at the outer diameter of the discharge housing located as shown in Sections G-G, H-H, J-J, K-K, and L-L of Fig. 17. In addition, two pairs of static pressure ports which measure the pressure inside of the rotating assembly are shown in Sections M-M and S-S in Fig. 17.







SECTION





4MS45-10/19/79-C1F

Figure 18. Discharge Housing

## Nonmodeled Components.

Bearings. The LSES propulsor rotating elements are supported on oil-lubricated spherical ball bearings at the forward end and on a water-lubricated rubber bearing at the aft end. The ball bearings are jet fed with cooled oil from the facility lubrication delivery system. The aft bearing is lubricated by water circulated within the propulsor during propulsor operation.

The LSES model pump bearing package consists of two single-row spherical ball bearings that carry forward thrust and one single-row spherical ball that carries reverse thrust and radial loads. Lubrication of the forward bearings accomplishes both heat removal and separation of rolling surfaces. Adequate cooling is obtained by circulating a quantity of oil through the bearings sufficient to remove the heat of mechanical and viscous friction with a moderate oil temperature rise. Lubricants are delivered to the bearings through a jet directed toward the interior of the bearing at the gap between the inner and outer races. This places fresh lubricant where it produces maximum benefit, i.e., at the roller ends. Bearing motion also provides circulation of oil to other parts of the bearing, providing effective cooling. After passing through the bearings, the oil is gravity-drained through a three-hole drain duct into a reservoir.

The aft end of the rotating pump elements is radially supported by a water-lubricated bearing that is formed of a molded rubber compound bonded into a metal liner. The advantages of the rubber material are in its low friction coefficient when wet, its ability to survive water-carried particulate contamination, and its ability to absorb overloads. The inside surface of the bearing is composed of a series of flat surfaces whose junctures form axial grooves that permit the lubrication and cooling water to flush out solid contaminants.

Driveline. The driveline for the LSES propulsor is shown in Fig. 5 and consists of a facility shaft, a flexible coupling, and the propulsor main shaft. Torque is transmitted from the torquemeter to a quill shaft (not shown in Fig. 5)

and then to the facility shaft through the splines at the forward end of the facility shaft. The aft end of the facility shaft is mated to the coupling hub by a keyway. The centerbody of the coupling is bolted to the coupling hub on both ends, and the flexible elements in the coupling are located on both ends of the centerbody between the centerbody and hub. The forward end of the propulsor main shaft is splined to mate with the coupling hub. Torque is transmitted from the coupling to the main shaft through the splines and then is transmitted to the inducer by a keyway located at the aft end of the shaft.

## HYDRODYNAMIC DESIGN

### Overview

Three components have had design modifications since the release of the Design Report.\* These three are the inducer, axial rotor, and straightening vanes. The purpose of this section is to describe these three designs and relate their design predictions to test results from the model program.

### PJ-46 Inducer Design

Design Requirements. The pump hydrodynamic design was approached with the goals of developing the maximum possible sub-hump thrust with a pump capable of fitting within the space envelope. Table 1 shows the design point requirements of the PJ-46 Inducer.

TABLE 1. DESIGN POINT FOR SES INDUCER

Flow, gpm	138,000
Head, feet	622
Speed, rpm	1,000

During hump operation, the inducer must be capable of generating sufficient head rise to keep the stator out of cavitation at 5% less flow at a total inlet head (TIH) of 40.3 feet. This suction requirement leads to a required suction specific speed based on the pump inlet head of 22,279 where

$$Q = 138,000 * 0.95 = 131,100 \text{ gpm}$$

$$N = 1000 \text{ rpm}$$

$$\text{NPSH} = 40.8 - 0.6 = 40.2 \text{ ft}$$

$$\text{Vapor Head} = 0.6 \text{ ft}$$

---

\*R-9765, 2K SES Waterjet Propulsor Design Disclosure Summary

The sum of the inlet evaluation and hydrodynamic losses are an additional 6 feet leading to an NPSH of 34.2 feet and a required inducer centerline suction specific speed of 25,600. These defined requirements were to be met with a design that achieves

1. Long life by minimizing blade cavitation damage
2. High efficiency by minimizing hydrodynamic losses
3. Relatively uniform discharge conditions to avoid cavitation damage or large losses in the downstream stator

The flow coming into the inducer is assumed to be relatively uniform both with regard to inlet velocity and head. This uniformity is assumed to hold even with a relatively strong distortion upstream of the inlet elbow based on tests showing the effectivity of the elbow in reducing upstream distortions

Design Geometry. The inducer consists of tandem blade rows fixed to a common hub. The inlet blade set consists of four full blades plus four splitter blades. The second blade row (kicker blades) consists of 16 airfoil shaped blades. The inlet portion of the inducer permits operation at low pump inlet head values. This portion of the inducer is an improved version of the Powerjet 20 inducer with a proportionally reduced inlet hub diameter and increased tip diameter. At corresponding radius ratios, the inlet blade angles are the same. The profile view of the inducer is shown in Fig. 19. This inlet design was selected to ensure both good suction performance and long life by operating without cavitation damage. The similarity with the Powerjet 20 design provides the confidence in the design based on demonstrated performance both in the laboratory and in seawater operation.

The front blade row thickness distribution is also similar to that of the Powerjet 20. The camber distribution is similar in the leading edge region, but more camber is introduced towards the trailing edge of the front row blades. This added camber provides a higher head rise in the front row and results in more margin for the kicker blade row to minimize the loss potential due to kicker blade cavitation.

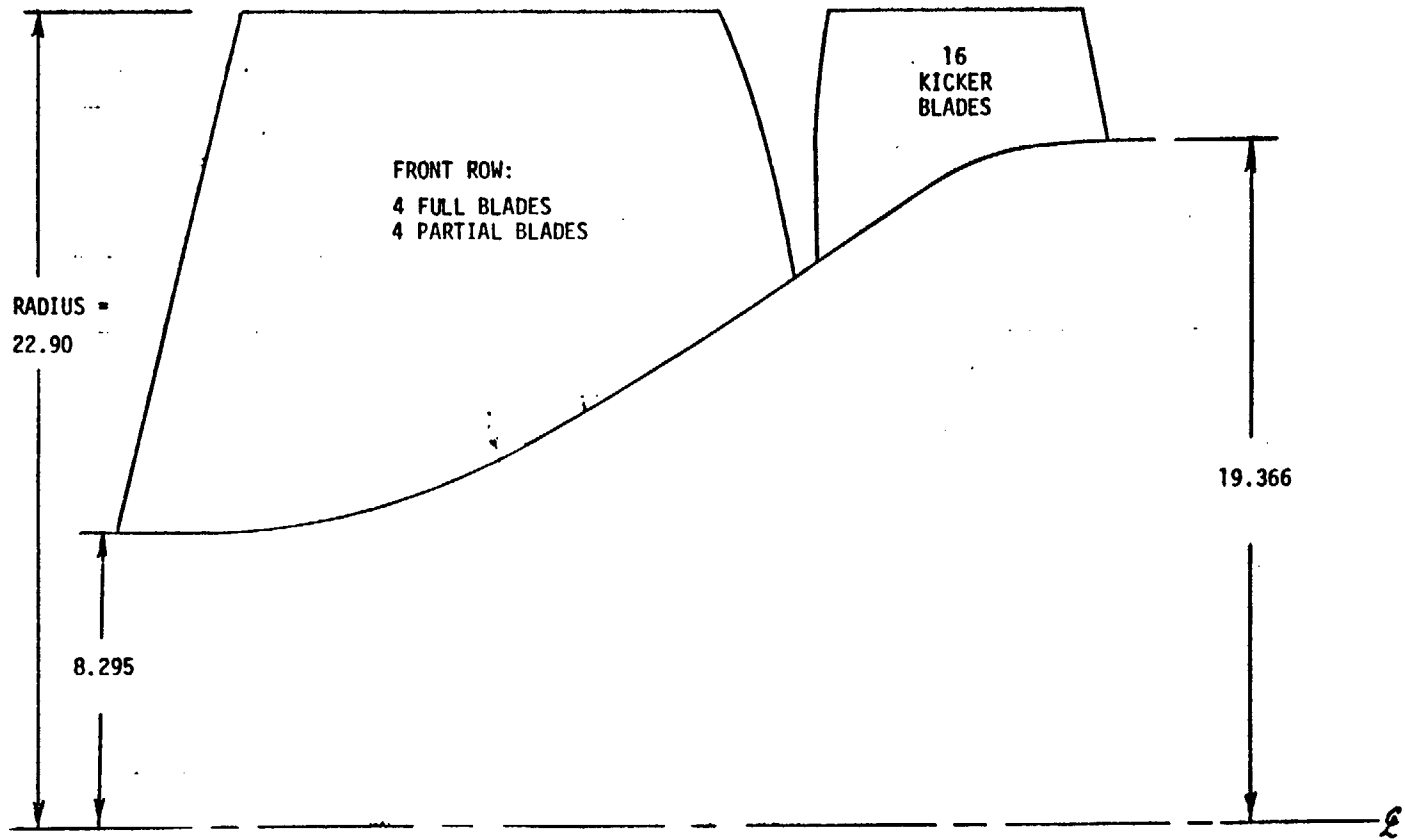


Figure 19. 3K SES Inducer Profile

Figure 20 shows a typical blade-to-blade profile shape with the partial in place. Even with the extra camber, the diffusion factor for the front blade row is moderate so that no problem would be expected with front row boundary layer separation. The tip solidity of the inducer was also reduced slightly as compared with the Powerjet 20 to help provide maximum efficiency.

The waterjet design computer program was used to obtain the design flow vectors for the inducer. The design program was derived from the NASA compressor design program. This is a nonisentropic complete radial-equilibrium program that includes the effects of wall curvature and variations in efficiency from hub to tip along required streamlines, including both hub and tip boundary layers. The design flow vectors selected by the program for the discharge of the PJ-46 inducer front row are shown in Table 2. Table 3 presents similar data for the kicker blade discharge. Note that the program demands constant head from hub to tip leaving the inducer, and thus, provides more work where the inducer efficiency is lower near the wall. This keeps the head uniform and minimizes mixing losses.

The head split between the front blade row and the kicker blade row was selected to be 50/50. This provides a good cavitation margin at the kicker leading edge and analytically shows good overall efficiency. The first kicker stage tested resulted in an overall inducer head rise that exceeded the desired head rise. The inducer head as measured was 682 feet at the tip and 742 feet at the hub as compared with a design head of 622 feet. This additional head rise is attributable to the kicker stage and indicated that the blade profiles selected were giving significantly more fluid turning than the design value. These profiles were modified NACA-65 series airfoils, and the additional turning is believed to be due to the added benefit of the three-dimensional flow effects in the inducer. For example, these effects are largest at the hub where the head rise was also largest. These profiles were trimmed at the trailing edge to lower the head rise, but this also resulted in a reduced efficiency. Therefore, the decision was made to redesign the kicker blade row to achieve an optimum design from both a head rise and efficiency standpoint.

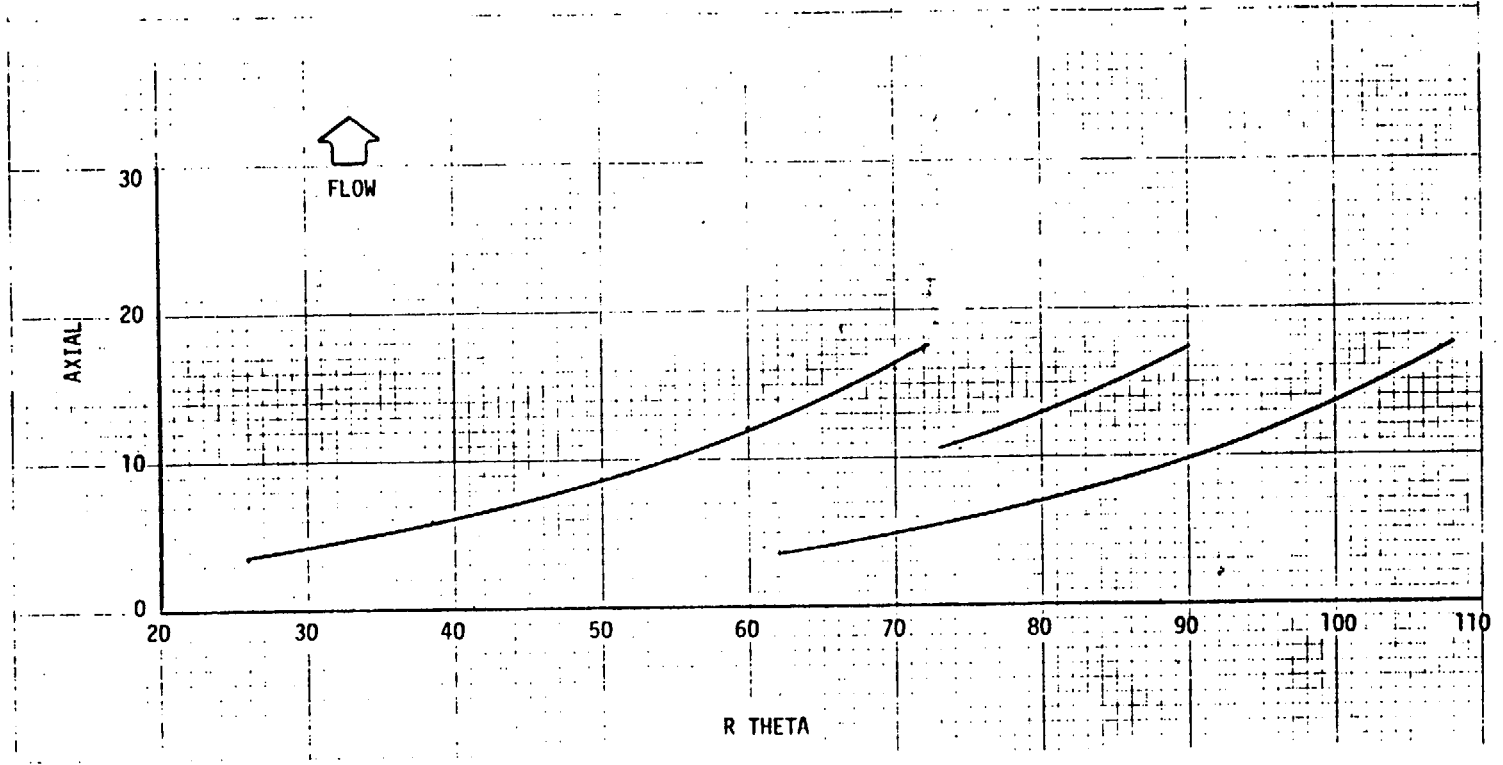


Figure 20. Blade Centerline Profile at Tip

TABLE 2. INDUCER FIRST BLADE ROW DISCHARGE DESIGN VECTORS

STREAMLINE NO.	RADIUS (IN.)	AXIAL COORD. (IN.)	AXIAL VEL. (FT/SEC)	MERID. VEL. (FT/SEC)	TANG. VEL. (FT/SEC)	ABS. VEL. (FT/SEC)	ABS. FLOW ANGLE (DEG)
TIP	22.900	17.100					
1	22.900	17.100	62.94	62.94	46.72	78.38	36.59
2	22.372	17.177	65.84	65.88	43.85	79.14	33.65
3	21.853	17.277	67.39	67.53	43.05	80.08	32.52
4	21.337	17.406	68.36	68.69	42.70	80.86	31.87
5	20.821	17.555	69.03	69.65	43.02	81.86	31.70
6	20.301	17.708	69.47	70.50	43.42	82.80	31.63
7	19.776	17.853	69.68	71.31	43.89	83.73	31.61
8	19.240	17.990	69.31	71.78	44.73	84.58	31.93
9	18.685	18.118	67.92	71.62	46.55	85.42	33.02
10	18.099	18.238	64.93	70.49	49.19	85.95	34.91
11	17.458	18.357	58.94	67.45	53.57	86.14	38.46
HUB	17.458	18.357					

STREAMLINE NO.	R/R TIP	REL. FLOW ANGLE (DEG)	REL. TANG. VEL. (FT/SEC)	REL. VEL. (FT/SEC)	WHEEL SPEED (FT/SEC)	EFF.	DIFFUSION FACTOR
TIP	1.0000						
1	1.0000	67.66	153.12	165.55	199.84	0.7542	0.2447
2	0.9770	66.48	151.38	165.09	195.23	0.8224	0.2142
3	0.9543	65.42	147.65	162.36	190.70	0.8576	0.1943
4	0.9317	64.42	143.50	159.09	186.20	0.8857	0.1739
5	0.9092	63.33	138.67	155.18	181.69	0.9008	0.1532
6	0.8865	62.20	133.75	151.19	177.16	0.9154	0.1265
7	0.8636	61.01	128.69	147.12	172.58	0.9296	0.0906
8	0.8402	59.77	123.17	142.56	167.90	0.9376	0.0437
9	0.8159	58.42	116.40	136.76	163.06	0.9276	-0.0172
10	0.7904	57.05	108.76	129.60	157.95	0.9063	-0.1143
11	0.7624	55.67	98.78	119.61	152.35	0.8627	-0.3190
HUB	0.7624						

TABLE 3. INDUCER DISCHARGE DESIGN VECTORS

STREAMLINE NO.	RADIUS (IN.)	AXIAL COORD. (IN.)	AXIAL VEL. (FT/SEC)	MERD. VEL. (FT/SEC)	TANG. VEL. (FT/SEC)	ABS. VEL. (FT/SEC)	ABS. FLOW ANGLE (DEG)
TIP	22.900	27.544					
1	22.900	27.544	92.33	92.33	115.70	148.03	51.41
2	22.546	27.644	98.27	98.27	112.41	149.31	48.84
3	22.202	27.739	101.41	101.42	111.77	150.92	47.78
4	21.862	27.831	103.36	103.36	111.71	152.19	47.22
5	21.521	27.921	104.65	104.66	112.66	153.77	47.11
6	21.180	28.009	105.75	105.76	113.70	155.28	47.07
7	20.836	28.095	106.83	106.84	114.84	156.85	47.07
8	20.489	28.181	107.20	107.21	116.68	158.46	47.42
9	20.135	28.265	106.34	106.34	119.92	160.28	48.43
10	19.769	28.347	102.74	102.75	124.98	161.79	50.58
11	19.366	28.430	92.01	92.01	135.78	164.02	55.88
HUB	19.366	28.430					

STREAMLINE NO.	R/RTIP	REL. FLOW ANGLE (DEG)	REL. TANG. VEL. (FT/SEC)	REL. VEL. (FT/SEC)	WHEEL SPEED (FT/SEC)	2ND BLADE ROW EFF.	ROTOR OVERALL EFFICIENCY	OVERALL DIFFUSION FACTOR
TIP	1.0000							
1	1.0000	42.34	84.14	124.92	199.84	0.9441	0.8674	0.526
2	0.9845	40.64	84.34	129.50	196.75	0.9599	0.9067	0.470
3	0.9695	38.95	81.98	130.41	193.75	0.9677	0.9294	0.436
4	0.9547	37.42	79.07	130.14	190.78	0.9736	0.9408	0.404
5	0.9398	35.68	75.15	128.84	187.81	0.9750	0.9476	0.374
6	0.9249	33.92	71.12	127.45	184.83	0.9763	0.9540	0.338
7	0.9099	32.09	66.99	126.11	181.83	0.9776	0.9602	0.285
8	0.8947	30.09	62.12	123.90	178.80	0.9741	0.9609	0.227
9	0.8793	27.68	55.79	120.09	175.71	0.9649	0.9515	0.151
10	0.8632	24.82	47.52	113.20	172.50	0.9432	0.9299	0.058
11	0.8457	19.85	33.22	97.83	169.00	0.8799	0.8738	-0.072
HUB	0.8457							

The redesigned kicker blade was selected to have the same profile type as the original design, i.e., a modified NACA-65 series. This profile shape had been shown to provide excellent lift capability with good efficiency. Testing on the first design had also indicated a good suction performance and life capability with the original kickers. Thus, the kicker leading edge blade angles and profile shape had demonstrated a good match with the flow discharging from the front blade row. Therefore, this same leading edge configuration was selected for the redesign.

The blade camber required to achieve the design head rise was adjusted by using a combination of empirical and analytical techniques. The tested inducer provided results that could be compared with results from two-dimensional cascade tests of the same basic profile shape. This provided a two-to three-dimensional correction factor. The blade profiles were then analyzed with the Rocketdyne three-dimensional analysis program using techniques that provided a match to the original data and a predicted performance for the new profiles. These techniques provided confidence in the new design.

The selected profile shapes for the final design are summarized in Table 4. The profile varies linearly between the two radii shown in the table. The blade profile is held constant below the inner radius shown in the table. This profile variation was required to match the incoming flow.

TABLE 4. KICKER PROFILE SHAPE

Radius In.	Lift Coefficient	Solidity	Chord	Stagger Angle, Dec.
22.90	1.20	1.25	11.241	49.11
19.366	1.77	1.50	11.408	44.75

Figure 21 depicts the cavitation free range of the kicker tip which is the most critical region of the kicker for cavitation. The lower curve in Fig. 21 is a locus of points representing the maximum velocity overspeed on the blade leading edge. These points were generated using a two-dimensional potential flow program that provides good accuracy in the leading edge region. As can be seen from the curve, a deviation from reference angle of attack in either direction tends to cause the local velocity to increase. When the local velocity, relative to the inlet velocity, reaches 1.38 the minimum local static head drops to vapor head, assuming the hump conditions of 40.8 feet of total inlet head and 1000 rpm pump speed. The curve shows substantial margin for avoiding leading edge cavitation on the kicker. The margin along the abscissa (relative to the inlet flow angle) is important to provide cavitation-free range for all kickers which are positioned at various positions relative to the suction and pressure sides of the upstream blade rows, and thus are subject to some blade-to-blade variations.

Model Test Data. Verification of the front row design is obtained by comparing the suction performance and life of the part and by comparison of the measured and analytical tip wall static pressure distribution. The suction performance achieved during early testing matched design predictions indicating a satisfactory design. The suction performance did tend to degrade with subsequent testing, but has always been sufficient to provide comfortable thrust margins for the overall pump during the low boat speed operation. The inducer front row has also shown excellent life characteristics. After 29 hours of testing, no indication of cavitation damage was observed. After an additional 13 hours, giving a total of 42 hours at hump conditions, only slight frosting near the tips of some of the blades was observed. These results demonstrate the ability of the front row to meet the life requirements of the pump.

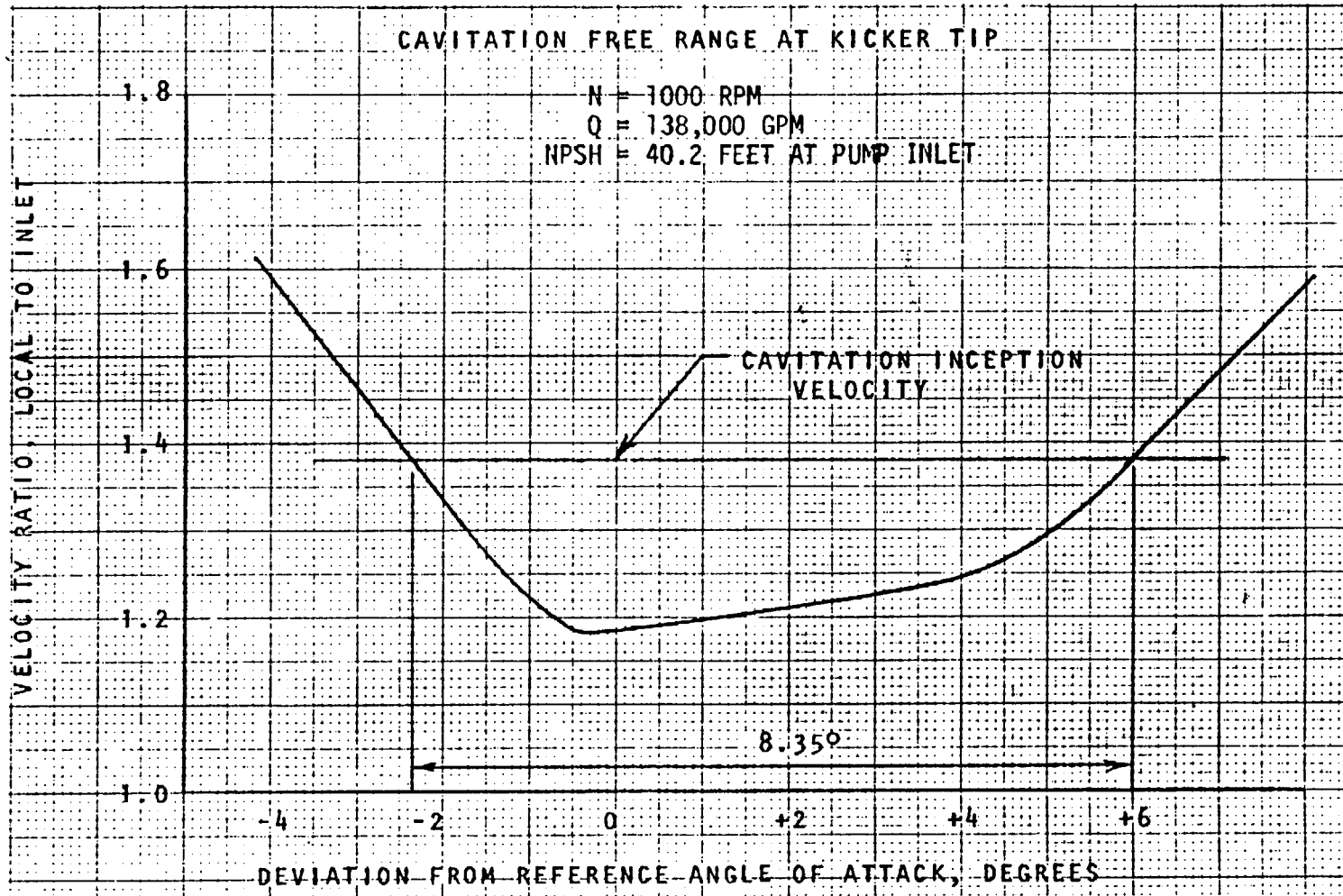


Figure 21. Kicker Cavitation Margin at Tip

Figure 22 shows the static pressure rise measured along the tip of the inducer front row. The analytical prediction for this parameter is also shown. Both test data and analysis show a monotonically increasing static pressure rise as desired, and the two show very good agreement. By varying the amount of blockage in the analysis, the results could be made to agree even better, but the results shown are believed to be adequate to substantiate the design as performing per the analysis.

Another circumstantial evidence of the successful performance of the front blade row is the favorable performance of the kicker blades. In particular, the kicker blades were observed through a plastic view tunnel during cavitation testing and indicated no significant blade cavitation on the kicker blades until the front blade row had experienced deep cavitation. The tip vortex cavities on the kickers also showed that the blades were loaded in the right direction without any major differences blade-to-blade. These observations show that the front blade row discharge flow angles are close enough to the design values to provide a good match with the kicker inlet blade angles.

Downstream of the kicker blades, head surveys were made to establish the radial gradient. Figure 23 shows typical data from a design-flow test. It shows a flow-weighted head rise of 597 feet which is within 19 feet of the design value. This was considered good agreement considering the accuracy of the data. The data are plotted using an expanded scale and show the head higher at the mid-radius than either boundary. The head drop towards the hub is considered moderate, but that at the tip is larger than desired. The tip data may not be as accurate using the yaw probe due to the stronger gradients experienced because of the tip backflow.

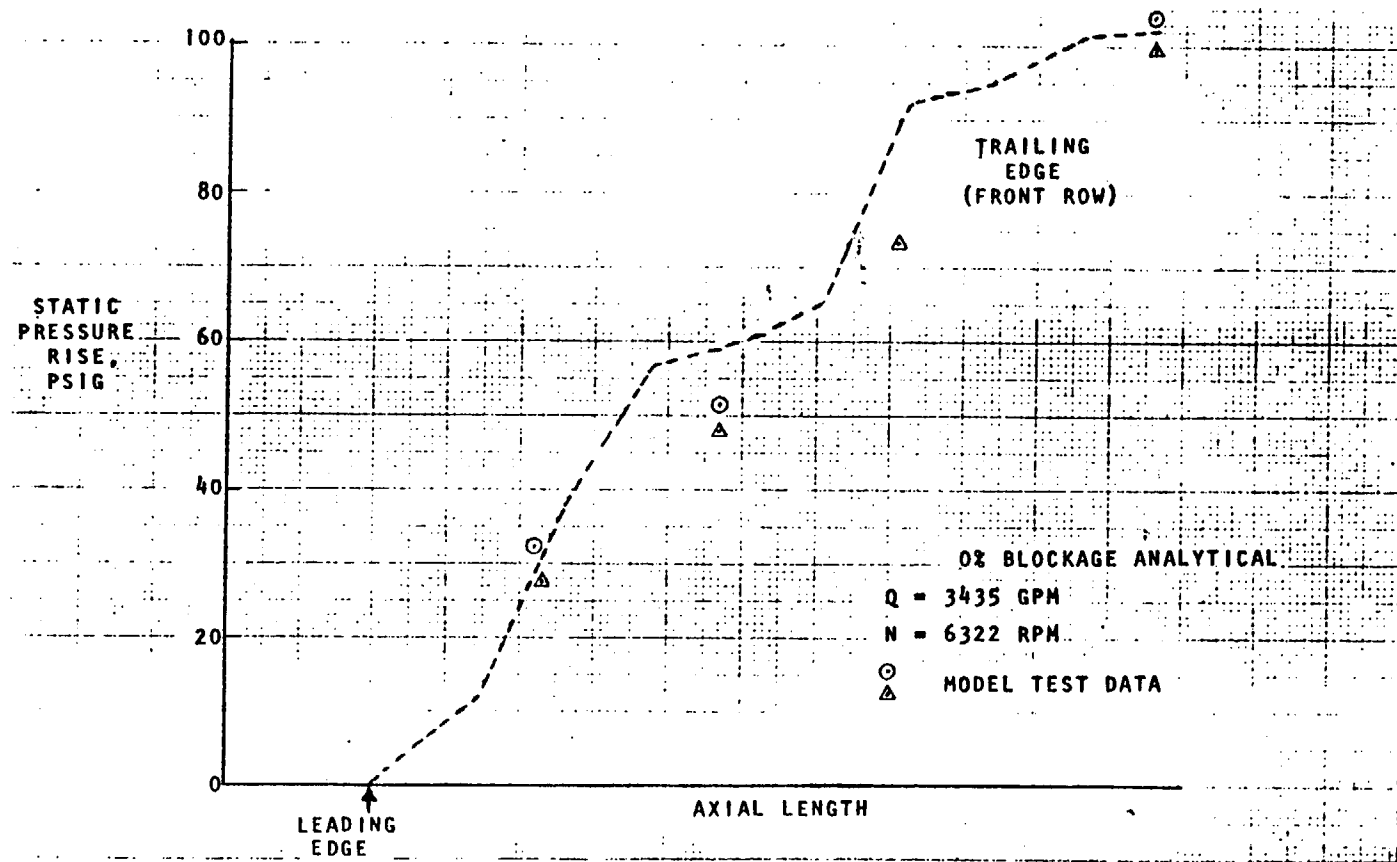


Figure 22. Inducer Front Row Static Pressure Rise Vs. Axial Length

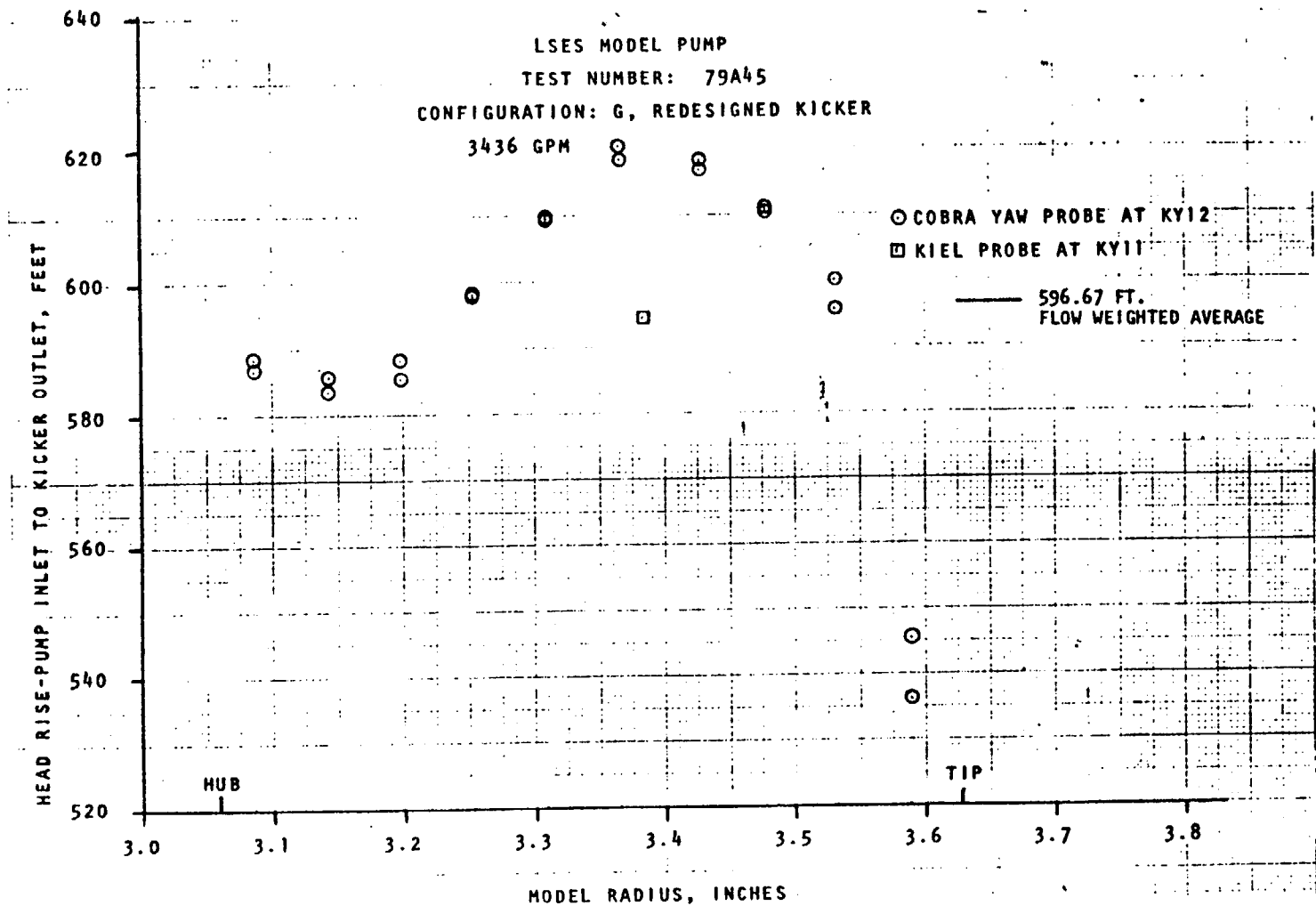


Figure 23. Inducer Head Rise Vs Radius

Figure 24 shows the measured fluid angles as a function of radius. The angles are reasonably close near the hub, but show more difference at larger radii than would be expected considering the relative agreement of the head rise. This variation is due to the redistribution of the streamlines as the flow experiences the three-dimensional effects of the inducer passage. The axial velocity at the tip is dropping off and more flow is pushed into the hub region. These flow angles are acceptable if the stator life is satisfactory, and life tests indicate this to be true.

#### PJ-46 Axial Rotor Design

Design Requirements. System studies have led to an optimum overall pump head requirement of 942 feet (from pump inlet to nozzle discharge) with a design flow of 138,000 gpm at 1000 rpm. Actual propulsor operation in the ship will be at a slightly higher speed and flow, but operating with scaled performance and at the same ratio of flow-to-speed as the design requirement. This system requirement led to a required head rise downstream of the axial rotor of 967 feet above pump inlet total head. This was based on estimated losses of 25 feet through the straightening vane. This loss has subsequently been increased, thereby resulting in slightly less overall pump head; the effects of this adjustment are discussed in a later section. However, the design of the axial rotor was based on a required discharge head of 967 feet with an integrated average rotor inlet head of 598 feet. Thus the required design head rise of the axial blade row was 369 feet.

Inlet conditions to the axial rotor are shown in Fig. 25 and 26. Figure 25 illustrates the rotor inlet absolute flow angles as a function of radius as determined by model test surveys behind the axial stator. Figure 26 shows two alternate rotor inlet total head gradients which were derived from test survey data. Two head gradients with identical flow-weighted average values were used for analysis purposes because it was felt that a large clearance between the stator and the hub might be causing modifications to the head gradient in the model which would be corrected in the full size pump. It was later found through analysis that rotor head rise performance was relatively

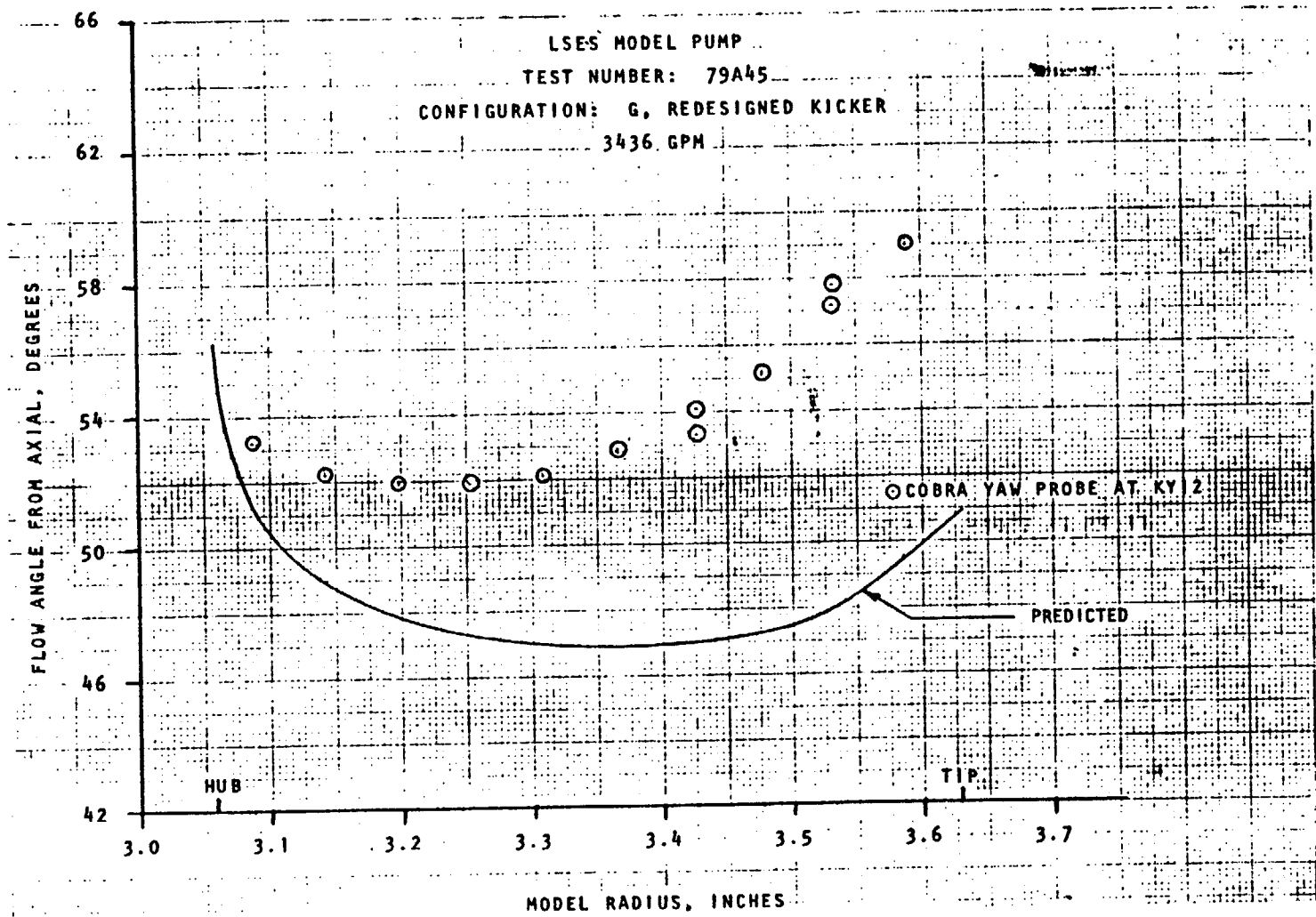


Figure 24. Inducer Discharge Flow Angle

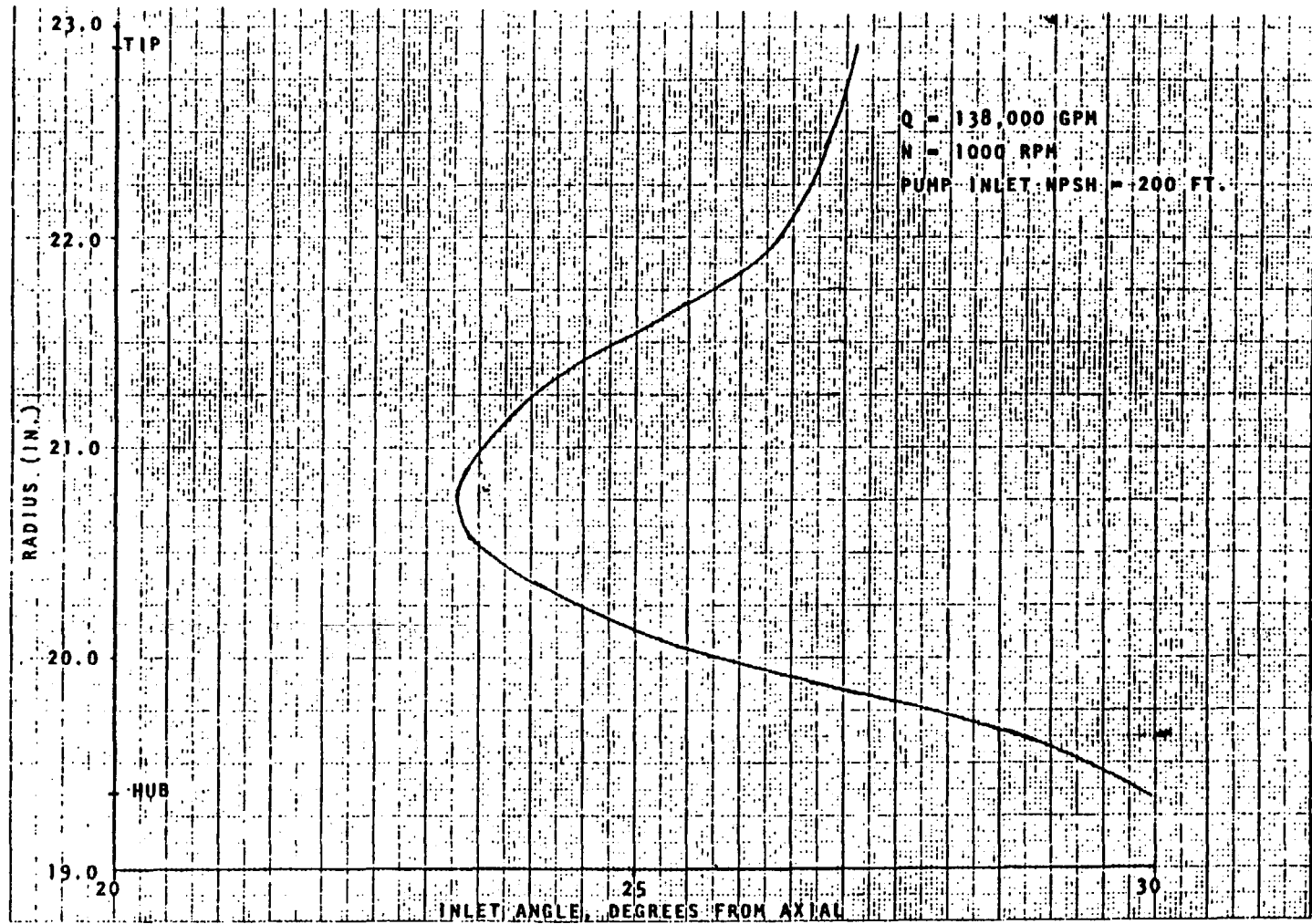


Figure 25. Axial Rotor Inlet Absolute Flow Angle

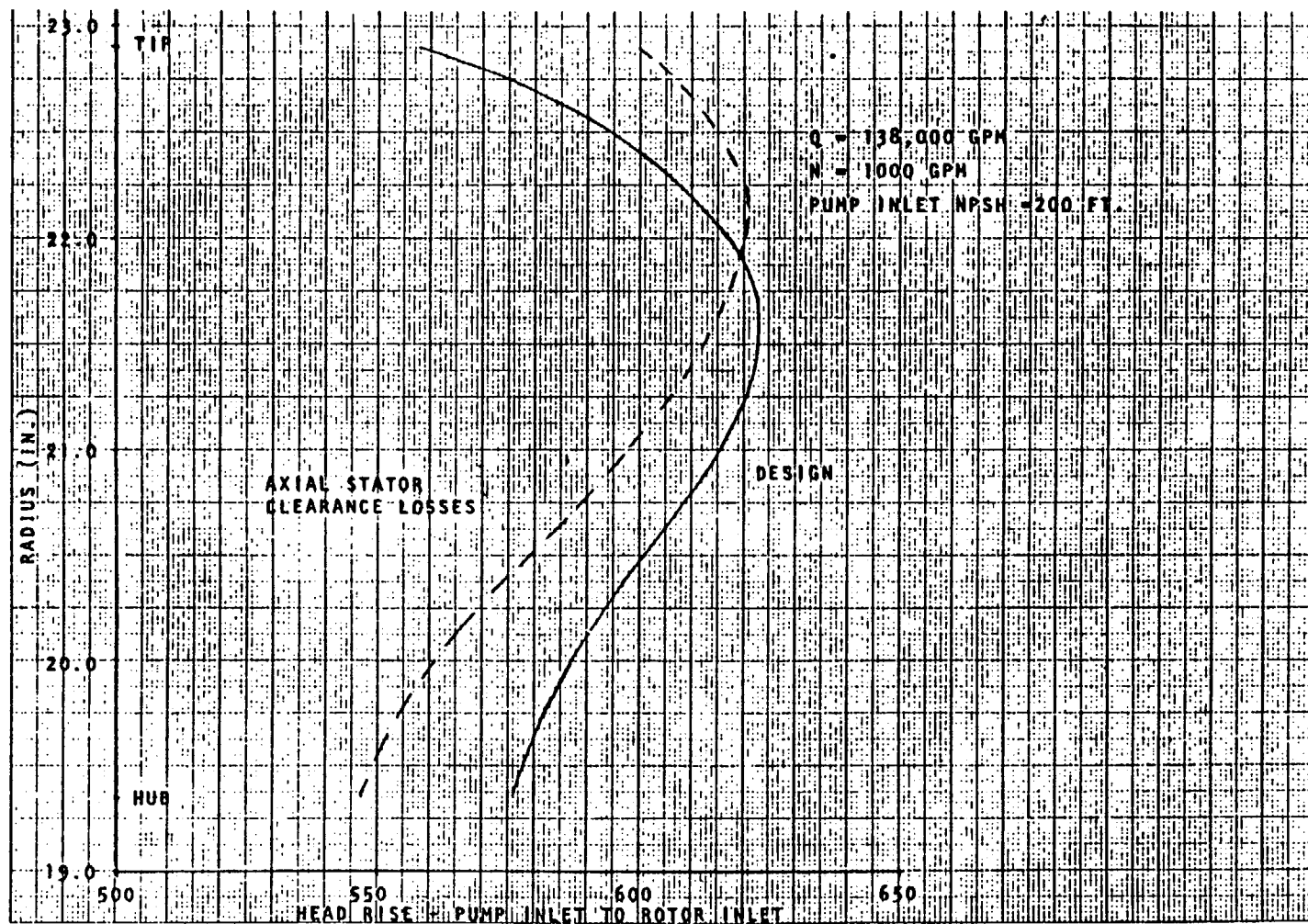


Figure 26. Axial Rotor Inlet Total Head

insensitive to inlet total head gradients. In the rotor analysis, other flow variables were changed to bracket the rotor performance and account for possible variations from the most probable performance.

The rotor should be configured so that the inlet conditions in Fig. 25 and 26 will not result in cavitation on the rotor blade. Furthermore, the rotor should be able to operate at the 95% flow, or hump condition (pump inlet total head - 40 feet) without cavitation damage. Finally, the rotor discharge flow should match well enough with the straightening vanes that cavitation does not occur on the vanes, and axial thrust is kept within bearing limits.

Blade Geometry. The rotor blades are defined at five radii to provide the best leading edge match with the inlet fluid flow. There are 17 blades consistent with the original design to maintain the same axial length with an appropriate solidity. The defining sections are either NACA-65 series blades or extrapolations of that series with similar appearance and performance. This blade shape has been shown to be effective in minimizing cavitation and in giving good efficiency. Basic design characteristics of the blades are defined in Table 5. The defining cylindrical blade sections are connected with straight line surface elements. Surface coordinates are given with respect to the stacking axis.

Performance Prediction. Determination of rotor blade relative discharge angles relied in part upon two-dimensional (2-D) cascade test data for NACA-65 series blades. However, analysis of model test data gathered from the previous rotor design indicated that three-dimensional effects were causing the relative flow turning done by the blade row to deviate from that predicted by 2-D cascade data alone. The amount of 3-D deviation  $\delta\theta_{3-D}$  from 2-D relative turning  $\Delta\theta_{2-D}$  was tabulated as a function of radius and used to determine the turning expected by the new design. To bracket rotor performance, three different rotor outlet relative angles were obtained as functions of radial distance, as can be seen in Fig. 27. The 2-D cascade case assumed that blade sections turned the flow as though they were two dimensional. The 3-D compensated case assumed that  $\Delta\theta_{2-D}$  for the new design blade sections was corrected by  $\delta\theta_{3-D}$  as defined above. The expected angle is labeled as the design case, and for this case the correction

TABLE 5. AXIAL ROTOR DESIGN CHARACTERISTICS

Design Flow, gpm	138,000	
Rotor Speed, rpm	1,000	
Head Rise, pump inlet to rotor inlet, ft.	598.4	
Head Rise, pump inlet to rotor discharge, ft.	967.3	
Rotor Head Rise, ft.	368.9	
Number of Blades	17	
Tip Diameter, in.	22.900	
Hub Diameter, in.	19.366	
Tip Radial Clearance, in.	0.080	
Hub Fillet, in.	0.375	
	<u>Radius, In.</u>	<u>Solidity</u>
		<u>Stagger Angle, Deg.</u>
	19.3660	1.51
	20.5125	1.42
	21.1250	1.38
	21.8125	1.33
	22.9000	1.26
		50.40
		49.65
		49.09
		47.70
		44.81

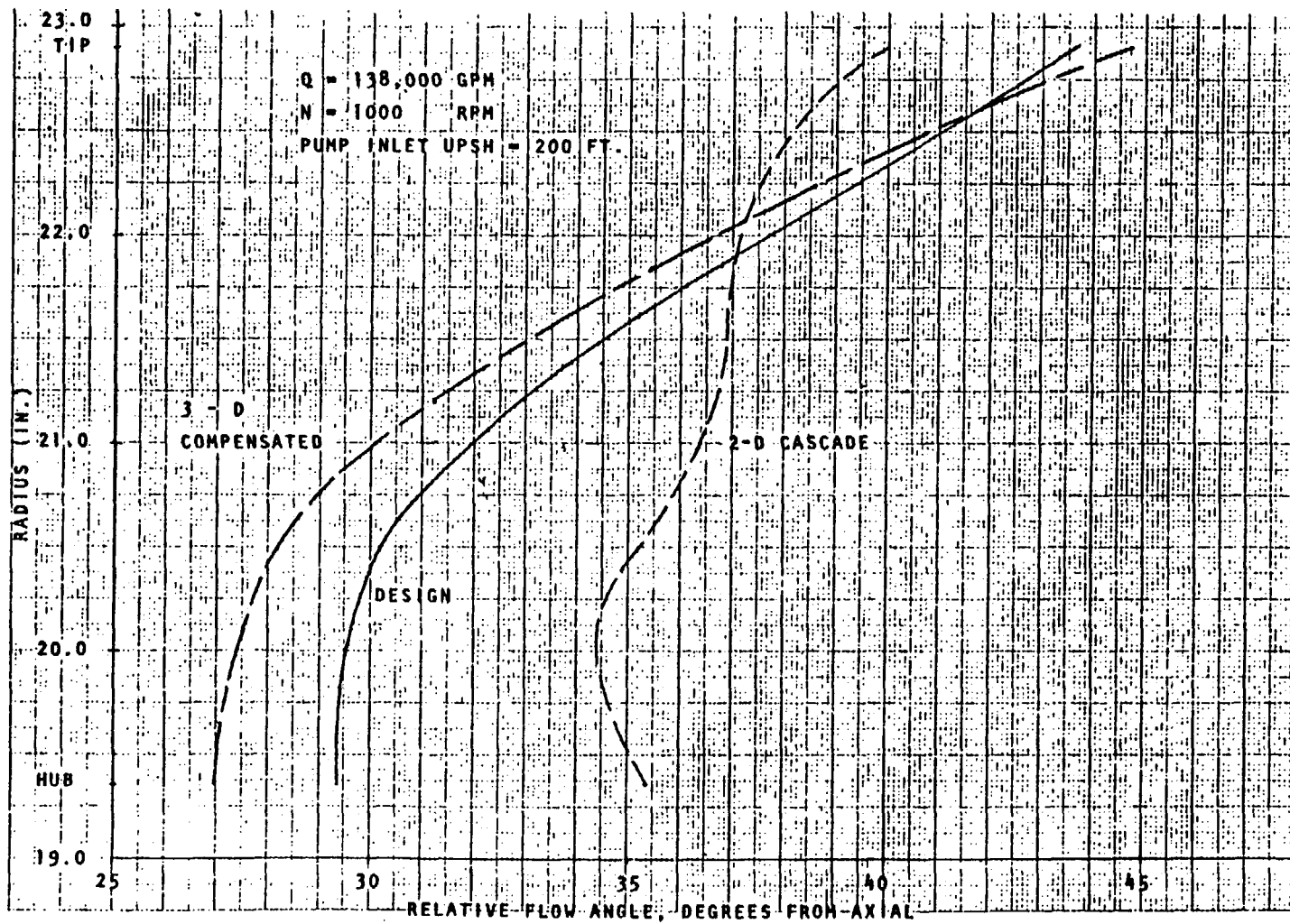


Figure 27. Rotor Discharge Relative Flow Angle

for three-dimensional effects from the 2-D cascade turning was assumed to be proportional to the total constant radius flow turning. The proportionality constant was derived from previous data. Velocity triangles for the most likely set of flow conditions are shown in Fig 28.

In Fig. 29, two efficiency gradients for the blade row are plotted: (1) a design case, assumed to be most likely, and (2) a case where large end wall losses are assumed. These efficiency gradients were derived from previous test data by matching the computer analysis with test data. The large end wall losses are the potential result of large tip clearances in the stator or rotor.

The rotor blade performance was analyzed using the Rocketdyne Three-Dimensional Analysis Program (R3DAP) with the data in Fig. 25, 26, 27, and 29 as program inputs. Five computer runs were made to bracket blade row performance, with run 1 combining the most likely set of inputs. A summary of the inputs for each of the runs is given in Table 6. Figure 30 shows rotor discharge flow angles as functions of radius for the five runs. Results are consistent; there is a scatter of no more than 3 degrees at constant radius between the different cases. In Fig. 31, the discharge velocities as functions of radius are plotted, and again, there is little variation between the different cases. Rotor head rise performance as a function of radius does vary somewhat between runs, as can be seen in Fig. 32, and the flow-weighted head rise performance is tabulated in Table 7. Rotor discharge total head rise above pump inlet total head is seen to range between 940.5 and 986.5 feet, with 967.3 feet considered as the most likely case.

To evaluate the cavitation performance of the rotor blade, blade sections at tip, mean, and hub were run in the Douglas-Neumann program for varying angles of attack. The maximum relative velocity encountered on the blade surface is divided by inlet velocity to form the ratio plotted against inlet relative flow angle to form the cavitation "buckets" shown in Fig. 33 through 35. Cavitation limits were then determined for the cruise and hump conditions for the two rotor inlet cases shown in Fig. 25 and 26 (cases A and B). Cavitation limits at tip, mean, and hub for cruise and hump at the two different possible inlet conditions A and B are all seen to fall within the cavitation free range shown in Fig. 33 through 35. Therefore, cavitation problems are not expected on the rotor blade.

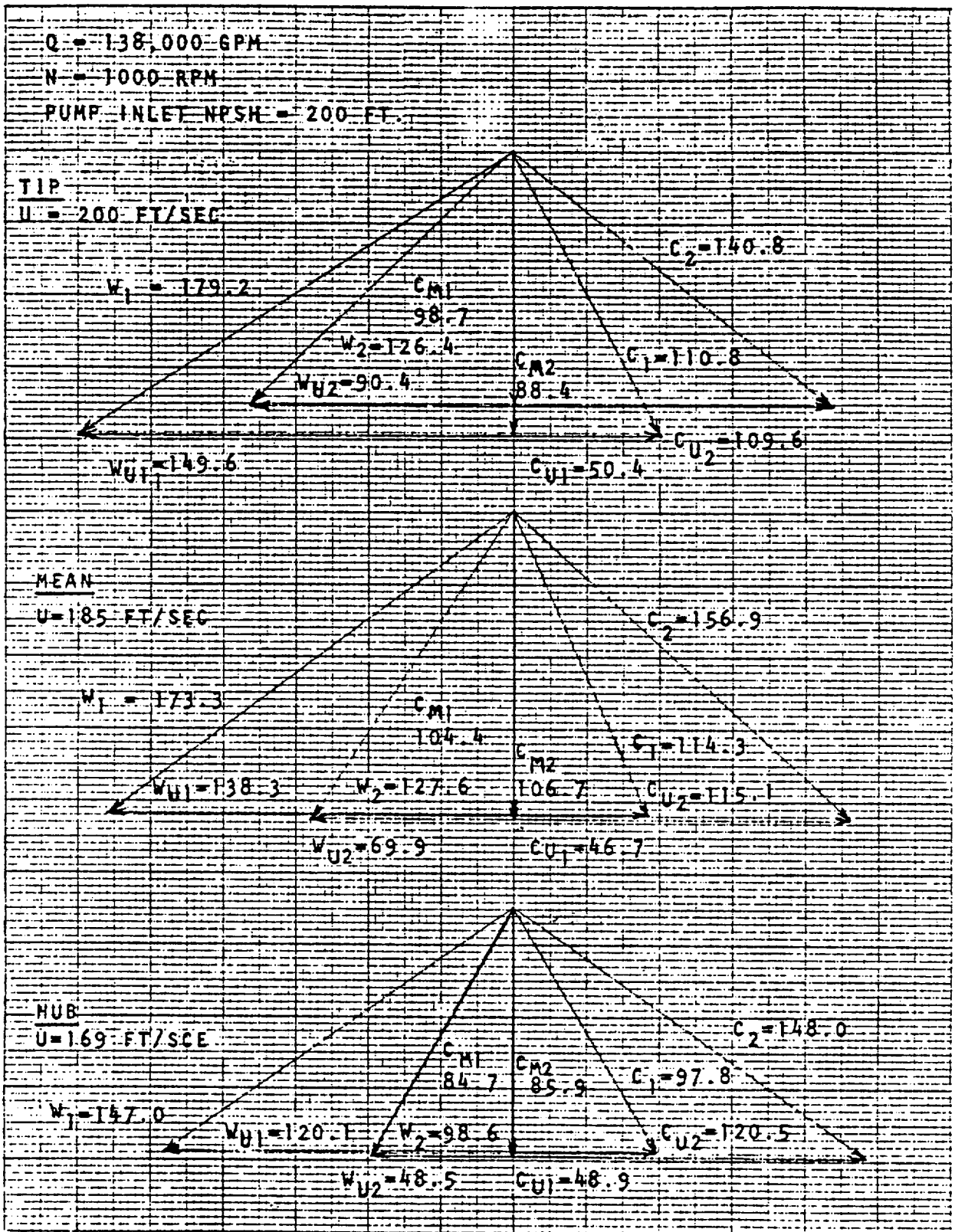


Figure 28. Rotor Vector Diagrams

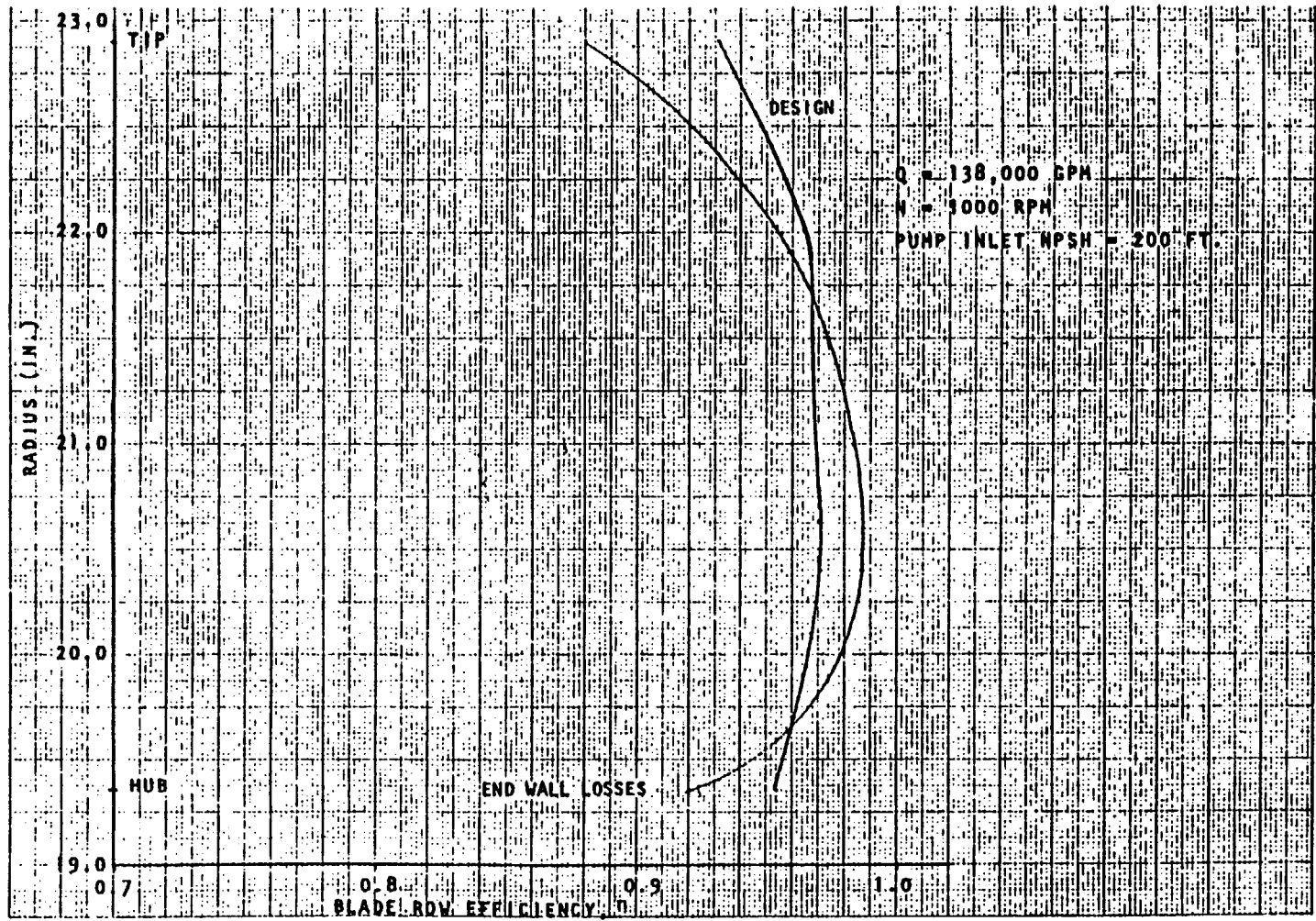


Figure 29. Axial Rotor Efficiency

TABLE 6. ROCKETDYNE THREE-DIMENSIONAL ANALYSIS PROGRAM INPUTS  
FOR AXIAL ROTOR

Run No.	Efficiency	Inlet Head	Rotor Discharge Relative Flow Angle
1	Design	Design	Design
2	Design	Axial Stator Clearance Loss	Design
3	End Wall Losses	Design	Design
4	Design	Design	2-D Cascade
5	Design	Design	3-D Compensated

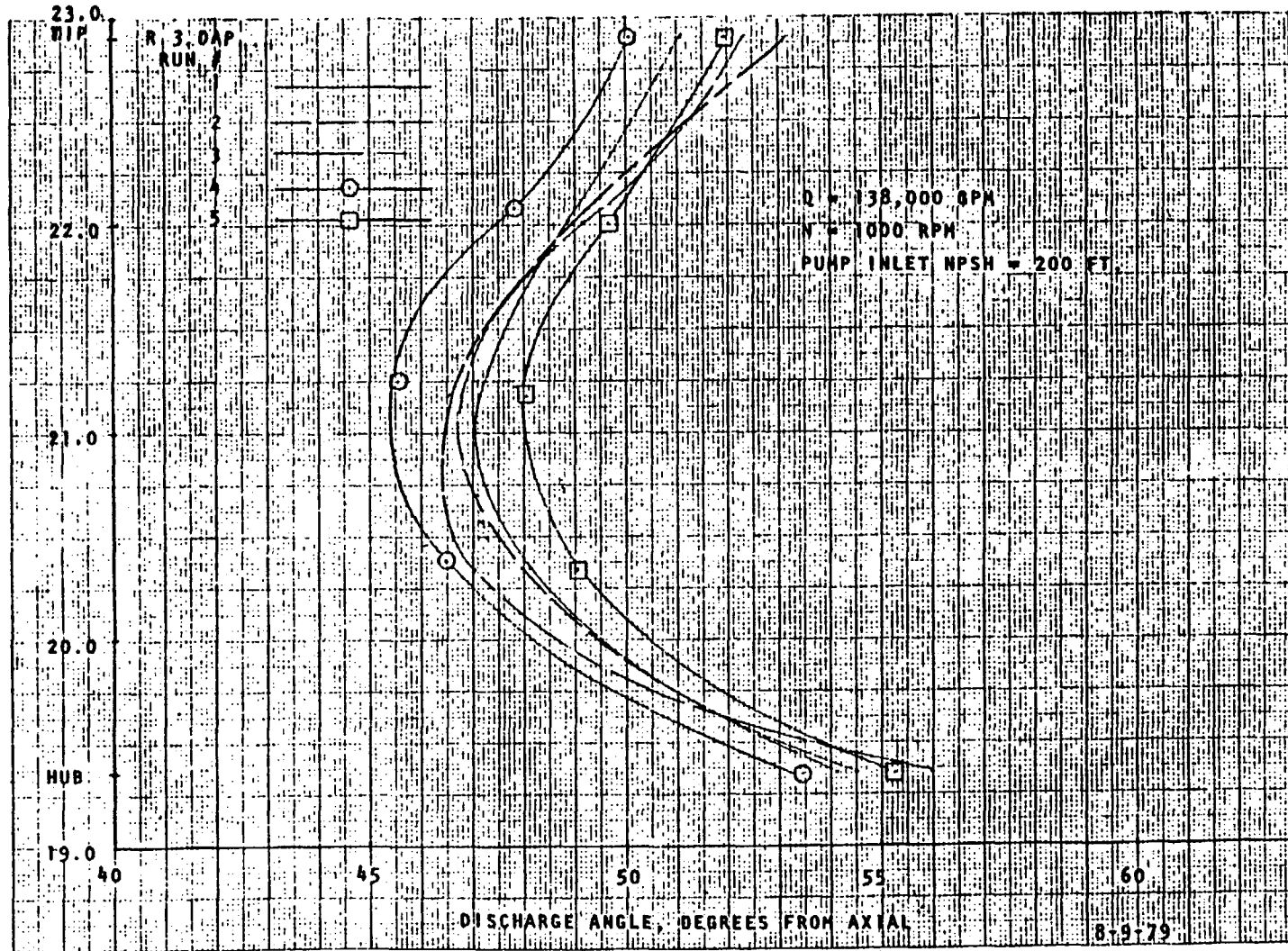


Figure 30. Rotor Discharge Flow Angles

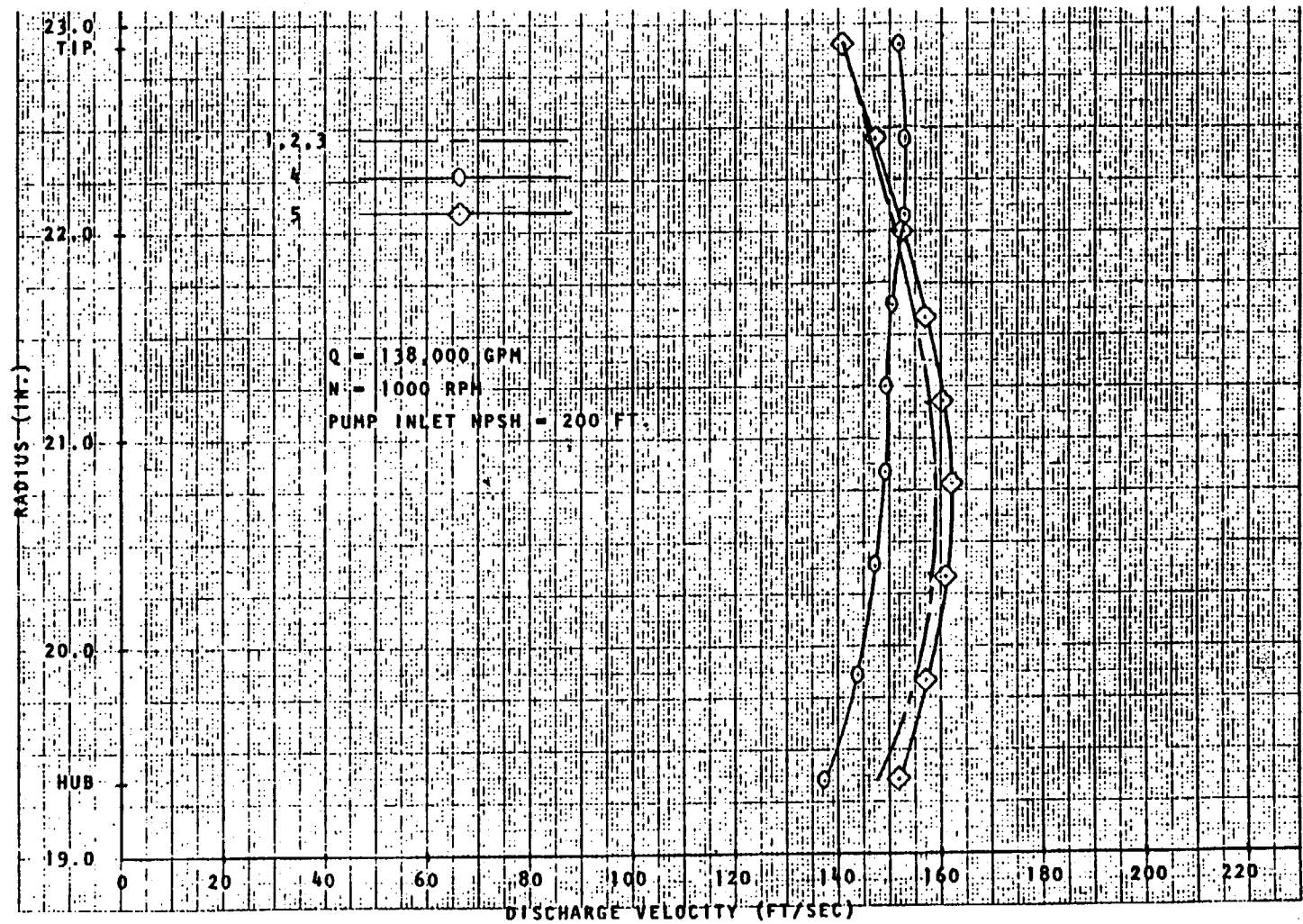


Figure 31. Rotor Discharge Flow Velocities

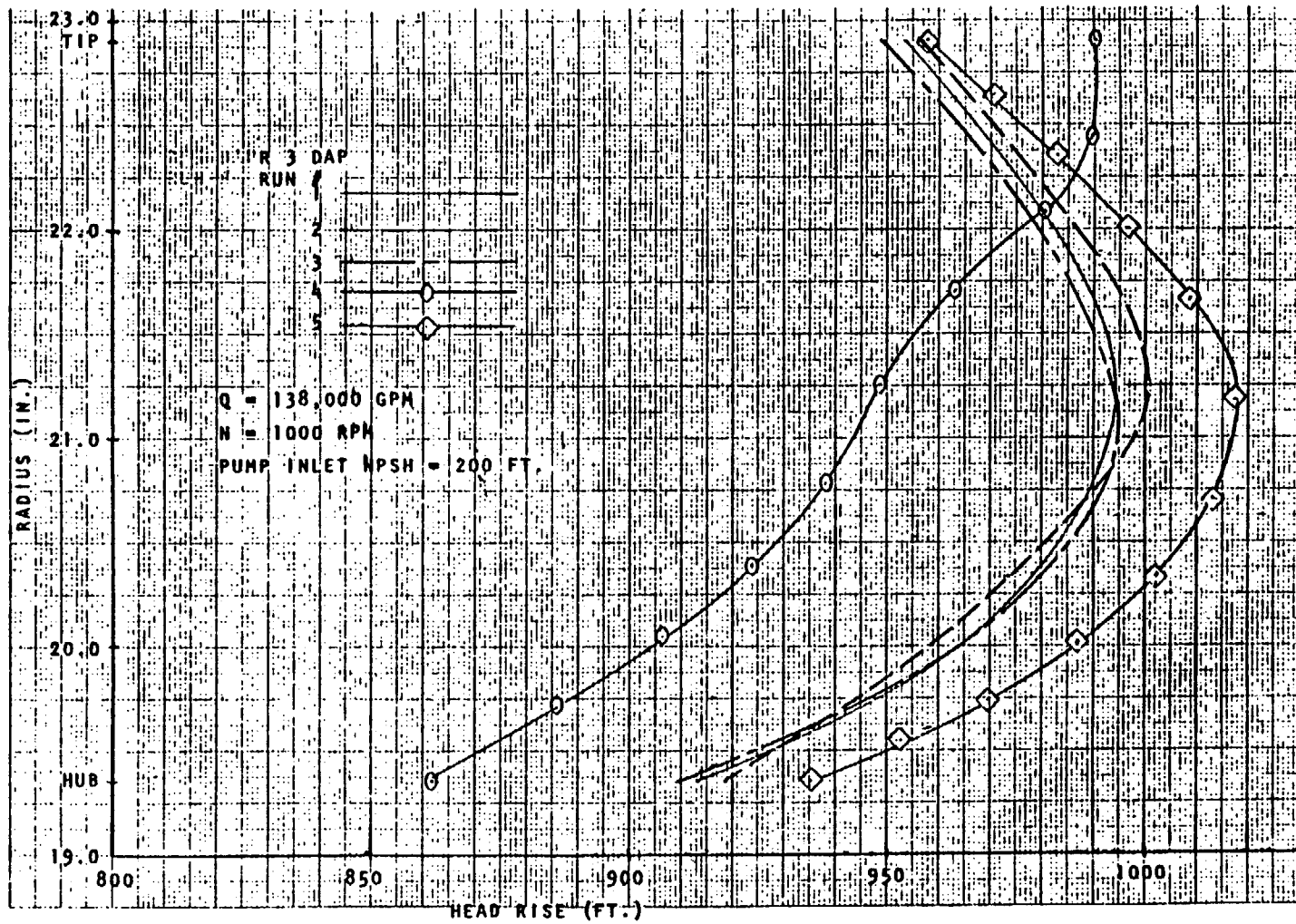


Figure 32. Total Head Rise, Pump Inlet to Rotor Discharge

TABLE 7. PREDICTED AXIAL ROTOR DISCHARGE HEAD

R3DAP Run #	Head Rise, Pump Inlet to Rotor Discharge, Ft.
1*	967.3
2	970.3
3	966.6
4	940.5
5	986.5

\*Design and most likely case

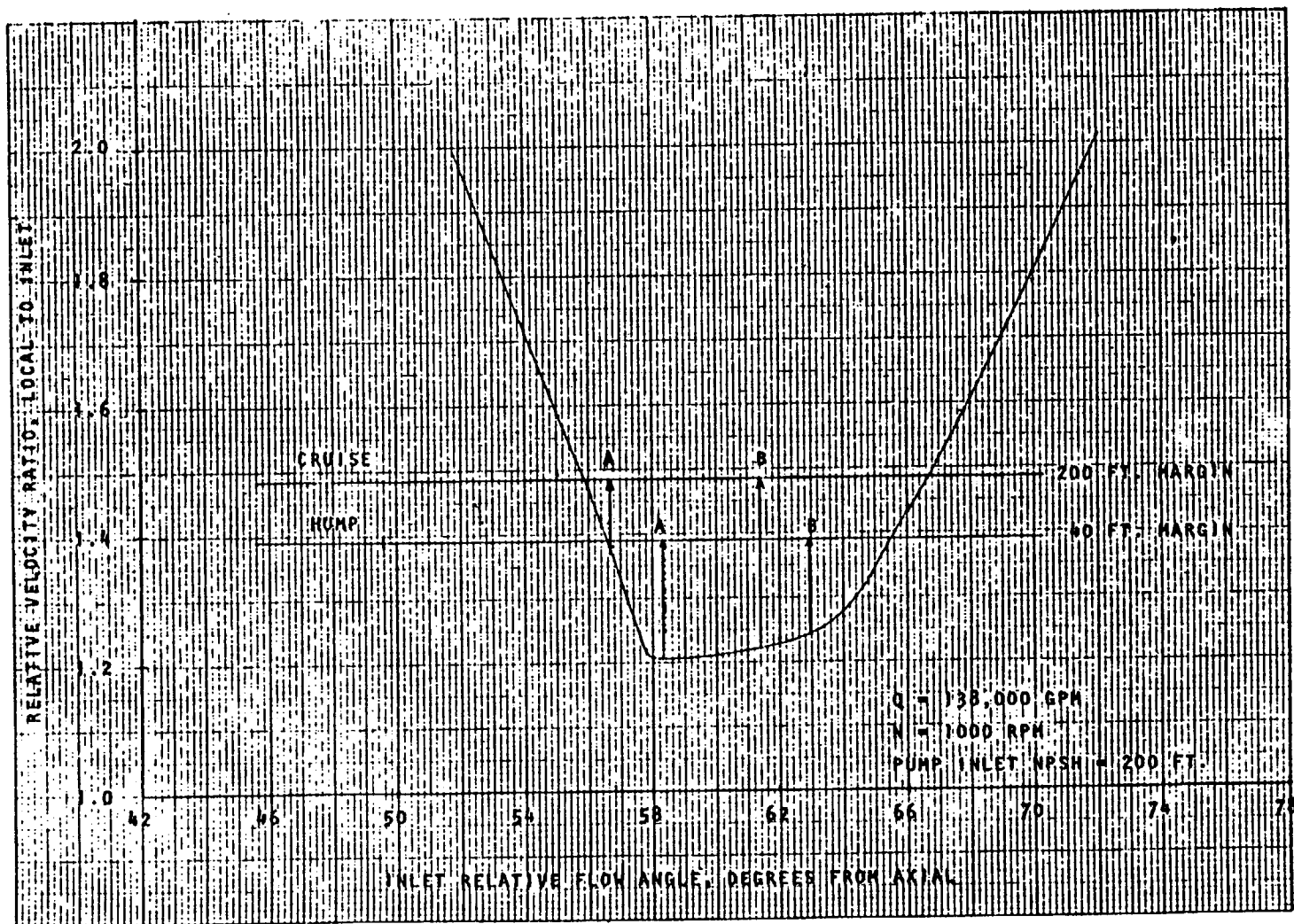


Figure 33. Axial Rotor Tip Cavitation Performance

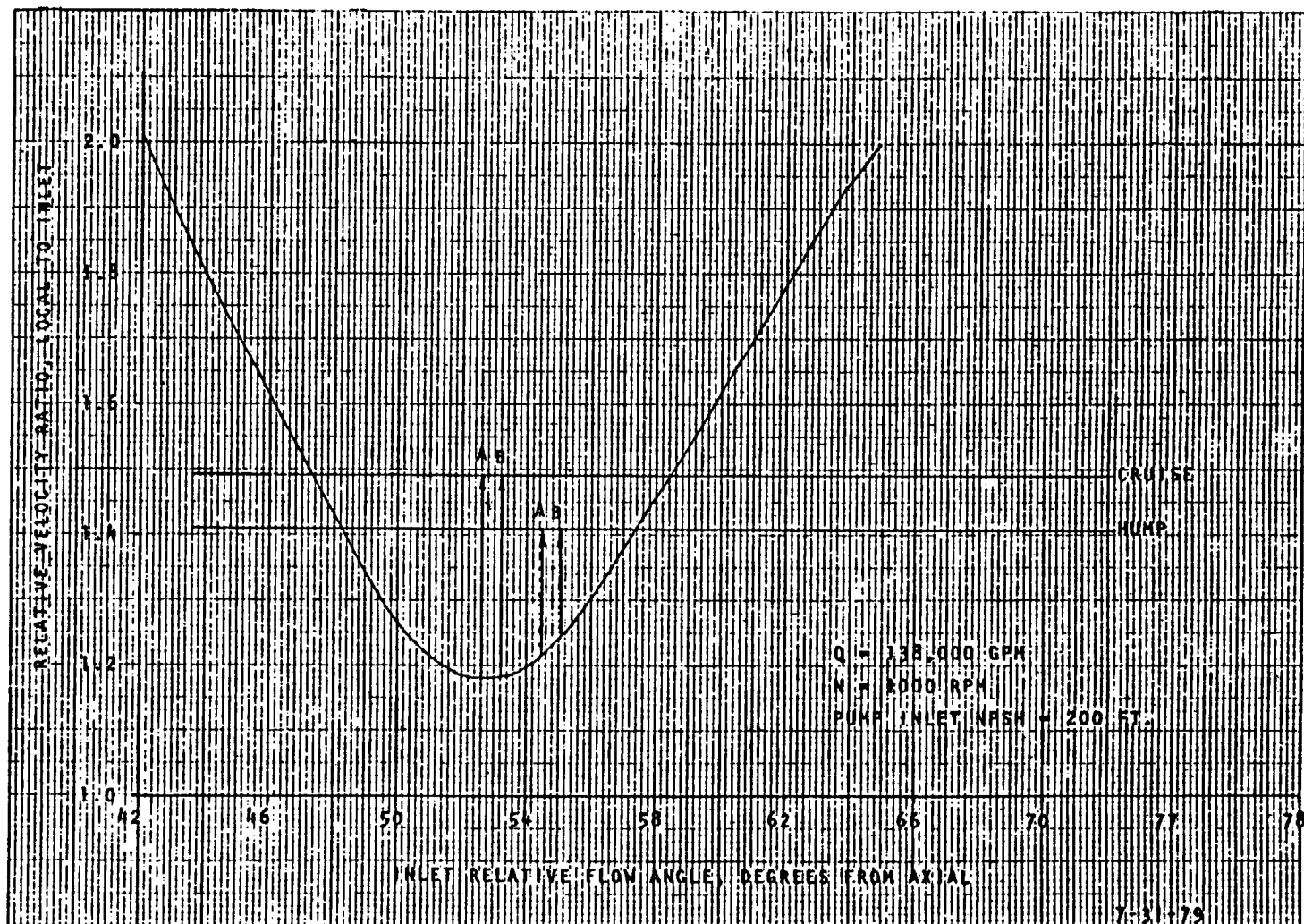


Figure 34. Axial Rotor Mean Radius Cavitation Performance

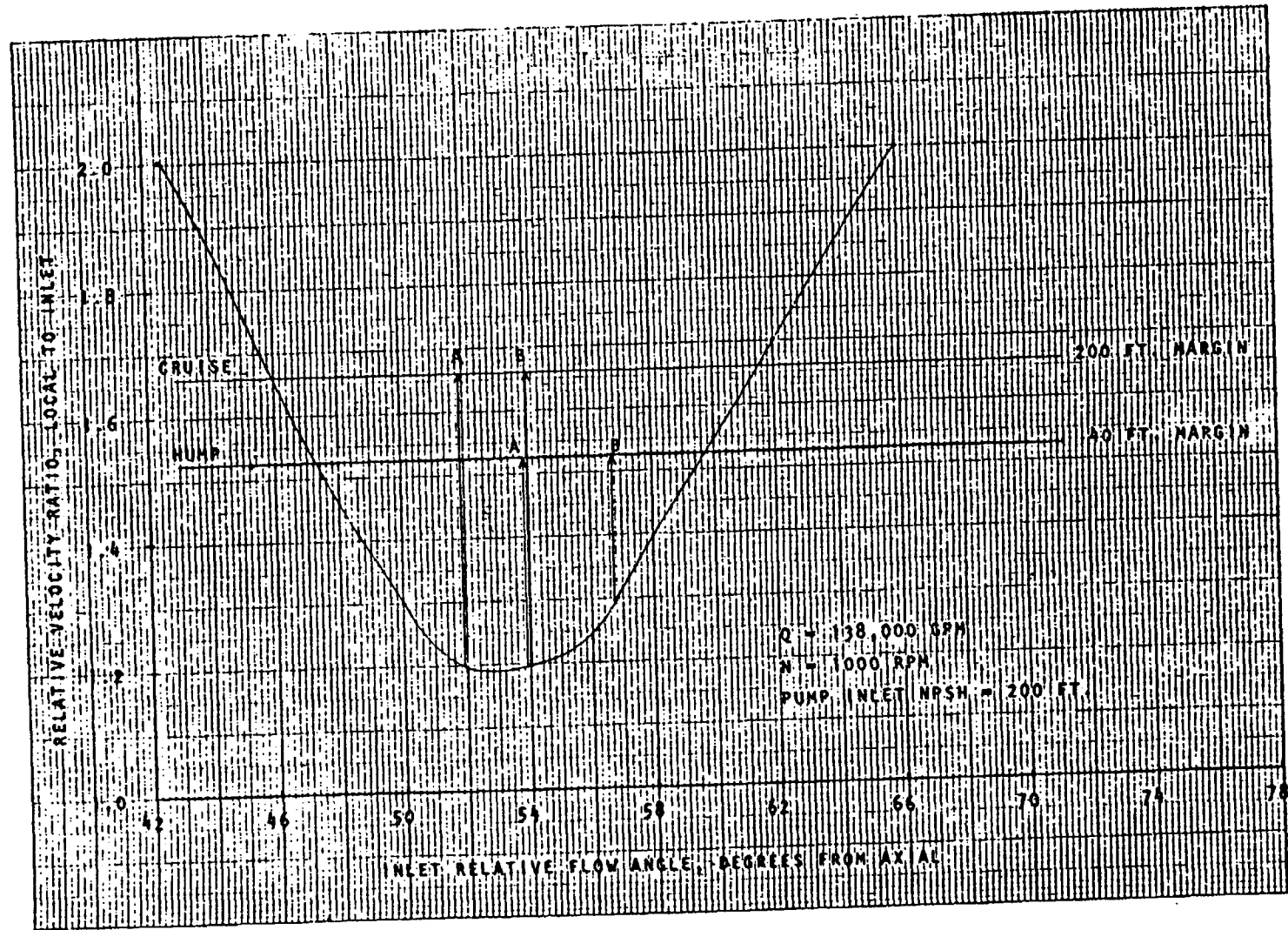


Figure 35. Rotor Hub Cavitation Performance

Blade loading ( $\Delta P$ ) profiles as functions of blade length are plotted in Fig. 36. Profile shapes were obtained from the Douglas-Neumann 2-D potential flow computer program, but overall loading magnitude was scaled from the R3DAP analysis program.

Model Test Data. Tests were run on a PJ-46 scale model (rotor tip diameter of 7.232 inches) and surveys were taken behind the axial rotor. Total head measurements were taken with kiel and yaw probes while flow angles were provided by the yaw surveys. Figure 37 shows all survey head rise data along with the run 1 R3DAP prediction corrected to model size. A 10.3 feet lower head is predicted for the model pump than for the full-size pump due to Reynold's number scaling effects. The shape of the predicted curve agrees well with the test data. Comparisons of total head magnitude are provided in Table 8. Extrapolated curve fits of the kiel and yaw data gave pump inlet to rotor discharge total head rises of 957.7 and 949.5 feet, respectively, indicating in each case that the difference from the predicted head was less than 10 feet.

Figure 38 gives the test yaw measurements of the flow angle as measured. To satisfy continuity and radial equilibrium, the data points were shifted by a constant added angle of 8.28 degrees. This angle error is believed to be due to the effects of a relatively large probe for the passage height. The corrected angles show good agreement with the predicted angle gradient except at the tip. Some discrepancy between test data and prediction for the blade tip was noted also for the head gradients in Fig. 37. This may be due to viscous tip clearance effects not modelled exactly in the 3-D dynamic computer program. Figure 39 shows a comparison between predicted rotor discharge fluid velocities and discharge velocities calculated from test survey data after radial equilibrium and continuity have been satisfied.

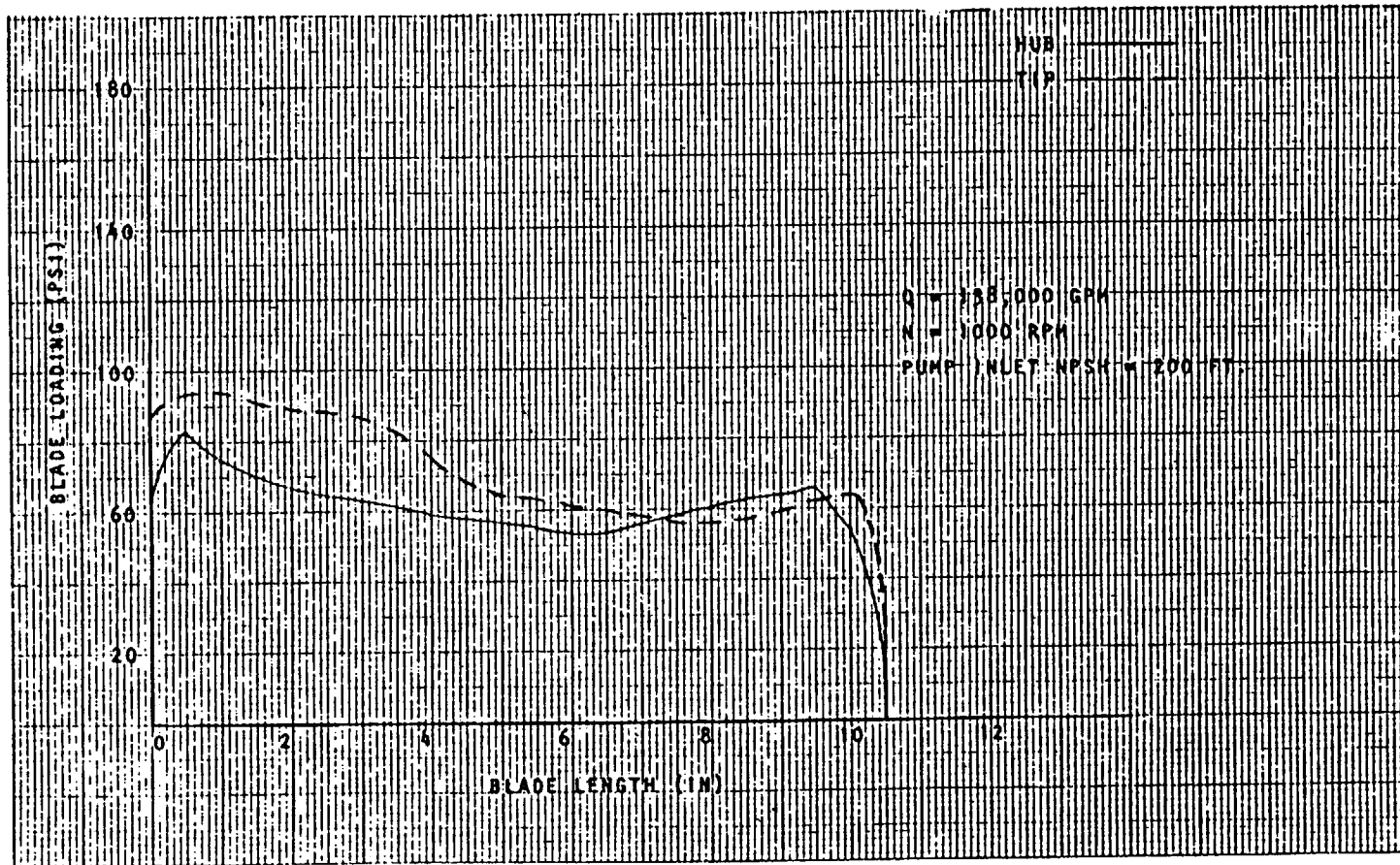


Figure 36. Axial Rotor Redesign Blade Loading Profiles  
From Douglas Neuman, Scaled From R3DAP

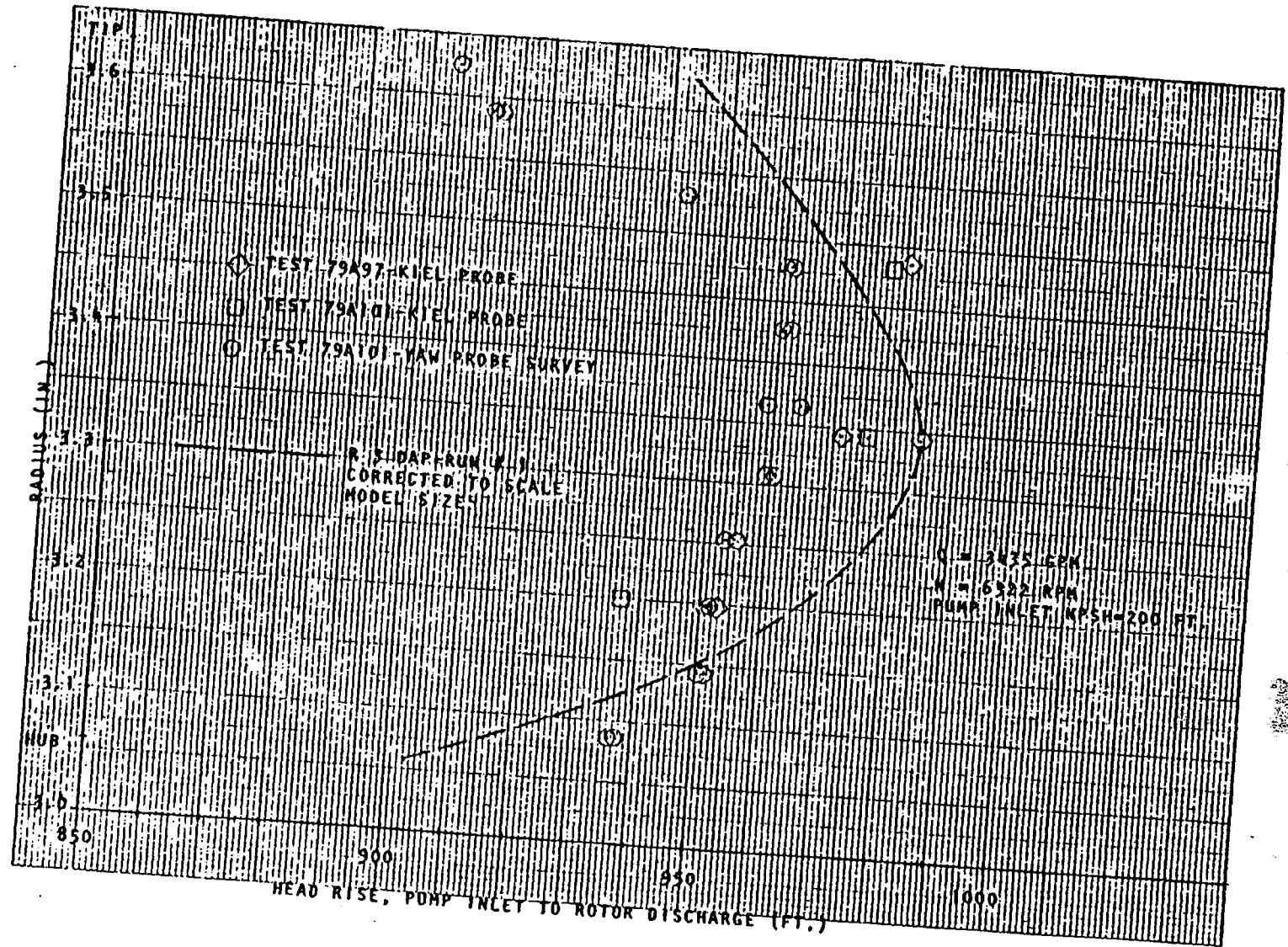


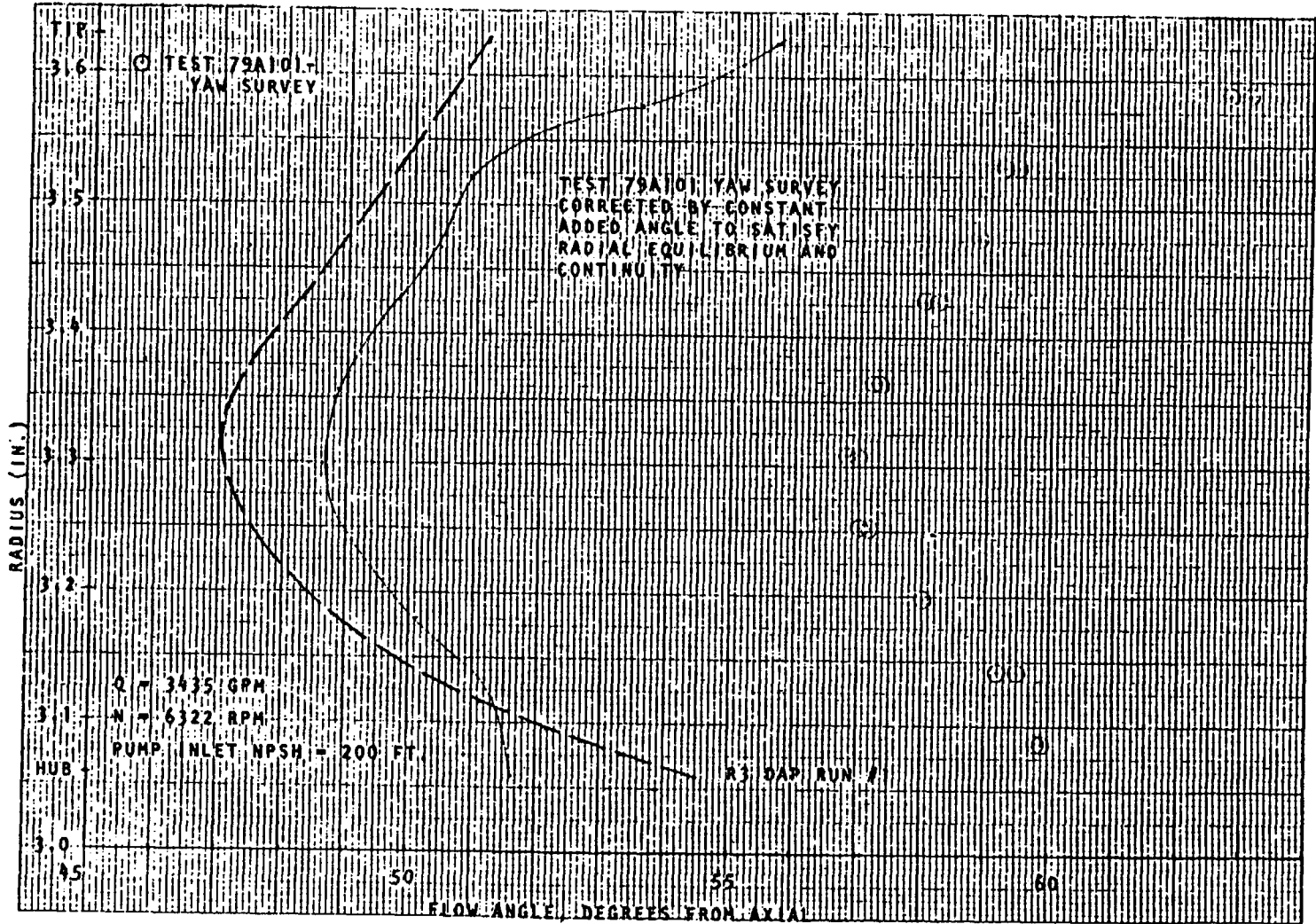
Figure 37. Axial Rotor Discharge Total Head

TABLE 8. COMPARISON OF PREDICTED AND MODEL TEST ROTOR  
HEAD RISE PERFORMANCE

R3DAP Run #	Full Size Discharge Head (ft)	10.3' Correction to Model Size (ft)
1*	967.3	957.0
2	970.3	960.0
3	966.6	956.3
4	940.5	930.2
5	986.5	976.2

Model Test: Extrapolated Curve Fit

	Rotor Discharge Head	R3DAP Run #1 Percent Error
Kiel Probe	957.7 ft.	0.07%
Yaw Probe	949.5 ft.	-0.79%



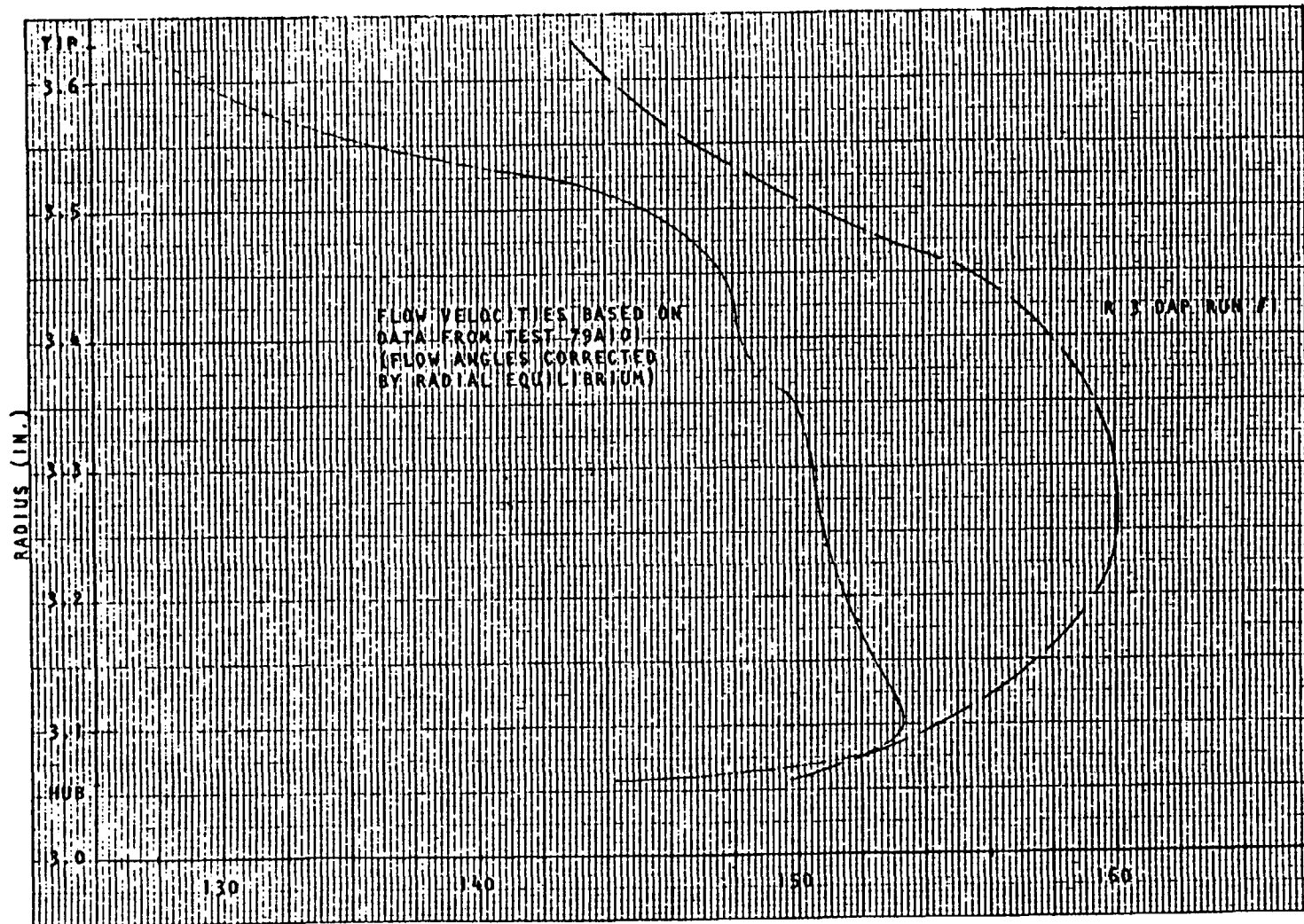


Figure 39. Axial Rotor Discharge Flow Velocities

Although cavitation on the blade was not predicted, slight damage on some of the model blades was noted after 17 hours at hump conditions on the suction side just above the fillet at the hub. The damage was not serious and would not impact the required life for the full-size propulsor. It may be caused by nonuniform leading edge hand benching or an improper leading edge fillet, either of which can be better controlled on the full-size part.

The rotor blade test data to date have shown good agreement with prediction. This supports the procedure of using more than two radial positions to define blades to obtain a good match with the inlet flow whenever significant gradients exist in the inlet flow.

#### PJ-46 Straightening Vane Design

Design Requirements. The inlet flow conditions used in analysis of the straightening vanes are shown in Fig. 30 through 32 of the rotor design section. Although the rotor discharge flow labelled "RUN 1" was considered most plausible, analysis was carried out for all five cases. (The straightening vanes had been designed for different inlet conditions, but the analysis was performed based on the new rotor discharge conditions as discussed above.)

The straightening vanes were designed to meet several requirements, as follows:

1. Produce axial discharge flow to recover the whirl energy from the rotor
2. Minimize the leaving axial thrust load by lowering the static pressure of the flow passing down the back face of the rotor drum to the rubber bearing
3. Minimize stator-nozzle losses, including no separations of the boundary layers along the blades
4. Maintain adequate margin for cavitation-free performance at both hump and cruise conditions
5. Provide sufficient blade thickness for structural integrity

Vane Geometry. The straightening vanes consist of 18 Rocketdyne-designed vanes specifically tailored to the design requirements described in the Introduction. Basic design characteristics are shown in Table 9. The vanes are defined along two cylindrical/hemispherical surfaces, as shown in Fig. 40. Straight line elements between the defining sections are extended to the hub and tip casings. A typical blade profile is shown in Fig. 41.

TABLE 9. STRAIGHTENING VANE CHARACTERISTICS

Design Parameter	Hub	Tip
Chord,*In.	14.67	16.86
Number of Vanes	18	18
Radius,*In. - LE	19.366	22.98
- TE	16.2081	18.8239
- Average	17.2081	20.902
Solidity - LE Spacing	2.17	2.10
- TE Spacing	2.59	2.57
- Average Spacing	2.38	2.34
Blade Angle,** Deg. - LE	51	55.5
- TE	-6	-8

\* Full Scale PJ-46

\*\* From Axial

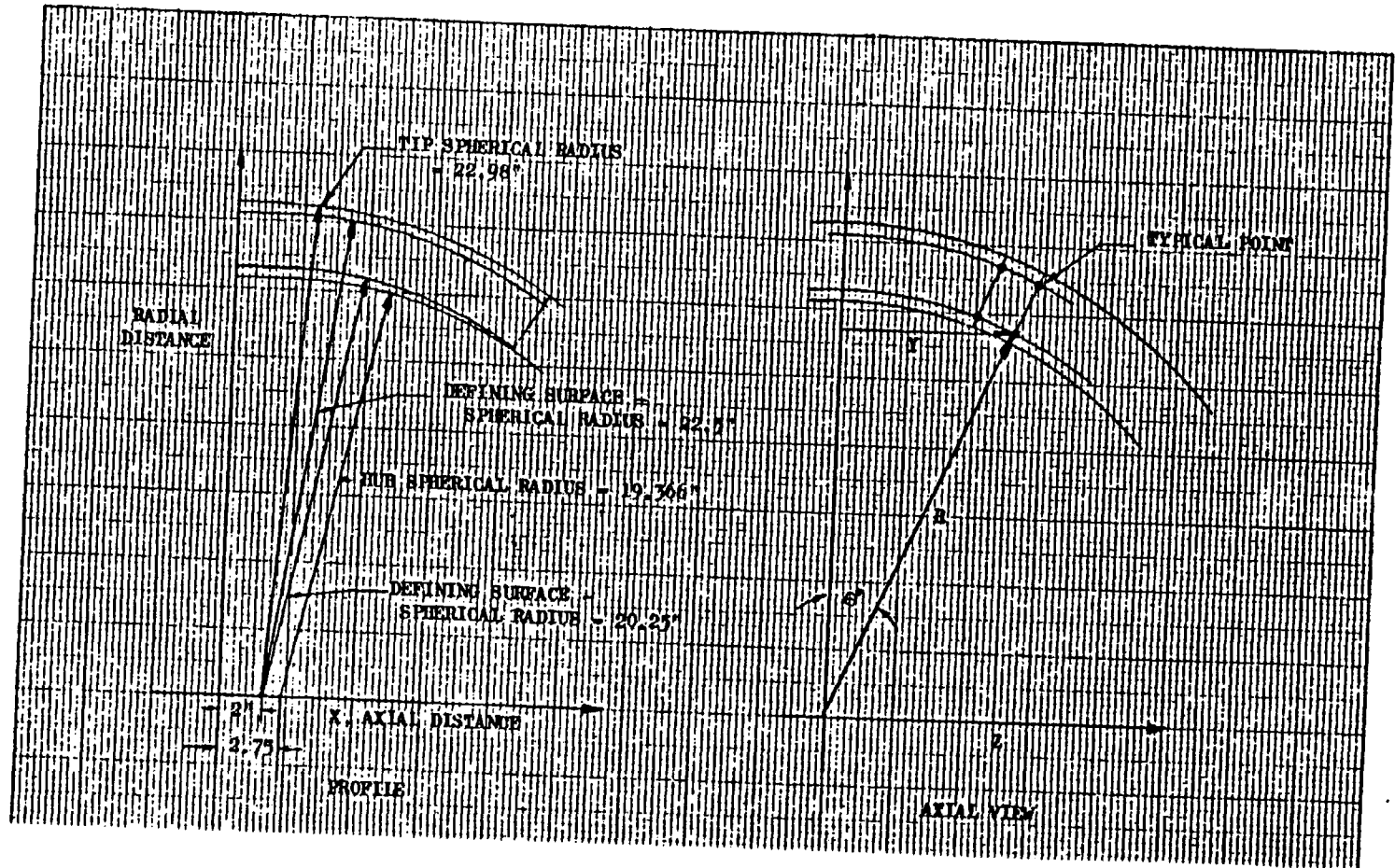


Figure 40. Straightening Vanes Defining Surface Definition.

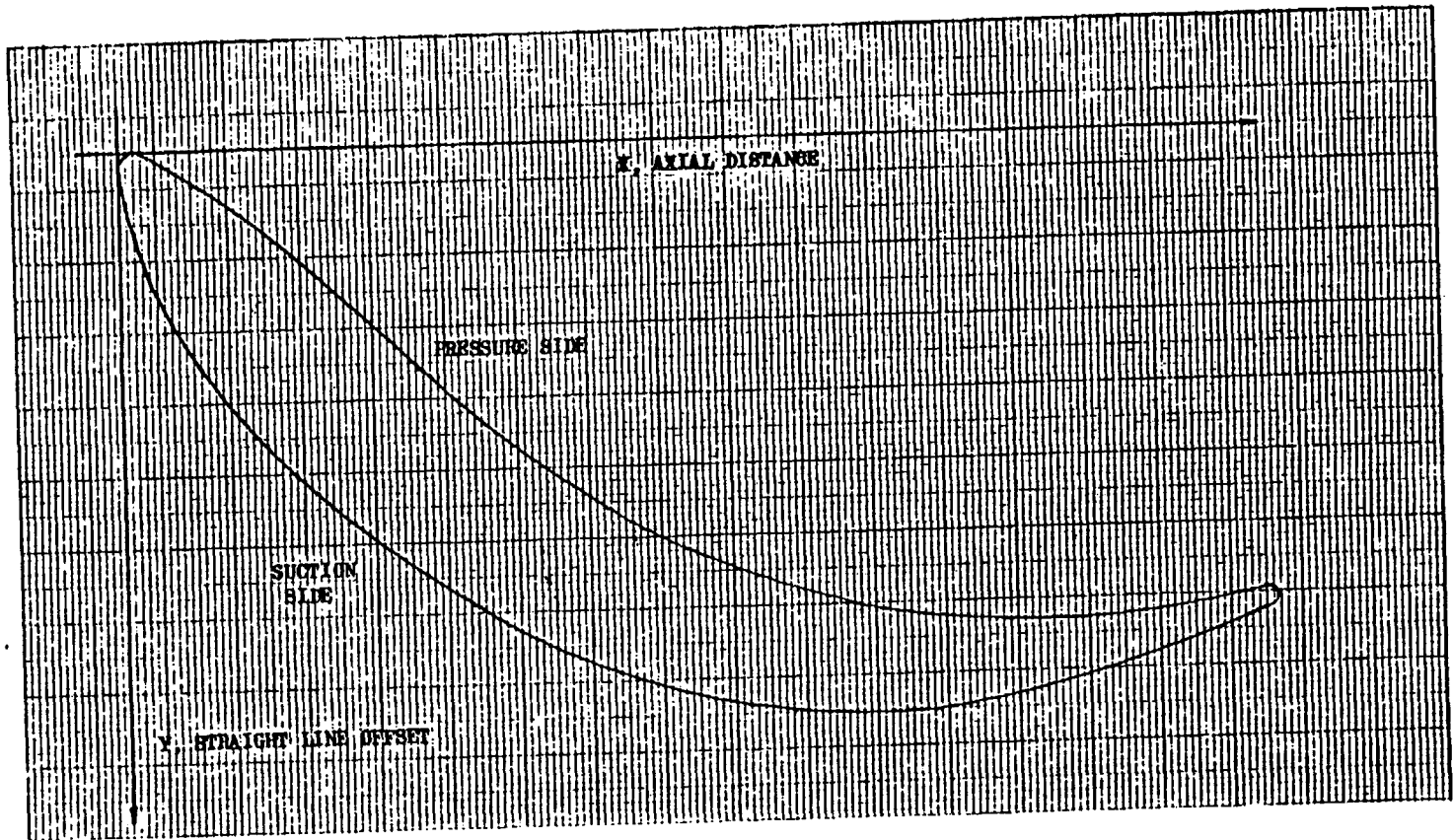


Figure 41. Straightening Vanes Typical Vane Contour

TABLE 10. AXIAL THRUST PREDICTIONS

Rotor Discharge Flow	Changes from Run 1		Net Axial Thrust*
	Rotor Blades	Rotor Drum	
1	-	-	261,143
2	+651	+2,659	264,453
3	-137	+16,179	277,183
4	-5,731	-11,445	243,969
5	+4,105	+8,706	273,954

\*Based on axial thrust calculations of 249,500 pounds before straightening vane/axial rotor redesign.

Component Performance. Component performance was analyzed for all 5 rotor discharge conditions, as well as for both model and full size configurations. Unless specified, the results below refer to RUN 1 inlet conditions in the full size waterjet:

1. Axial Discharge Flow

Carter's Rule was used to calculate the deviation angle for the vanes. Carter's rule is a theoretical and empirical formula relating the amount of turning in the vane row to the solidity and inlet fluid conditions. Since the solidity varied depending upon the vane spacing used whether leading or trailing edge as shown in Table 9, a range of expected deviations was calculated.

These deviation angles result in predictions of the flow being from 1 to 1.75 degrees underturned at the hub, and from 2.5 to 4.3 degrees underturned at the tip, with a linear variation between. This would result in a thrust loss of less than 0.1%.

2. Axial Thrust

The straightening vanes were analyzed using the Rocketdyne Three-Dimensional Analysis Program (R3DAP) to calculate the static pressure over the gap leading to the passage between the rotor drum and the discharge housing. The vane number and leading edge thickness distribution were both designed to drop the static pressure over the rotor drum discharge gap to provide axial thrust control. This unique hydrodynamic feature eliminates the need for a mechanical seal to control thrust and which could suffer damage during seawater operation and result in a bearing failure. However, as pointed out below, this feature does make the hydrodynamic design more difficult from the standpoint of eliminating separation and minimizing losses in the stator. It was assumed that changes in the static pressure over the gap would result in uniformly raising the pressure on the rotor drum. The axial thrust changes between the various inlet conditions are summarized in Table 10. The thrust changes on the axial rotor are also shown for the various inlet conditions. Each of these calculated values are within the capability of the bearings while maintaining a long bearing life.

### 3. Straightening Vane Losses and Separations

Static pressures and flow velocities along the vane surfaces were calculated using R3DAP. Pressure distributions for each vane surface at hub, mean, and tip streamlines were supplied to the Rocketdyne Boundary Layer Program. The boundary layer program calculates the growth of the boundary layer along the vane surface, and predicts separations of the flow from the vane.

Figure 42 shows the boundary layer shape Factor H (the ratio of the displacement thickness to the momentum thickness) along the pressure side of a blade near the hub. This was the most critical surface on the straightening vanes, based on analysis. Separation of the turbulent boundary layer is predicted to occur for shape factors between 1.8 and 2.4, with 2.4 an upper limit for attached flow.

The difference in boundary layer behavior between model and full-scale pumps is shown in Fig. 42. The smaller dimensions of the model result in a lower Reynold's number, and separation is predicted. The full-size pump is predicted to be free from separations. Note that although separation is predicted on the model on the vanes pressure surface, secondary flow effects cause the separation to be observed on the suction surface across the vane passage. Table 11 shows the predicted separation positions for each of the rotor discharge flows in both model and full size pumps.

Losses were predicted using the Rocketdyne Axial Pump Program INDANA, which accounts for frictional losses from the vane surfaces as well as diffusion and incidence losses using empirical correlation. No loss is included to account for boundary layer separation. The vane losses were estimated at 25 feet of head in the full-size pump, and 30 feet in the model, exclusive of separation losses.

### 4. Cavitation Margin

Vane profiles at hub, mean, and tip were analyzed with the Douglas-Neumann Program for a wide variety of inlet flow angles. The maximum velocity ratio on the surface of the vanes is plotted as a function of inlet angle to produce the cavitation charts shown in Fig. 43 through 46. The maximum velocity ratio without cavitations is also shown as a

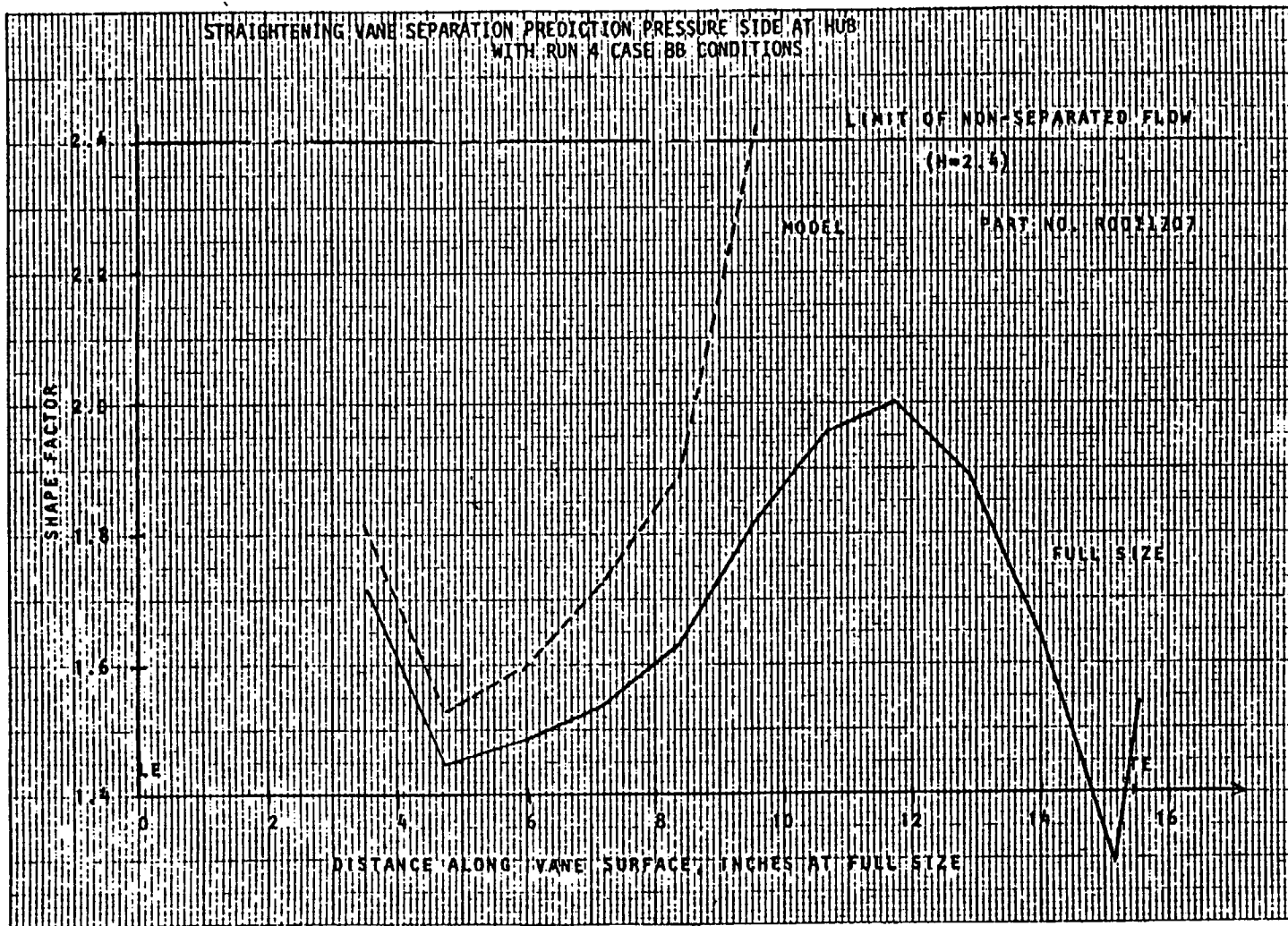


Figure 42. Straightening Vane Boundary Layer Separation Prediction

TABLE 11. PREDICTED BOUNDARY LAYER SEPARATION  
LOCATIONS ON STRAIGHTENING VANES

Run	Model Pump	Full Scale
1	49-68% of chord at hub, mean, and tip	No separation
2	65-68% of chord at hub, mean, and tip	No separation
3	49-68% of chord at hub, mean, and tip	No separation
4	61-90% of chord at hub and mean	No separation
5	49-68% of chord at hub and tip	No separation

horizontal line for each set of rotor discharge flows in Fig. 43 and 44 (cruise and hump flows at hub), while the limit is shown for rotor run 1 in Fig. 45 and 46. The results show a satisfactory cavitation margin at both hump and cruise conditions.

#### 5. Vane Loadings

Vane load as a function of vane meanline distance was calculated from the R3DAP results as used for boundary layer and axial thrust predictions. Results are shown in Fig. 47 for hub, mean, and tip streamlines at Run 1 conditions.

Model Test Data. Model tests were performed on a scale model of the PJ-46. Information on straightening vane performance was gathered through kiel and yaw probe surveys at the vane inlet and discharge, static taps inside the axial gap between rotor drum and discharge housing, and by flow visualizations along the hub and tip casings downstream of the straightening vanes. All data represent cruise conditions unless stated otherwise.

Inlet conditions to the straightening vanes, as determined by the model test, are discussed in the rotor design section. The test inlet conditions are similar to the analysis inlet conditions.

Figures 48 through 50 show the wake downstream of the straightening vanes. The wake is shown as going from the pressure side of one vane across the flow passage to the suction side of the next vane, however, the probes are actually spaced behind several vanes as shown in Fig. 51. The head rise is presented from inlet total head. The large wake shown at the mean and near the hub represents flow separation, and agree with the predictions for the model as shown in Table 12.

The straightening vane performance is shown in Fig. 52 both with and without the wake regions shown in Fig. 49 and 50 included. The overall model pump performance is listed in Table 12. Table 13 presents the projected full-size pump performance based on the model tests. It is assumed that separation will not occur on the full-size pump, but a maximum wake loss of 2% is included, leading to a projected full-size pump head rise of 926.5 feet at 86.6% efficiency with design

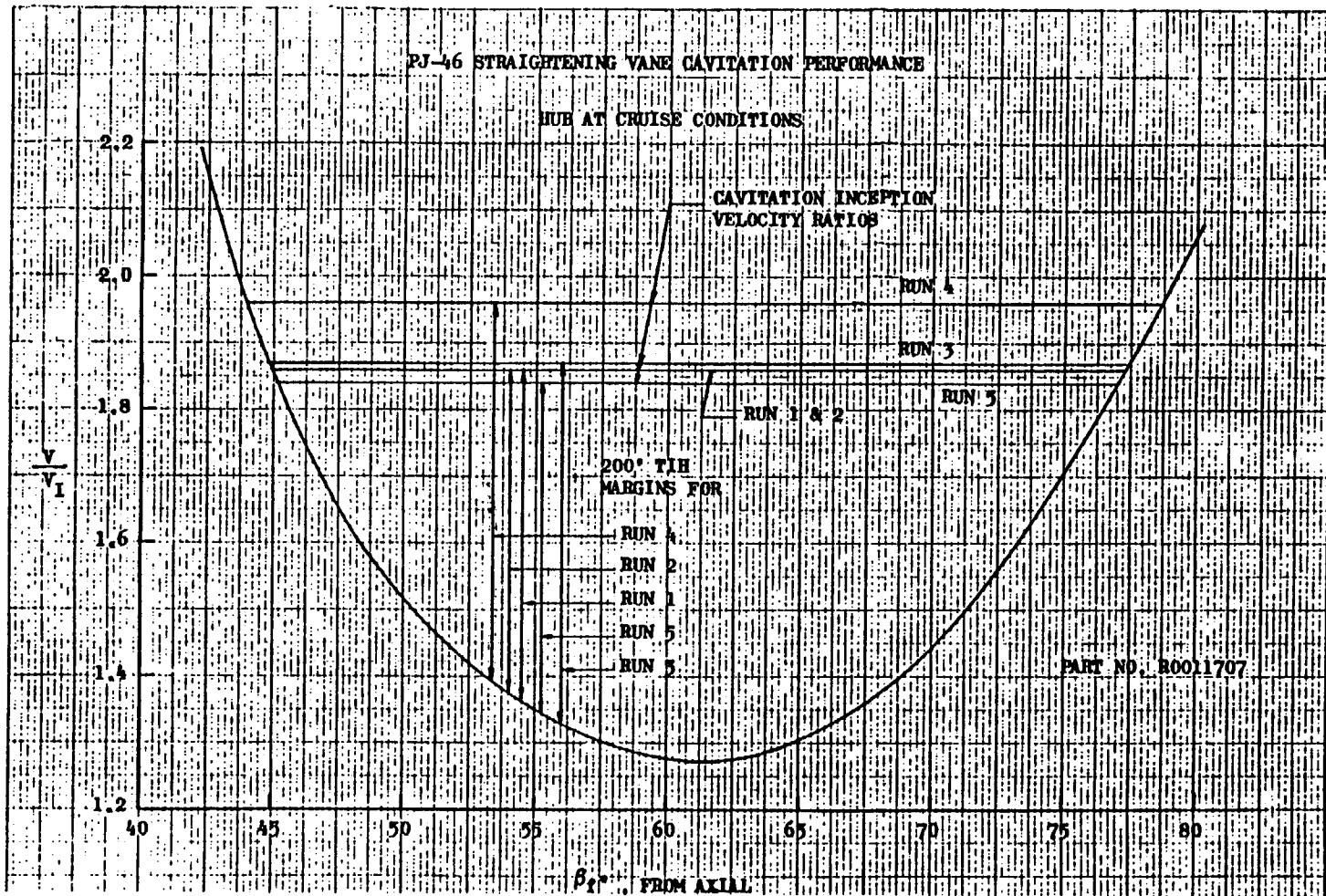


Figure 43. Straightening Vane Cavitation Performance With Hub at Cruise Conditions

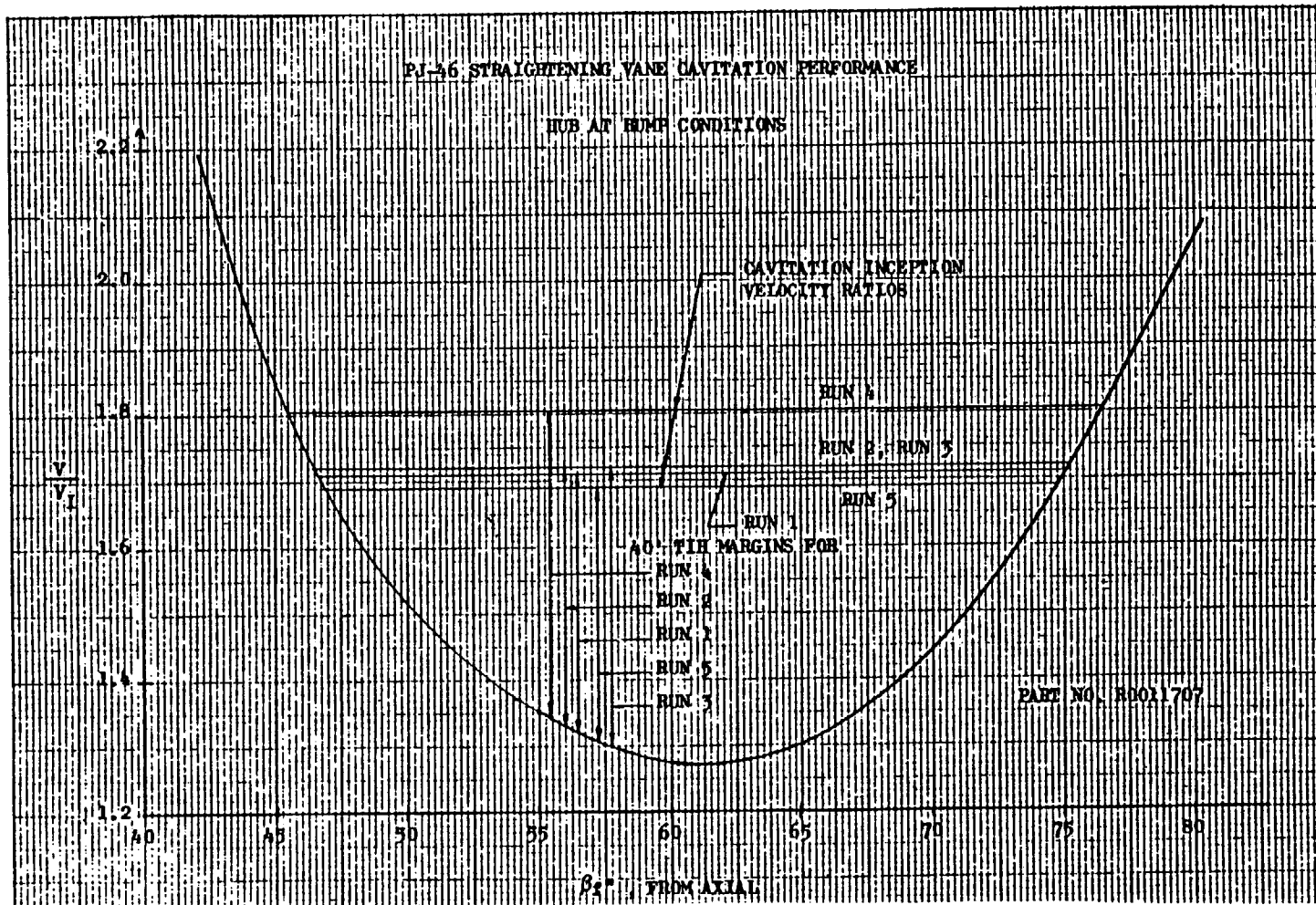


Figure 44. Straightening Vane Cavitation Performance With Hub at Hump Conditions

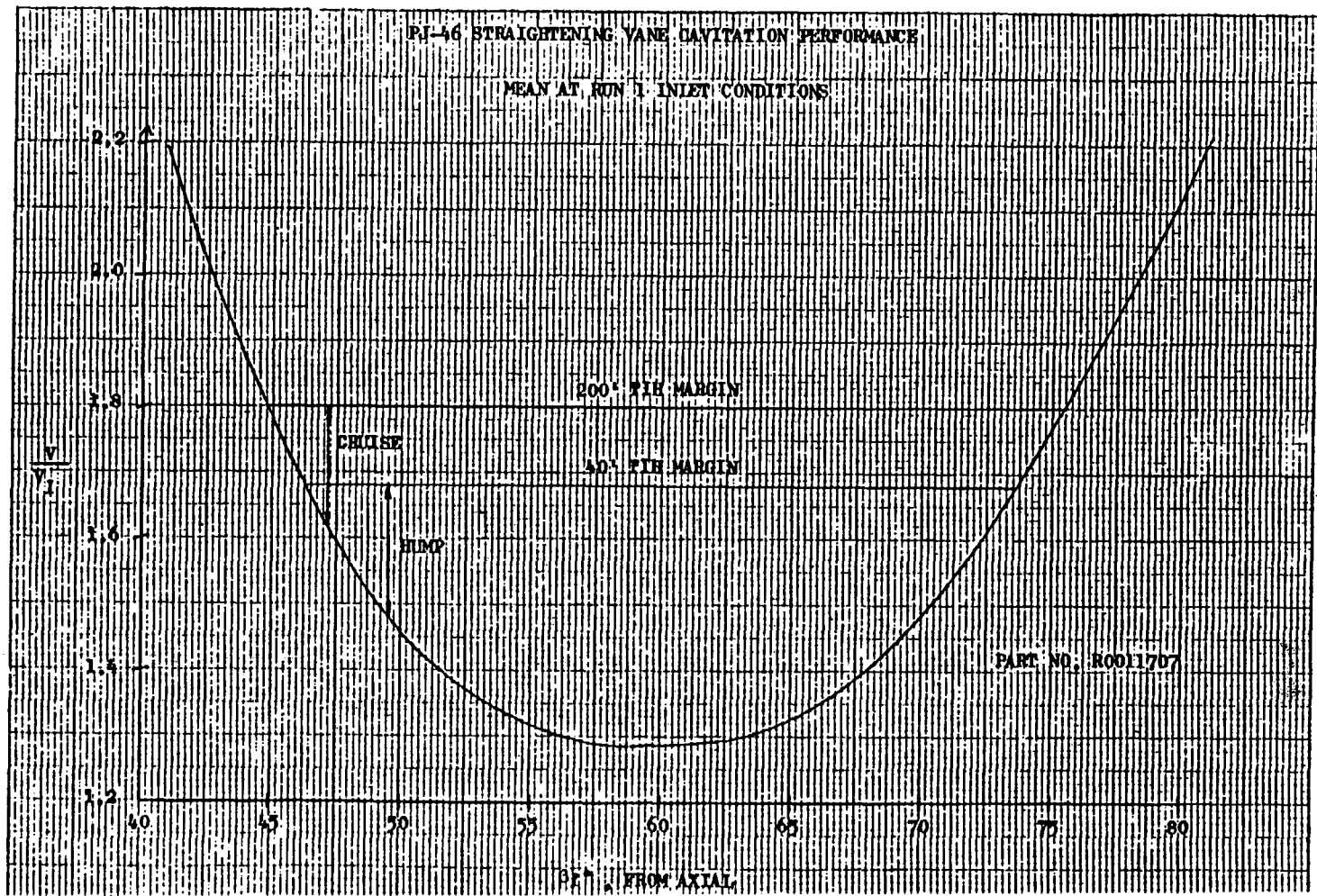


Figure 45. Straightening Vane Cavitation Performance With Mean at Run 1 Inlet Conditions

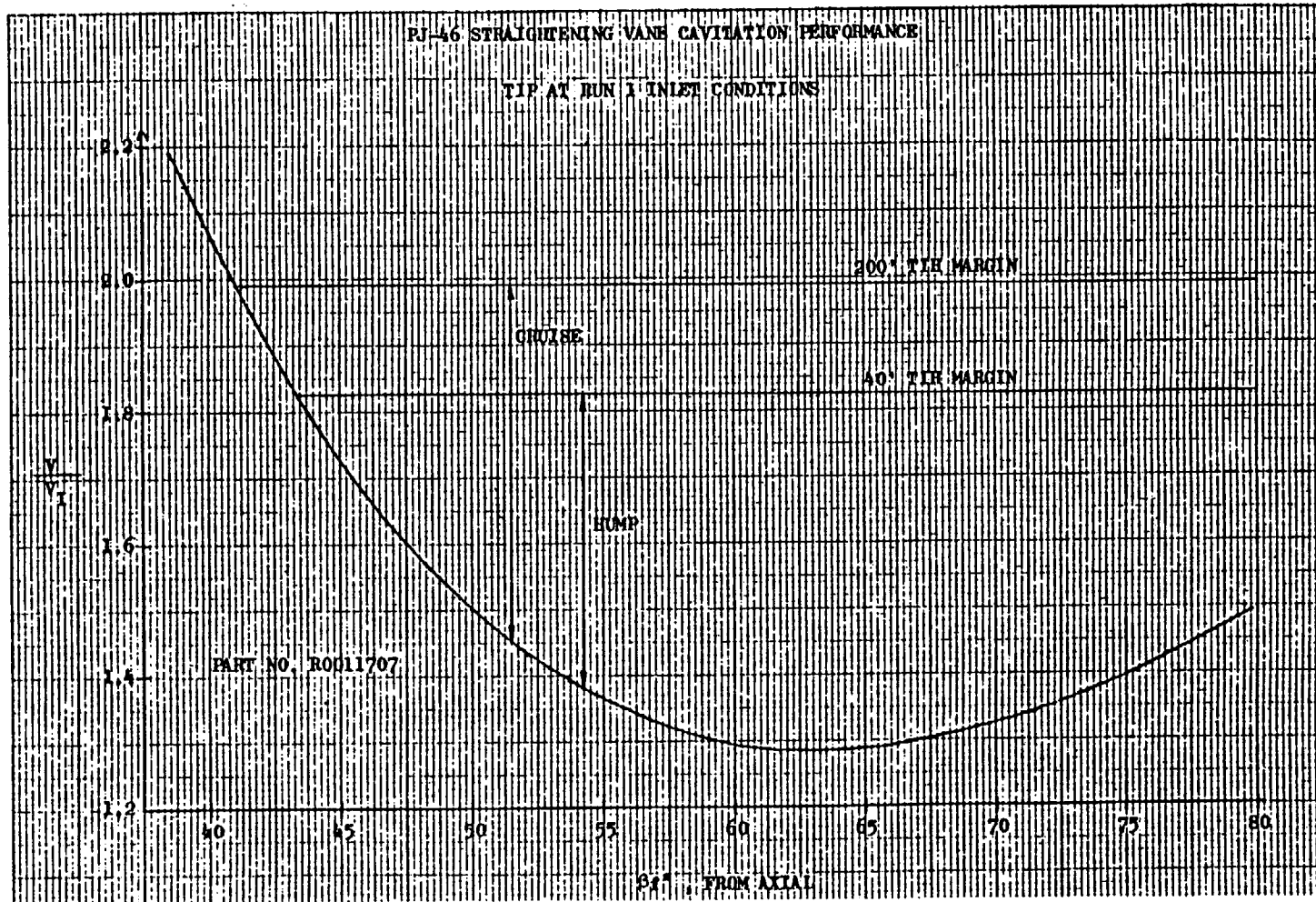


Figure 46. Straightening Vane Cavitation Performance  
With Tip at Run 1 Inlet Conditions

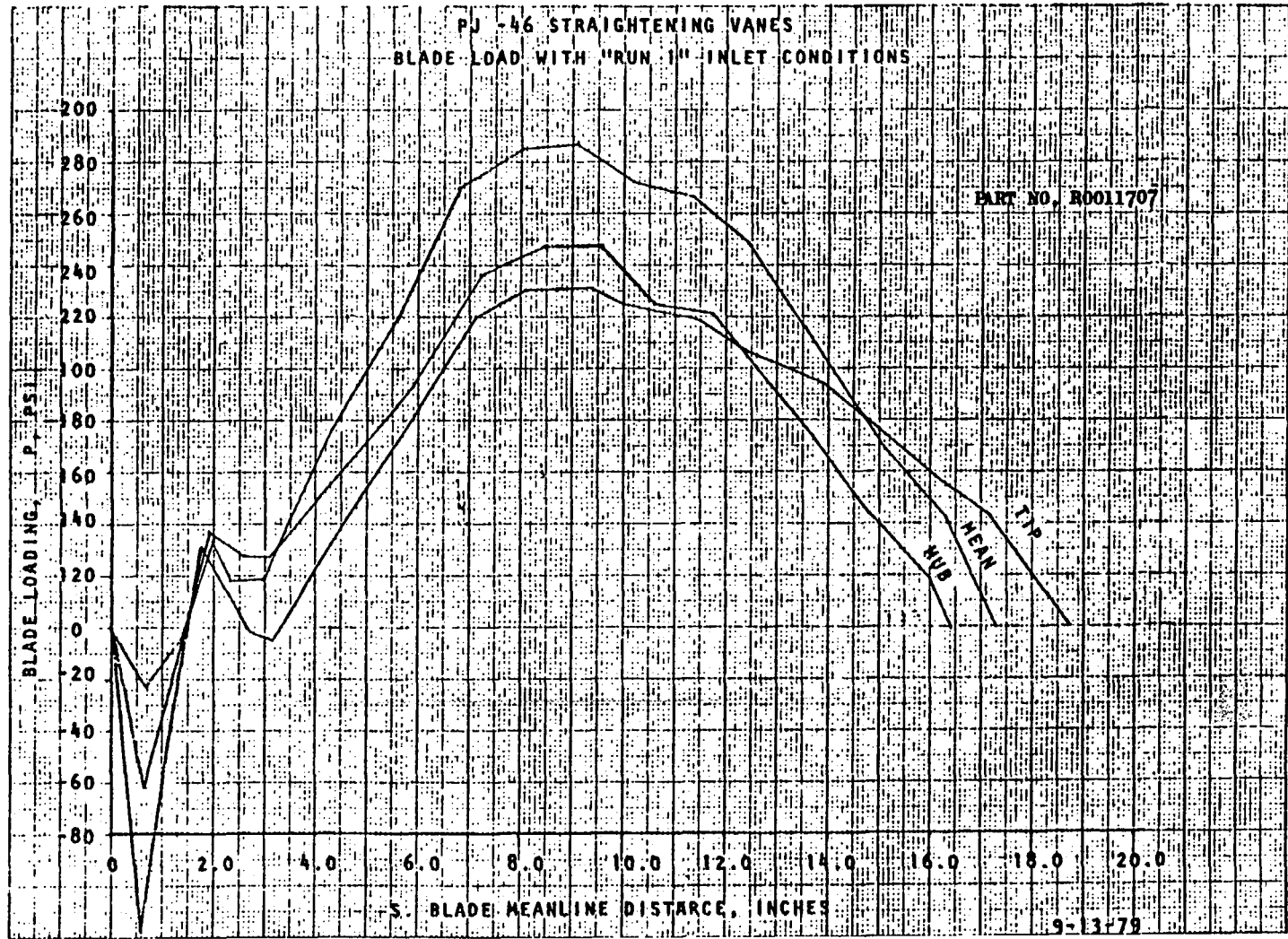


Figure 47. Straightening Vanes Blade Load With Run 1 Inlet Conditions

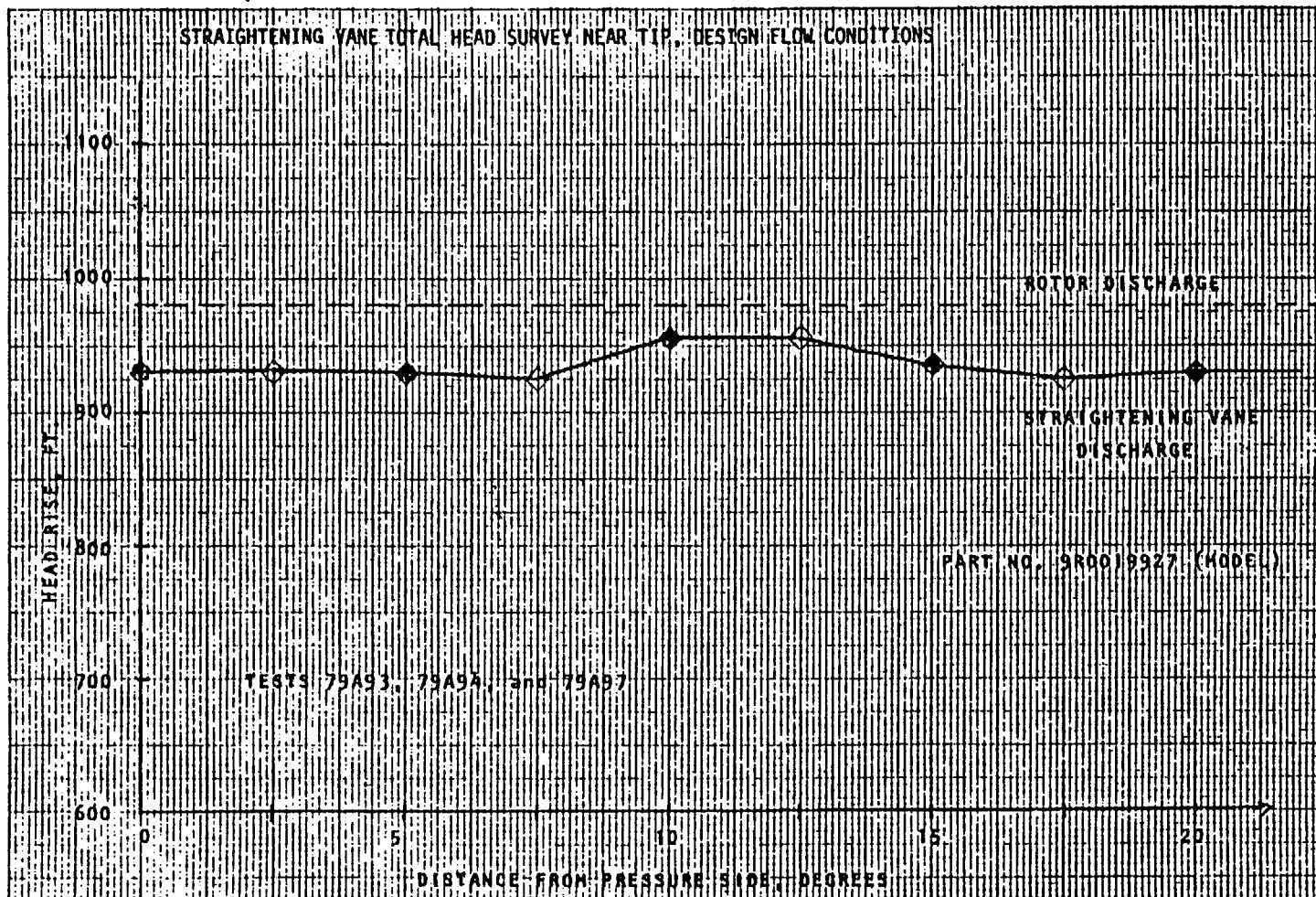


Figure 48. Straightening Vane Total Head Survey Near Tip at Design Flow Conditions

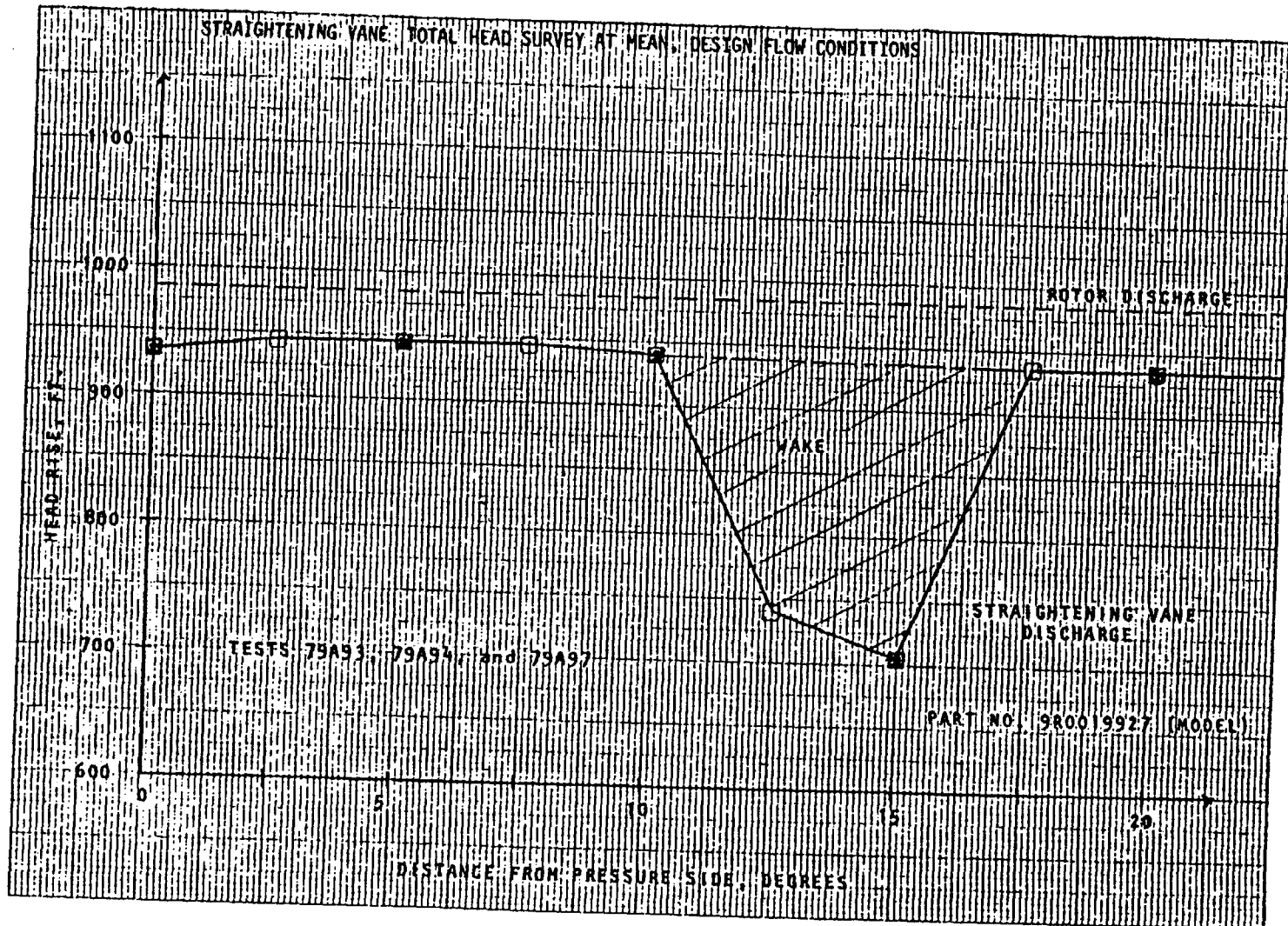


Figure 49. Straightening Vane Total Head Survey at Mean at Design Flow Conditions

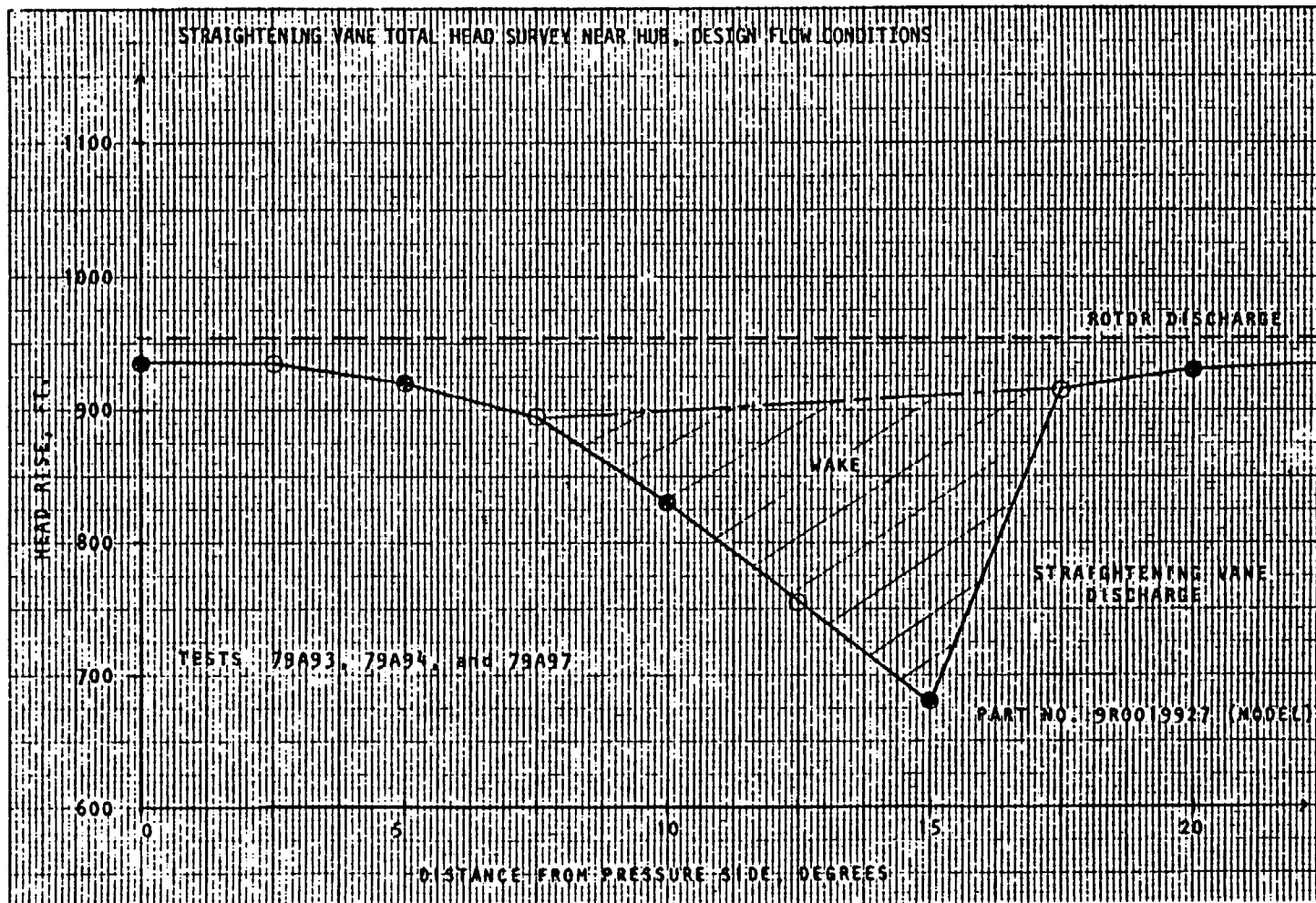


Figure 50. Straightening Vane Total Head Survey Near Hub at Design Flow Conditions

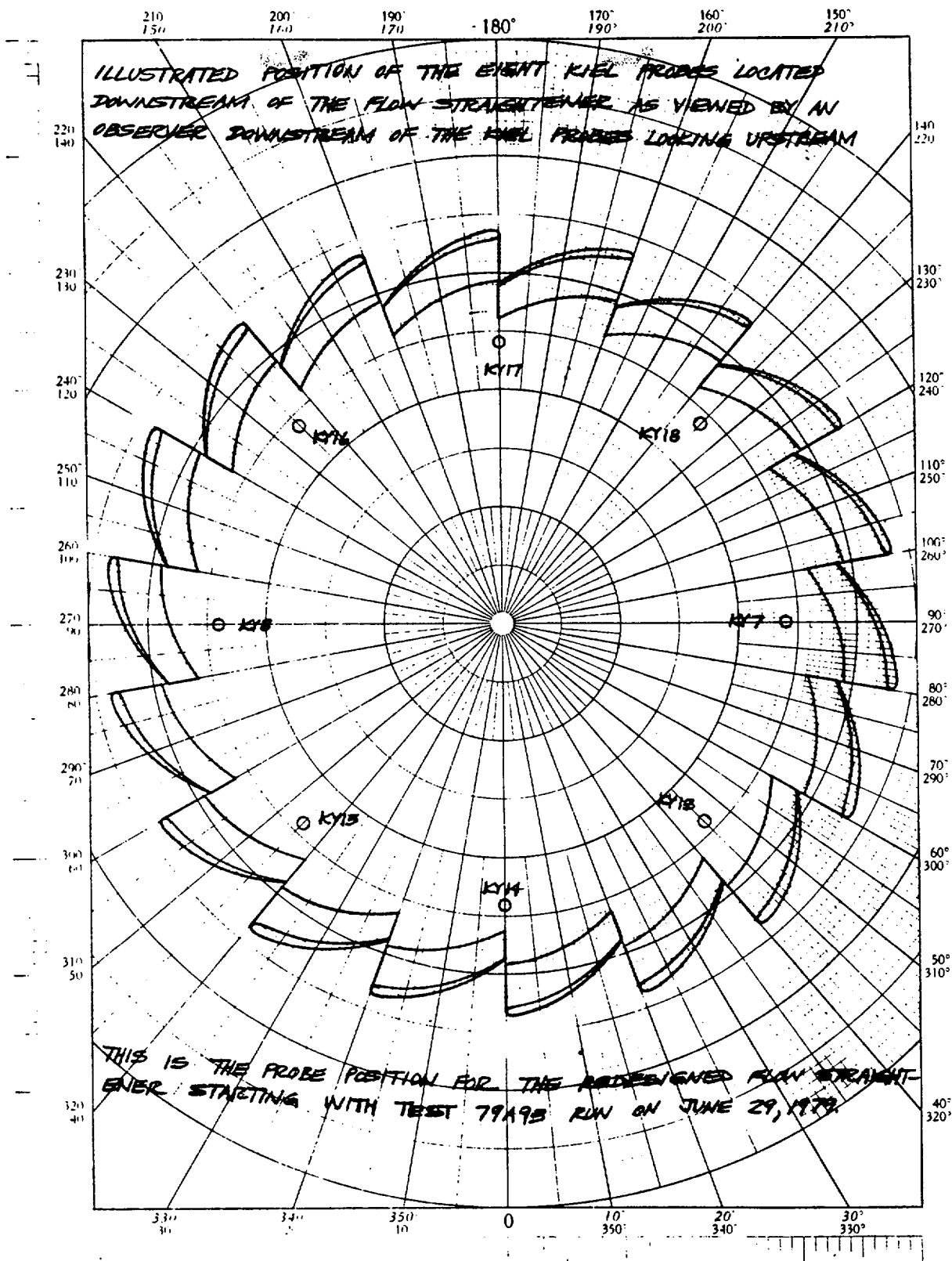


Figure 51. Kiel Probe Locations Relative to Flow Straightener

TABLE 12. COMPARISON OF PREDICTED/MEASURED MODEL PERFORMANCE

Location and Parameter	Predicted	Measured
At Discharge of Axial Rotor		
Head Rise, feet	957	958
Efficiency	88.5	88.3
Straightening Vane Loss, feet	30*	73 Including wakes 26 Without wakes
At Pump Discharge		
Head Rise, feet	927	885
Efficiency	85.7	81.6
*Assumes no separation		

TABLE 13. PROJECTED FULL-SIZE PUMP PERFORMANCE

Parameter	Head	Efficiency
Measured Model Pump Performance	885	81.6
Model → Full-Scale Hydro Correction	+17.3	+2.7
Model → Full-Scale Elevation Correction	- 3.8	-0.3
Predicted Full-Scale Performance with Separation	898.5	84.0
Maximum Straightening Vane Loss without Separation (2% Wake Loss)	45.0	-
Predicted Full-Scale Performance without Separation	926.5	86.6

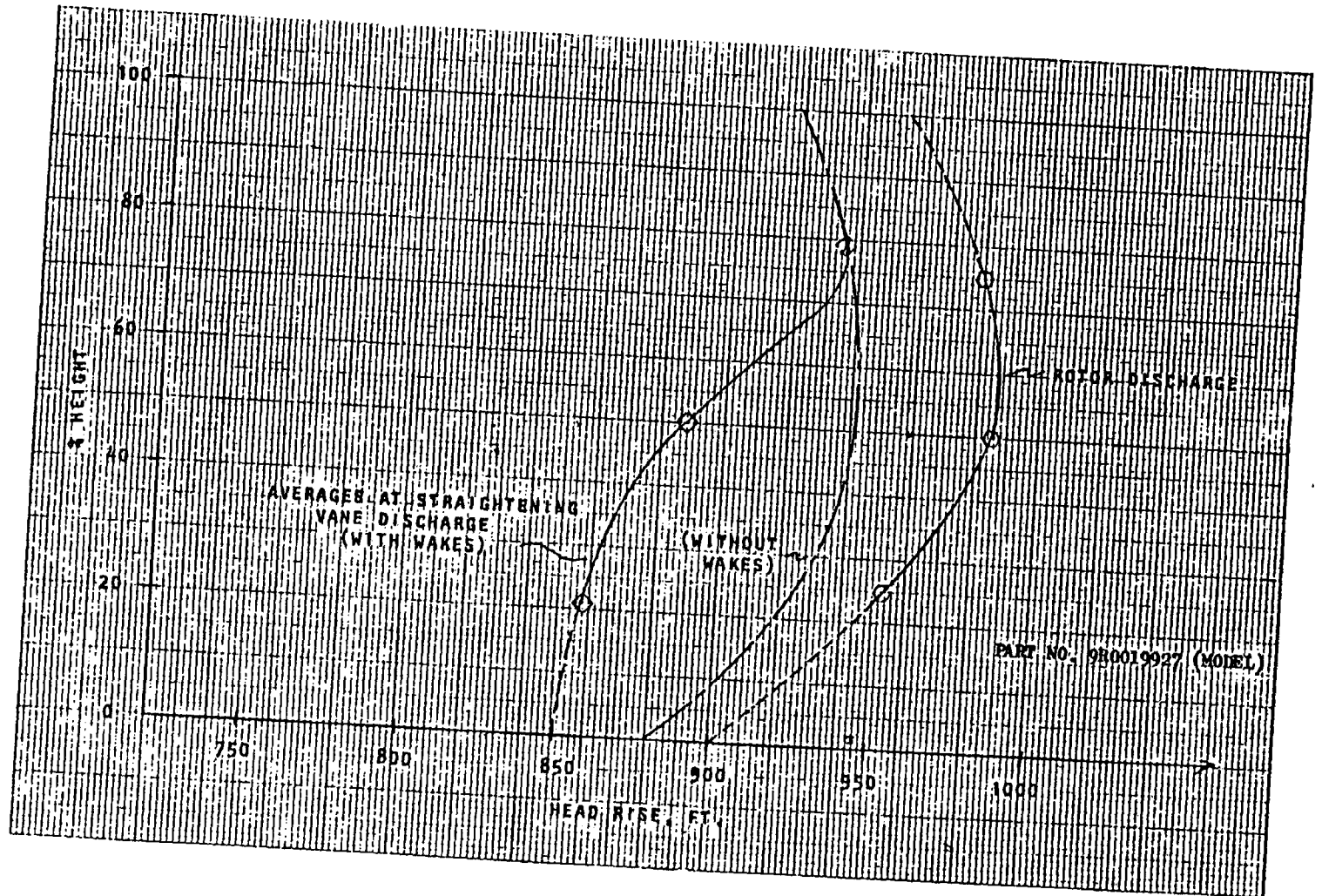


Figure 52. Straightening Vane Performance at Design Flow

flowrate of 138,000 gpm and at 1000 rpm. With the assumed wake loss, the overall loss in the stator does exceed the original prediction of 25 feet of loss.

Yaw survey results downstream of the straightening vanes are shown in Fig. 53. The two surveys were done on different sides of the wake. The tangential pressure gradient due to the wake is believed to cause the divergence as the large wake at the mean is approached. However, near the tip, a discharge flow angle of approximately 1.5 degrees underturned is shown.

Slight cavitation damage was observed on the pressure side of some of the vanes near the hub after 17 hours at hump conditions. It is believed that this was caused by flow through the gap between the rotor drum and straightening vane leading edge. The bottom edge of the straightening vane over the rotor drum will be smoothed before the life testing is continued. The damage was not serious, and would not represent a life problem even if not corrected. No damage was observed that could be attributed to leading edge flow conditions in agreement with predicted cavitation margins.

Axial thrust was not measured directly on the model pump, but may be calculated from a static tap located inside the gap between discharge housing and rotor drum. To compare the static pressure with predictions, the measurement must be adjusted by the assumed radial pressure gradient between the measurement point and the bottom of the straightening vanes. This yields an axial thrust prediction of 279,000 to 313,000 pounds, (with the test rotor head change taken into account) depending on the radial pressure gradient used. This is higher than the predictions in Table 10, but only two data points were available. More test data will be checked when testing continues, and the actual radial pressure gradient will be established by using several taps inside the gap.

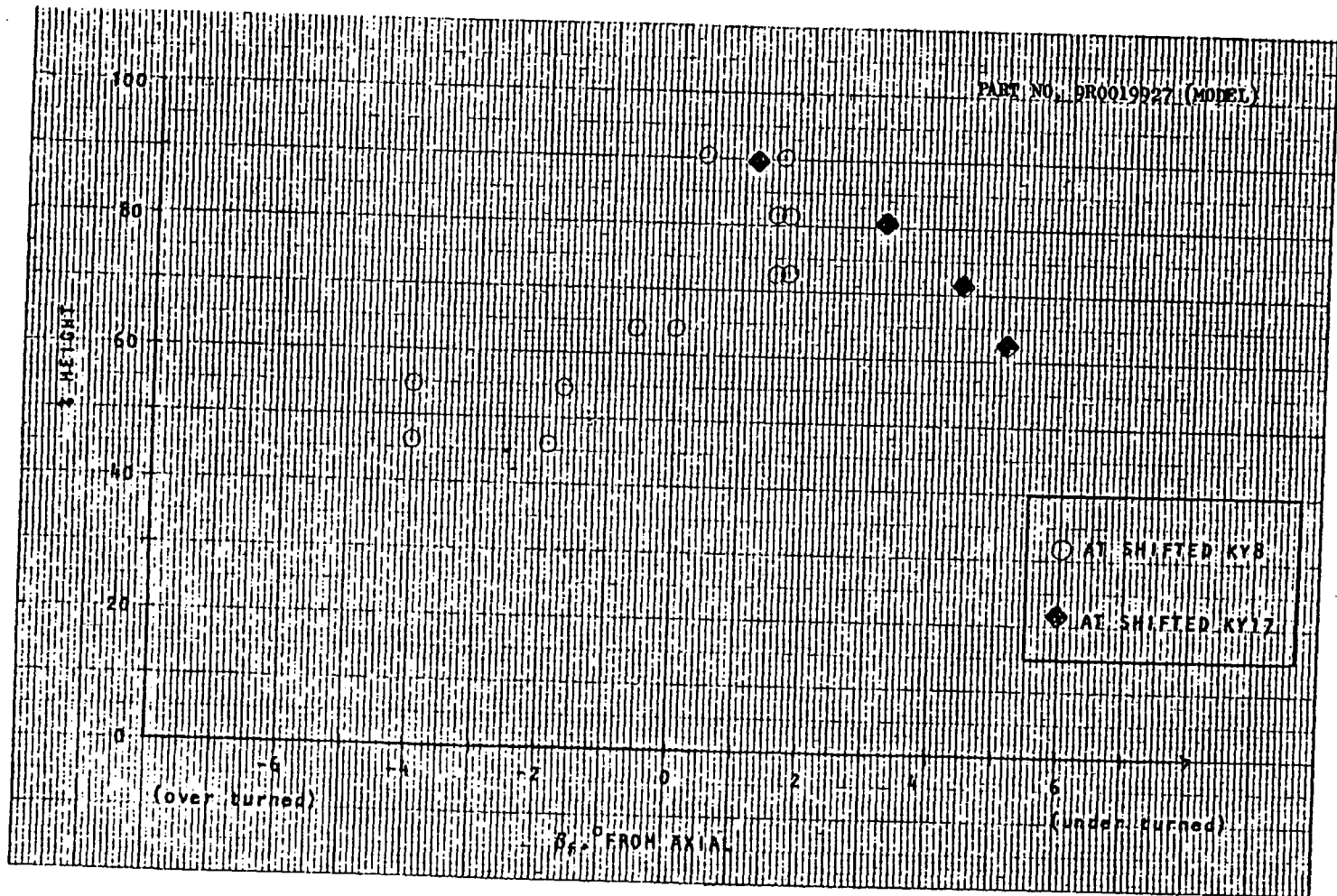


Figure 53. Yaw Probe Surveys at Discharge of Straightening Vanes

## FACILITY MODIFICATION DESIGN

The pump test facility at Rocketdyne is designed to test single-stage pumps (inducer or rotor with integral deswirl vanes and discharge volute). Figure 54 shows the model LSES inducer installed using the facility discharge volute. Flow enters the inducer axially from the right (foreground) and is discharged normal to the axis of rotation (small diameter pipe in background). LSES inducer-only testing was performed using this standard facility installation.

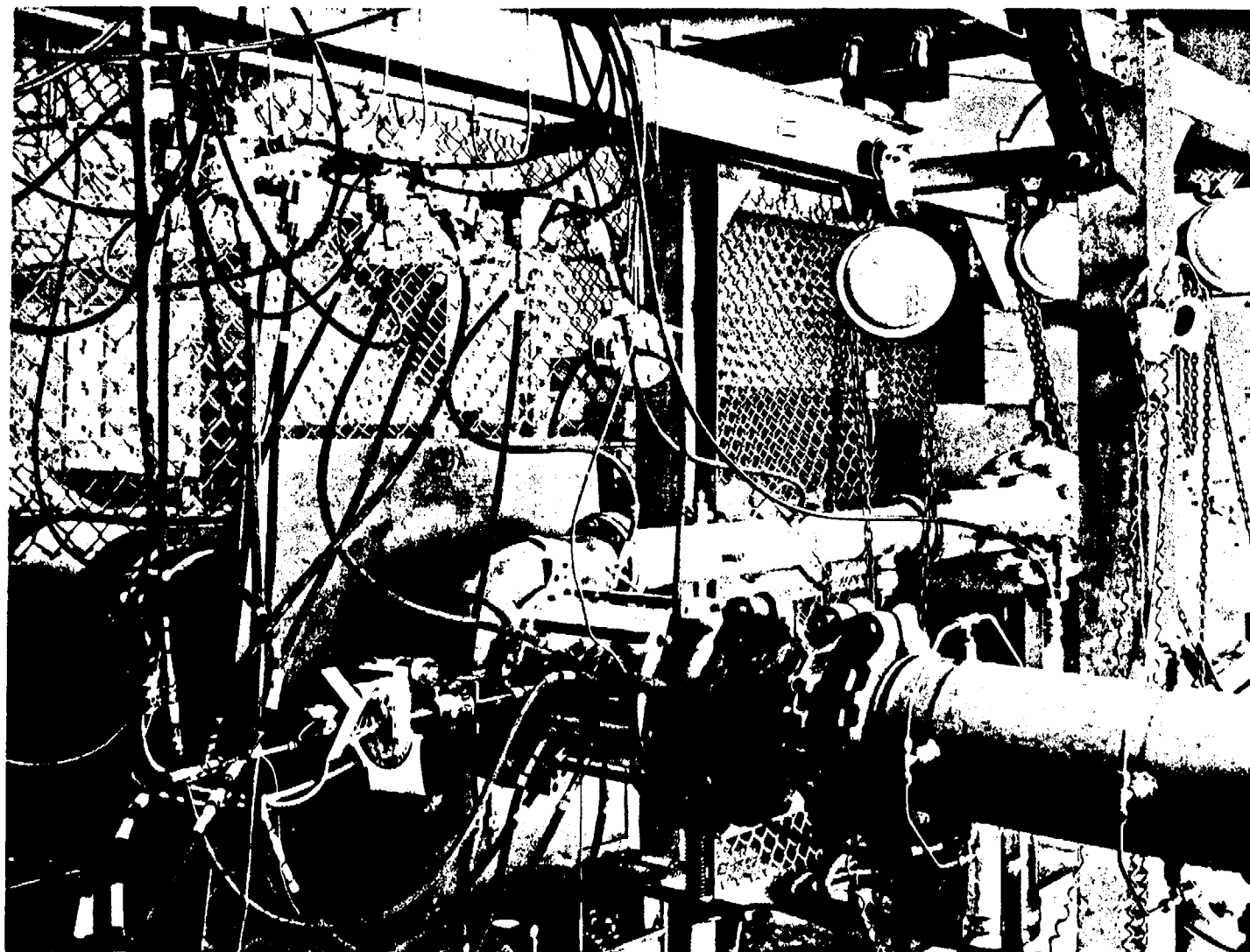
Testing the entire model pump required the modification of the facility to allow the flow to enter the pump at 55 degrees (from axial) and discharge axially. Figure 55 details the modifications required. The plan view (upper left) shows the point of connection (POC) for the inlet and discharge systems.

### Inlet Piping System

The inlet system is constructed of 8-inch ASTM A53, schedule 40, welded seamless pipe. Section A shows the inlet and discharge piping looking east. The inlet flow is turned 90 degrees by a vaned elbow. The distortion effects of the turn are decreased by these vanes shown in Detail 7. The inlet transition section, Detail 3, reduced the pipe ID from 7.98 to 6.79 inches (the model pump inlet elbow ID).

### Discharge Piping System

After passing through the model pump, the flow is discharged as a small-diameter (3 inches), high-velocity (250 ft/sec) jet. The jet is contained by the discharge spool section, Detail 1, and diffused (velocity reduced) by the facility transition section, Detail 2. A 1-1/8-inch spacer between the spool and transition section allows for variation in pump length. The remainder of the discharge system consists of three 90-degree elbows and various lengths of 8-inch ASTM A53, schedule 40, welded seamless pipe.



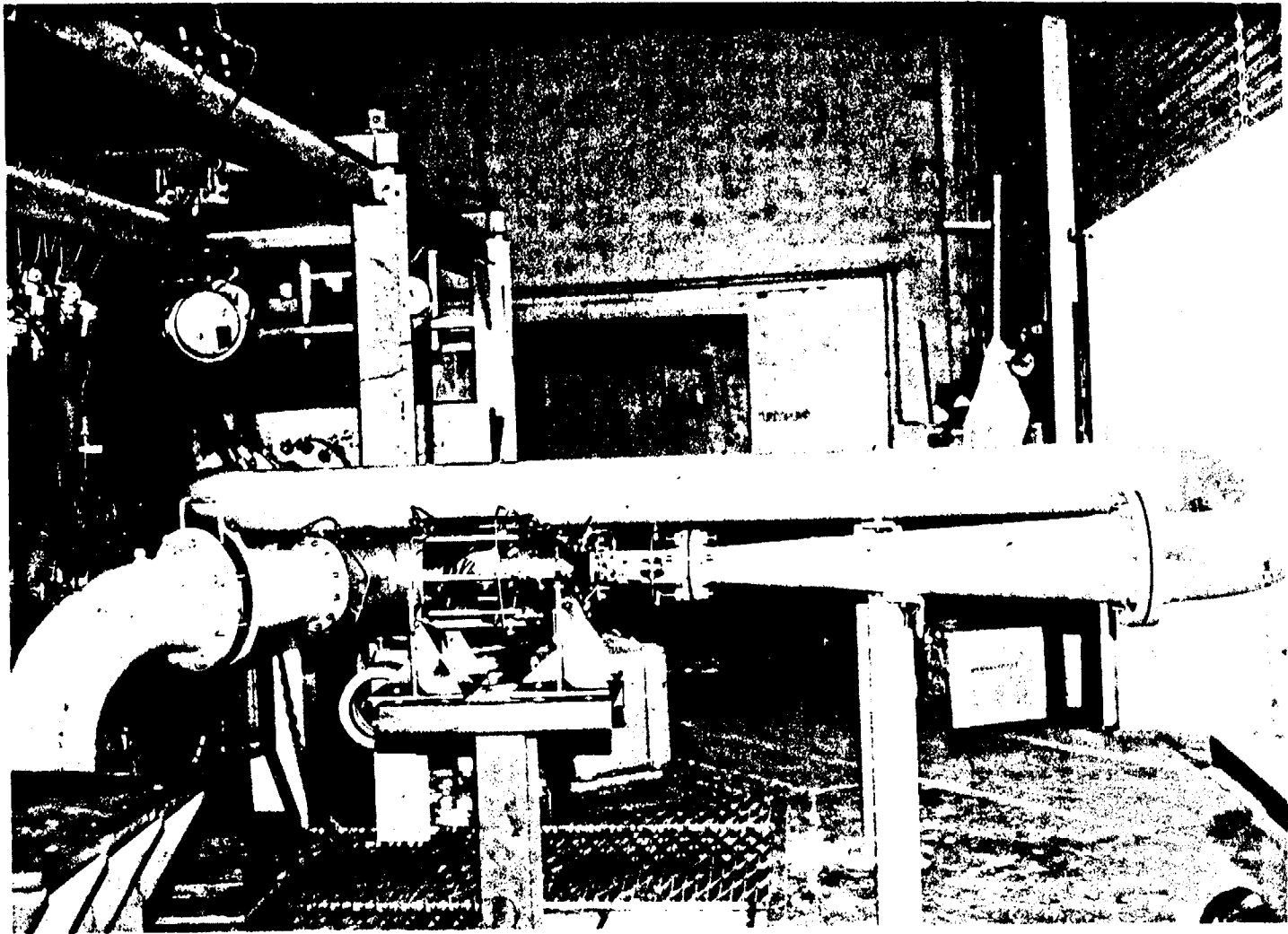
4MA44-7/24/79-C1A

Figure 54. Inducer-Only Test Setup



### Support System

The model pump is supported on 10-inch wide channel which is welded to an 8-inch beam which, in turn, is connected to an 18-inch square base plate, as shown in Detail 6. Figure 56 shows the facility modification shortly after completion.



4MA41-10/23/78-C1A

Figure 56. Initial Facility Modification

## FABRICATION AND FACILITY MODIFICATION (SOW TASK 3.2)

### PUMP FABRICATION

#### Fabrication Methods

The LSES model pump was fabricated using standard techniques. The inlet was cast by creating a wood pattern and sand cores and then a sand mold in which molten aluminum was placed. The stator vanes were formed by use of pantograph machining (3 to 1 expanded pattern). The inducer, rotor, and straightening vanes were machined on a numerically controlled, five-axis omnimill.

#### Materials

The materials used for construction of the LSES model pump were in part dictated by the PJ-46 (full size) pump design. Where a component was modeled, it was fabricated from the same material, e.g., the inlet is A357 aluminum, the inducer stator, rotor, and straightening vanes are commercially pure titanium. The remainder of the parts are made from various materials such as: 17-4 PH stainless steel for the main shaft, discharge duct, and inducer drive keys; acrylic plastic for viewing tunnels; carbon steel for the pump support cradles.

### FACILITY MODIFICATION

#### Initial Modification

In October 1978, the facility modification discussed above was installed. Pre-test checkout of the facility revealed that the inlet pipe was moving when the system was pressurized. This caused the quill shaft (later replaced by the flexible coupling) to bind and caused a delay in the initiation of pump testing.

#### Increased Stiffness Added

To solve the problem of quill shaft binding, the inlet pipe was welded at the location where a victaulic coupling is shown in the drawing (Fig. 55). In

addition, a support system was added at the facility inlet elbow which securely held it in place. Two angles were added at the discharge to hold the diffuser. Figure 57 shows the facility after the elbow support (left) and diffuser angles (right) were welded in place. The additional stiffness solved the binding problem (due to system pressurization). Tests were begun and the facility functioned satisfactorily.

113/114

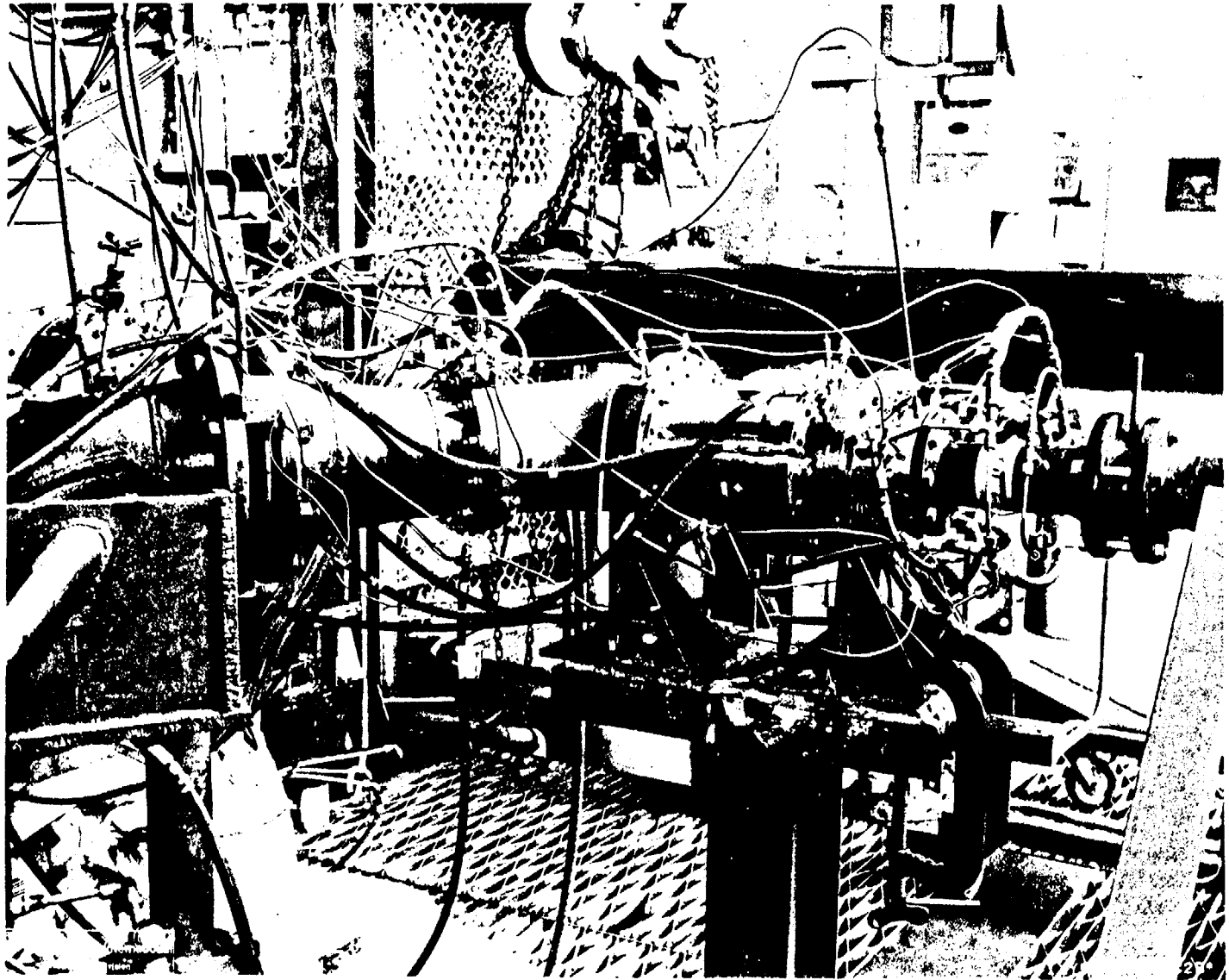


Figure 57. Modified Test Facility Inlet  
with Welded Elbow Support and Diffuser Angles

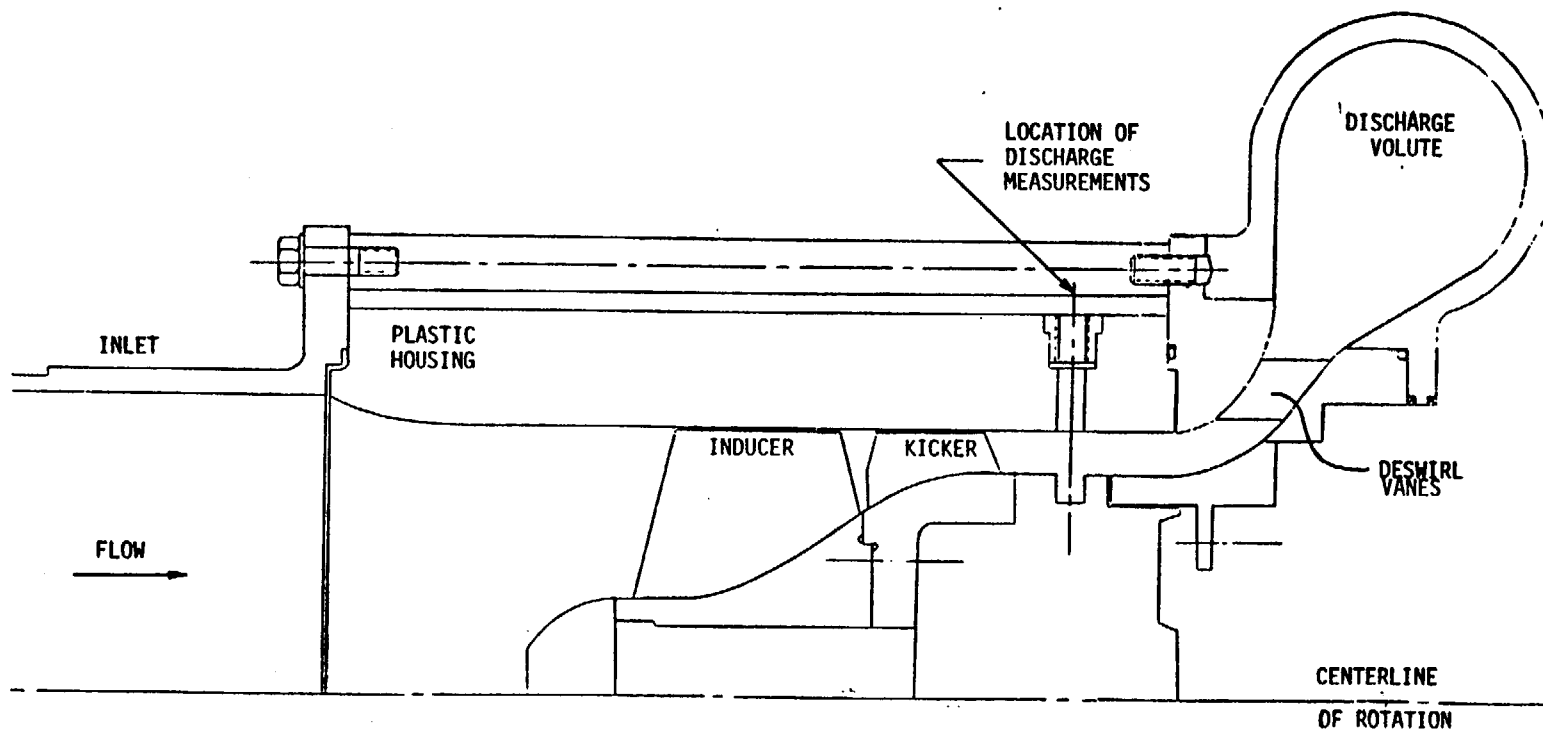


Figure 58. Model Pump Configuration A; Inducer only; Plastic Tunnel

## MODEL TEST RESULTS (SOW TASK 3.3)

### TEST PROCEDURES AND TECHNIQUES

#### Configurations

The LSES model pump is designed to allow maximum flexibility in regard to axial spacing of the hydrodynamic elements. This makes complete surveys of the inlet and discharge conditions of each component possible. A 1.1-inch space can be added at the kicker discharge, stator discharge, or rotor discharge. This added space allows for piezometer, total pressure, and yaw probe instrumentation to be installed. There are seven basic configurations, lettered A through G.

Inducer-only tests were performed using configurations A and B (Fig. 58 and 59). The flow entered along the axis of rotation after passing through a flow straightener. The inlet converges to the model pump diameter just upstream of the inducer full and partial blades (labeled inducer). After passing through the kicker section of the inducer, the flow conditions are monitored through several ports machined in the outer housing. The flow is then diffused into a facility discharge volute. In the A configuration, a clear plastic housing (lucite) is used. In the B configuration, a stainless-steel housing is substituted for the plastic.

Pump tests were performed using configurations C through G (Fig. 60 through 64). During pump tests, the flow (distorted) is turned by the model inlet elbow just upstream of the inducer. The inducer, stator, rotor, and straightening vanes are used during all tests. Various spacers are used to create axial space between the kicker and stator (configuration G), stator and rotor (configuration C), and rotor and straightening vanes (configuration D). Configurations E and F have the design spacing. Configurations C, D, E, and G have plastic housings over the inducer, kicker, and rotor. Configuration F is all titanium and is used for life verification testing.

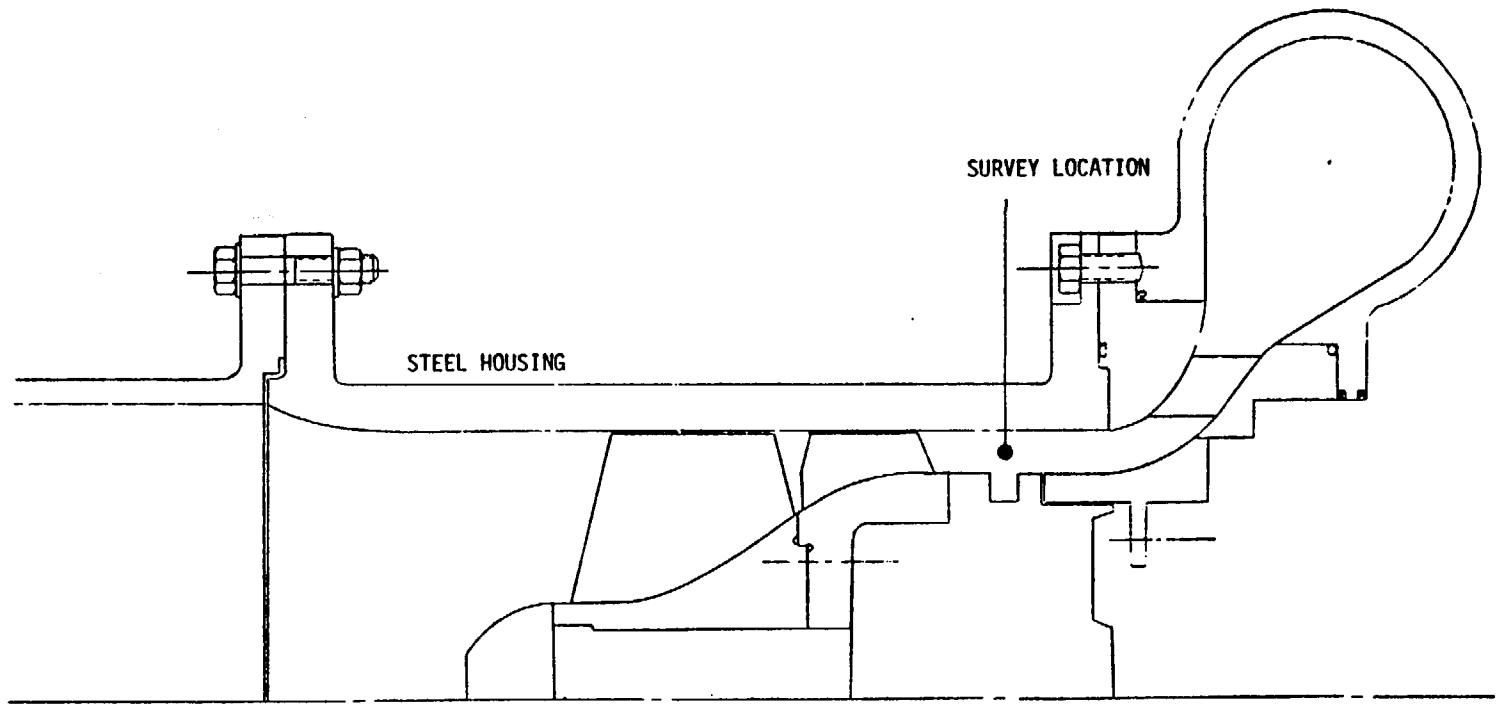


Figure 59. Model Pump Configuration B; Inducer Only; Steel Tunnel

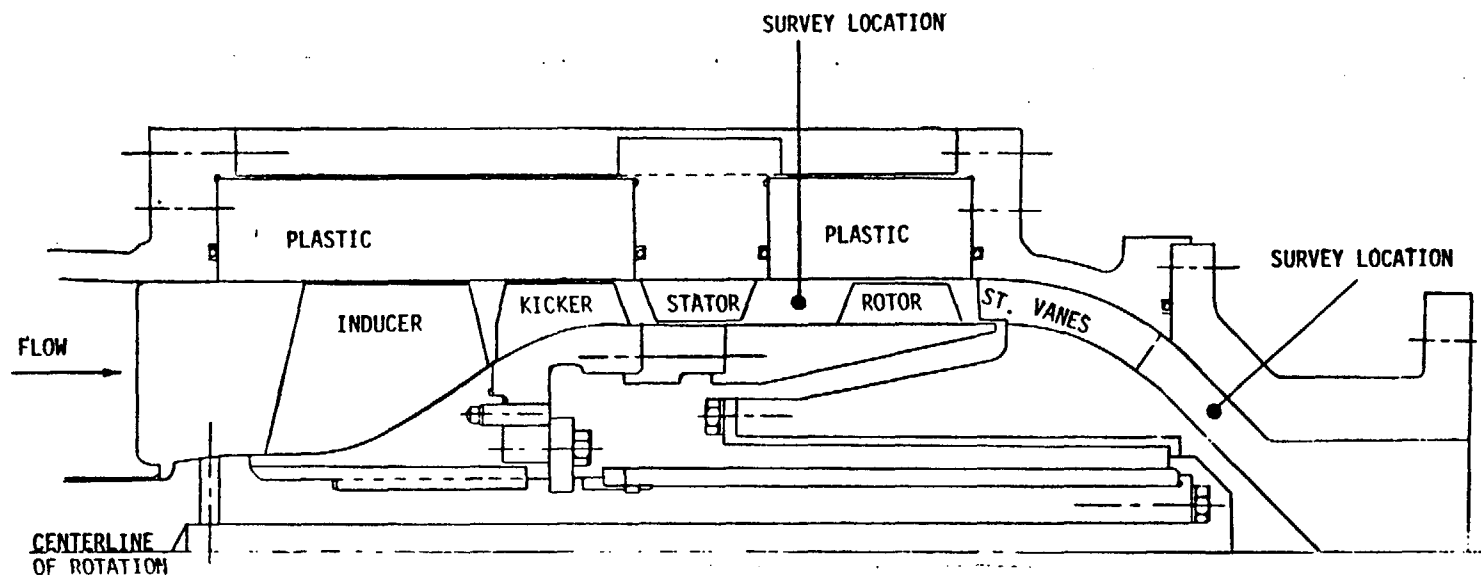


Figure 60. Model Pump Configuration C; Surveys at Stator Discharge

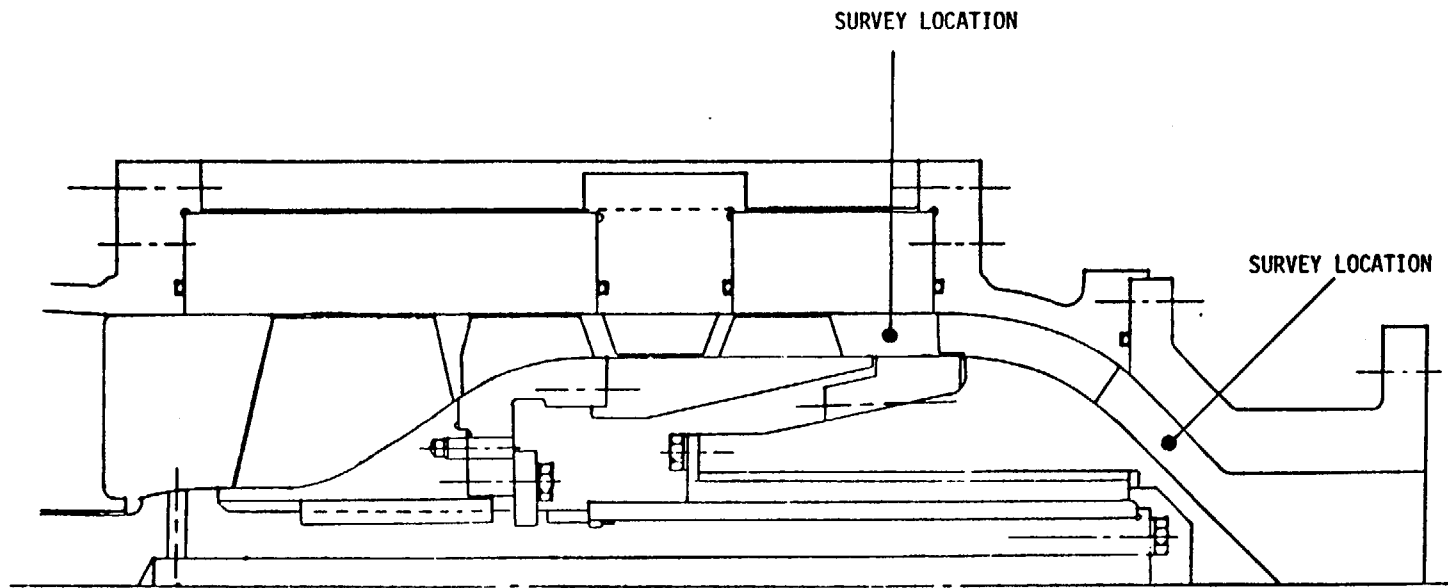


Figure 61. Model Pump Configuration D; Surveys at Rotor Discharge

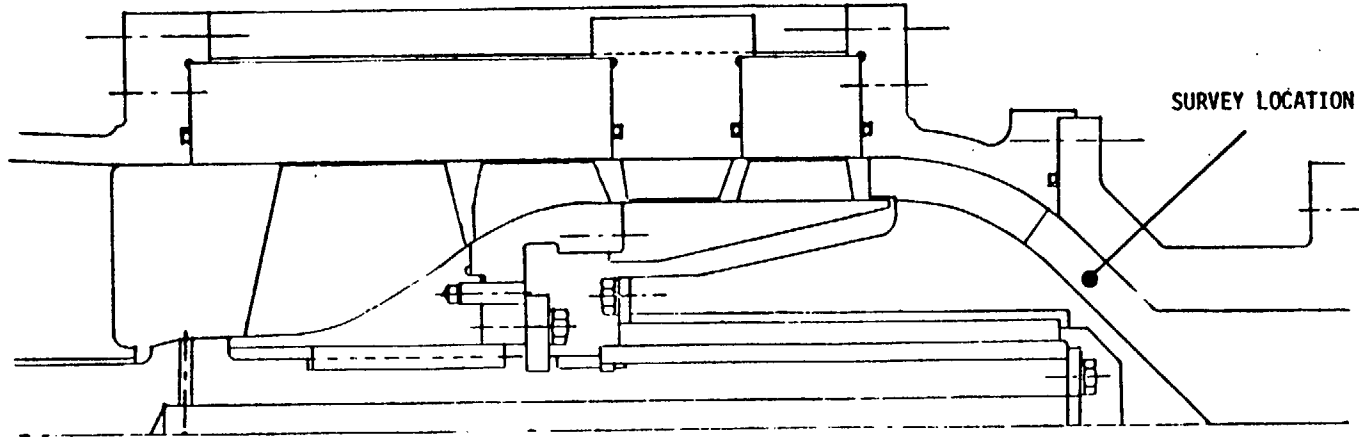


Figure 62. Model Pump Configuration E; Plastic Tunnel

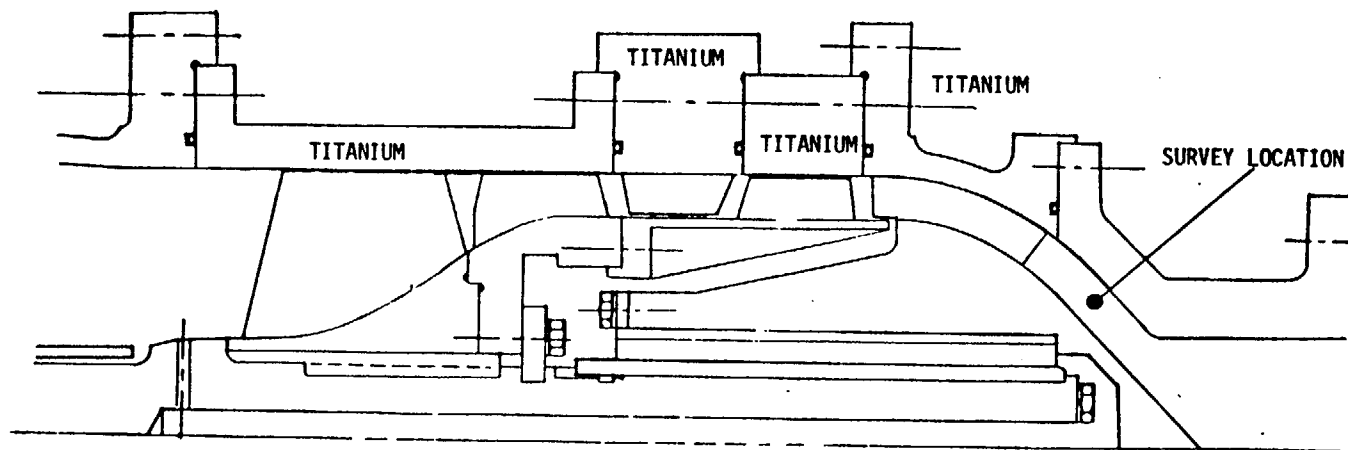


Figure 63. Model Pump Configuration F; All Titanium

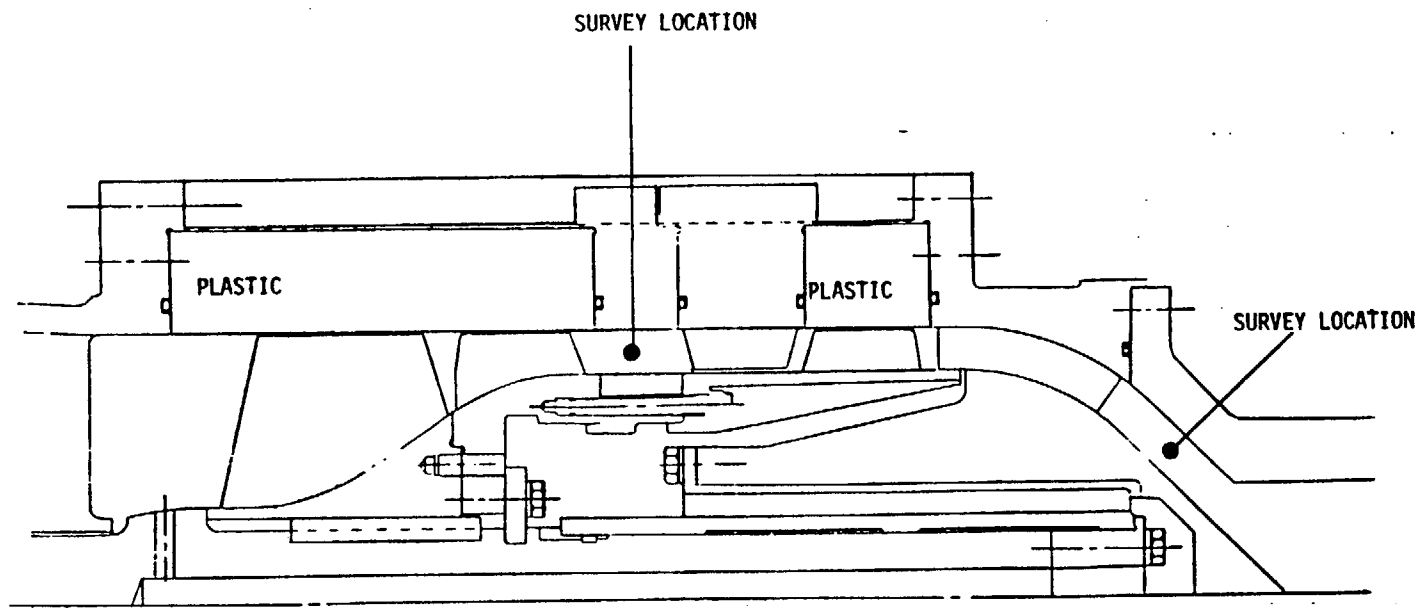


Figure 64. Model Pump Configuration G; Surveys at Kicker Discharge

## Instrumentation

The model pump is equipped with a large number of instrumentation bosses. Static pressure can be measured at the inlet and discharge flange of the inlet elbow, six locations over the inducer, four over the stator, four over the rotor, five over the straightening vanes, two inside the rotor drum, and several other locations. Total pressure and yaw probe ports are provided as shown in Fig. 65 (labeled KY).

## Pump Test Facility

The LSES model pump test facility is located at Rocketdyne's main facility in Canoga Park, California. A schematic of the facility drive system and flow loop is shown in Fig. 66. The pump drive consists of a 1200 rpm, reversible, synchronous electrical motor rated at 4000 hp. Two pump positions are available. A 4000-hp gearbox is capable of producing speeds of 3,976, 5,040, 6,322, 8,013 and 10,000 rpm. A torquemeter is located between the pump mounting pedestal and gearbox.

The flow loop is supplied with water from an 8000-gallon tank which is pressurized or evacuated as required. A heat exchanger, located adjacent to the tank, maintains a uniform fluid temperature at approximately 90 F. The inlet ducting consists of 8-inch, schedule 40 steel and aluminum piping rated at 125 psi. The discharge ducting is 6-inch, schedule 120 steel piping rated at 2000 psi. The discharge flow passes through a motor-operated throttle valve to the tank. It then passes through a series of baffles in the tank where it is smoothed out before recirculating through the facility.

Test data are recorded on magnetic disk by the Autodata 9 digital data acquisition system. The magnetic disk is then read into an IBM computing system which processes the data and presents it in digital form. Pump speed is measured using a magnetic pickup on a 60-tooth gear with the data recorded on a Berkeley counter. Flow measurements are made by a turbine-type flowmeter located in the

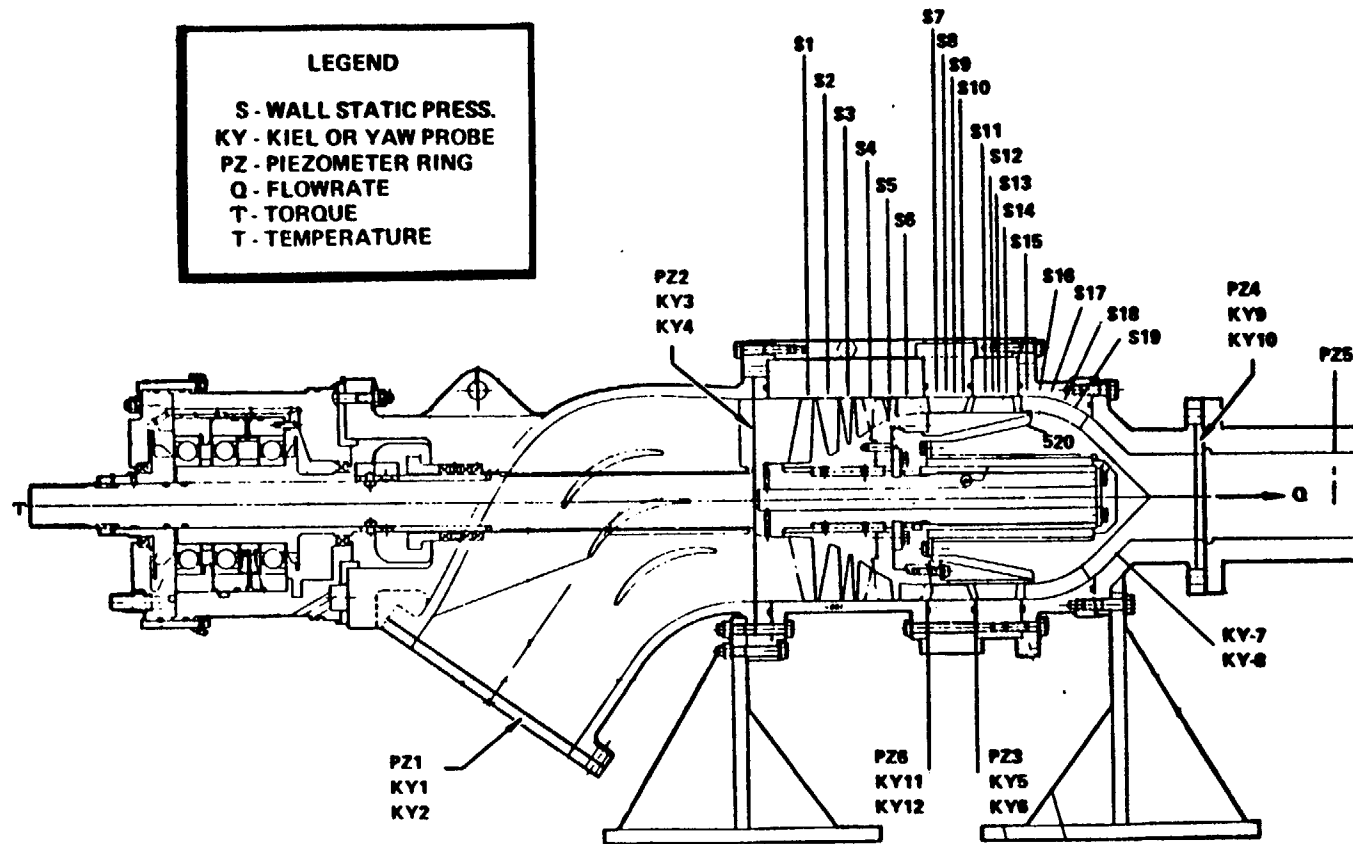


Figure 65. Model Pump Instrumentation Locations

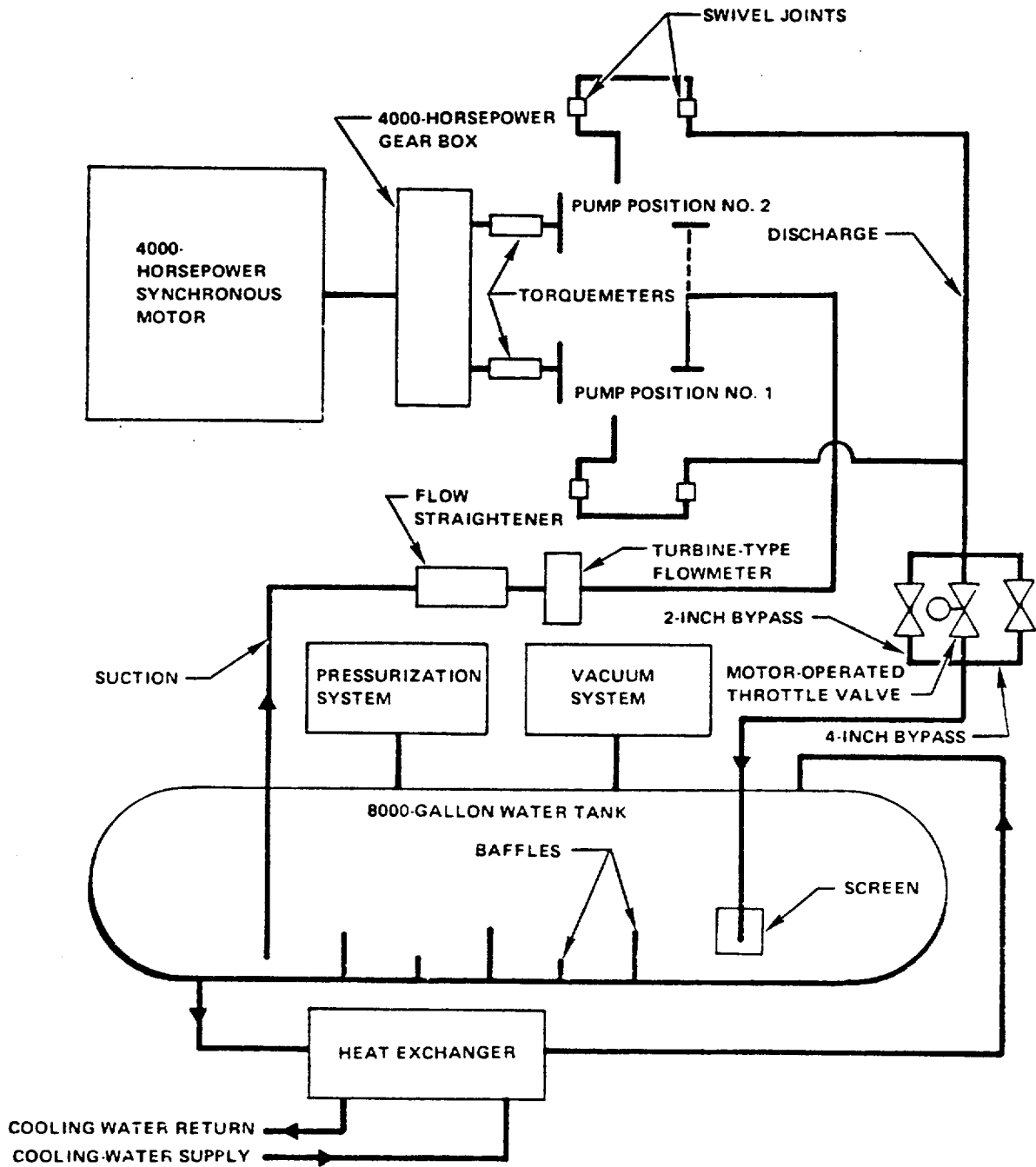
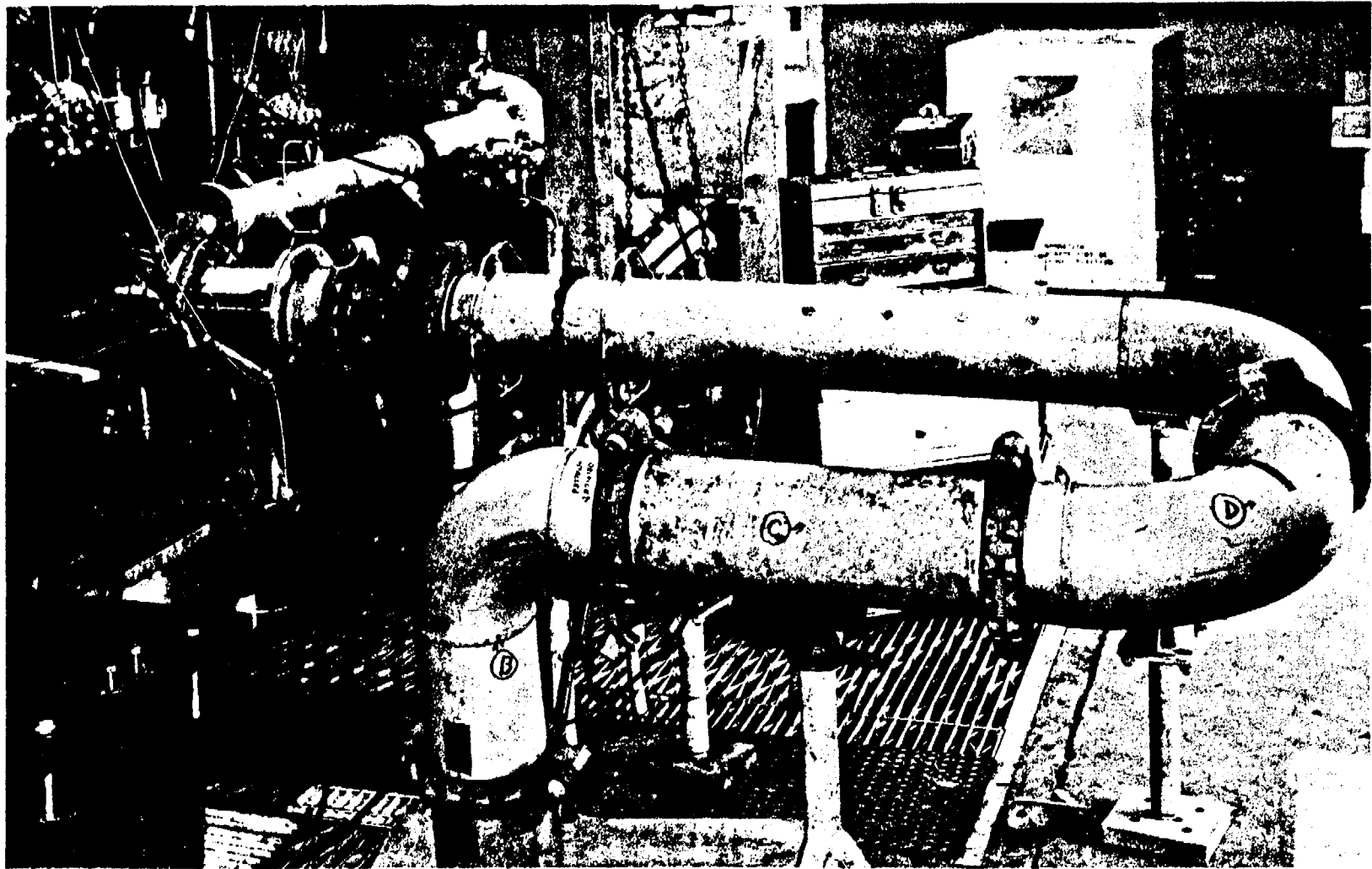


Figure 66. Model Pump Test Facility Schematic

inlet duct. Torque measurements are obtained by a Lebow torquemeter and recorded on Estaline Angus strip chart recorders (as well as the disk). Inlet and discharge pressures are measured via Teledyne Tabor strain gage transducers. Fluid temperatures are obtained by Rosemont platinum temperature sensors and recorded on the Autodata 9.

A typical inducer test setup in the model pump test facility is shown in Fig. 67. The water enters the facility through the floor at point A and flows through three bends. It then flows through a straightening section before entering the inducer. A steel tunnel is visible just upstream of the discharge volute. This tunnel is interchangeable with a clear plastic tunnel for motion picture coverage and visual observation. The flow from the inducer is collected by an existing vaned diffuser ring and scroll, and discharged into a 4-inch-diameter pipe which, in turn, discharges into the 6-inch discharge ducting.

The waterjet test facility configuration used for pump testing is shown in Fig. 68. The flow path of the water is indicated by the arrows marked on the facility. The water supplied by the tank flows through the vaned facility inlet elbow shown on the far left of the figure. The water is then directed into the pump inlet through a converging section, and it is turned by the guide vanes mounted in the pump inlet elbow before reaching the inducer. Fig. 68 shows the pump in its C configuration with a space provided for instrumentation behind the first stator. A piezometer ring is shown immediately behind the stator. A clear lucite housing covers the inducer and rotor sections of the pump. The pump section is anchored to the ground by a mounting pedestal and supported by two cradles on either end. The water exits the pump through the discharge housing which contains straightening vanes for removing whirl and a pseudo nozzle and pintle combination for accelerating the fluid. The water then passes through a 3-inch-diameter spool section which is followed by the facility diffuser section. Also shown in Fig. 68 are several pressure lines running from the static pressure ports in the pump to the transducers.



4MA45-9/7/78-C1A

Figure 67. Test Facility, Inducer-Only Test

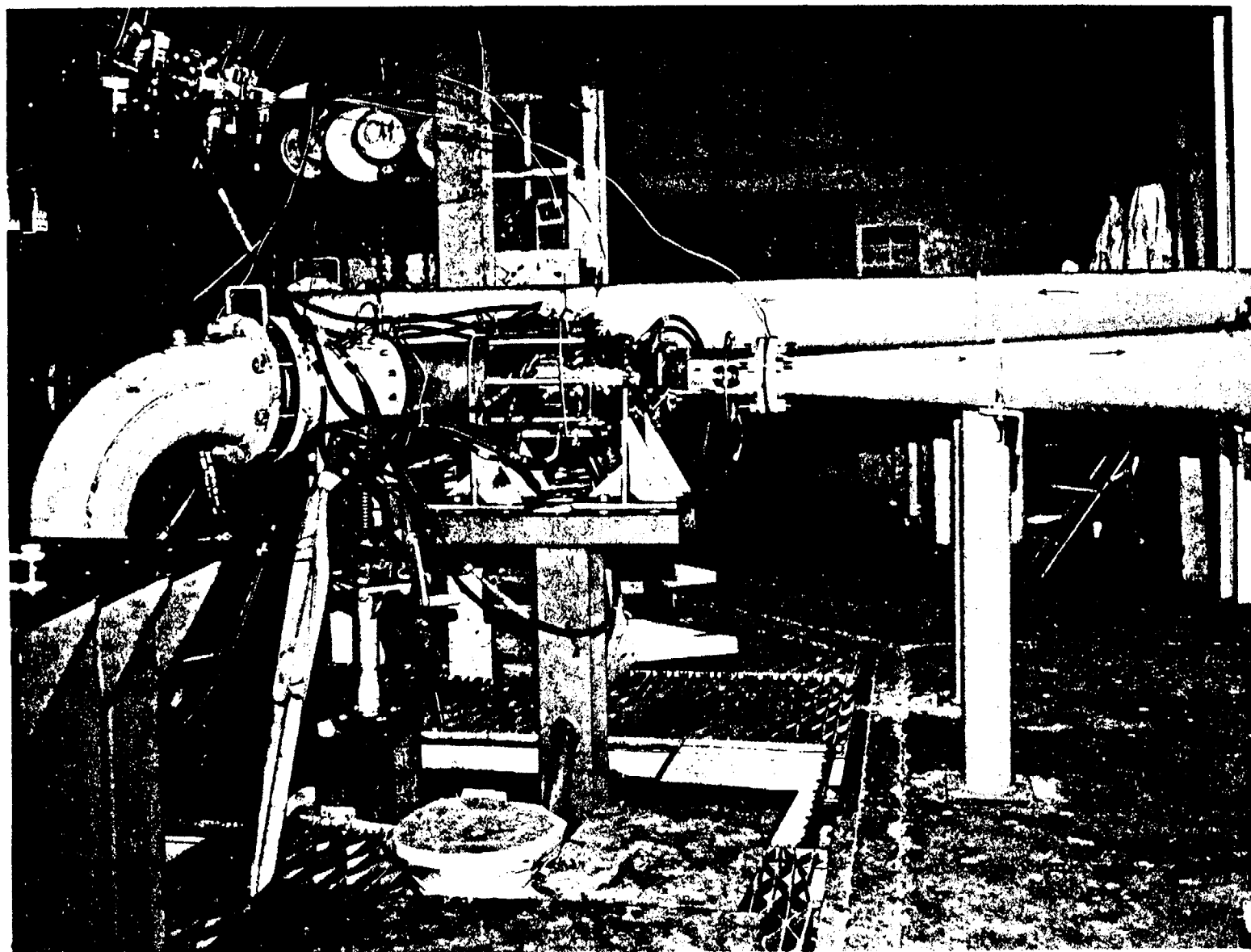


Figure 68. Model Pump Test Facility for Complete Pump Test

## PROBLEMS ENCOUNTERED

### Bearing Failure

After approximately 2 hours of pump testing (configuration C), the ball bearings (used to react the shaft axial thrust) failed. The calculated  $B_{10}$  life of the matched set of bearings is greater than 30 hours. The cause of the failure was determined to be inadequate lubrication flowrate. The lubrication pump was adjusted to provide an increased flow. The pump was subsequently operated for approximately 150 hours, with bearing changes at about 25-hour intervals, with no bearing failures.

### Kicker Excess Head Rise

During inducer only testing, the head rise of the inducer was measured and determined to be approximately 100 feet higher than design. The trailing edge of the kicker was trimmed, reducing the head to the design, however, this reduced the efficiency. The part was redesigned and retested with excellent results (see Test section).

### Straightening Vane Separation

During tests performed in January and February 1979, it was determined that the flow passing through the straightening vanes was separating, causing higher than expected losses. The part was redesigned and tested with sufficient performance to exceed the specified performance (see Test Results section).

### Facility Shaft Failure

The model pump was driven through a series of shafts consisting of the torquemeter output shaft, intermediate bearing package shaft, quill shaft (for most tests), and LSES main shaft. The splines used for the quill shaft were of such design that they allowed little misalignment (less than  $\pm 0.010$  inch). This caused problems throughout the test program. When installing the model pump, it was difficult to maintain this tight tolerance. On some occasions, the quill

shaft became very hot while operating. It was determined that a flexible element coupling would perform better. A design was initiated that would allow replacement of the intermediate bearing package shaft and quill shaft with a new bearing package shaft and a Rexnord flexible element coupling. While the design was in progress, the facility shaft just upstream of the quill shaft began to fail. A crack was initiated upstream of the drive splines which caused a shutdown of the facility due to vibration. Figure 69 shows the coupling and the location of the failure of both the facility and main shaft discussed below.

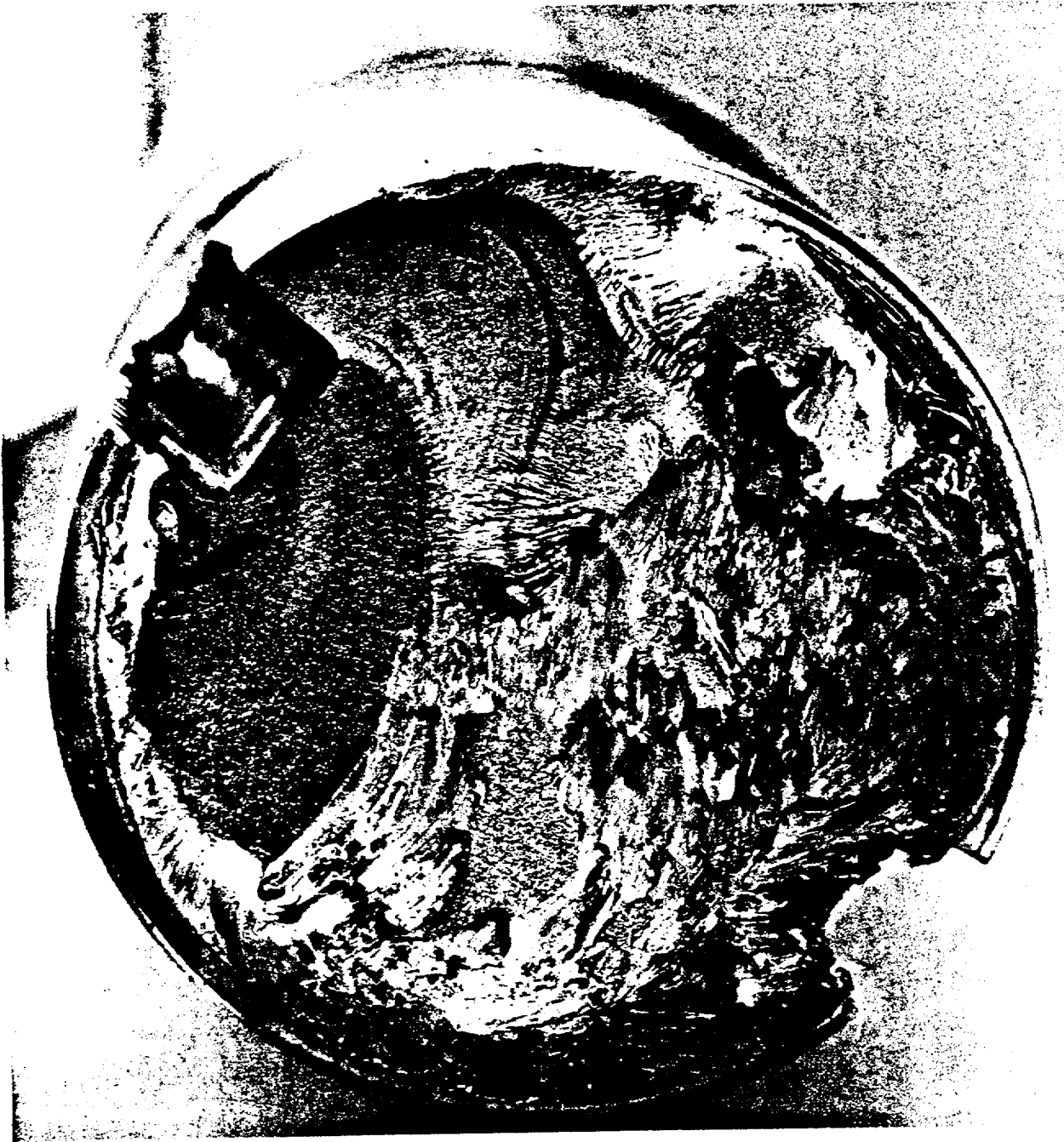
#### Main Shaft Failure

The flexible coupling discussed above was installed in early September 1979. While operating with the coupling, the vibration levels were significantly lower than with the quill shaft (2 g compared to 3 g). Approximately 27 additional hours of testing were logged when the vibration level began to climb from 2 g (p-p), the normal level, to greater than 5 g, which caused a malfunction shutdown. During the deceleration, the main shaft completely failed (Fig. 70). Analysis revealed that high cycle fatigue (initiated during quill shaft operation) caused the failure. The design of the shaft has been modified to increase the fatigue strength by removing stress risers such as threads, notches, and O-ring grooves.

#### Axial Rotor Optimization

The testing performed during the redesigned kicker verification revealed that the pump head was still slightly higher than design (20 feet). Analysis showed that the specified performance could be met, but that a lower head rotor would better match the ship performance goals. As a result, an effort to redesign the rotor and test it in parallel with other pump tests was funded by Rohr Marine. The performance of the redesigned rotor was excellent, as discussed in the Test Results section.





4MS45-10/19/79-C1A

Figure 70. Failed Shaft, End View

## TEST RESULTS

### Test Log

Table 14 presents a log of the model test program listing test numbers, dates, configurations, and types of tests for every test completed during the initial model program. The log is divided into 10 phases of consecutive tests. The first three phases were inducer-only tests. The subsequent seven phases were complete model pump tests. Each of these phases is summarized below in a chronological manner. The results are then presented in a subsequent section. The log shows the configuration tested in each phase.

Inducer-Only Tests (Full Blades and Kicker). The inducer test setup is shown in Fig. 67. Initial head-flow and cavitation tests of the inducer only (Phase 1) showed a head rise higher than predicted with suction performance less than predicted. The inducer leading edges were found to be thicker than designed by the Hydrodynamics Unit, so were reworked for thinning and finishing to the hydrodynamic designs. This thinning and finishing process was done in two steps with a test sequence (Phase 2) between the two. Subsequent tests (Phase 3) verified that the inducer head was higher than predicted, and the suction performance was essentially as predicted. The kicker was not trimmed to try to match the design head until the complete model pump testing was initiated to provide head margin potential if required.

### Complete Model Pump Tests.

Original Configuration. The pump test setup is shown in Fig. 68. Pump instrumentation was extensive including multiple pressure ports, both static and total. The instrument locations are shown in Fig. 65. In initial pump tests (Phase 4), the kiel probes moved radially outward during the test, providing unreliable data. The probes were subsequently brazed in the fittings to provide permanent radial positioning. The tester thrust bearings failed due to lack of lubrication, ending Phase 4. Test results showed a head rise higher than predicted at both the kicker and the overall pump discharge.

TABLE 14. LSES MODEL PUMP TEST PROGRAM TEST LOG

TEST PHASE	TEST NUMBER	TEST DATE	CONFIGURATION	TYPE OF TEST	COMMENTS
1	78A07	7/21/78	A	CAV	INDUCER VARIFICATION TESTS
	78A09	7/22/78	A	H-Q, CAV	
	78A10	7/22/78	A	YAW AT KICKER OUTLET	
2	78A15	8/10/78	A	H-Q, CAV	LEADING EDGE THICKNESS REWORKED
	78A16	8/11/78	A	H-Q, CAV	
	78A17	8/11/78	A	H-Q, CAV	
	78A18	8/15/78	A	CAV	
	78A19	8/16/78	A	H-Q	
	78A20	8/16/78	A	CAV	
	78A21	8/17/78	A	CAV	
3	78A29	8/30/78	A	H-Q, CAV	IMPROVED FINISH, BROUGHT LEADING EDGE THICKNESS TO HYDRO DESIGN
	78A30	8/30/78	A	YAW AT KICKER OUTLET	
	78A31	8/31/78	B	CAV	INDUCER PERFORMANCE ESTABLISHED

TABLE 14. (Continued)

TEST PHASE	TEST NUMBER	TEST DATE	CONFIGURATION	TYPE OF TEST	COMMENTS
3	78A33	8/31/78	B	20 MIN DYE TEST	NO DAMAGE
	78A34	9/ 1 /78	B	20 MIN DYE TEST	
	78A35	9/ 2/78	B	25 HR CAV	
	78A36	9/ 4/78	B	25 HR CAV	
4	78A63	11/7/78	C	H-Q	KIEL PROBES WERE NOT STATIONARY IN THE FITTINGS, DATA NOT RELIABLE
	78A64	11/8/78	C	CAV	
	78A65	11/9/78	C	CAV	KIEL PROBES SOLDERED TO FITTINGS MODEL PUMP BEARING FAILURE
	78A66	11/9/78	C	CAV	
	78A67	11/10/78	C	KIEL SURVEY AT STATOR (KY6) AND STRAIGHTENING VANE (KY8) OUTLETS	
5	78A72	11/28/78	C	KIEL SURVEY AT STATOR OUTLET (KY6)	SURVEY TO MID-CHANNEL (WEDGE PROBE, NO HUB GROOVE)  KICKER TRIM 1
	78A73	11/28/78	C	CAV	
	78A74	11/30/78	C	YAW SURVEY AT STRAIGHTENING VANE OUTLET (KY8)	
	78A75	12/1/78	C	YAW SURVEY AT STATOR OUTLET (KY6)	
	78A76	12/7/78	G	YAW SURVEY AT KICKER OUTLET (KY12)	
	78A77	12/7/78	G	20 MIN. DYE TEST AND H-Q	
	78A78	12/11/78	G	H-Q AND 20 MIN. DYE TEST	
	78A79	12/12/78	G	YAW SURVEY AT KICKER OUTLET (KY12)	

TABLE 14. (Continued)

TEST PHASE	TEST NUMBER	TEST DATE	CONFIGURATION	TYPE OF TEST	COMMENTS
5	78A80	12/15/78	G	YAW SURVEYS AT KICKER (KY12) AND STRAIGHTENING VANE (KY8) OUTLETS, H-Q AND 20 MIN. DYE TEST	KICKER TRIM 2, STRAIGHTENING VANE TRIM 1, NOZZLE MOD 1
	78A81	12/21/78	G	30 MIN REFERENCE TEST, YAW SURVEY AT KICKER OUTLET (KY12), 20 MIN. DYE TEST AND H-Q	KICKER TRIM 3
	79A01	1/ 5/79	G	H-Q AND YAW SURVEYS AT AXIAL ROTOR OUTLET (KY19)	
6	79A16	4/ 6/79	D	H-Q	INTRODUCED 8 KIEL PROBES AT STRAIGHTENING VANE OUTLET
	79A17	1/ 6/79	D	H-Q, H-Q	8 KIEL PROBES NEAR HUB
	79A18	1/ 6/79	D	YAW SURVEY AT AXIAL ROTOR OUTLET (KY5)	8 KIEL PROBES NEAR TIP, 8 KIEL PROBES AT MID CHANNEL
	79A19	2/ 7/79	F	20 MIN. DYE TEST	8 KIEL PROBES AT MID CHANNEL
	79A20	2/ 9/79	F	20 MIN DYE TEST	
	79A21	2/10/79	F	H-Q, CAV AND LIFE TESTS	COMPLETED 4 HRS. OF LIFE TEST (6 HOURS CUMULATIVE)
7	79A40	4/ 3/79	G	H-Q	INTRODUCED REDESIGNED KICKER
	79A41	4/ 4/79	G	H-Q	KIEL SURVEYS AT STRAIGHTENING VANE AND KICKER OUTLETS
	79A42	4/ 5/79	G	CAV	KIEL SURVEYS AT STRAIGHTENING VANE AND KICKER OUTLETS
	79A43	4/ 5/79	G	CAV	

TABLE 14. (Continued)

TEST PHASE	TEST NUMBER	TEST DATE	CONFIGURATION	TYPE OF TEST	COMMENTS
7	79A44	4/ 6/79	G	YAW SURVEY AT KICKER OUTLET (KY12)	INTRODUCED COBRA PROBE FACILITY LUBE PUMP FAILURE
	79A45	4/10/79	G	YAW SURVEY AT KICKER OUTLET (KY12)	
	79A46	4/11/79	G	YAW SURVEYS AT KICKER OUTLET(KY12)	
	79A47	4/13/79	D	YAW AND KIEL SURVEYS AT AXIAL ROTOR OUTLET (KY5 and KY6)	
8	79A55	5/ 5/79	C	H-Q AND CAV	8 STATOR DISCHARGE KIEL PROBES AT HUB, TIP AND MID CHANNEL FOR H-Q TESTS
	79A56	5/ 7/79	C	YAW SURVEYS AT STATOR OUTLET(KY21)	8 KIEL PROBES AT MID CHANNEL
	79A57	5/ 8/79	C	YAW SURVEYS AT STATOR OUTLET(KY20)	8 KIEL PROBES AT MID CHANNEL
	79A58	5/ 9/79	C	YAW SURVEYS AT STATOR OUTLET(KY19)	8 KIEL PROBES AT MID CHANNEL
9	79A93	5/28/79	D	CAV AND H-Q	INTRODUCED REDESIGNED AXIAL ROTOR STRAIGHTENING VANE, NOZZLE MOD 2 8 KIEL PROBES AT MID CHANNEL AND NEAR TIP FOR H-Q TESTS
	79A94	6/28/79	D	H-Q	8 KIEL PROBES NEAR HUB
	79A95	6/29/79	D	YAW SURVEY AT STRAIGHTENING VANE(KY8)	OTHER 7 KIEL PROBES AT MID CHANNEL, YAW PROBE BENT, NO DATA
	79A96	7/ 3/79	D	YAW SURVEY AT STRAIGHTENING VANE(KY8)	OTHER 7 KIEL PROBES AT MID CHANNEL, DABBED PAINT ON HUB, YAW PROBE BROKE
					STRAIGHTENING VANE HOUSING ROTATED 2.5 DEGREES
	79A98	7/10/79	D	YAW SURVEY AT STRAIGHTENING VANE (KY8)	OTHER 7 KIEL PROBES AT MID CHANNEL
	79A99	7/11/79	D	YAW SURVEY AT STRAIGHTENING VANE (KY17)	OTHER 7 KIEL PROBES AT MID CHANNEL, YAW PROBE BROKE
	79A100	7/12/79	D	YAW SURVEY AT AXIAL ROTOR OUTLET (KY19)	YAW TRAVERSE UNIT MALFUNCTION, NO USEFUL DATA

TABLE 14. (Concluded)

TEST PHASE	TEST NUMBER	TEST DATE	CONFIGURATION	TYPE OF TEST	COMMENTS
9	79A101	7/13/79	D	YAW SURVEY AT AXIAL ROTOR OUTLET(KY19)	COMPLETED 17.5 HRS OF LIFE TEST, MODEL PUMP BEARING ACCEL. READING TERMINATED LIFE TEST
	79A102	7/19/79	G	20 MIN DYE TEST	
	79A103	7/21/79	F	CAV, H-Q, START OF LIFE TEST	
	79A104	7/21/79	F	CONCLUSION OF LIFE TEST	
10	79A141	9/5/79	F	H-Q, CAV, START OF LIFE TEST	COMPLETED 11 HRS OF LIFE TEST COMPLETED 11 HRS OF LIFE TEST AT 105 PERCENT HUMP FLOW COMPLETED 2 HRS OF LIFE TEST THEN PUMP SHAFT BROKE AT DRIVE SPLINE
	79A142	9/7/79	F	CONCLUSION OF LIFE TEST	
	79A143	9/19/79	F	H-Q, CAV, LIFE TEST	
	79A144	9/20/79	F	H-Q, CAV, LIFE TEST	

The kicker was trimmed during Phase 5 three times to reduce the head rise. Tests showed the head was still higher than design and that the trimming process led to a nonoptimum design profile which impacted efficiency. Thus, it was decided to redesign the kicker to achieve the design head with the design efficiency.

Initial yaw probe surveys at the straightening vane discharge indicated overturning. The straightening vanes were trimmed to provide an axial discharge flow. Subsequent yaw probe surveys indicated underturning.

Test data downstream of the straightening vane had indicated some variances which led to a suspicion that the vane wakes were larger than expected. It was decided that additional kiel probes were needed to provide sufficient data to completely map the vane-to-vane head profile from hub to tip to establish the actual wake profiles. Kiel probe surveys with eight circumferential and three radial positions were added (Phase 6). The radial positions were varied from test to test. These 24 total pressure readings were then used to characterize the wakes. They indicated large wakes with significant head gradients downstream of the trimmed straightening vane. Yaw probe surveys also were performed at the rotor discharge and indicated the head was higher than predicted and relatively uniform. It was decided to redesign the axial rotor to optimize the head generation of the pump for the 3K SES, and the straightening vane was redesigned to achieve more margin for boundary layer separation and to improve performance. A 4-hour life test was performed to evaluate life characteristics. It showed significant cavitation damage on the stator suction surface at the leading edge root with the trimmed kicker. Further life testing was delayed until the redesigned kicker could be installed.

Redesigned Kicker Configuration. For Phase 7, the redesigned inducer kicker was introduced. A cobra-head yaw probe was used instead of the wedge probe to reduce channel blockage and attempt to get better angle measurements. Yaw surveys at the kicker discharge indicated a head rise for the overall inducer that was satisfactory. Yaw surveys at the stator discharge were performed in Phase 8 to provide input data to be used in the axial rotor redesign.

Redesigned Axial Rotor and Straightening Vane. Phase 9 was initiated with the redesigned axial rotor and straightening vane. With the changed number of vanes in the stator row, only four relative positions were recorded at the straightening vane discharge between the suction and pressure surface trailing edges. The outer housing serving as a probe ring was machined to be rotated 2.5 degrees circumferentially to provide for the total eight positions. Tests showed the average head at the straightening vane discharge was predicted. Paint tests were performed to help evaluate flow direction in the nozzle, and they showed axial flow at the hub and tip downstream of the straightening vane. Yaw surveys confirmed the near-axial flow at the tip. Cobra probes failed in the high velocity and turbulent flow at the straightening vane discharge, preventing yaw surveys to the hub.

A total of 42 hours of life testing was achieved in Phase 10 at the hump flow conditions. Modifications to the stator profile to meet nominal dimensions and to reduce fillet radii eliminated stator erosion after 29 hours of testing.

Testing was terminated by fatigue failure of the tester shaft at the drive spline.

### Overall Performance

The final model configuration included redesigns of the kicker blade row of the inducer and the axial rotor to reduce pump head and redesign of the straightening vane to provide more margin against separation. The overall average head rise versus flowrate for the model pump is shown in Fig. 71. This head is based on the average of the multiple kiel probe readings downstream of the straightening vanes and just upstream of the nozzle. Thus, this head represents the head at the nozzle, the loss in head between the measurement point, and the nozzle itself being only approximately 2 feet. The average head rise was 885 feet at the model design flowrate of 3435 gpm. The average overall efficiency versus flowrate is shown in Fig. 72 as determined from the head, flow, and torque from the torquemeter. Average efficiency at design flow was 81.5%.

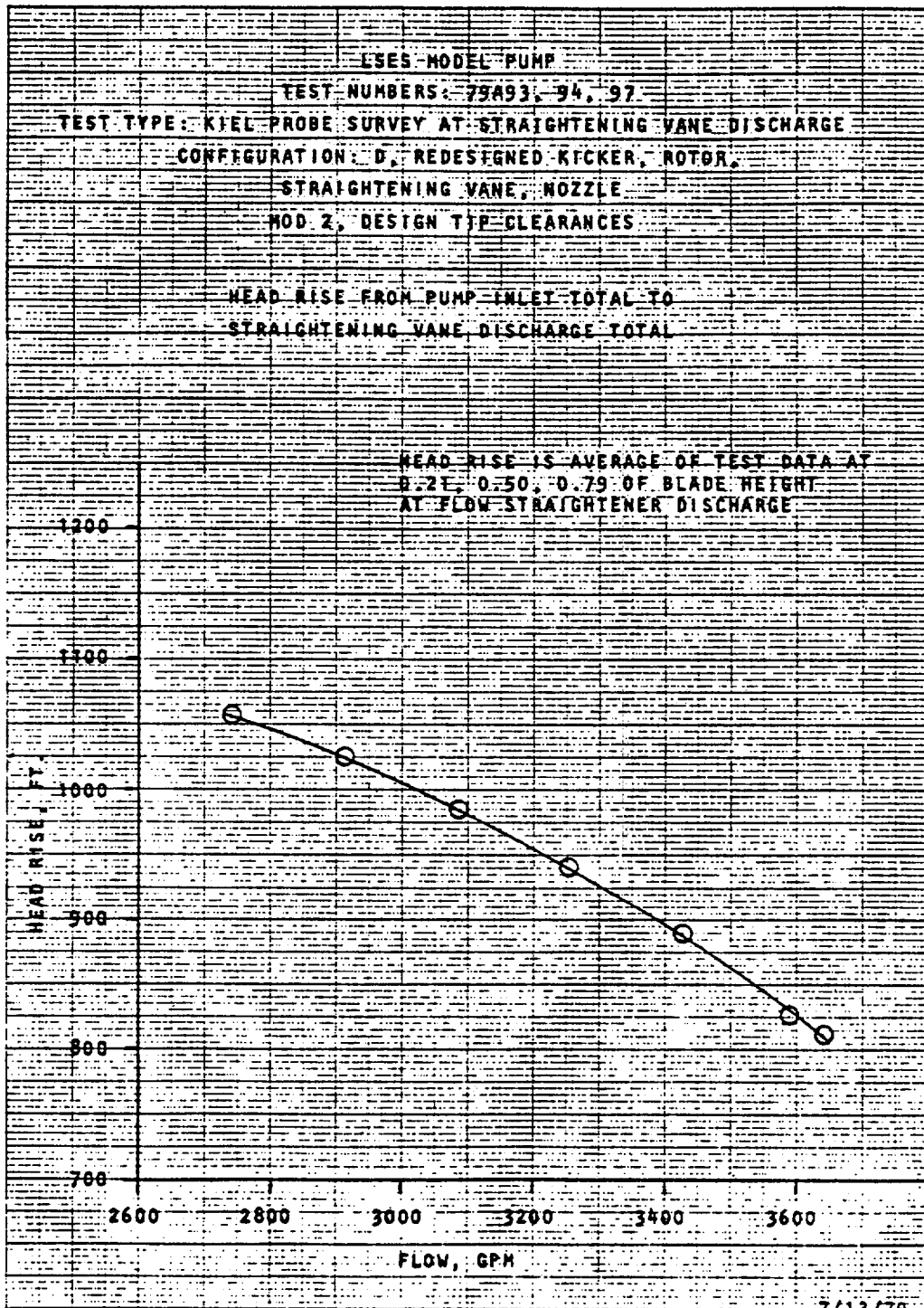


Figure 71. Pump Head Rise Versus Flowrate

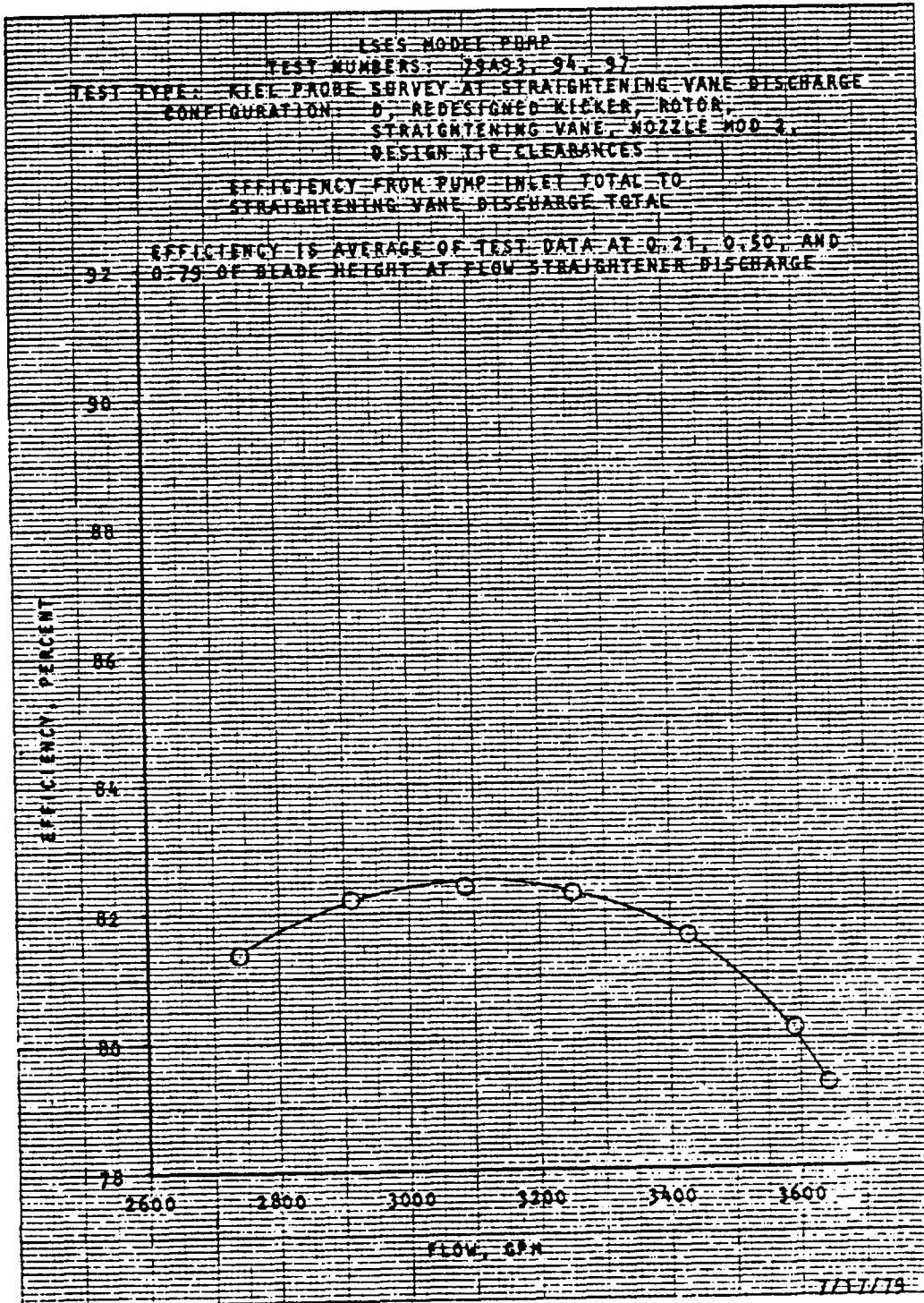


Figure 72. Pump Efficiency Versus Flowrate

Average head rise and efficiency were determined from the pump inlet flange total pressure and the average total pressure at the straightening vane discharge. Eight circumferentially equally spaced kiel probe positions with two circumferential orientations were used downstream of the redesigned straightening vane. At each position, total pressure was measured at three radial positions: 21, 50, and 79% of the channel height. The average of the 24 total pressure measurements (8 circumferential and 3 radial) were used to determine performance. The model pump performance does not include a loss due to vertical head from the inlet flange to the inducer centerline because the model pump has a horizontal inlet. This, and a factor for nozzle loss, are included in projections for full-size performance.

Based on the model pump performance and characteristics of both the model and full-size pump, the performance of the full-size pump can be projected with good confidence in the result. This is shown in Table 15 with explanations of each step included below.

TABLE 15. PROJECTED FULL-SIZE 3K SES PERFORMANCE

	Head, feet	Efficiency, %
Measured Model Performance	885	81.6
Model to Full-Size Hydrodynamic Correction	+17.3	+1.7
Model to Full-Size Parasitic Loss Correction	-	+1.0
Model to Full-Size Elevation Loss Correction	-3.8	-0.3
Predicted Full-Size Performance With Separation	898.5	84.0
Predicted Full-Size Performance Without Separation	926.5	86.6

The model performance shown is the same as quoted above. The hydrodynamic correction in going from model to full size is due to Reynold's numbers effects and surface finish in scaling the pump. The corrections have been calculated directly by the Rocketdyne axial flow pump performance computer program which

has size and hydrodynamic parameters as input and calculates each individual hydrodynamic loss through the pump. This correction is believed to be well founded in theory and based on previous comparisons may even be somewhat conservative. The parasitic loss comparison is due to difference between the two pumps in the bearing and seal area. The model pump has two extra bearings as compared with the full size, and there was no attempt to scale the bearings and seals in the model. The calculated full-size efficiency gain was 1.2 points, but this was conservatively rounded off to only 1.0 point.

The elevation loss is due to the elevation difference between the pump centerline and the inlet elbow inlet centerline on the full size, whereas the model had a horizontal inlet elbow. These corrections lead to the indicated full-size performance assuming that the full-size pump has a separation problem in the straightening vane just like the model. However, boundary layer calculations have shown that the full-size pump should not experience separation even though the model does (analytically and experimentally). Straightening vane losses without any wakes were calculated (as presented in another section). This would improve the head rise by 47 feet. However, there will be some wakes even without separation, and these are estimated to cost between 1 and 2% of the overall head rise. Using the larger number, an additional wake loss of approximately 19 feet of head was estimated. Thus, the net effect of no separation in the full-size straightening vane would be a gain of 28 feet of head and 2.6 points of efficiency. Factoring in these benefits leads to the bottom line of Table 15 and a conservative estimate of the expected performance of the full-size pump. Rocketdyne's pumps would provide the required thrust even with the head and efficiency shown with separation. If the performance shown in the last line of Table 15 without separation, is achieved, a comfortable margin is provided.

Figure 73 presents the pump static pressure distribution along the wall from pump inlet to the nozzle. The pressures were determined by subtracting the pump inlet static pressure from static pressures measured along the outer diameter. The pressure rise is seen to be monotonically increasing throughout the pump until the straightening vanes are reached. There is one decrease in

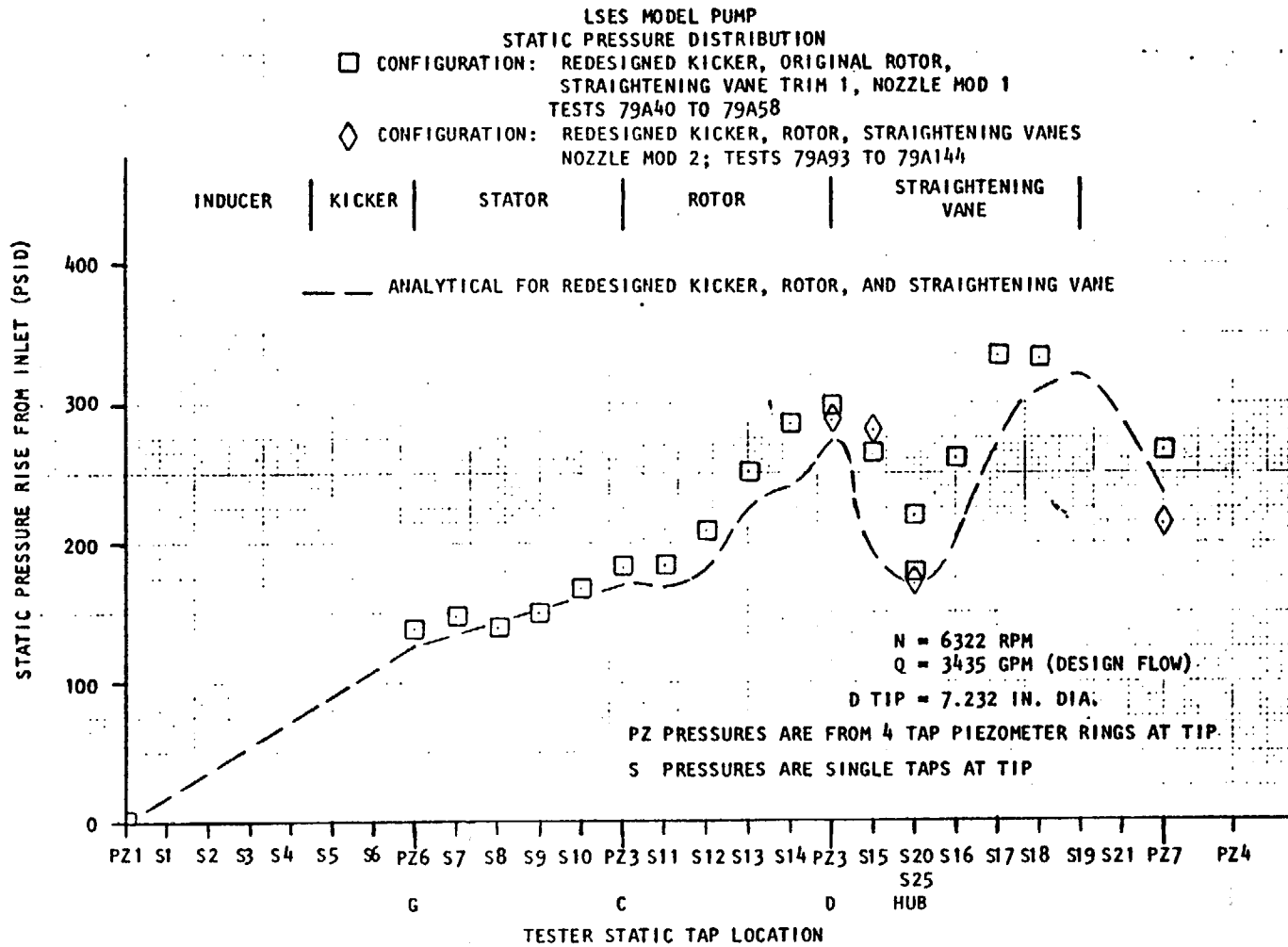


Figure 73. Static Pressure Distribution

pressure at the inlet of the straightening vane to help control axial thrust, and then the pressure drops again as the flow is accelerated in approaching the nozzle. The agreement of the data with analysis is seen to be good.

Suction Performance. Suction specific speed versus flow ratio for the final configuration is shown in Fig. 74. Characteristic lines are shown for the break point with no head falloff due to cavitation and for 5, 10, and 20% head falloff. This suction performance is based on an average of numerous tests run during Phases 7 through 9 of the test program. Some previous tests during Phases 4 and 5 had indicated better suction performance, but some test-to-test variations were noticed. It is believed that these variations are primarily a function of the model pump and, particularly, the small clearances required which are difficult to achieve. In fact, the model pump has shown evidences of rubbing during testing which has actually changed the clearances during the test process. Thus, the suction performance shown in Fig. 74 is believed to be conservative relative to the full-size pump. The suction performance does exceed the requirement of minimum suction specific speed of 24,000 rpm at the hump flow ratio of 0.95. Figure 75 shows the suction performance achieved during earlier tests and is believed to be more representative of full-size capability.

Life Testing. A total of 42 hours of life testing was accomplished during Phases 9 and 10 on the final configuration at hump flow and TIH conditions. Thirty-one hours were at a design flow ratio of 0.95 (3263 gpm) and suction specific speed of 24,000 rpm. Eleven hours were at 105% of the 0.95 flow ratio (3426 gpm) and suction specific speed of 24,927 rpm. This latter operating point was selected to investigate the life characteristics at a flow condition of 105% of the design value, which has potential benefits for ship operation.

The first test series accumulated 18 hours at 3263 gpm and 24,000 rpm suction specific speed. No cavitation damage occurred on the redesigned straightening vanes. Minor frosting was observed on a few of the inducer, kicker, and axial rotor blades, but no consistent pattern was observed, and the long life of the part is ensured. Minor cavitation damage was observed on the stator suction surface near the leading edge fillet (which is at the outer diameter). Modifications were made to six vanes to correct the suction surface leading edge profile

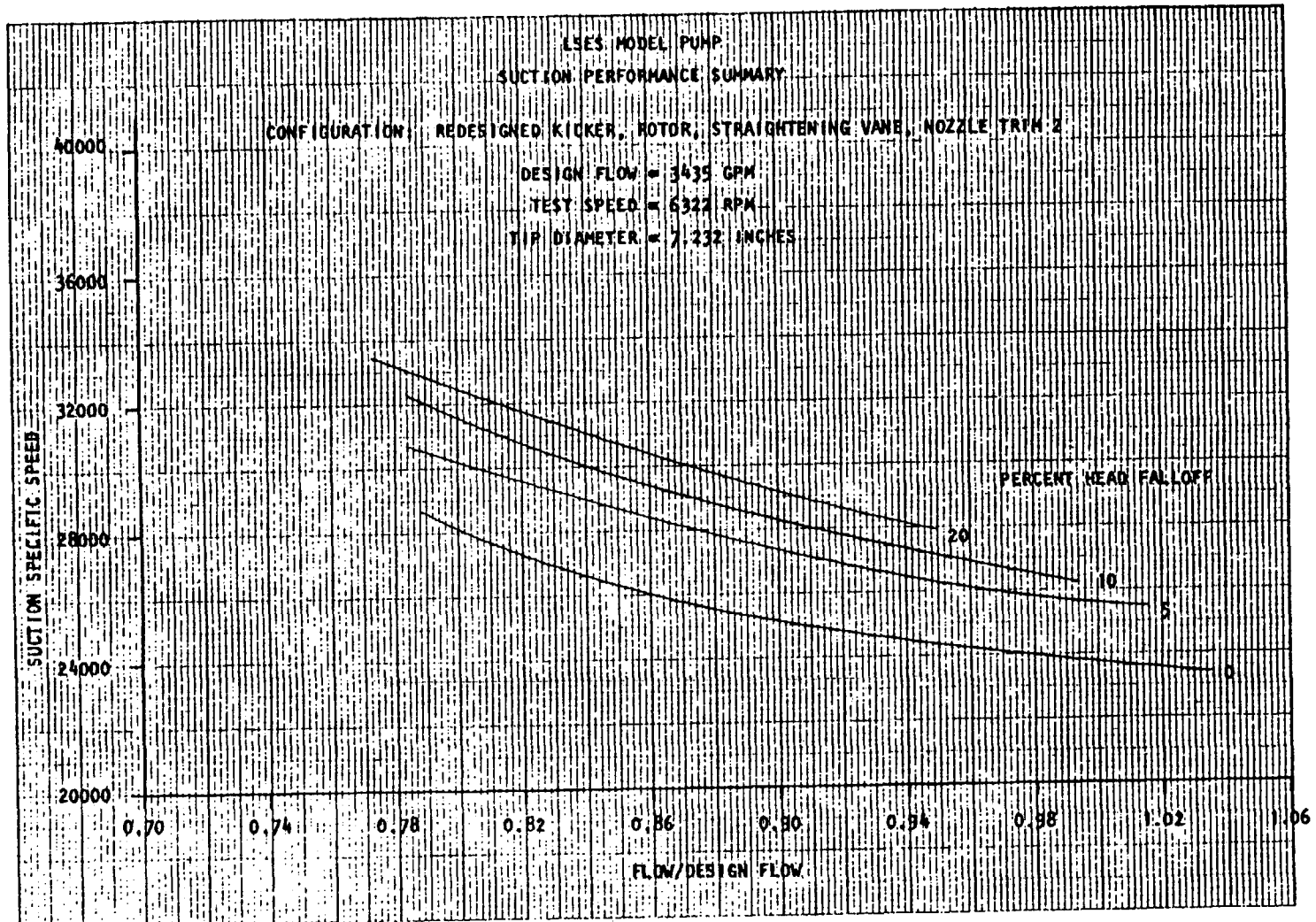


Figure 74. Current Model Suction Performance

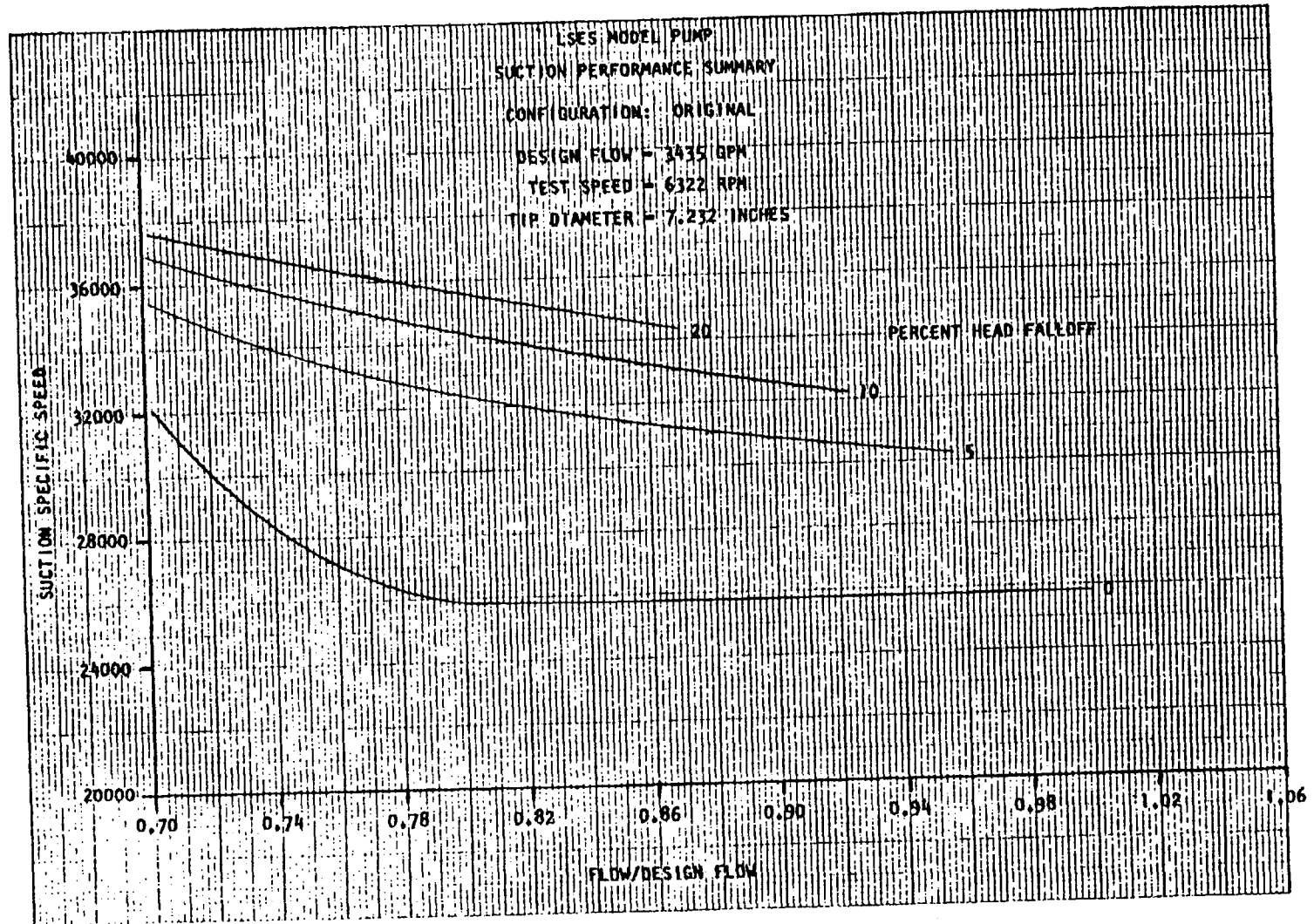


Figure 75. Projected Full-Scale Suction Performance

contour to the design nominal contour (Fig. 76). Modifications (Mod 1) were made to six other vanes to correct the contour and reduce the fillet radii.

The second test series accumulated 11 more hours at 3263 gpm and 24,000 rpm suction specific speed. The unmodified vanes showed increased damage. The vanes with only leading edge modification showed a moderate increase in damage. Vanes with modified leading edges and fillets showed slight to no damage. Three of the previously unmodified vanes were smoothed at the leading edge and modified (Mod 2) with the smaller fillets.

The third test series ran for 11 hours at the new hump flow condition of 3426 gpm and 24,927 rpm suction specific speed. Only one vane showed a slight increase in damage.

The fourth life test series was terminated after 2 hours by the tester shaft failure. Very light damage was noted on one stator vane.

Life tests have shown that when the model stator vanes were modified to the original design contour and reduced fillet radii, cavitation damage was either nonexistent or minimal. Operating at the new 105% hump flow condition almost eliminated stator cavitation damage completely. Based on these results, the full-size 3K SES waterjet is expected to be able to operate over the full projected life with no detriment to performance due to cavitation damage.

### Inducer

Inducer-Only Tests. The SES model inducer was first tested in Rocketdyne's 8000-gallon closed-loop water test facility as an individual component. Figure 77 shows the model inducer instrumented and installed in the test facility. Head-flow, cavitation, and yaw survey tests were conducted in Phase 1. Following these tests, the leading edges of the inducer were thinned to improve suction performance.

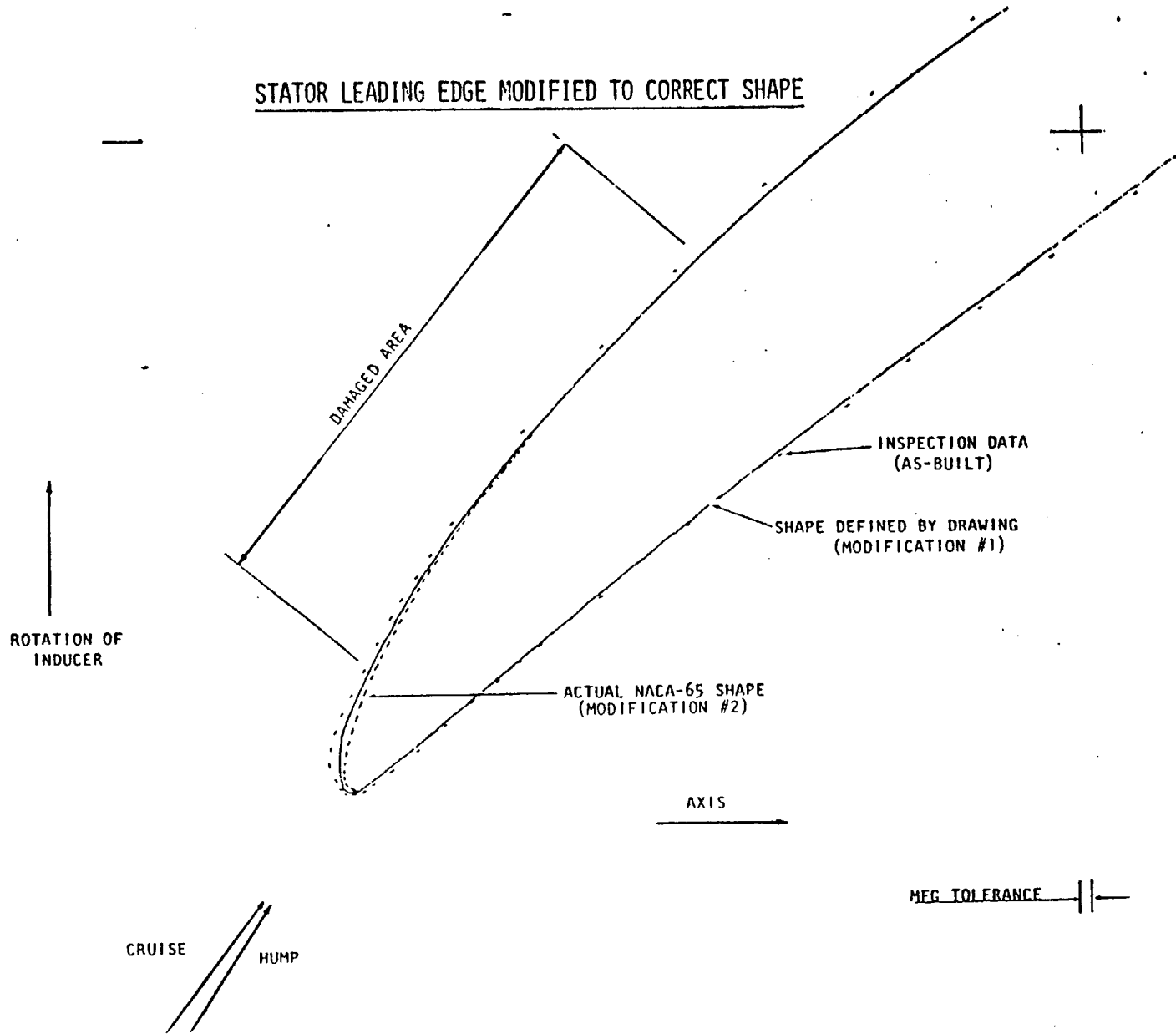
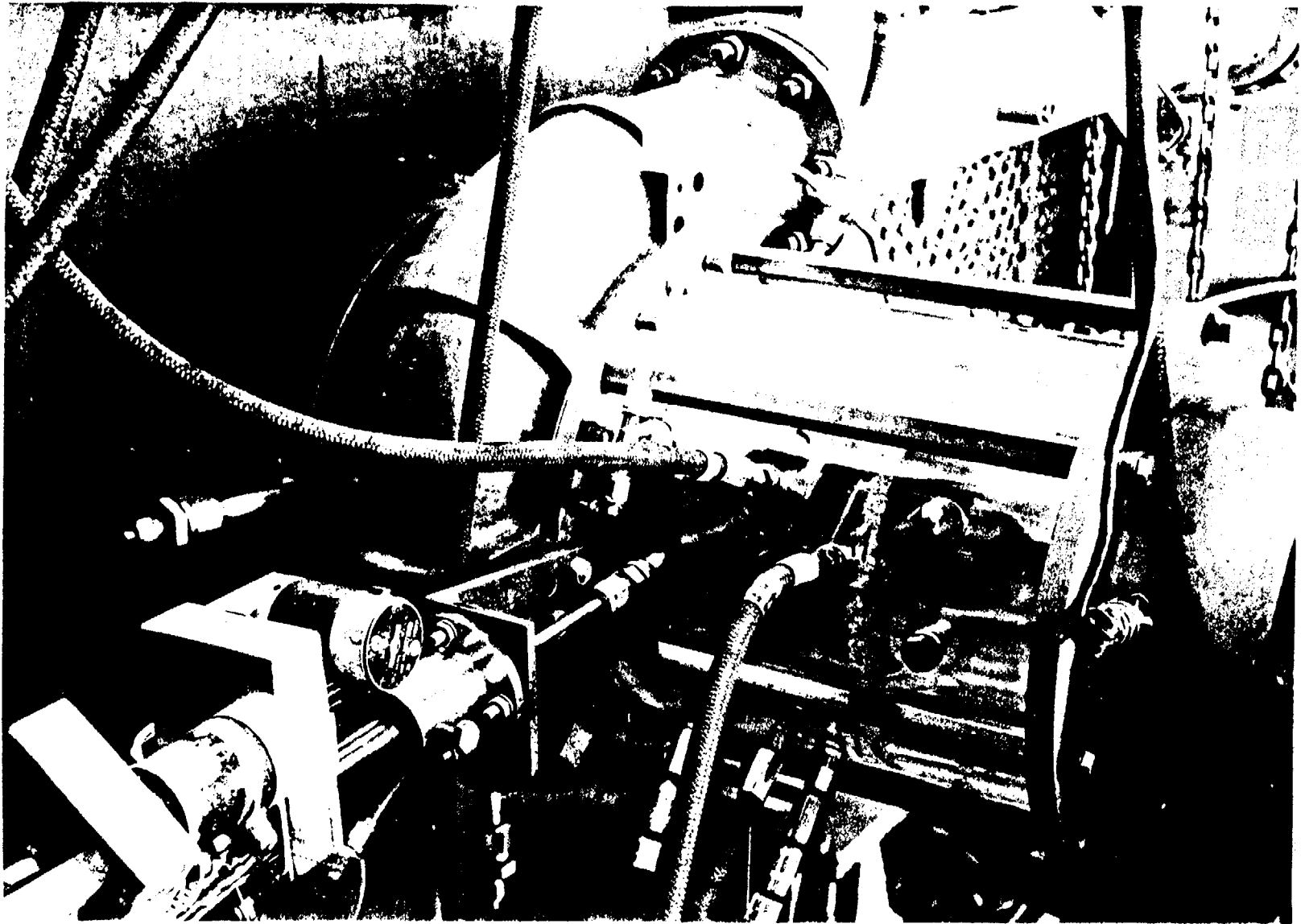


Figure 76. Stator Modifications



4MA44-7/24/78-C1C

Figure 77. Inducer Only -Plastic Housing

In Phase 2, head-flow and cavitation tests were conducted, additional thinning was done posttest to improve the leading edges to the hydrodynamic design requirements.

During Phase 3, head-flow, cavitation, yaw survey, and 20-minute dye tests were conducted verifying the inducer performance.

Figure 78 shows representative head rise and efficiency results for the inducer-only configurations tested in Phase 2. The head rise is actually 16% higher than the predicted at the cruise flow condition. The slope of the curve is flatter than predicted at lower flows and approaching the design slope at the cruise flow. The inducer efficiency also shows more slope change than predicted, but it exceeds the design prediction in the operating region.

Rework of the inducer leading edges had very little effect on the inducer head rise or efficiency as expected.

In addition to making the blade thickness of the model inducer agree with design specifications, reducing the leading edge thickness improved the suction performance. Suction specific speed versus flowrate for Phase 3 is shown in Fig. 79. The suction performance at 95 and 100% of design flow is significantly better than the final suction performance presented in the previous section. The suction performance at 90% of design flow is comparable in these tests with that of the final tests.

Thinning the leading edges did not significantly affect the yaw survey results. A wedge probe (United Sensor part number W-250-24-CD) was used to survey at the kicker discharge. Total and static pressures and fluid flow angles were measured at six equally spaced radial positions. Figure 80 presents the head rise at the kicker discharge as a function of model radius. The head was designed to be uniform from hub to tip, and uniformity was achieved over most of the blade height. However, at the tip, a significant drop in head was measured but may be at least partially due to wall boundary layer interference problems. The

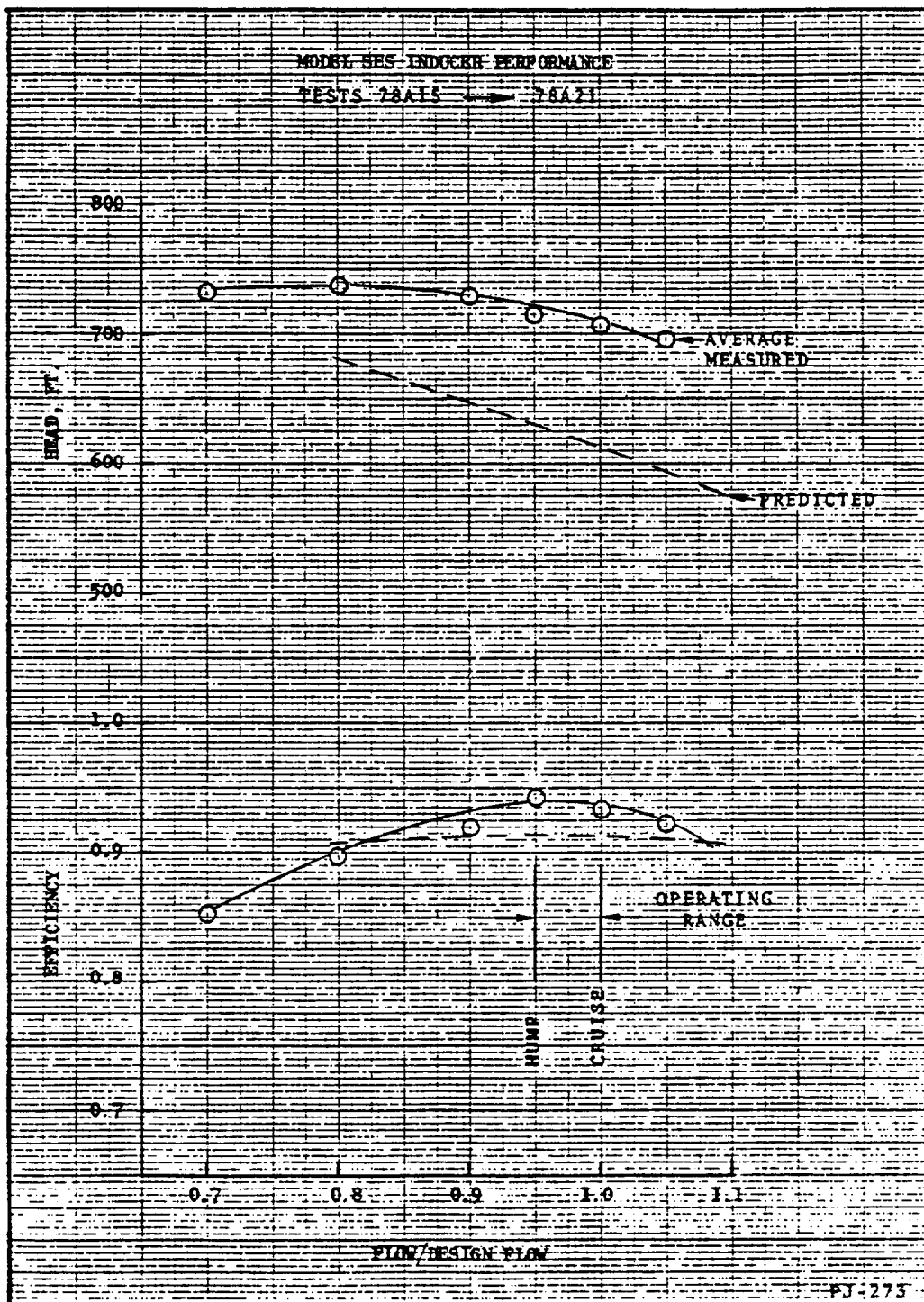


Figure 78. Inducer Performance

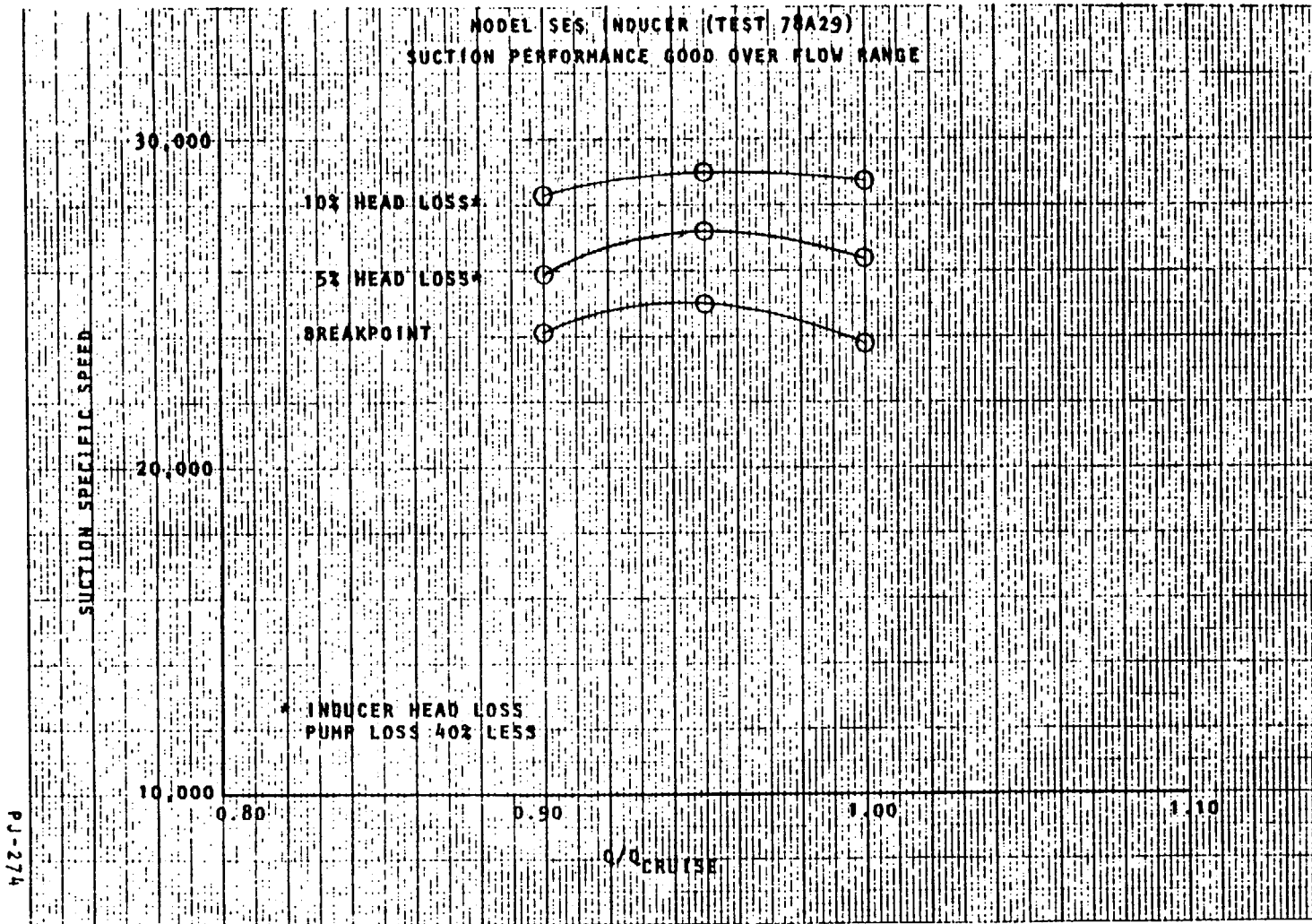
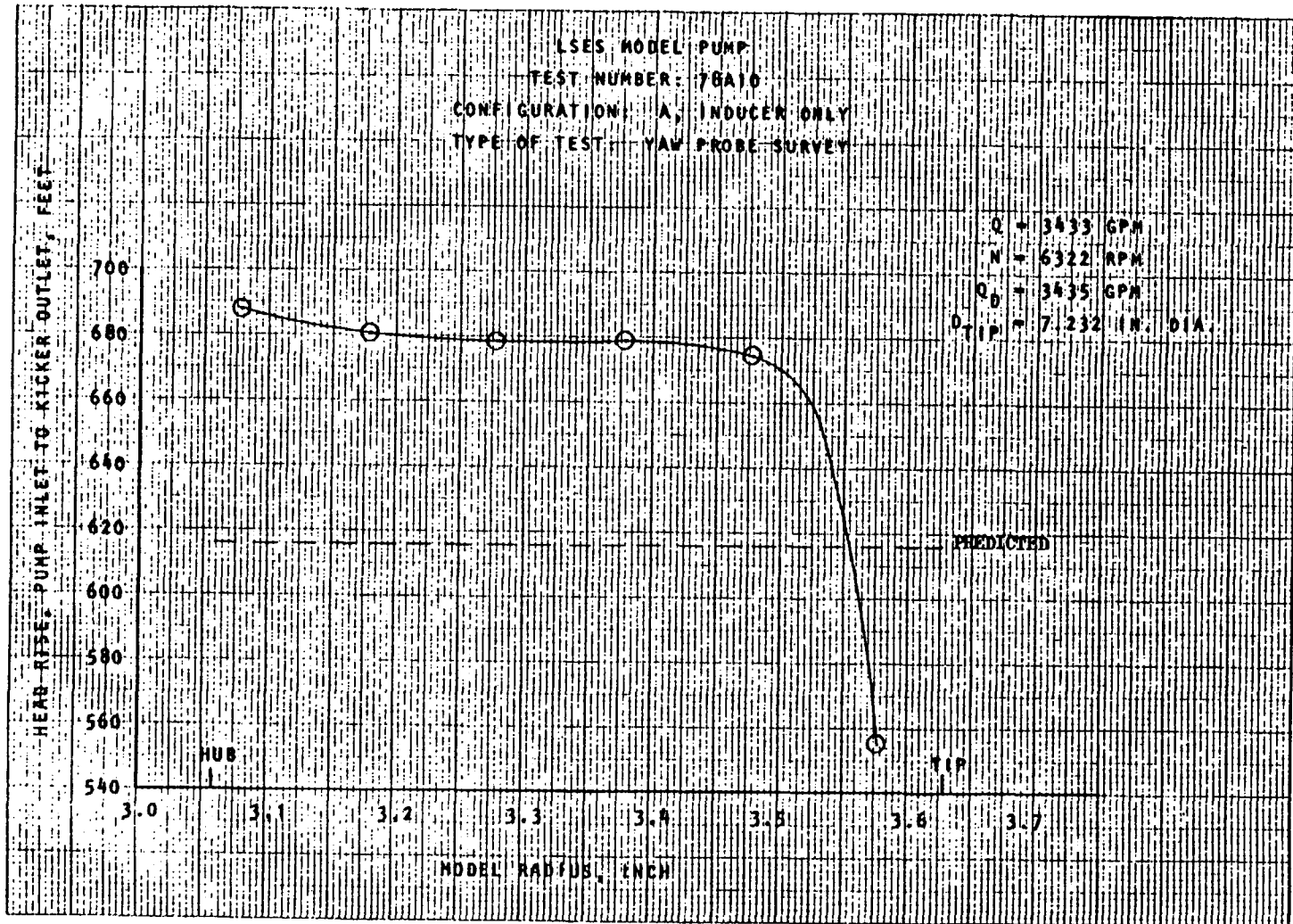


Figure 79. Inducer Suction Performance



absolute fluid angle measured from tangential versus model radius is shown in Fig. 81. The slope of the curve is parallel to predicted, but the angle is more tangential as expected, with the head rise being significantly higher than predicted.

To determine areas of potential cavitation damage, a water insoluble dye was applied to the inducer full blades. Figure 82 shows the slight amount of dye removal from the inducer blades following the completion of a 25-hour cavitation test. Dye tests are normally run for 20 minutes, not 25 hours, so that the results shown in the photograph are very positive in establishing the design. There was no indication of cavitation damage anywhere on the inducer, demonstrating the long-life potential of the part.

Before trimming the inducer to reduce the head rise, it was desirable that the entire pump be tested so the overall pump head rise could be determined. If any significant loss were found in any of the other pump components, the inducer could be trimmed to compensate for the loss.

Model Pump Tests. The complete SES model pump is shown in Fig. 83 installed in the 8000-gallon closed-loop water test facility. In Phase 4, head-flow, cavitation, and kiel probe survey tests were conducted. The testing was terminated due to a bearing failure in the model pump.

Phase 5 included kiel probe surveys, cavitation, yaw survey, dye, and head-flow tests. During this test phase, the kicker was trimmed three times to reduce the inducer head rise. This was necessary because the flow-weighted average head rise for the original kicker was 104 feet higher than the predicted level. After the first kicker trim, the head rise was 77 feet higher than the predicted level. The kicker was conservatively trimmed a second time to produce further reduction in head rise. The results showed the inducer head rise was 45 feet higher than the predicted level. The kicker was trimmed a third time to get the head rise to match the predicted. The test data show the inducer head rise was 27 feet higher than the predicted level. The decision was made to redesign the kicker

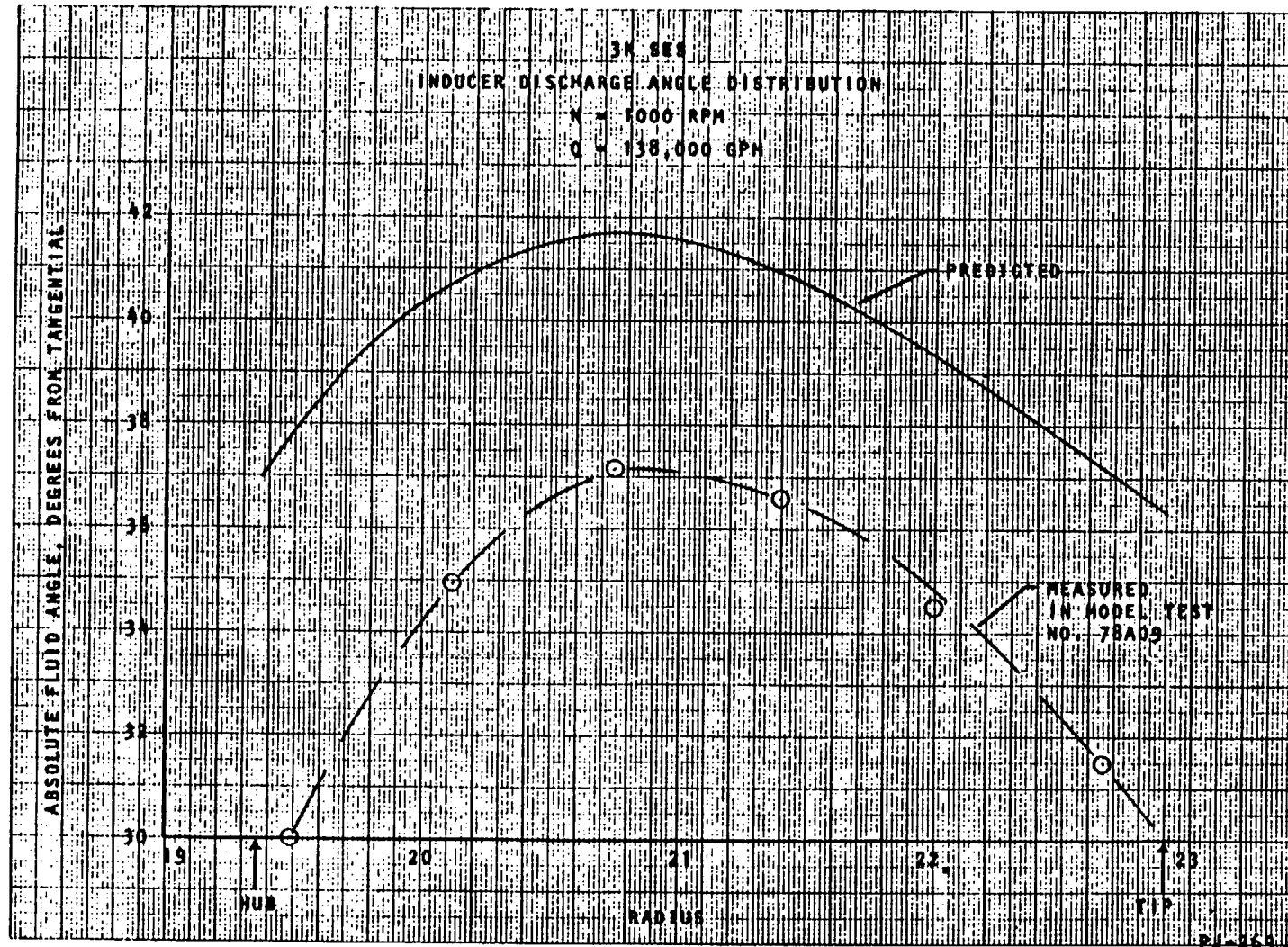
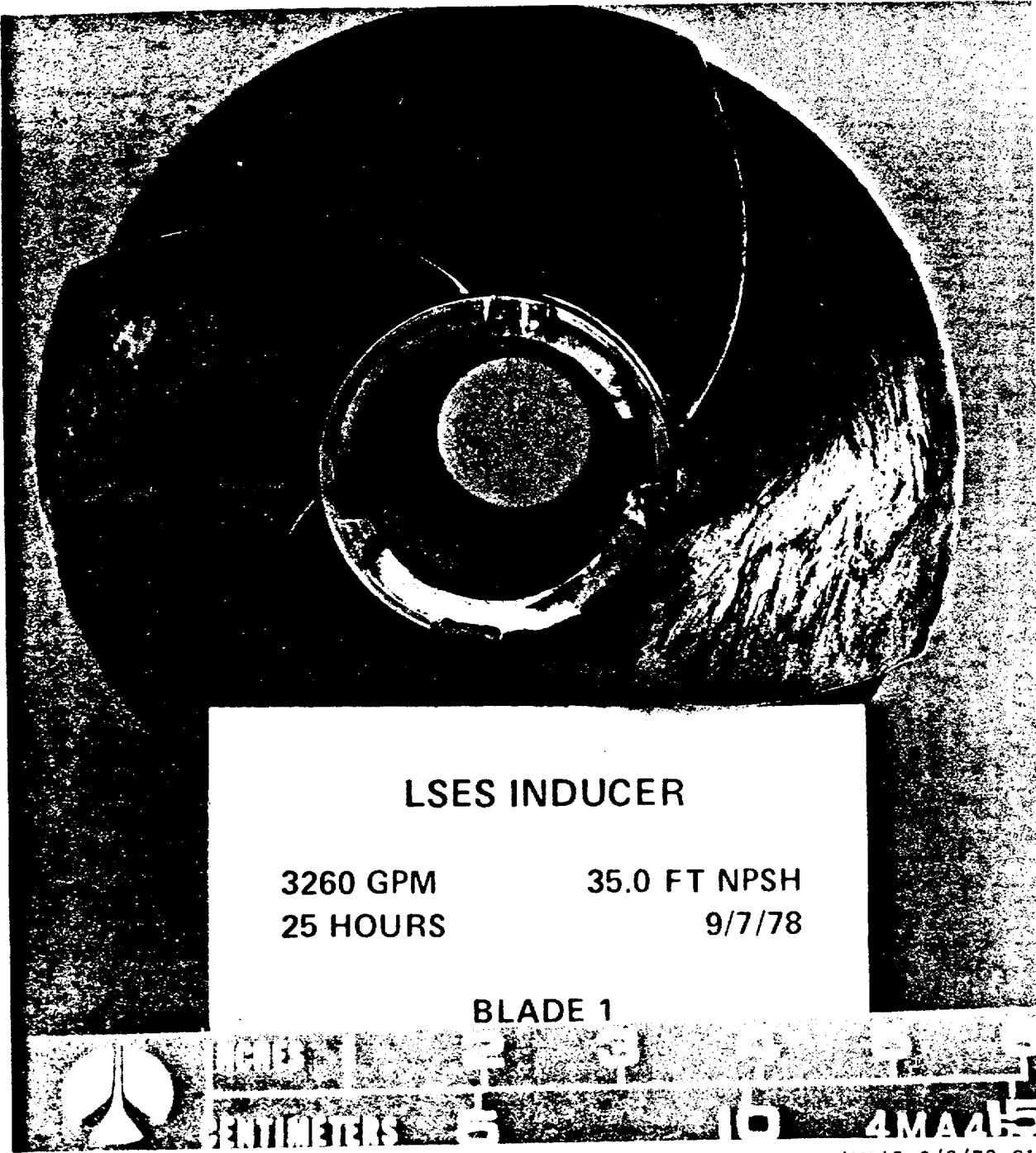


Figure 81. Inducer Discharge Angle Survey



**LSES INDUCER**

**3260 GPM  
25 HOURS**

**35.0 FT NPSH  
9/7/78**

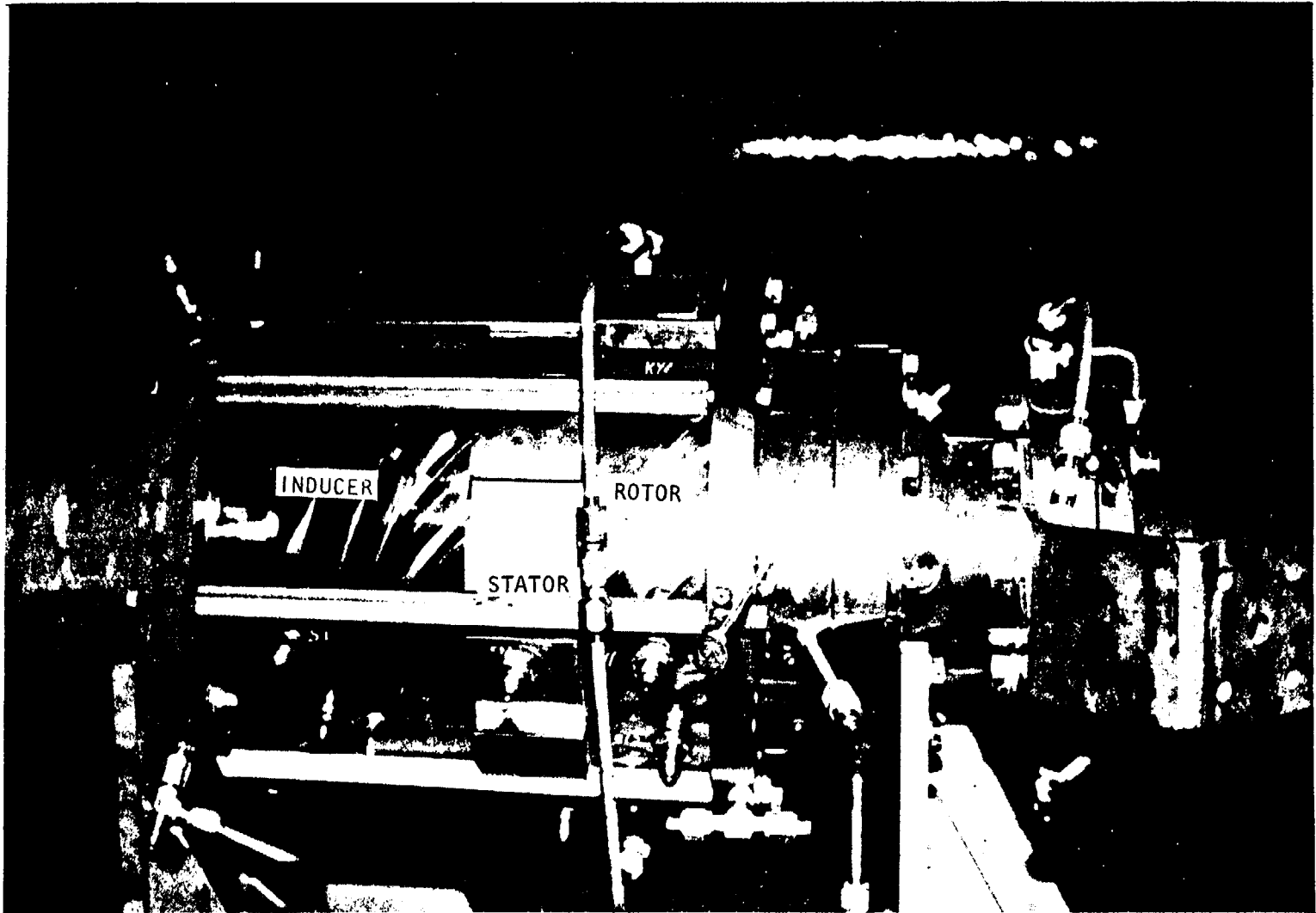
**BLADE 1**



INCHES 1 2 3 4 5 6 7 8 9 10 4MAA15

4MA45-9/8/78-C1F

Figure 82. Inducer Post-Test, 25-Hour Life Test



4MA41-10/23/78-C1B\*

Figure 83. Pump With Plastic Housings

incorporating the knowledge derived from test Phases 5 and 6. This was necessitated because the successive trims had resulted in decreasing the pump efficiency. It was determined that a redesign could result in the proper head without an efficiency penalty.

The total head rise versus model radius for each kicker configuration at design flow is shown in Fig. 84. The flow-weighted average head rise also is noted. The average head for the original kicker was 720 feet compared to the design of 616 feet. After the third trim, the kicker head average 643 feet, and pump efficiency had been reduced. The redesigned kicker average head rise was 597 feet, within 19 feet of the original design requirement (Fig. 84). The head rise is seen to be relatively uniform but, again, the head tends to drop near the tip.

The kicker discharge absolute flow angle versus radius is shown in Fig. 85 for each of the trims and the redesigned kicker configuration. The angles were corrected by constant valves to match continuity of flow with the measured flowrate. The angle as measured with the redesigned kicker still does not show as good a correlation with prediction as desired. However, the probes used in the high-velocity water medium were too large for the channel height, creating a blockage effect and gradient effects that resulted in angle measurement problems. Thus, the total head distribution is believed to be accurate, but the static pressure, velocity, and angle distributions are not as accurate as normally expected.

The effect of total inlet head (TIH) on inducer head rise at hump flow is shown in Fig. 86. The inlet static pressure of 79.8 psia at hump flow is equal to 197 feet TIH. The inlet static pressure of 10.7 psia is equal to 37 feet at hump flow. The average head drop for this decrease in inlet pressure or TIH was 26 feet, as shown in Fig. 86. The decrease was relatively uniform over the full blade height.

Photographs of the inducer and redesigned kicker after 29 hours of life testings at hump flow conditions are shown in Fig. 87 and 88. No erosion is observed on the inducer suction surface. Very slight erosion was observed on the kicker

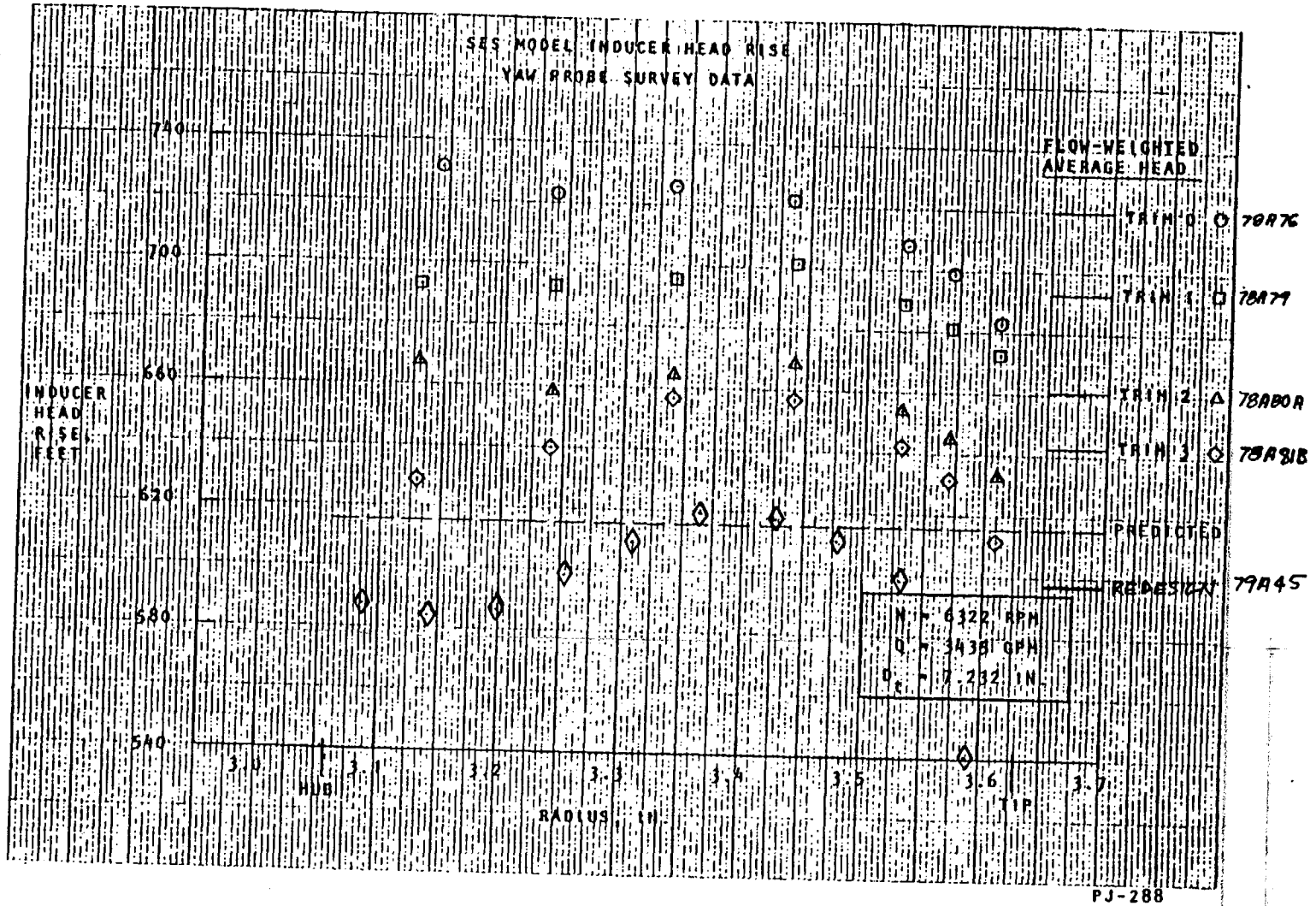


Figure 84. Kicker Discharge Pressure Survey

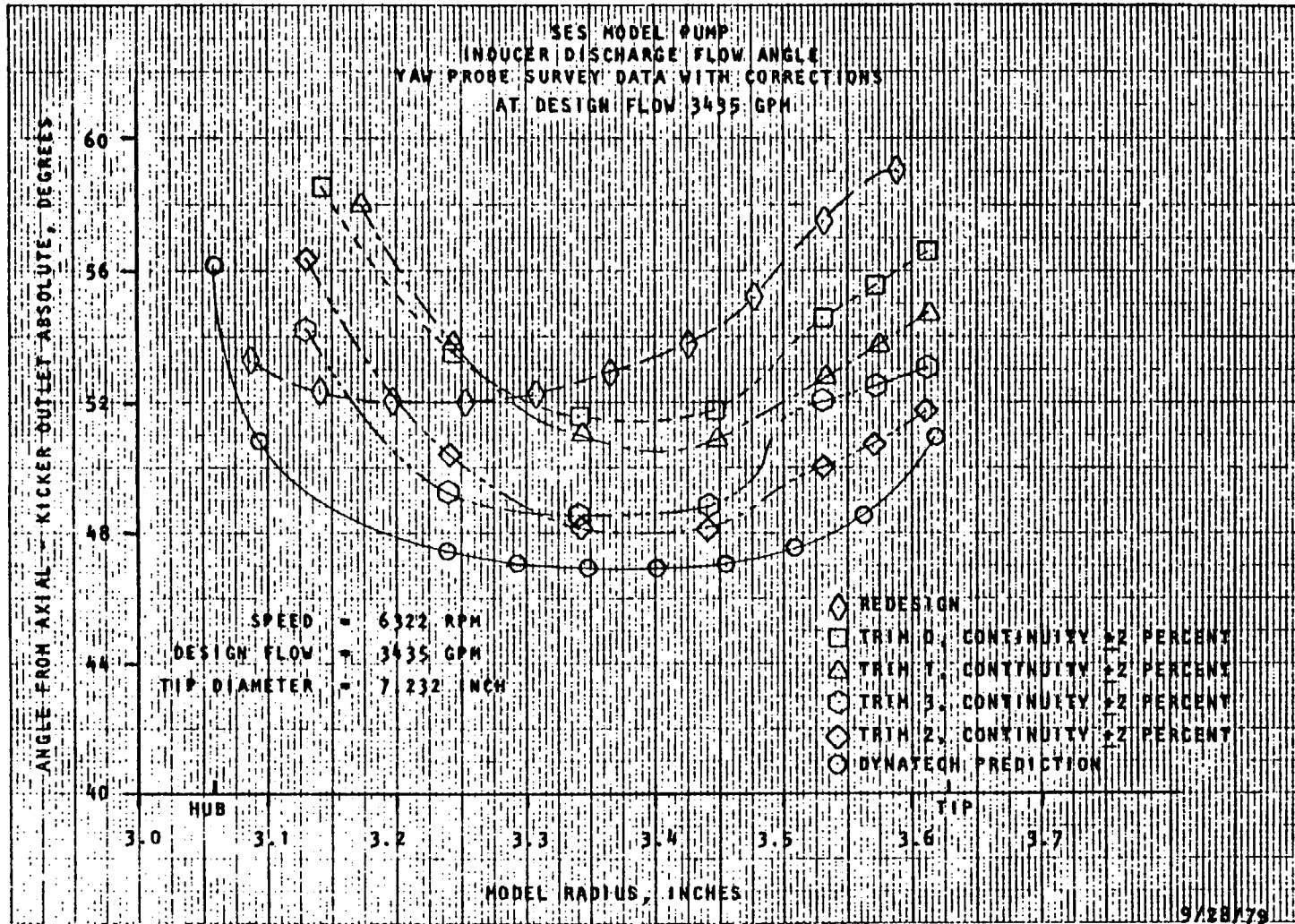
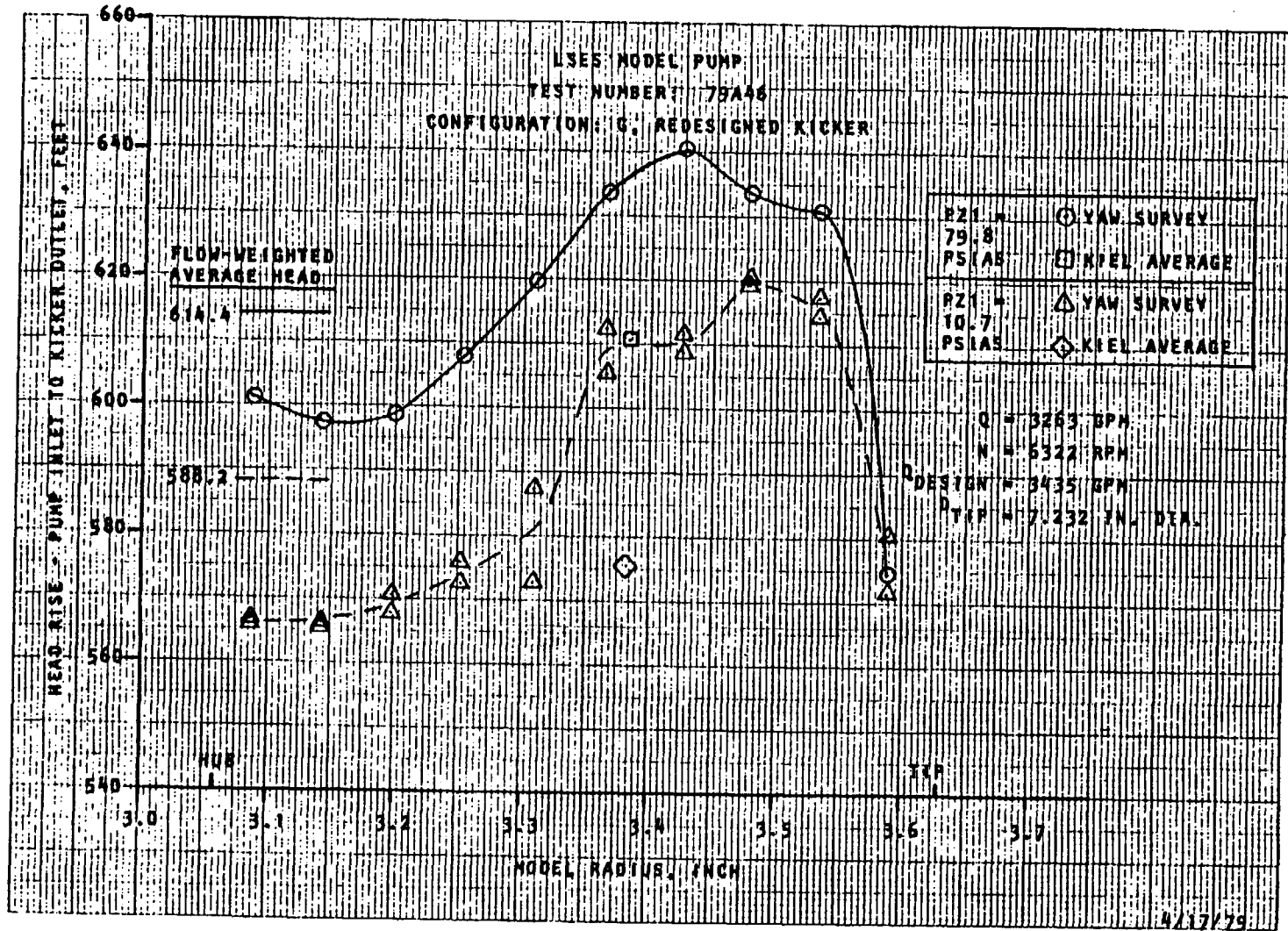
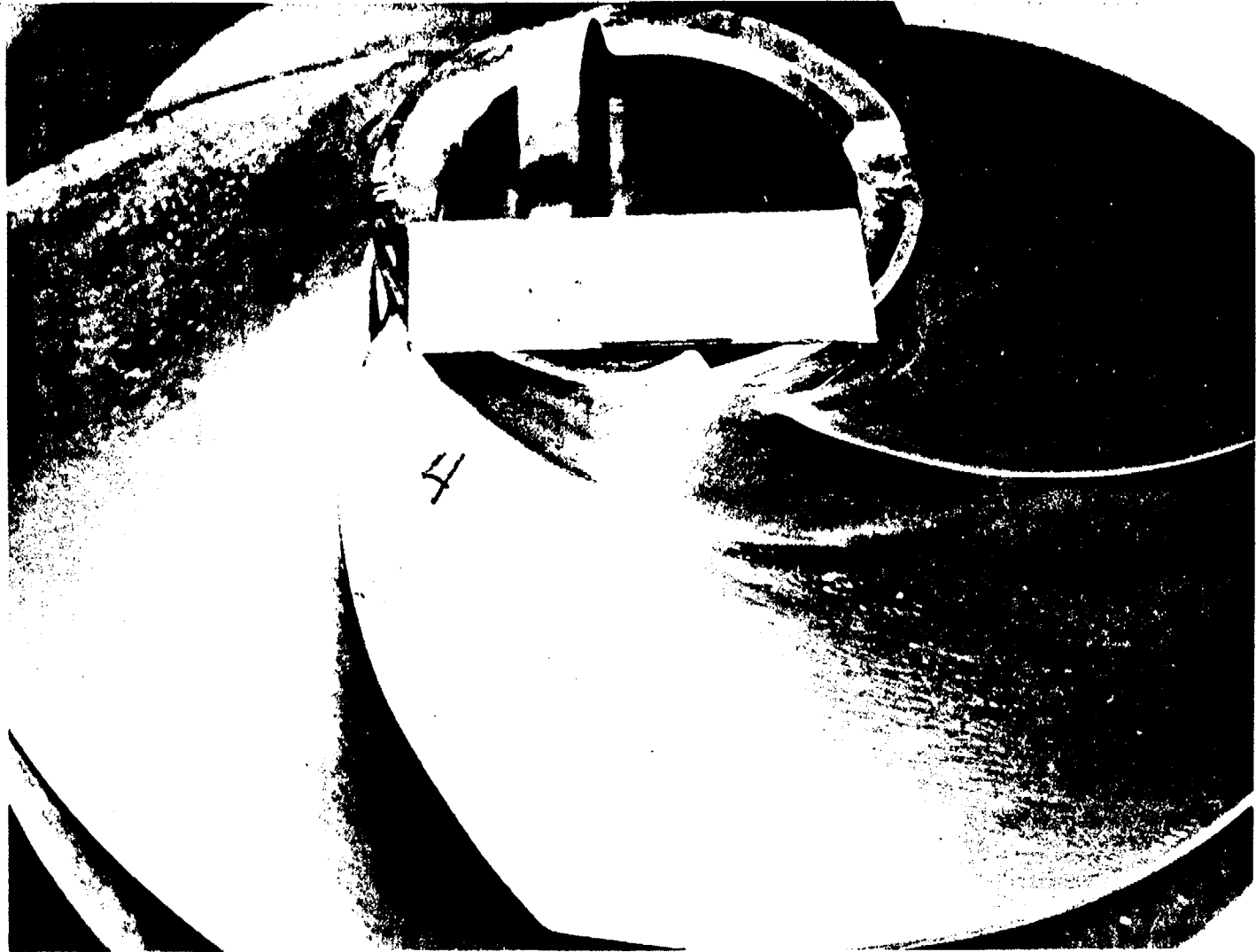


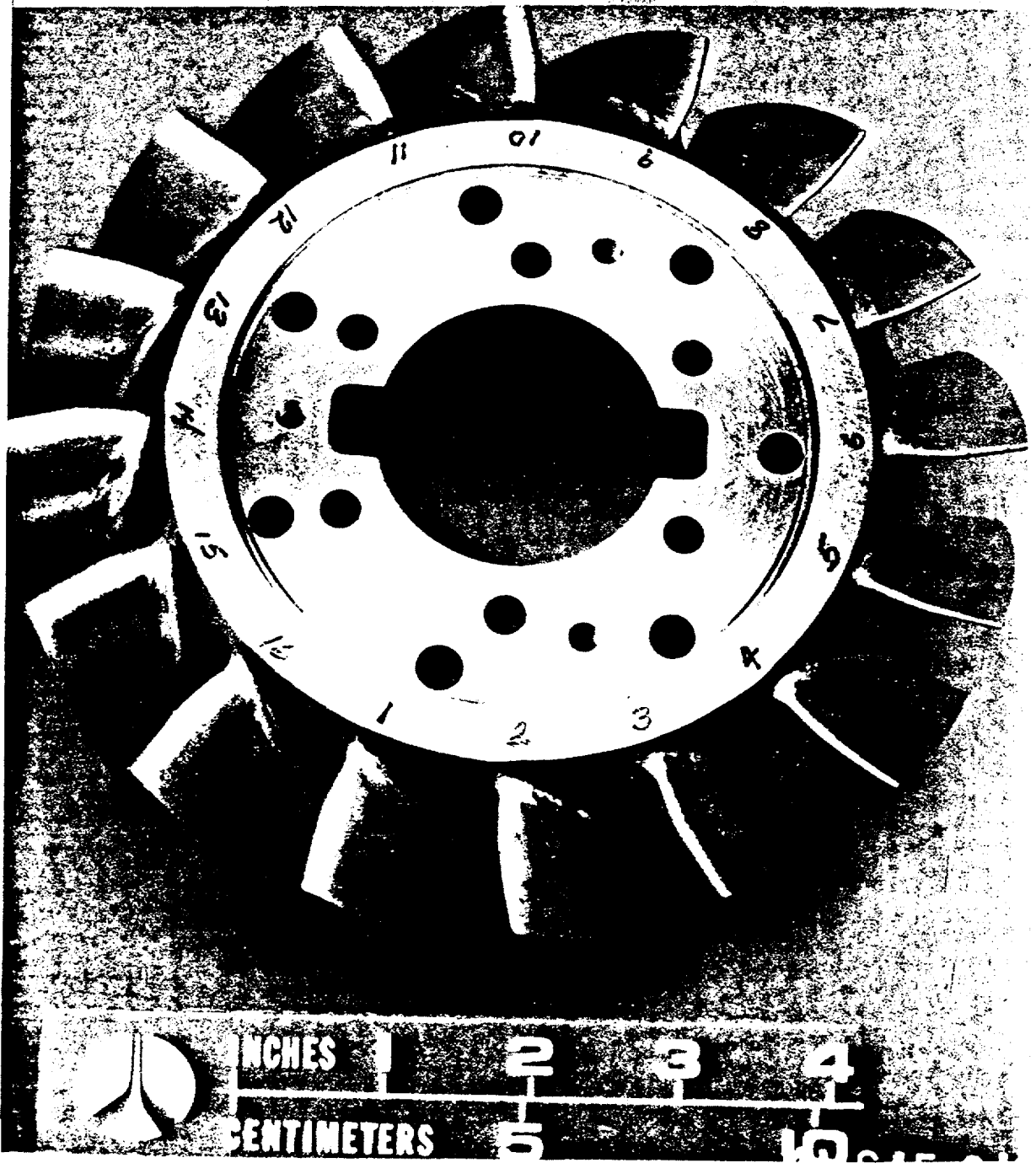
Figure 85. Kicker Discharge Angle Survey





4MS45-9/10/79-1-C2S

Figure 87. Inducer Post-Test, 25-Hour LVT



4MS45-9/10/79-C1A

Figure 88. Kicker Post-Test, 25-Hour LVT

suction surface of blade numbers 7 and 15 near the tip. An additional 13 hours of life testing were accumulated without further erosion on the kicker. Slight erosion was observed near the leading edge tips of the full and partial inducer blades numbered 2 and 4. The additional 13 hours included 11 hours at the new hump flow condition of 3426 gpm and 24,900 rpm suction specific speed.

Thus, the average total head rise was approximately as predicted and indicated that with the redesigned kicker a good inducer-kicker configuration had been achieved. After 42 hours of life testing, only very slight cavitation erosion has been observed on the inducer and kicker. This "frosting" has been sporadic and occurs on only a few of the blades, indicating it may be due more to local idiosyncrasies of the model build rather than an actual design problem. The part will definitely meet the life requirements of the full-scale design.

### Axial Stator

Pump configuration C used for the axial stator verification is shown in Fig. 60. Stator performance with the redesigned kicker was determined in Phase 8. Eight kiel probe positions were located 0.94 inch axially downstream of the stator mid-height trailing edge. The eight positions were equally spaced circumferentially and vane to vane to permit evaluation of the vane wake size. Kiel probe surveys were made during H-Q tests at three radial positions: 25, 50, and 75% of the channel height. Three yaw (cobra probe) surveys at design flowrate were run in and out of the vane wakes as determined from the kiel surveys. Static pressures were measured at the tip upstream and downstream of the stator with four tap piezometer rings and at four axial tip stations along the stator.

The arithmetic average total head rise versus flowrate is shown in Fig. 89. The average includes the 8 circumferential and 3 radial positions (24 total). The predicted head rise at design flow for the original configuration was 600 feet. The model test value was 573 feet with the redesigned kicker. The stator head rise is less than predicted by approximately the same amount as the redesigned kicker was below predicted. The total head loss through the stator for the

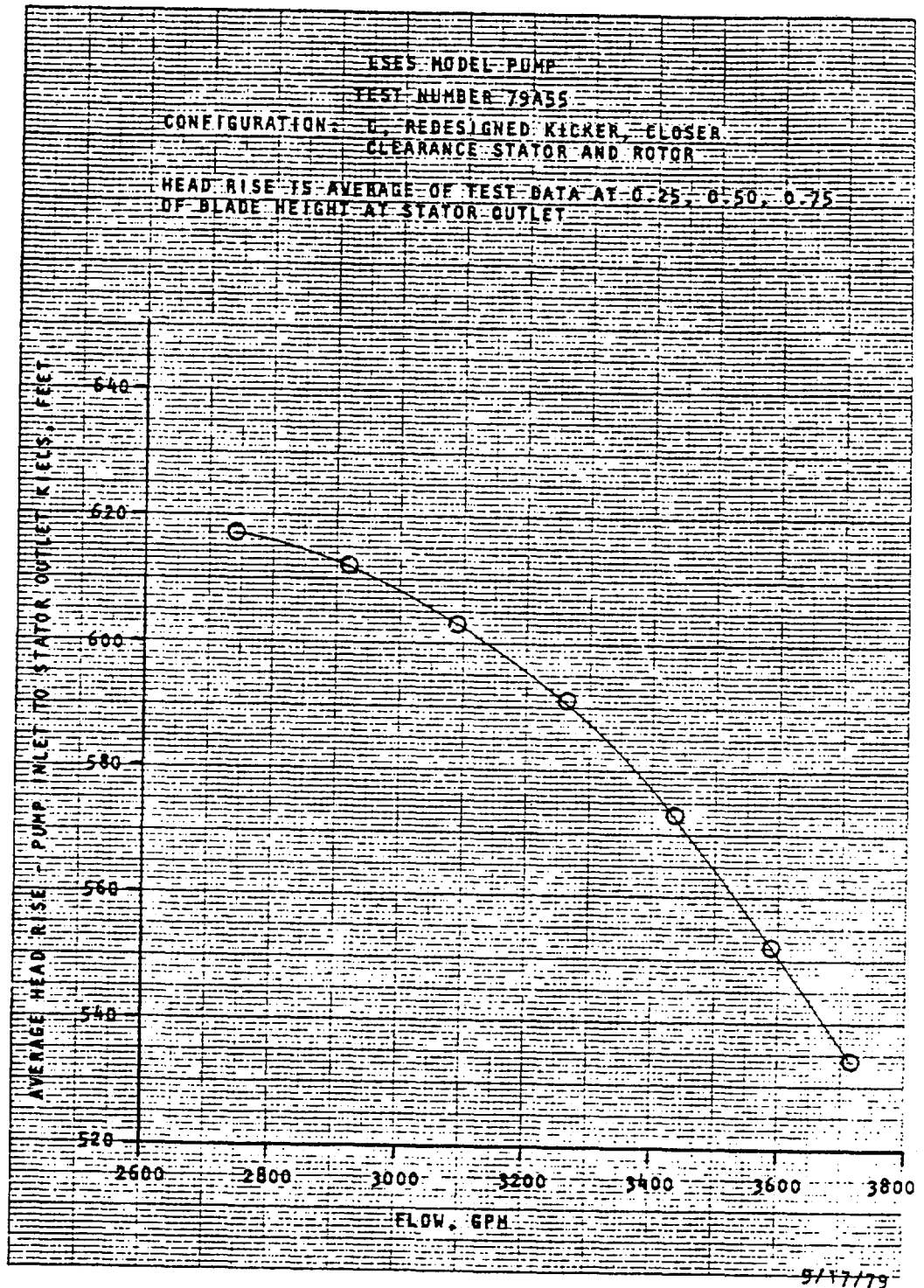


Figure 89. Stator Discharge Pressure Versus Flow

original prediction was 15 feet (615 feet total head at kicker discharge minus 600 feet at the stator discharge). The stator loss for the model testing was 24 feet based on the average head downstream of the redesigned kicker of 597 feet minus the 573 feet at the stator discharge.

The total head distribution vane to vane at design flow is shown in Fig. 90. The probe positions with respect to the trailing edge were determined by projecting the tip chord angle to the probe locations. The expanded scale used in the figure makes the head gradients appear to be large. The  $2\sigma$  band on the average was  $\pm 10\%$ . The head falloff in the wake at the 75 and 50% heights were at the same location with a slightly smaller falloff at mid-pitch. The wakes at the 25% height were offset and of greater magnitude. The wake width and the velocity head differential in the wake at the two outer radii are both reasonable from a magnitude standpoint. The wake width is relatively large near the hub. The diffusion factor is higher near the hub (approximately 0.51) but should not cause separation unless there is an interaction between the clearance flow and the boundary layers that is strongly affecting the wake. Obviously, the hub data have a major impact on lowering the overall head. The major importance of the flow field distribution at the stator discharge is the match between the flow vectors and the downstream rotor. The rotor performance determined by head, efficiency, and life has shown no problems due to mismatch of the rotor leading edge.

Radial yaw probe surveys using the cobra probe were run at the three locations shown in Fig. 91: KY19, KY21, and KY20. Yaw probe total head rise versus radius is shown in Fig. 911. The yaw survey data show good agreement with the kiel probe data from Fig. 92 at the two radii closest to the hub. However, the agreement is not very good at the tip, the cobra probe showing a significant dropoff of head near the tip at both KY19 and KY21 positions. Figure 92 shows kiel probe data from the same three tests as used for the cobra probe surveys, but the two kiel probes are always located at the two positions not being used by the cobra probe. However, these data show repeatability from test to test, agreeing with previous kiel probe data and disagreeing with the cobra probe at the tip. The cobra probe consistently shows a head dropoff near the tip, as was

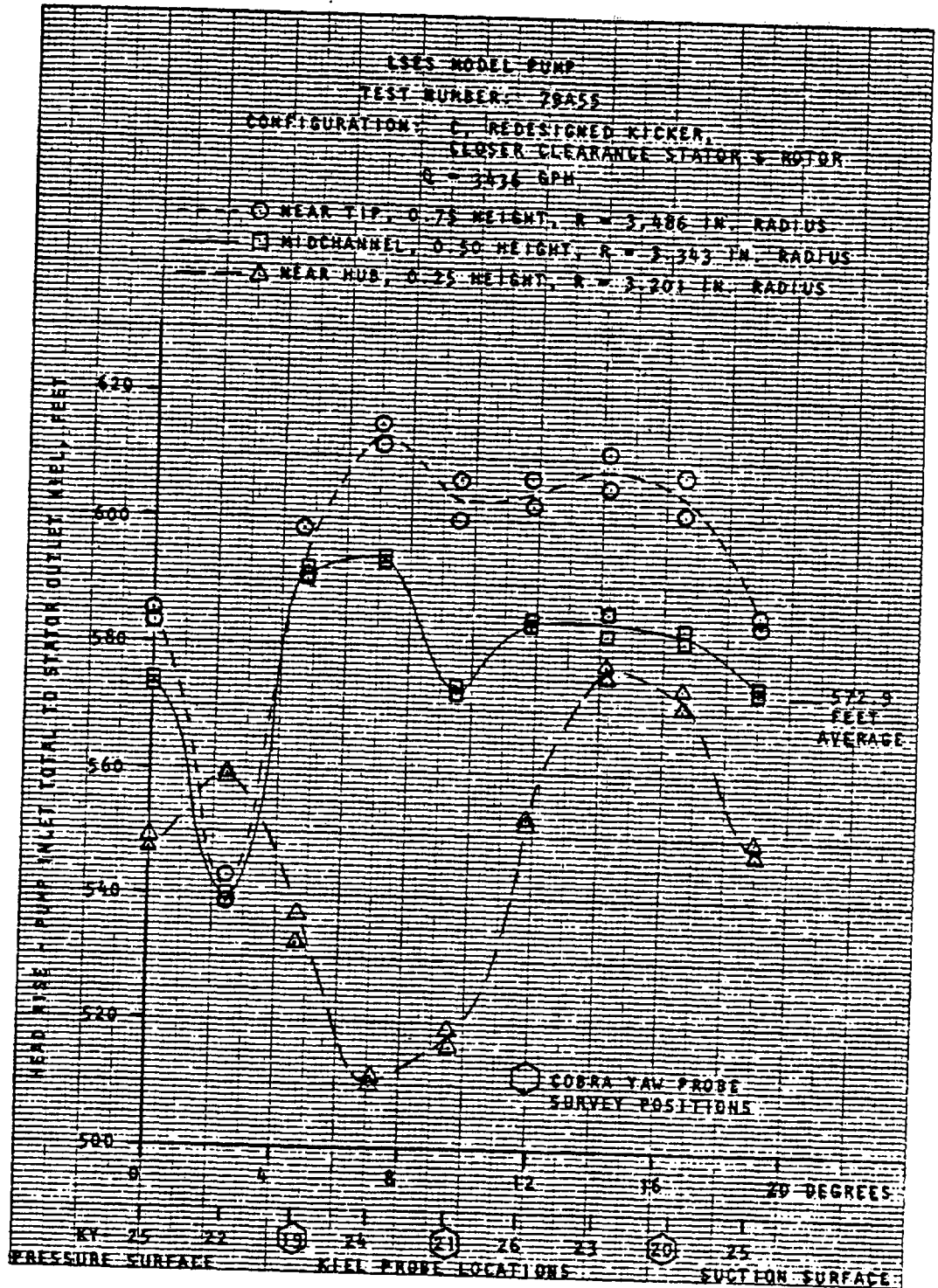


Figure 90. Stator Discharge Pressure Survey





witnessed behind the inducer. It is suspected that the cobra head yaw probe is losing accuracy near the tip even though it is typically expected to be a better probe near the boundary layer regions.

The measured absolute flow angle versus radius for the yaw probe surveys is shown in Fig. 93 along with the predicted values. Close agreement is shown for most of the blade height with greater deviation at the hub and tip. The hub difference could again be indicative of insufficient turning at the hub due to separation or tip clearance interaction. The disagreement shown at the tip may be due to inaccuracies in the cobra head probe. No indication of an angle matching problem with the downstream rotor was observed, except for some sporadic blade frosting at the root of some of the rotor blades. However, this would not prevent usage of both parts as is, and may be more indicative of minor profile differences on the rotor.

In conclusion, the stator performance was verified by showing the total head loss was near the predicted. The only area indicating less desirable performance was the significant head gradients observed near the hub showing large vane wakes.

#### Axial Rotor

Figure 61 shows pump configuration D used during the axial rotor verification in Phases 6, 7, and 9. Phase 6 involved head-flow and yaw probe survey tests using the original rotor and trim-three kicker. During Phase 7, cobra yaw probe and kiel probe surveys were conducted with the original rotor and redesigned kicker at flowrates of 3435 and 3263 gpm. Test Phase 9 included head-flow, cavitation, and yaw probe surveys using the redesigned axial rotor and redesigned kicker.

The total head rise at design flow for the original rotor with the redesigned kicker is shown in Fig. 94. The flow-weighted average head rise was 1030 feet compared with 1010 feet predicted. Head falls off toward the tip, but the fall-off is not considered serious (note the expanded scale in Fig. 94). The cobra yaw probe head agrees closely with the kiel probe head, but it has a tendency to drop off near the tip more quickly, as observed previously.

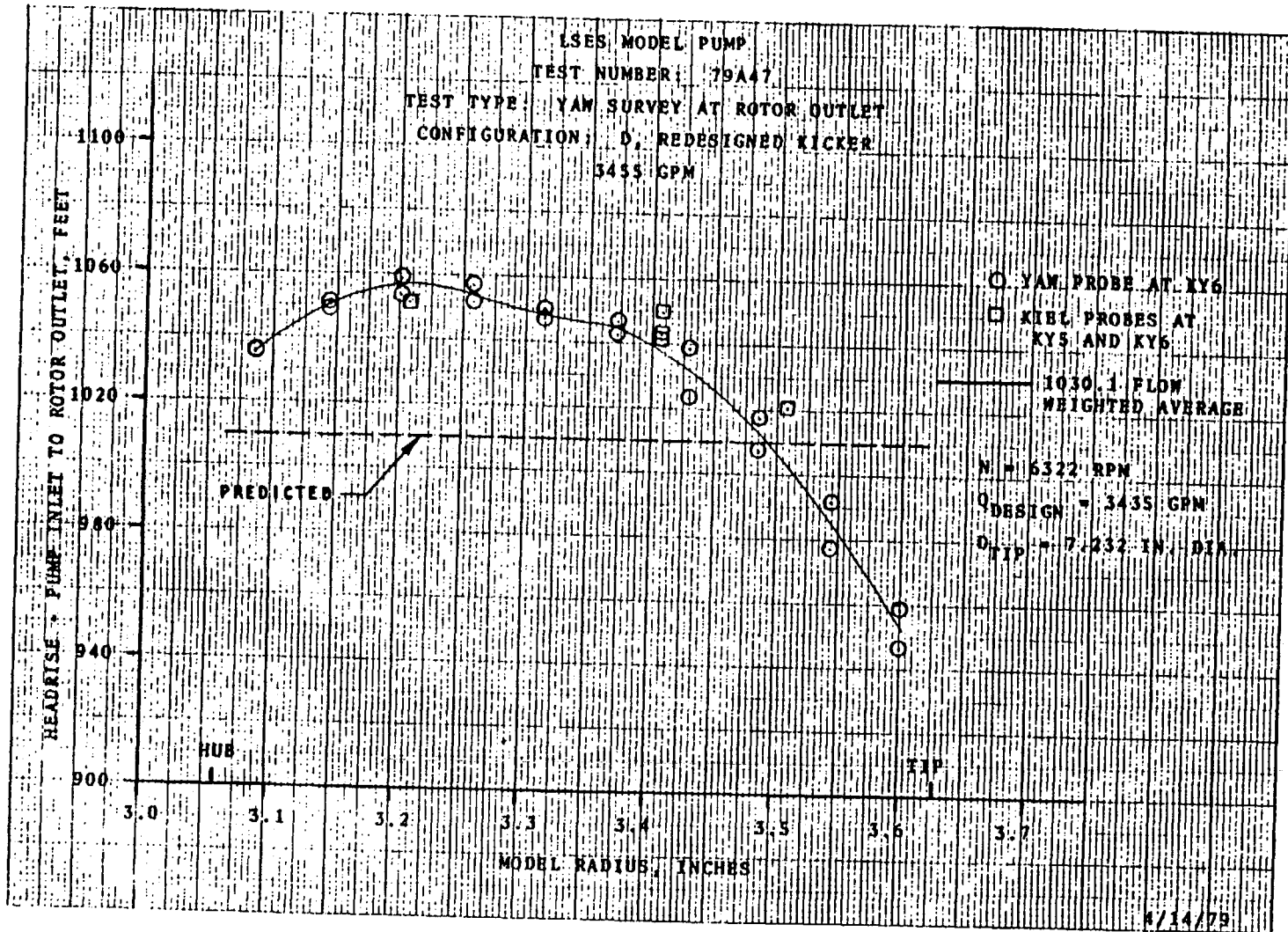


Figure 94. Rotor Head Rise Survey

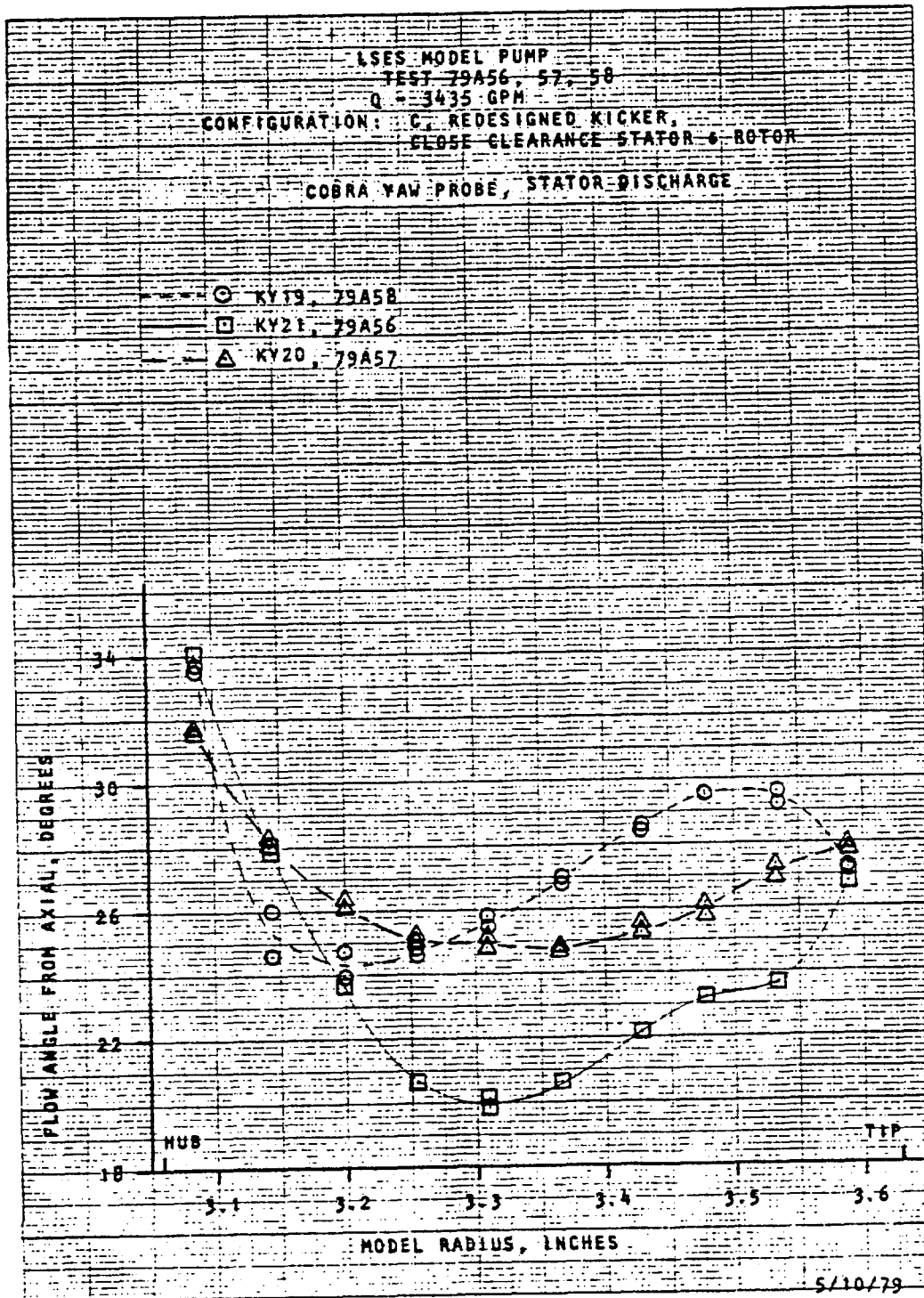


Figure 93. Stator Discharge Angle Survey

The absolute flow angle from the axial at the rotor discharge at design flow is shown in Fig. 95 versus radius. The angle was corrected 3.3 degrees toward axial to match continuity. Close agreement with the predicted is shown throughout, particularly near the hub and midchannel. The deviation toward the tip may be due to yaw probe inaccuracies in that region.

Total head rise versus flowrate for the original rotor at three radial positions is shown in Fig. 96. The head falloff toward the tip is shown increasing with increasing flowrate. Total efficiency based on the head rise from the pump inlet to the rotor discharge is shown versus flow in Fig. 97. Efficiency at the mid-channel at design flow was 86.6%.

The total head rise at design flow for the redesigned rotor (with the redesigned kicker) is shown versus model radius in Fig. 98. The flow-weighted average was 950 feet, down 80 feet from the original rotor. The redesigned rotor has a somewhat flatter head characteristic than the original rotor with less head falloff toward the tip. The agreement of the head rise with design prediction is seen to be excellent. The absolute flow angle at the redesigned rotor discharge is shown in Fig. 99. Close agreement with the prediction also is seen here.

A total of 42 hours of life testing at hump flow conditions was accumulated on the redesigned rotor. Figure 100 is an overall view of the rotor after 29 hours and shows no cavitation damage. Some frosting at the suction surface root is shown in Fig. 101 which was approximately typical of 8 of the 17 blades. The other nine blades showed no frosting. No further erosion was observed after 13 more hours of testing, of which 11 hours were at the 105% hump flow condition. The frosting observed was so light that no detriment in performance would be expected over the life of the part.

#### Straightening Vane

Overall head rise and efficiency at the straightening vane discharge for the design flowrate of 3435 gpm is summarized in Table 16, covering the different phases of testing.

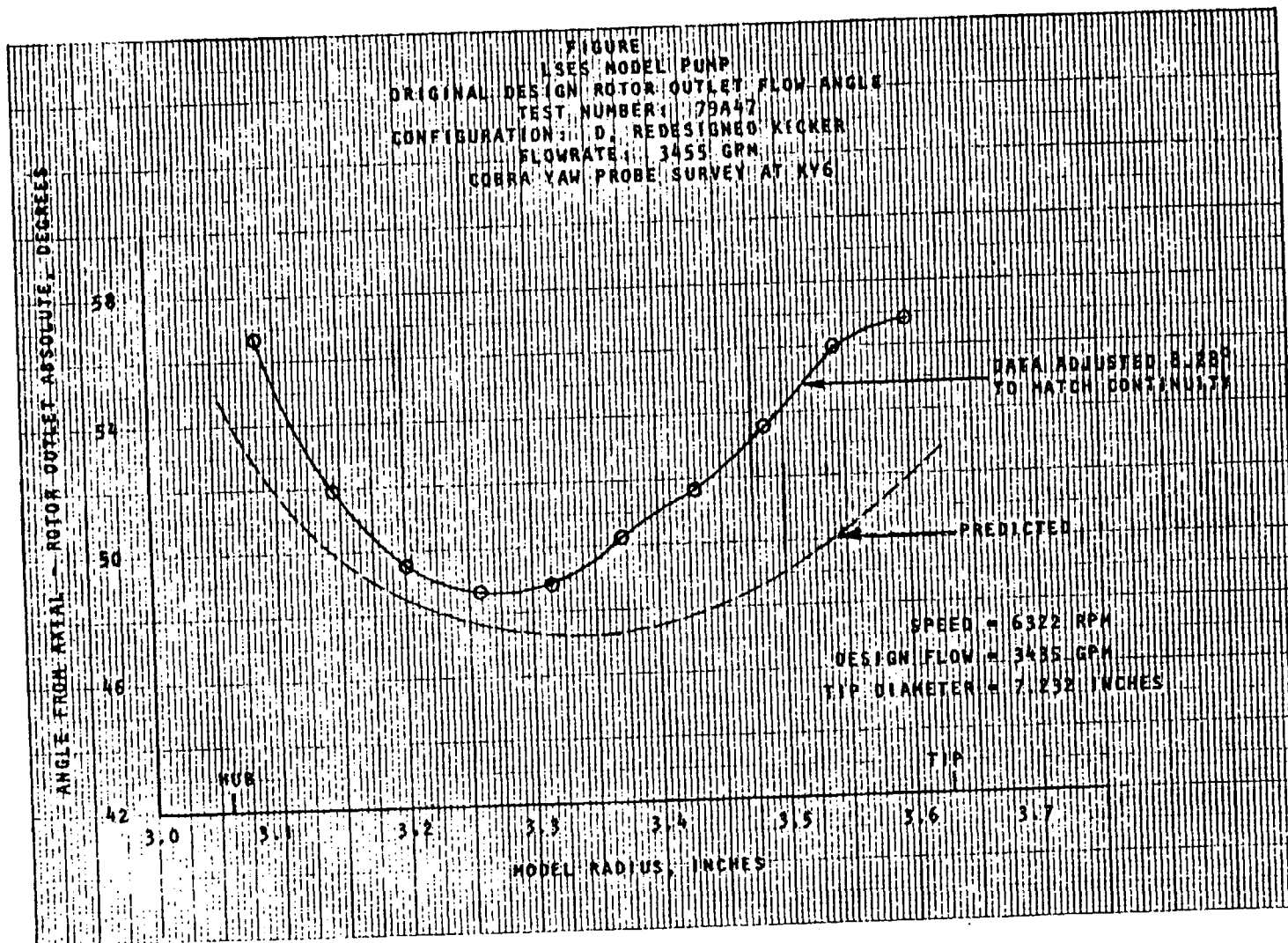


Figure 95. Rotor Discharge Angle Survey

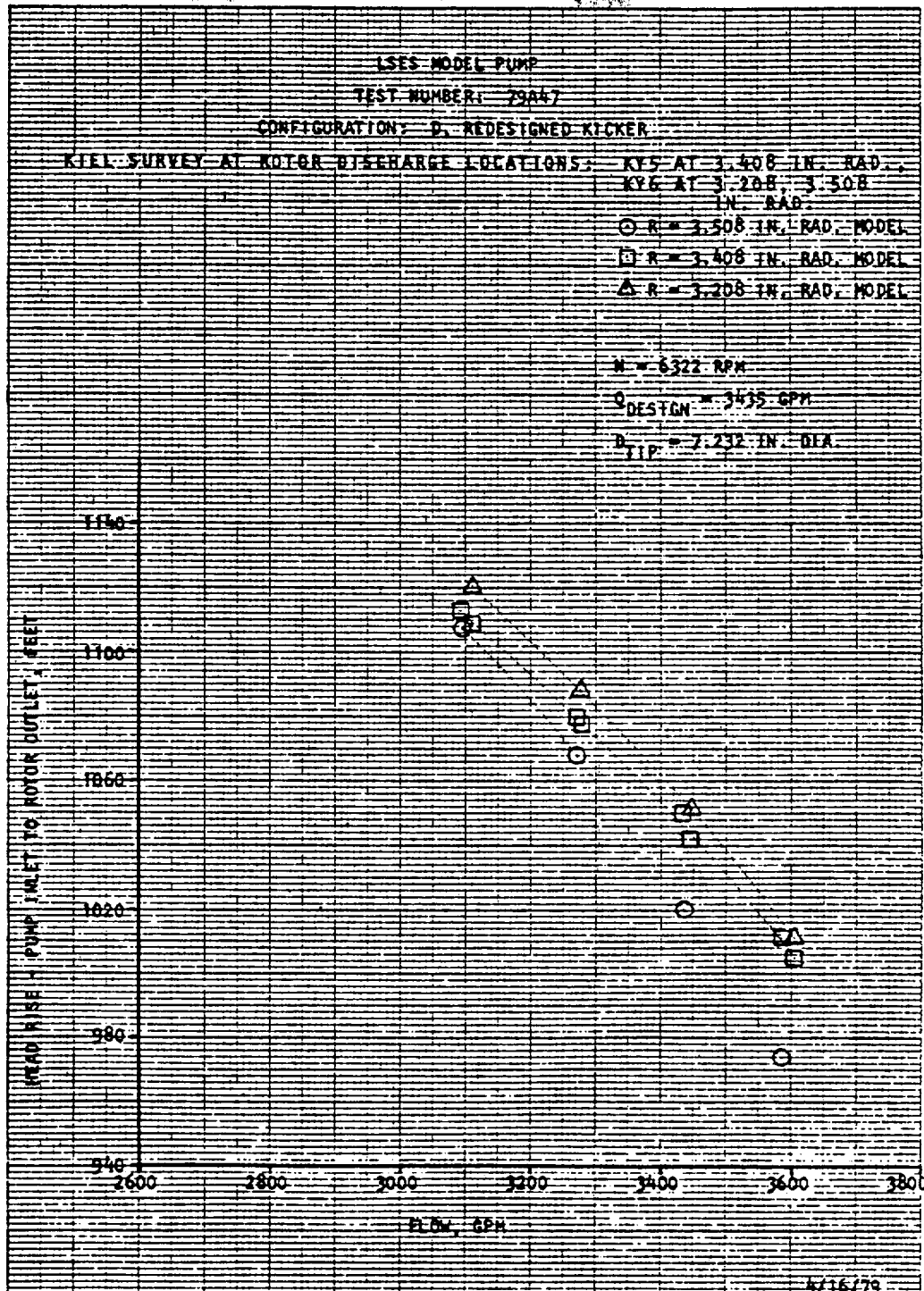


Figure 96. Rotor Head Rise Versus Flow

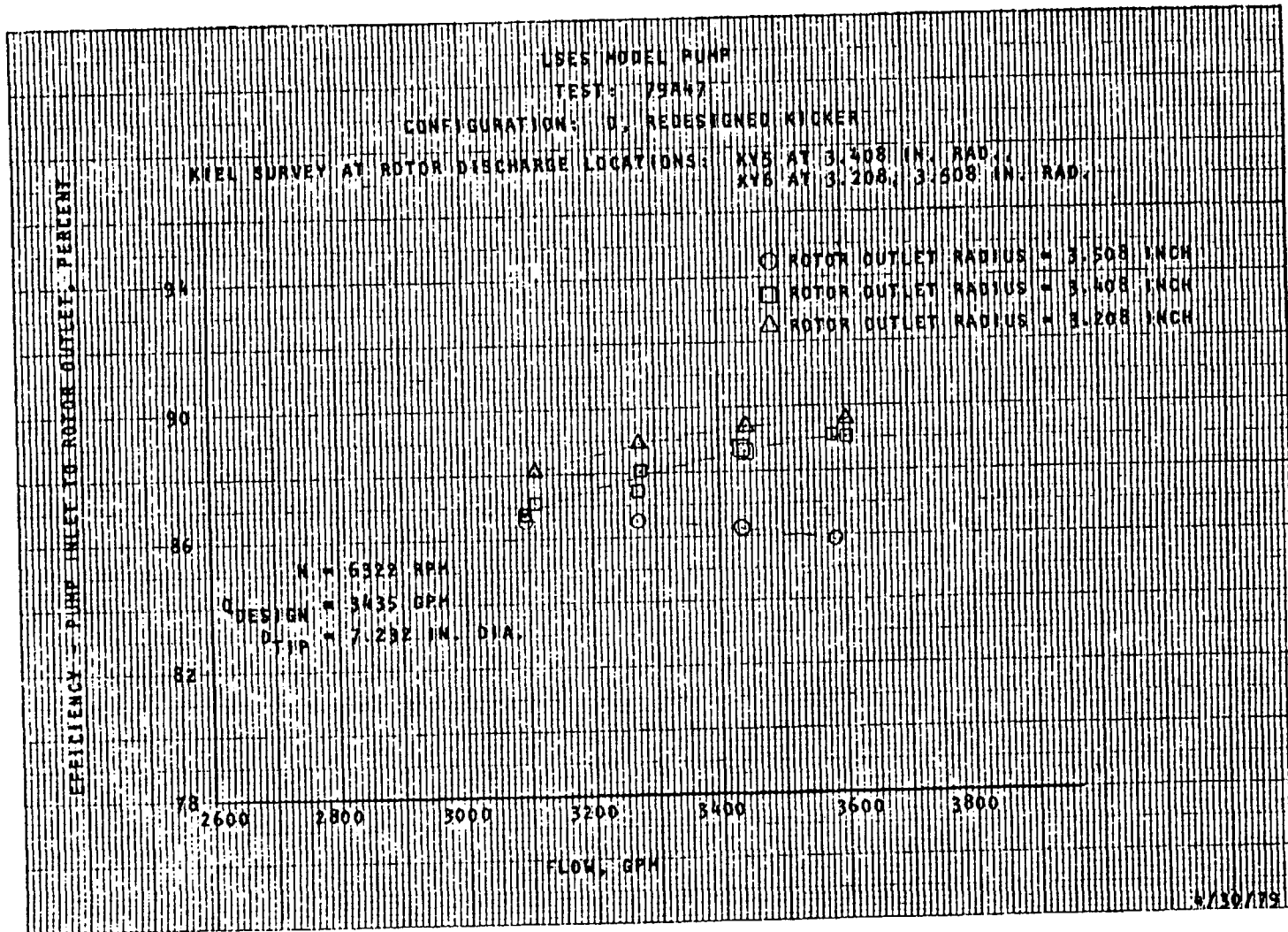


Figure 97. Rotor Discharge Efficiency Versus Flow

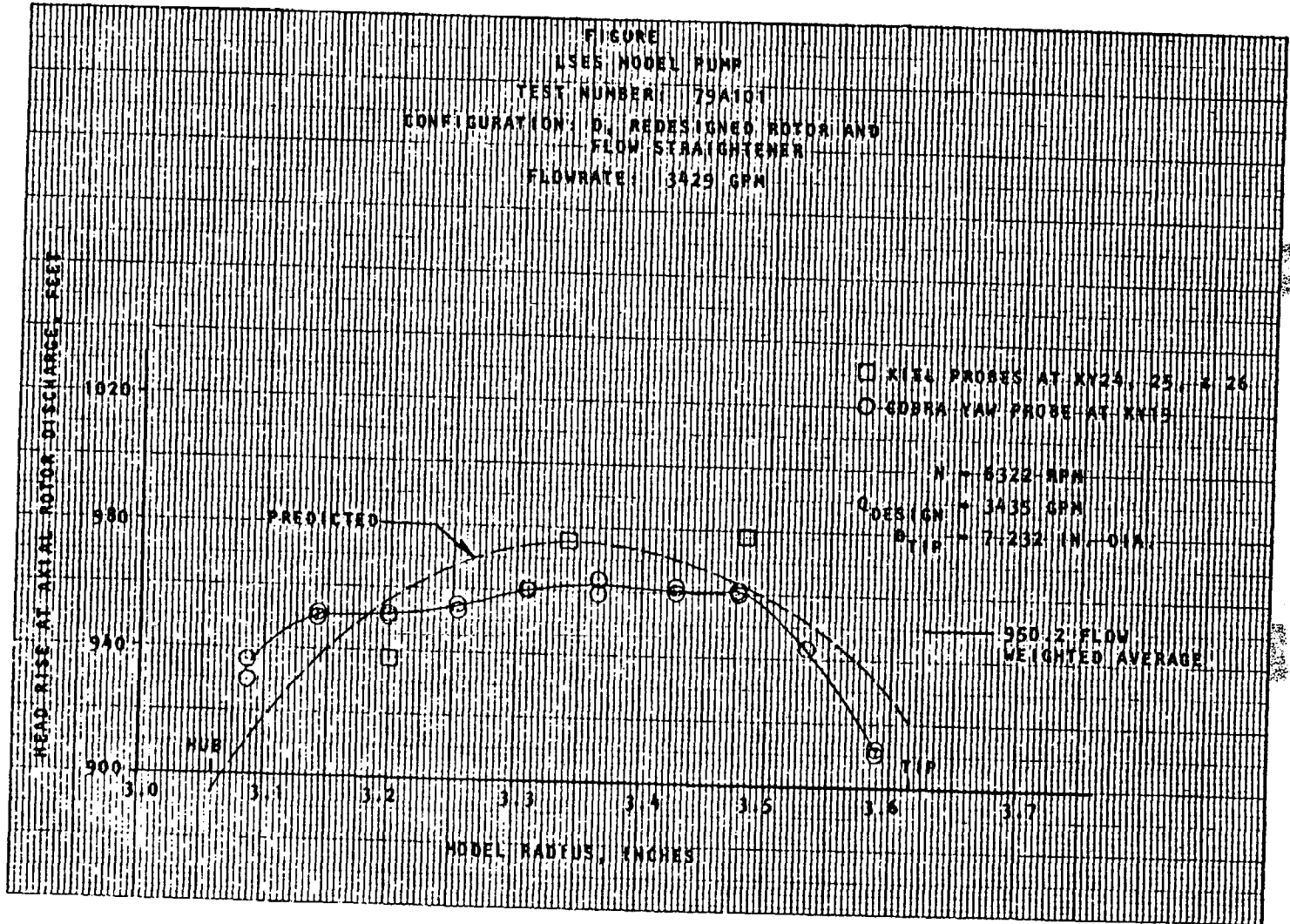


Figure 08 Rotor Discharge Head Rise

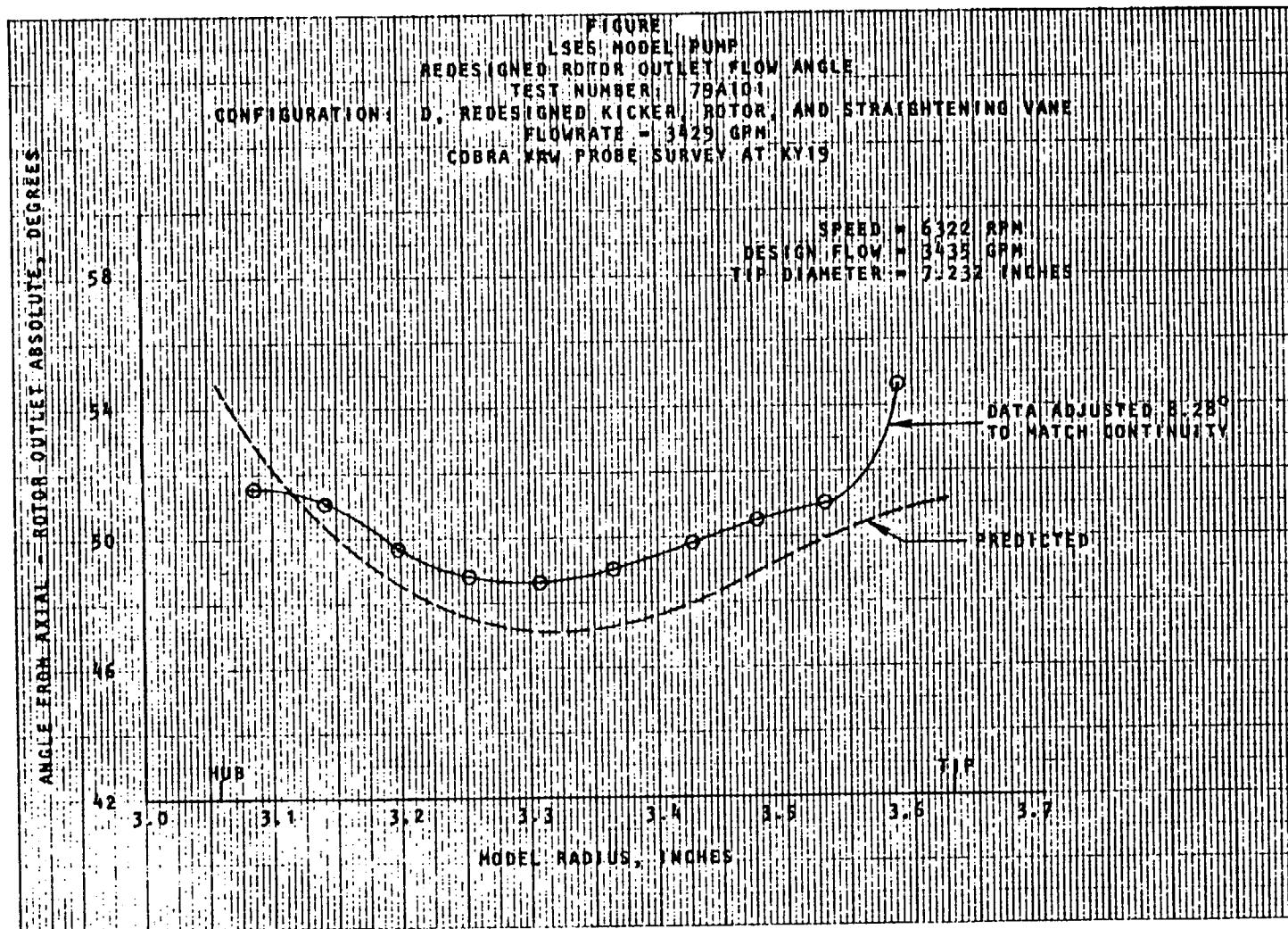
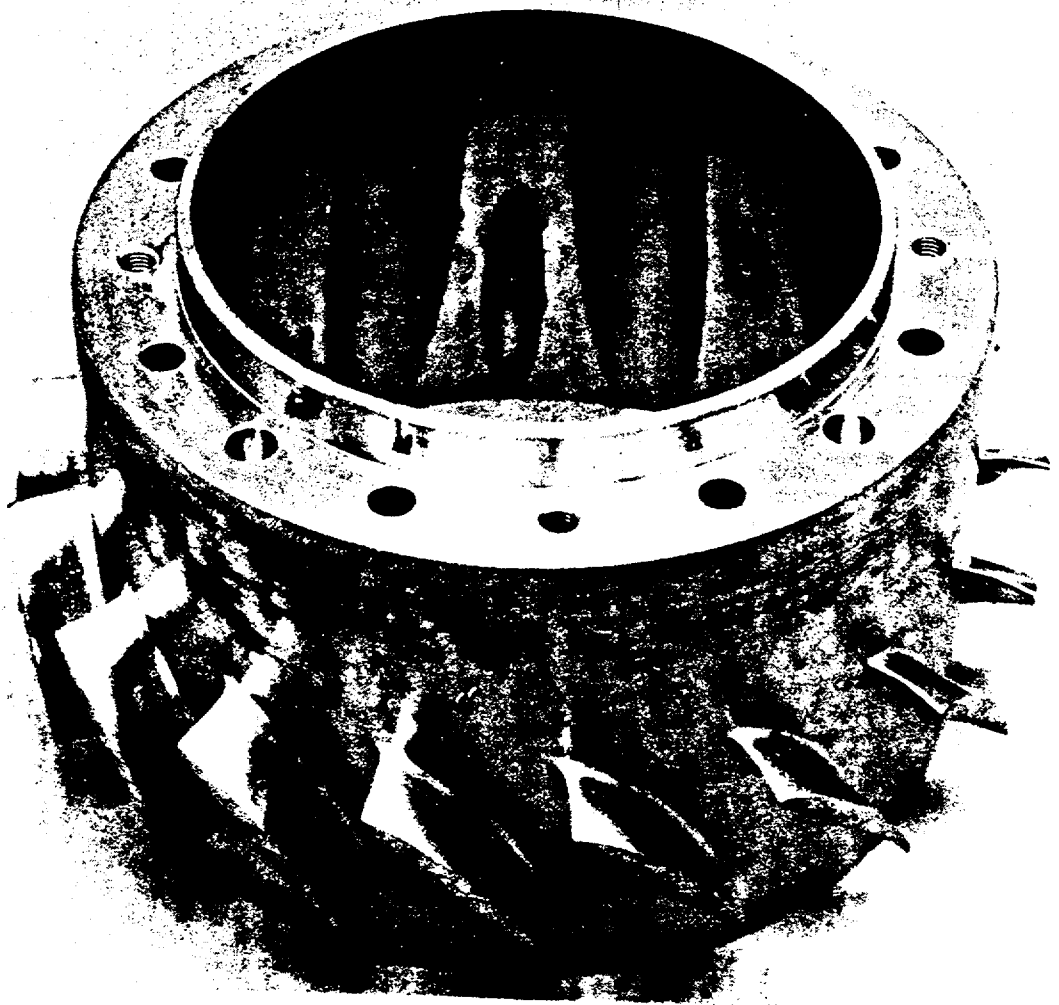
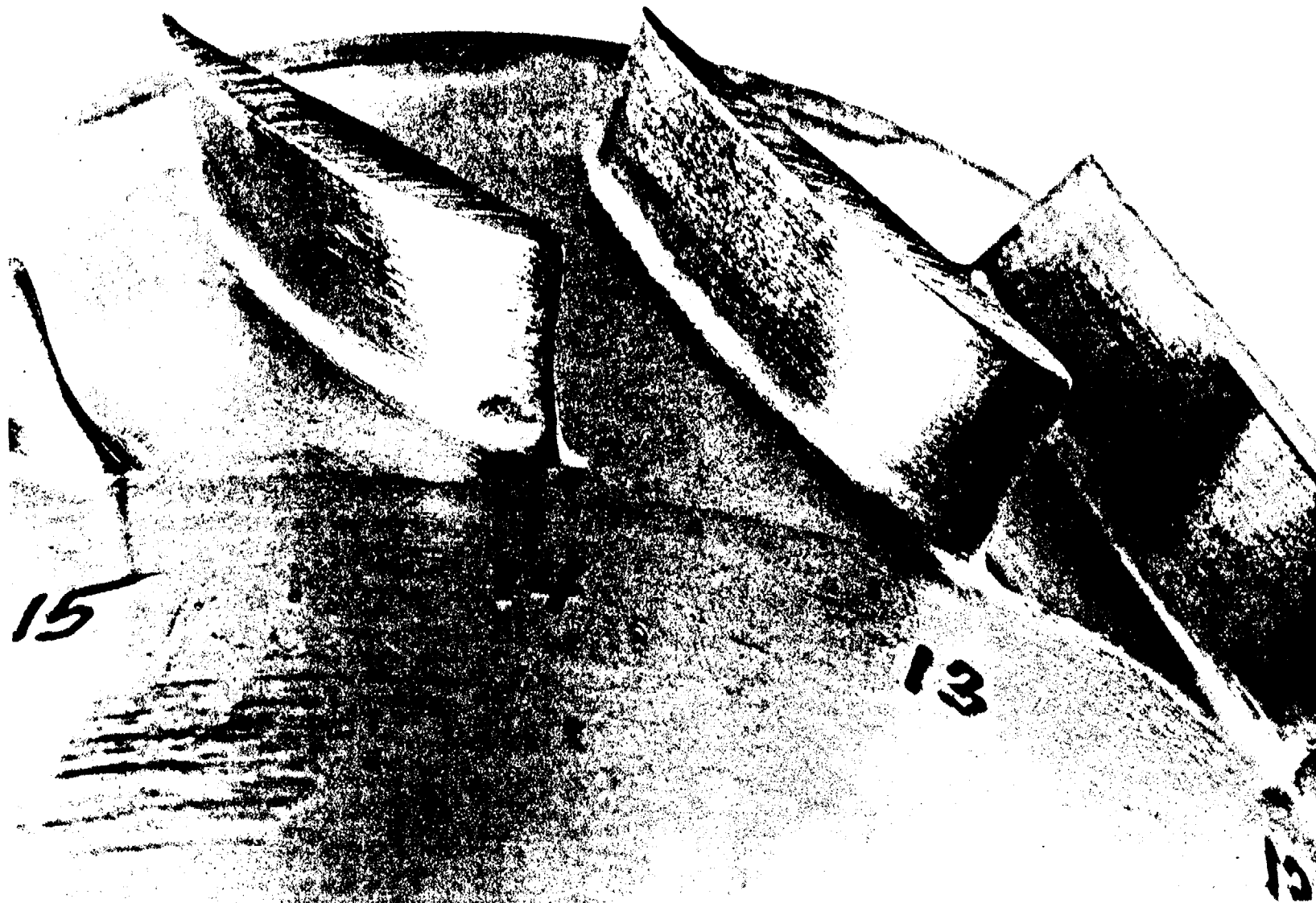


Figure 99. Rotor Discharge Angle Survey



4MS45-9/10/79-1-C3W

Figure 100. Rotor



4MS45-9/10/79-1-C3P

Figure 101. Rotor Blades 13 and 14

TABLE 16. LSES MODEL PUMP OVERALL PERFORMANCE AT DESIGN FLOW, 3435 GPM

CONFIGURATION	PHASE	HEAD RISE, FEET			EFFICIENCY		
		KY7 <sup>(1)</sup>	KY8 <sup>(1)</sup>	AVERAGE <sup>(2)</sup>	KY7 <sup>(1)</sup>	KY8 <sup>(1)</sup>	AVERAGE <sup>(2)</sup>
1. Original	4,5	1134	1037	-	0.875	0.801	-
2. Kicker Trim 1	5	1104	1026	-	0.882	0.820	-
3. Kicker Trim 2, Straightening Vane Trim 1, Nozzle Trim 1	5	1029	1004	-	0.839	0.817	-
4. Kicker Trim 3, Straightening Vane trim 1, Nozzle Trim 1	5,6	931	1013	989	0.762	0.830	0.809
5. Redesigned Kicker, Straightening Vane Trim 1, Nozzle Trim 1	7	960	1061	977	0.814	0.900	0.829
6. Redesigned Kicker, Rotor, Straightening Vane, Nozzle Trim 1	8,9,10	-	-	885	-	-	0.816

(1) Kiel Probes at 50 percent blade height at straightening vane discharge.

(2) Average for 8 Kiel probes at 25, 50 and 75 percent blade height at straightening vane discharge.

Pump testing during Phases 4 and 5 used two kiel probe locations (KY7 and KY8) downstream of the straightening vane to determine overall head rise and efficiency. The KY7 and KY8 kiel probes were: (1) at 50% vane height radially, (2) 180 degrees apart, and (3) at different circumferential locations relative to the straightening vane suction and pressure surfaces. Since the probes were not directly downstream of trailing edges, it was expected that the head rise for each should be equal, assuming that the wake widths off the vanes were relatively small.

Initial tests indicated KY7 was significantly higher than KY8, as shown in Table 16. It was thought that the low reading on KY8 was influenced by the wake (or possibly a plugged probe) and, therefore, not representative of the total flow. The higher value was used in presenting initial test results and as a basis for kicker trimming to achieve design overall head. Figure 102 presents performance after the first complete pump test series, Phase 4. Head rise and efficiency were higher than predicted.

The results of yaw (wedge probes) surveys at KY8 in Phase 5 are shown in Fig. 103 and 104. The total head rise versus vane heights showed head falloff near the hub which was greater at the higher flowrate. The head at the KY7 kiel probe located midchannel indicated the higher head consistent with Fig. 103. The flow angles from axial are shown in Fig. 104, indicating significant overturning.

The straightening vane was trimmed to eliminate the overturning when the kicker was trimmed for the second time. After the straightening vane trim, the yaw probe survey indicated the KY8 head rise was significantly higher than KY7, as shown in Fig. 105. The higher KY8 reading was essentially the same as the previous KY7 head shown in Fig. 103, even though the average kicker head rise had been reduced 59 feet by trimming. The absolute flow angle for the KY8 survey is shown in Fig. 106. Substantial underturning resulted from the straightening vane trim.

After the third kicker trim, yaw surveys were run at KY7 and KY8 for the same configuration. Total head versus radius and absolute flow angles are shown in

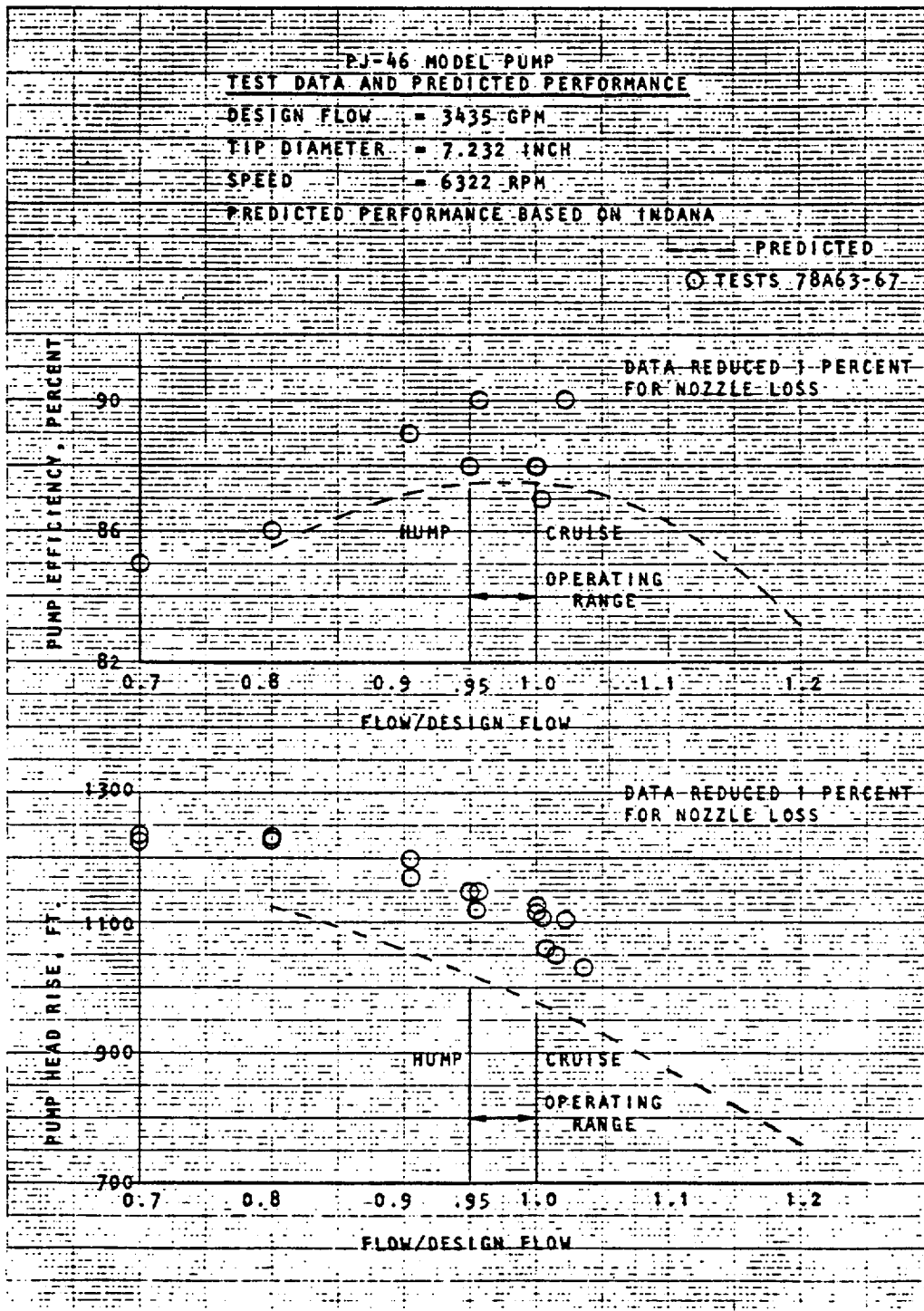


Figure 102. Pump Performance

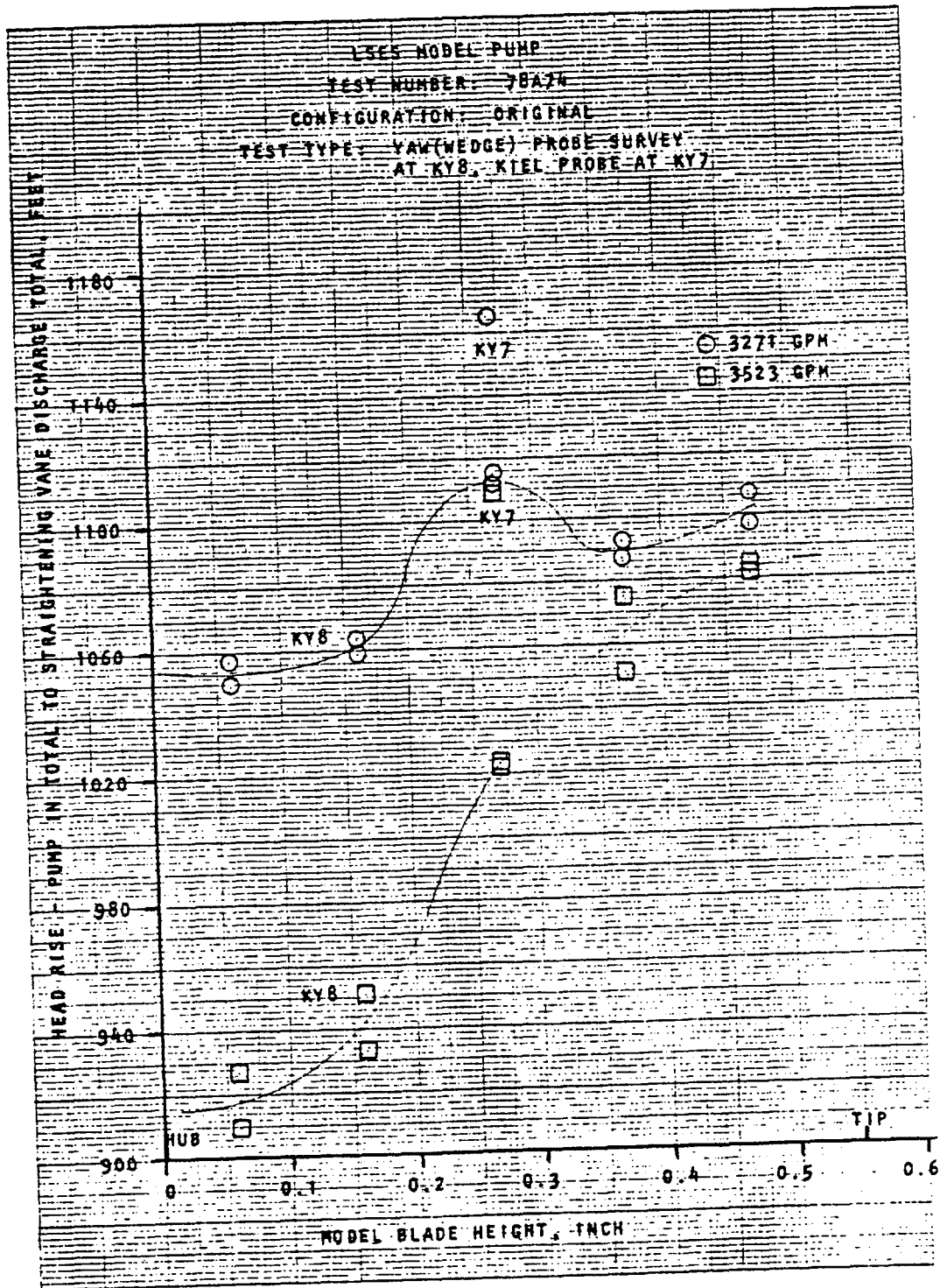


Figure 103. Pump Head Rise Survey



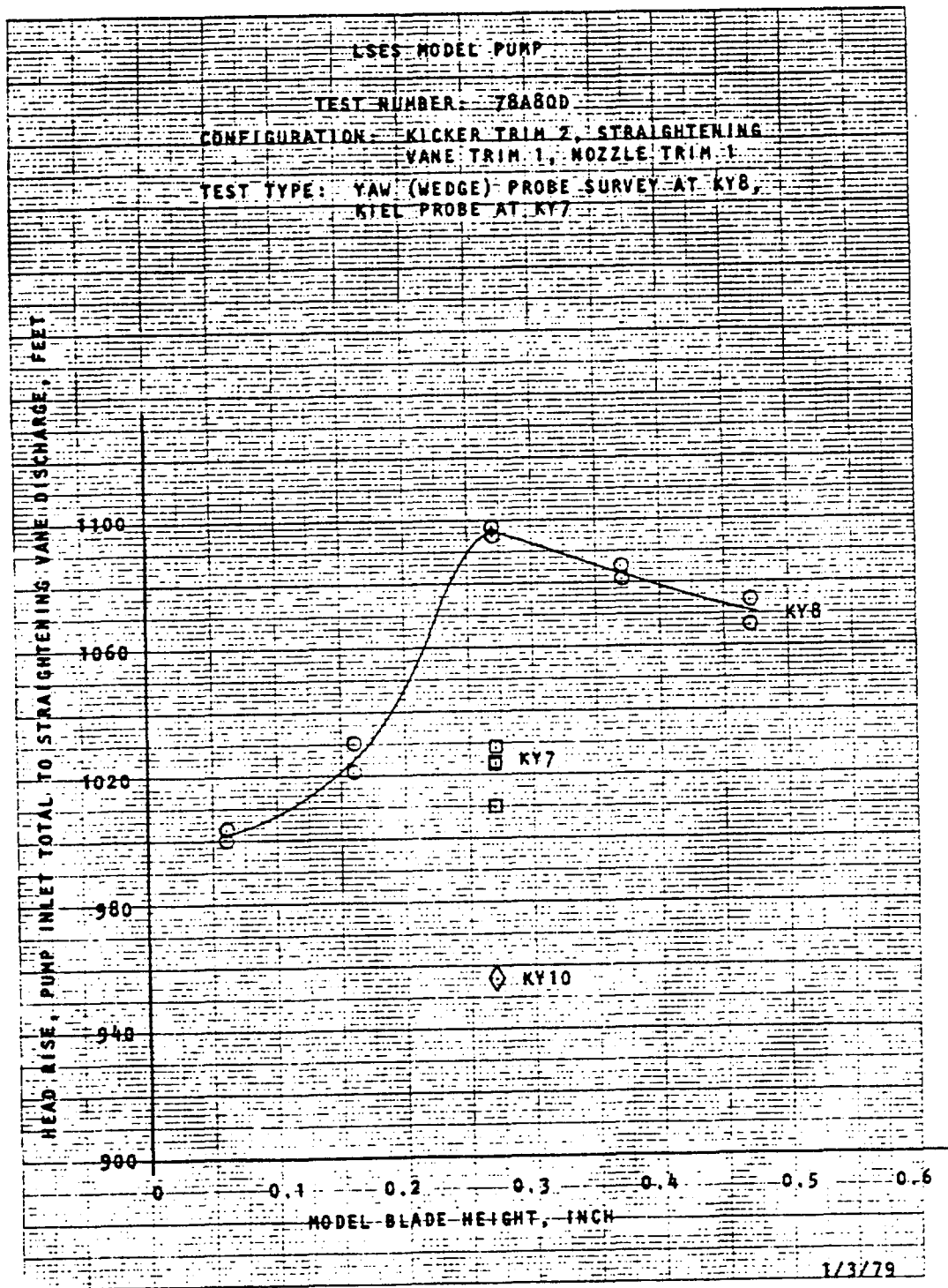


Figure 105. Pump Head Rise Survey



Fig. 107 through 110. Configurations of the head and angle trends seen in the earlier tests are shown with the level reduced by the kicker trim.

The variations observed in KY7 and KY8 and in the radial surveys clearly indicated larger boundary layer wakes than had been expected. Thus, a decision was made to add sufficient total pressure probes to map out the vane-to-vane profile. Six more kiel probe ports were added before Phase 6 in the same axial plane as KY7 and KY8 to give eight equally spaced circumferential locations at the straightening vane discharge. The eight ports were spaced between the pressure and suction surface trailing edges to completely map the vane-to-vane field assuming circumferential equilibrium, i.e., the flow field between any two vanes was assumed to be identical to that between any other two vanes.

Tests were run with the eight kiel probes at 25, 50, and 75% of the vane height. The head rise at design flow as a function of vane pitch is shown in Fig. 111 for the trim-three kicker and the trimmed straightening vane. The arithmetic average total head of the 24 kiel probe measurements was 989 feet. Large head gradients are shown for 50 and 25% blade heights.

The same kiel survey procedure was used in Phase 7 with the redesigned kicker. Straightening vane discharge total head versus pitch is shown in Fig. 112. Average head rise was 977 feet. Similar large head gradients are shown as with the trim three kicker.

The straightening vane was redesigned to provide axial discharge flow with minimum wakes. The number of vanes was increased from 15 to 18. The new vane number resulted in only four equally spaced stations vane to vane for the first kiel probe survey. The kiel probe housing was machined to rotate 2.5 degrees or one-half of the four-space increment to provide eight equally spaced vane-to-vane stations when the survey test was run again. The same kiel probes were used with the redesigned straightening vane which has a smaller vane height than the original design. The radial positions with the redesigned straightening vane were 21, 50, and 79% of the channel height. The vane-to-vane head rise for the

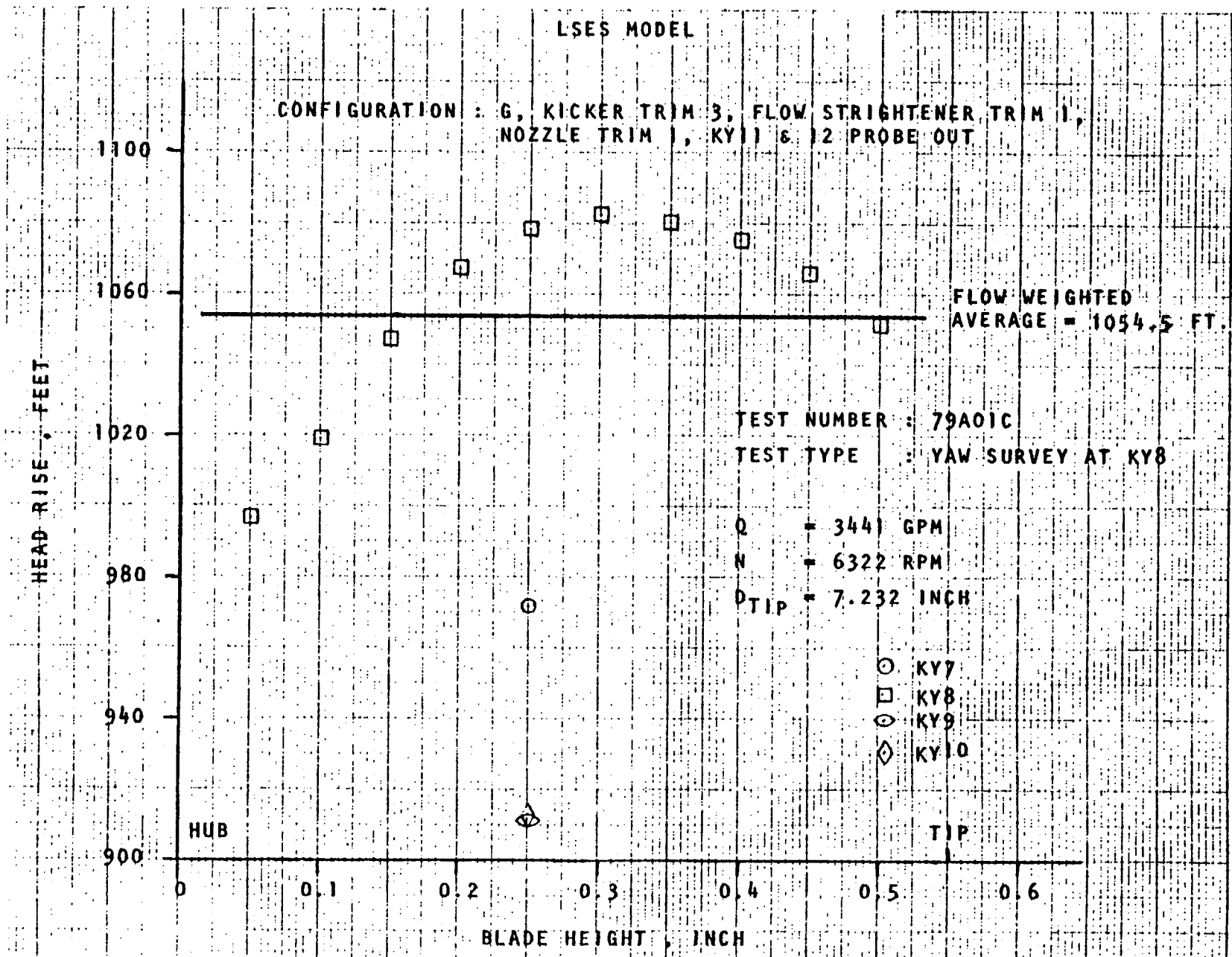


Figure 107. Pump Head Rise Survey (Test 79A01C)







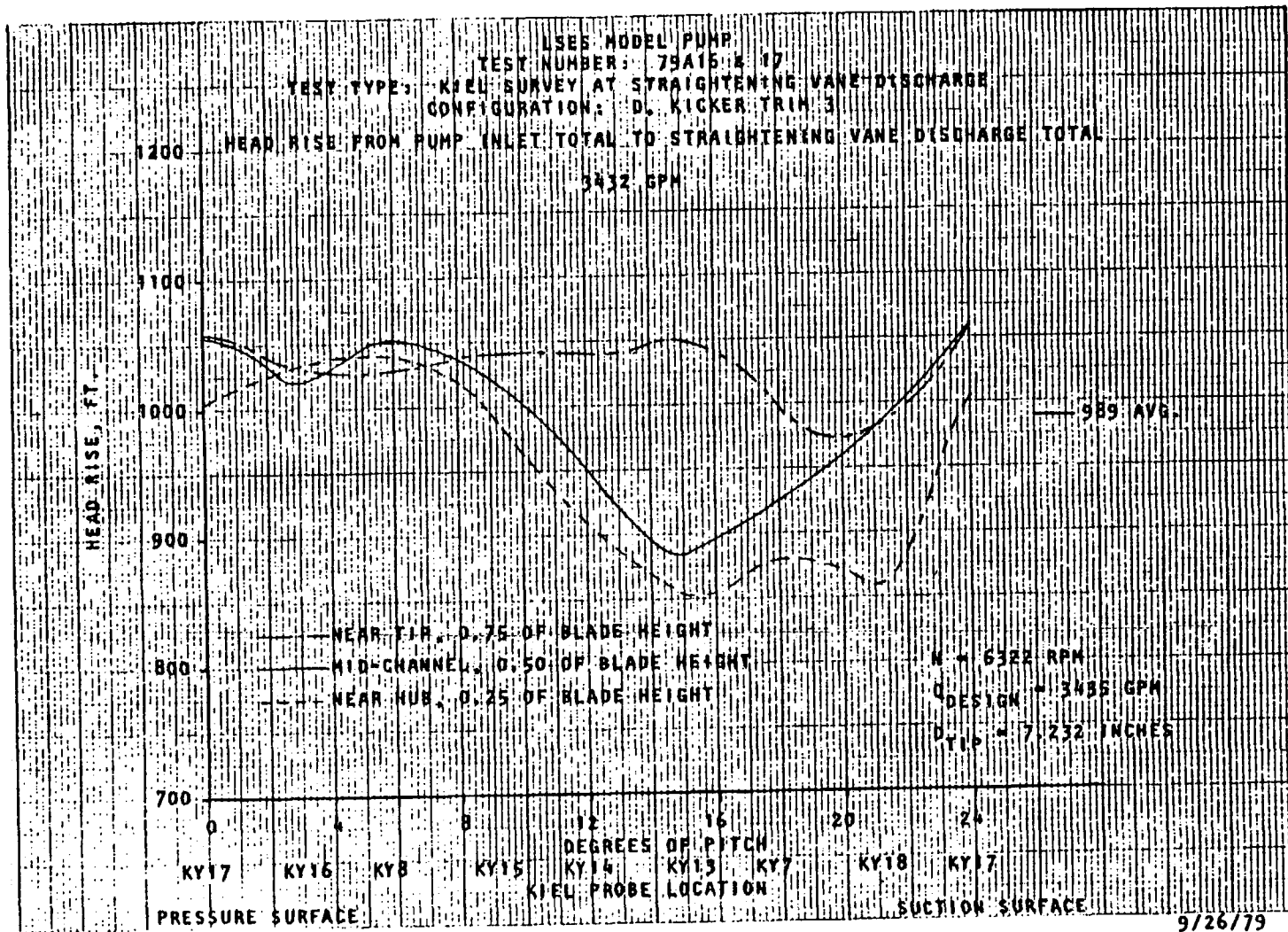


Figure 111. Pump Head Rise Survey (Test 79A16 and 79A17)

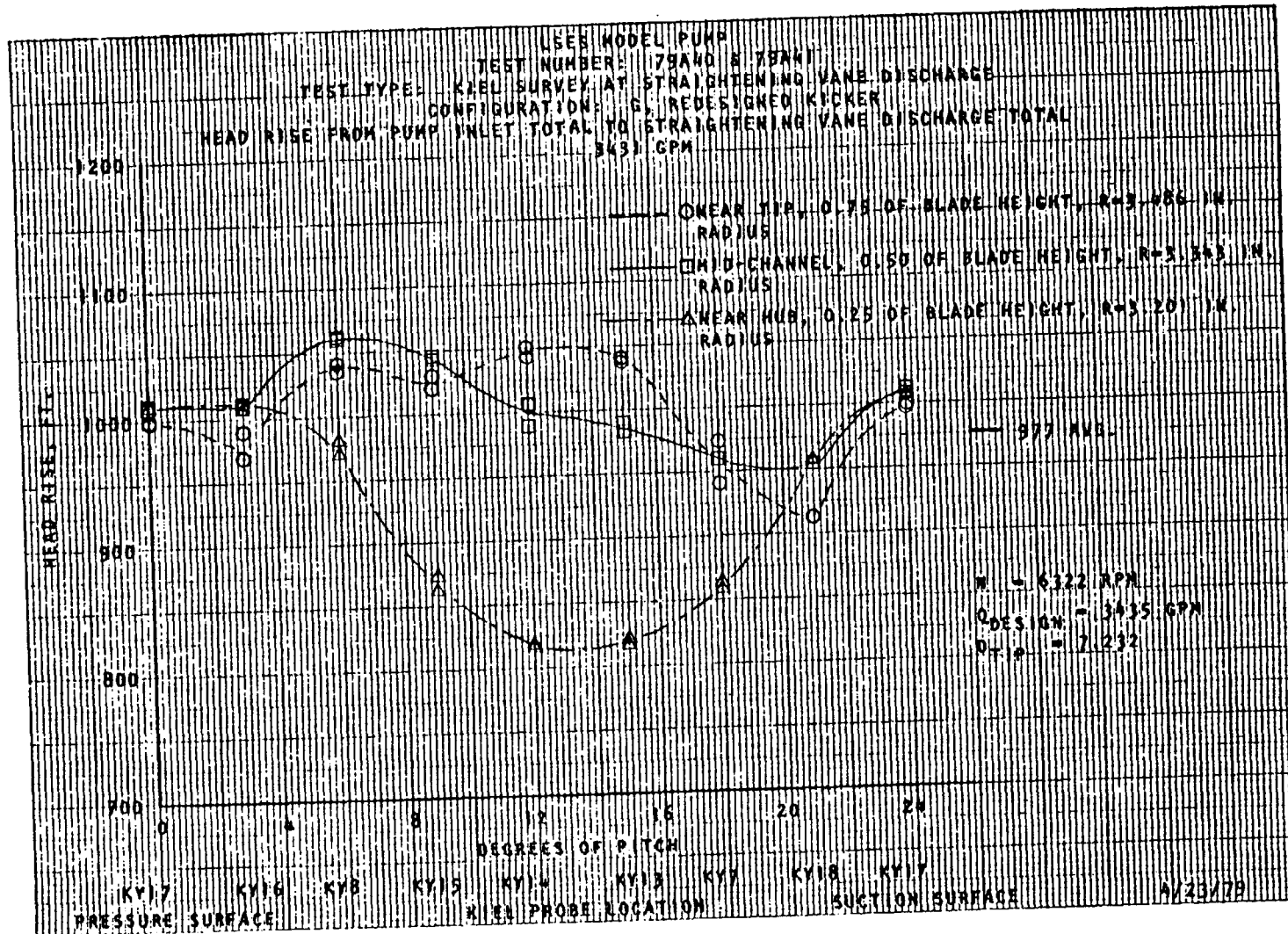


Figure 112. Pump Head Rise Survey (Test 79A40 and 79A41)

redesigned straightening vane is shown in Fig. 113. The average head rise was 889 feet. Substantial reduction in the wake effects is shown at the 79 and 50% heights. However, the wakes are still large due to boundary layer separation which was expected on the model pump but is not predicted for the full-size pump.

Cobra probe yaw surveys were attempted downstream of the redesigned straightening vane at KY8 and KY17 in the rotated position. The KY8 location was known to be in the wake from the kiel probe survey results shown in Fig. 113. The survey was run from the tip to midchannel and back to minimize the chance of the yaw probe breaking in the high-velocity, turbulent flow. Head rise versus radius is shown in Fig. 114. Head falloff in the wake is shown below the 2.29-inch radius. Flow angle is shown in Fig. 115 and indicates near-axial flow as designed. The KY17 was not in the wake as shown in Fig. 113. The cobra probe broke at 64% vane height. The head rise versus radius is shown in Fig. 116. The head rise from the tip is not as steep as at KY8. The flow angle is shown in Fig. 117, indicating near-axial flow at the tip.

An oil-base paint was applied on the hub and tip surfaces downstream of the straightening vane prior to testing. The paint was distributed in test and the results are shown in Fig. 118 through 120. Axial flow is shown at both the hub and tip. The lines in Fig. 118 connect the vane trailing edge to the cone tip.

Overall head rise and efficiency were calculated as the arithmetic average of the data taken at the eight circumferential and three radial positions downstream of the straightening vane. The average overall head rise versus flowrate is shown in Fig. 121 for the three configurations: (1) trim-three kicker with original rotor and trimmed straightening vane, (2) redesigned kicker, and (3) the final configuration of redesigned kicker, rotor, and straightening vane. The head rise for the trim-three kicker and the redesigned kicker were approximately the same and near the original design requirement of 978 feet at 3435 gpm. The final configuration head rise at design flow was 885 feet. The head change

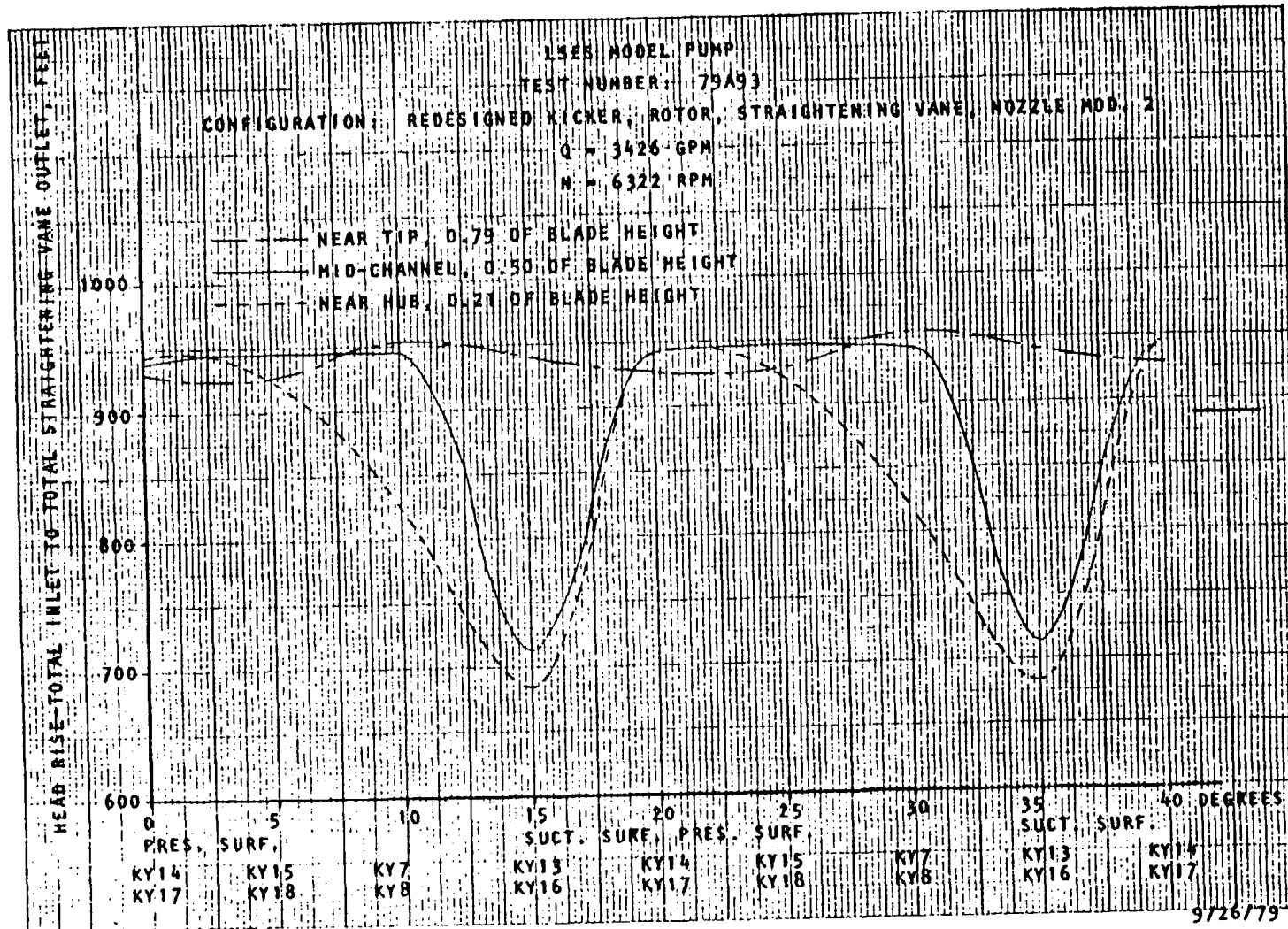


Figure 113. Vane-to-Vane Head Rise Survey



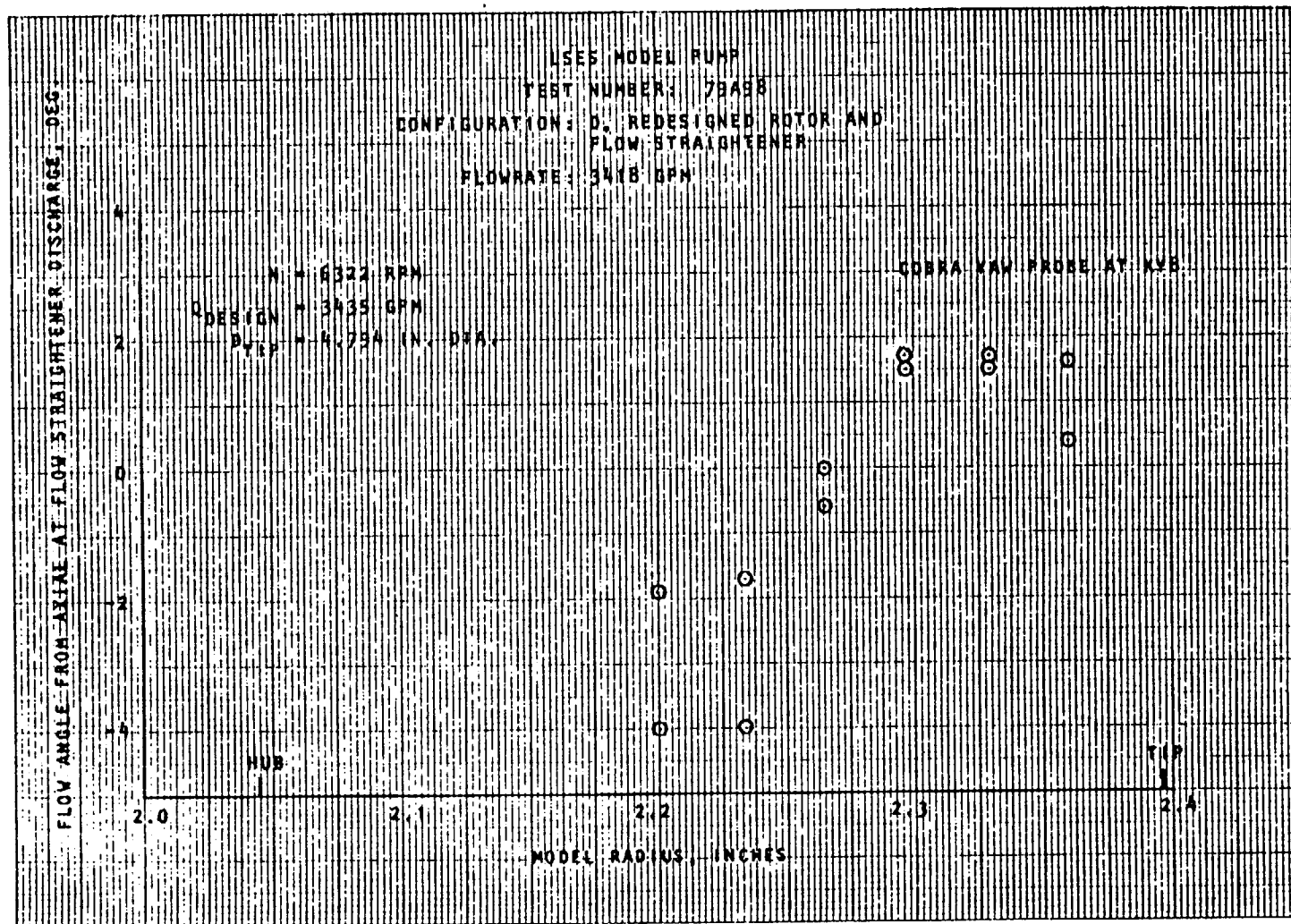


Figure 115. Flow Angle at Discharge



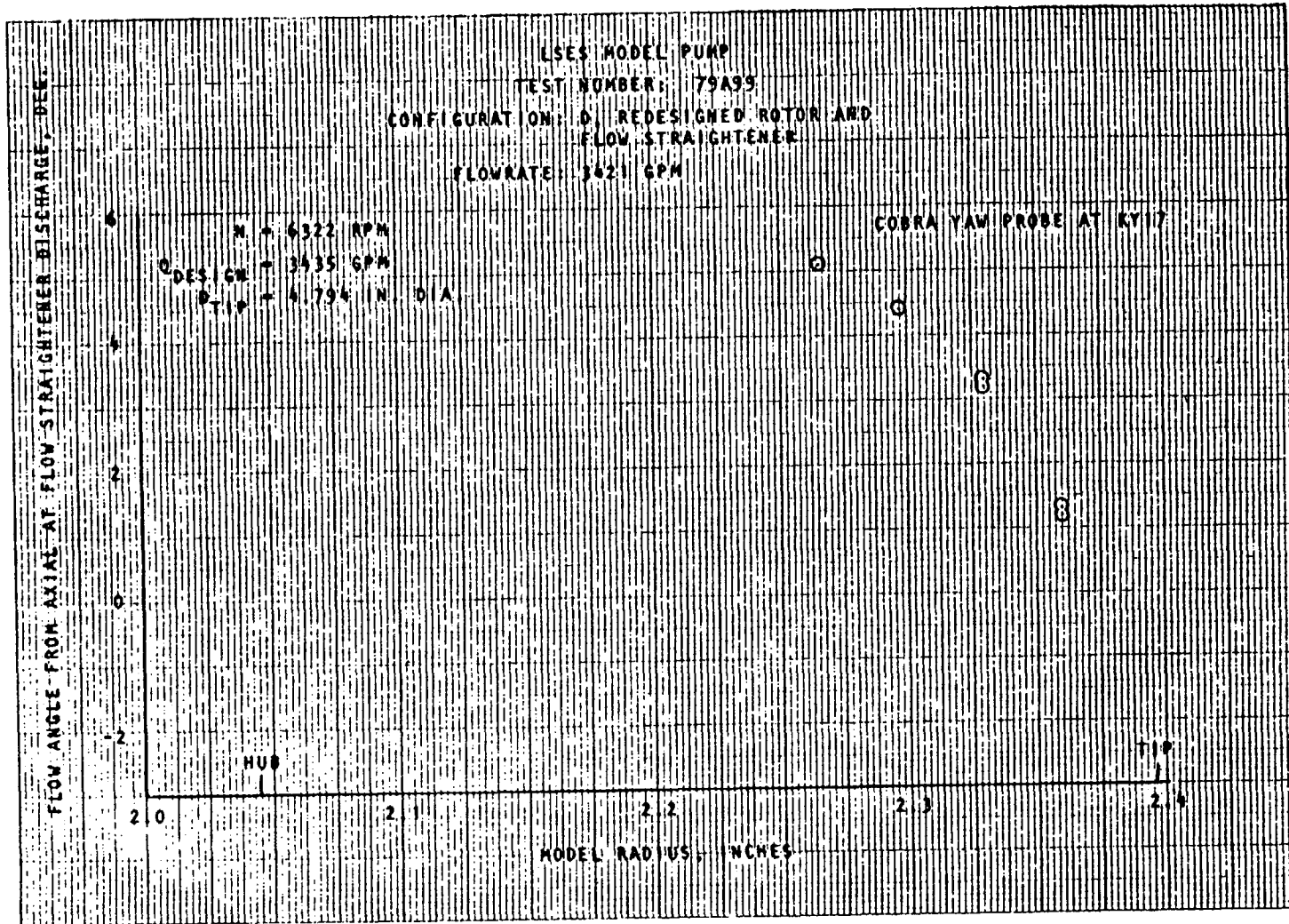
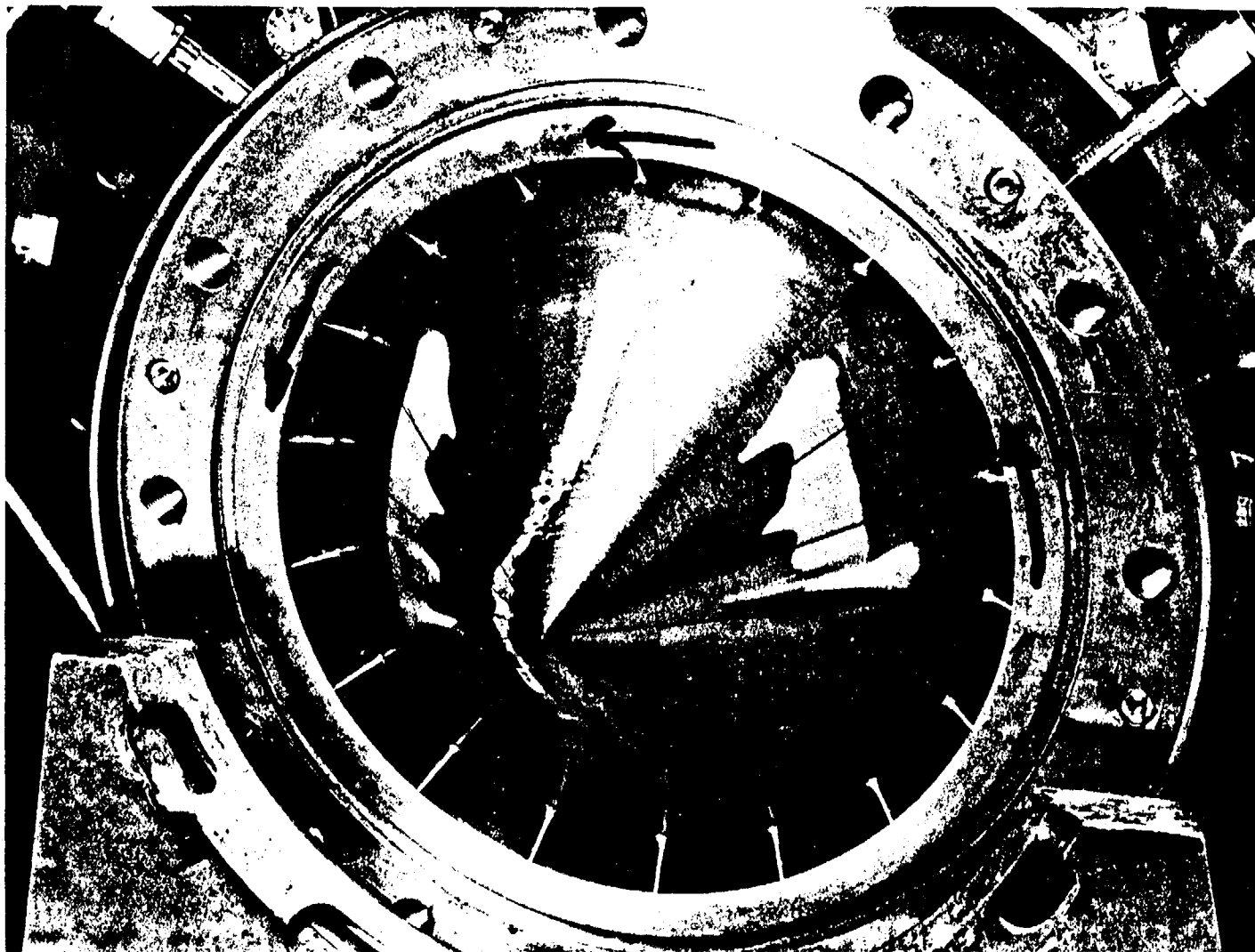
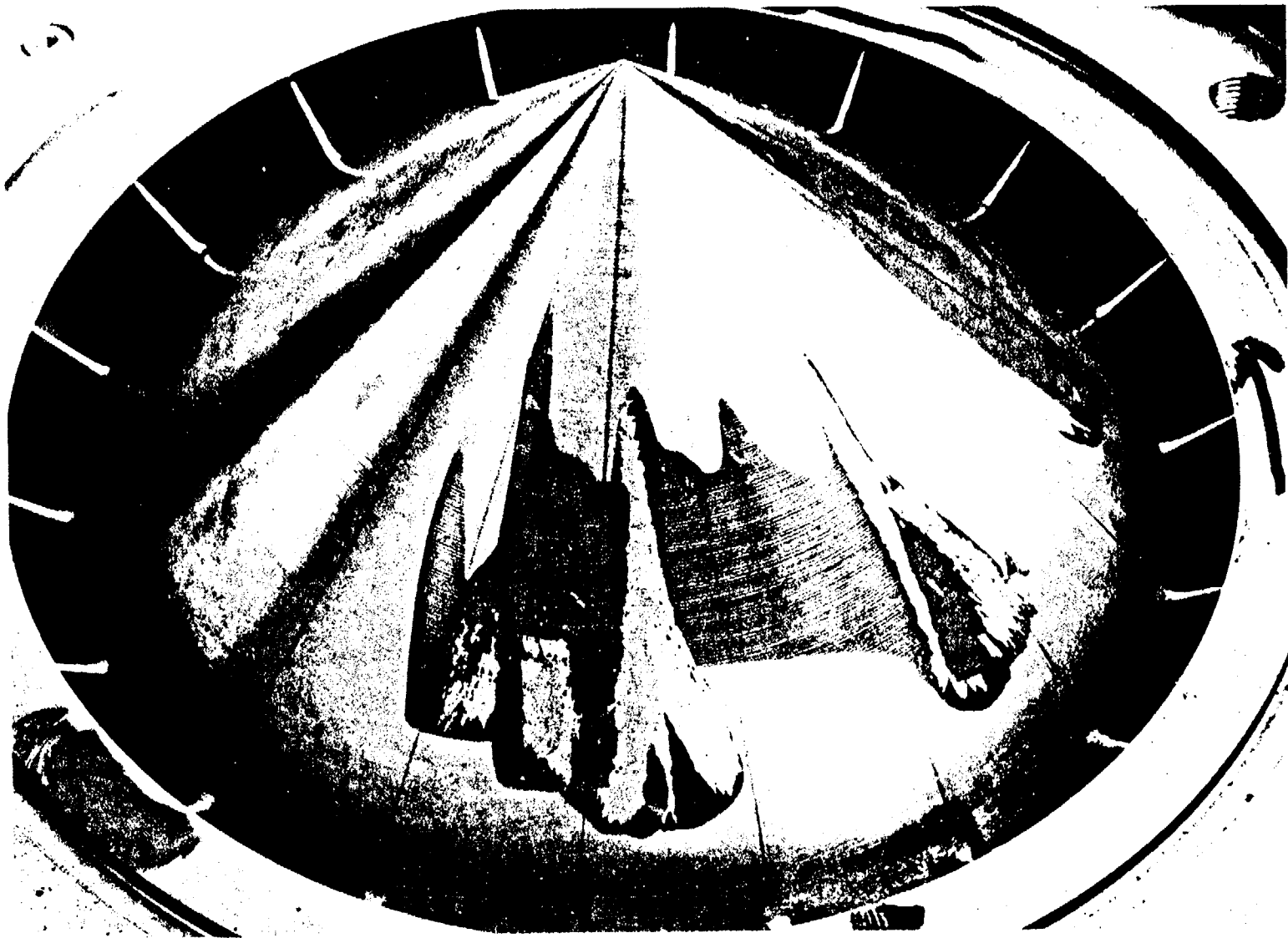


Figure 117. Flow Angle at Discharge



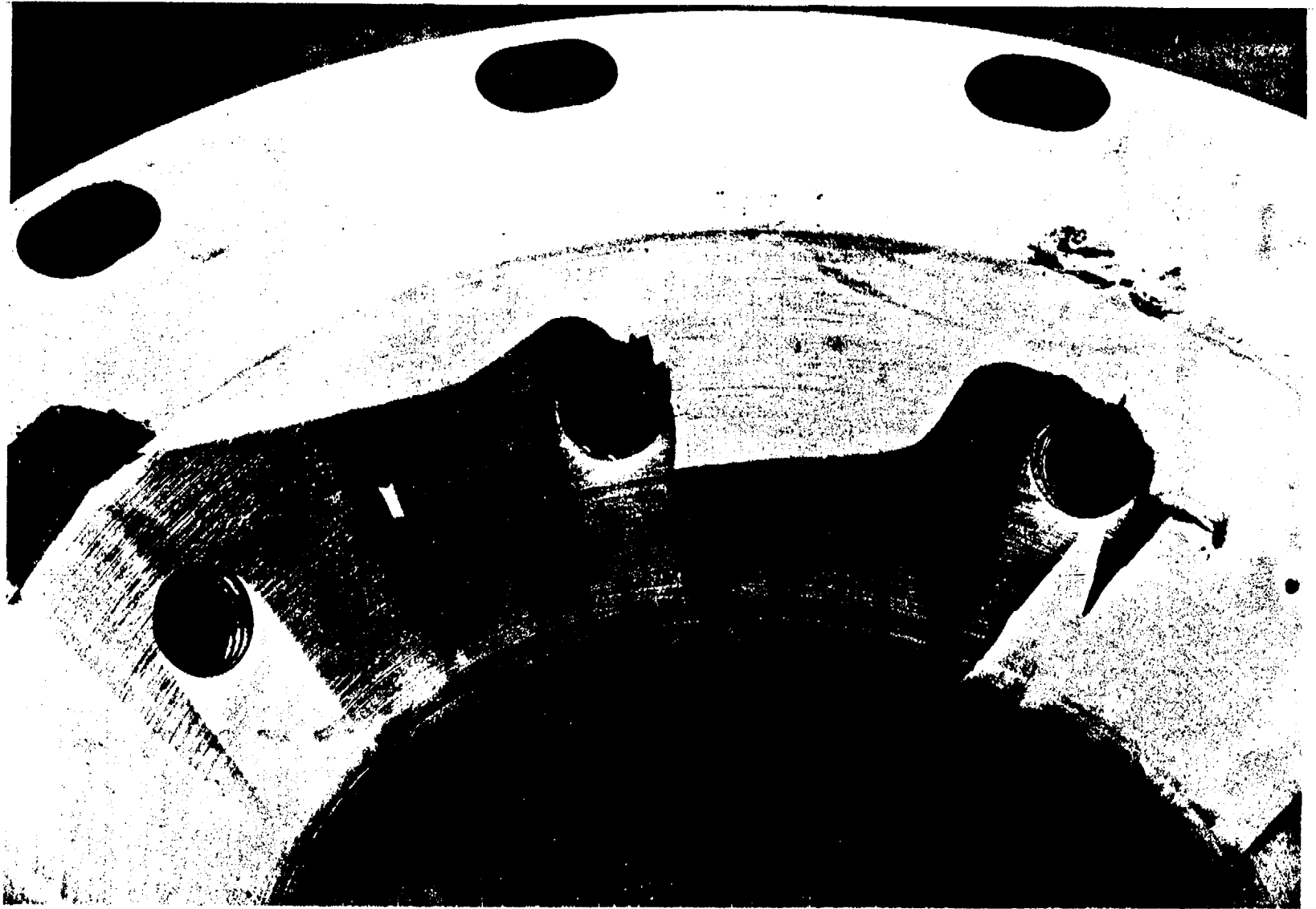
4MS45-7/6/79-C1B

Figure 118. Discharge Pintle



4MS65-7/16/79-C1A

Figure 119. Discharge Pintle



4MS65-7/16/79-C1E

Figure 120. Discharge Outer Housing

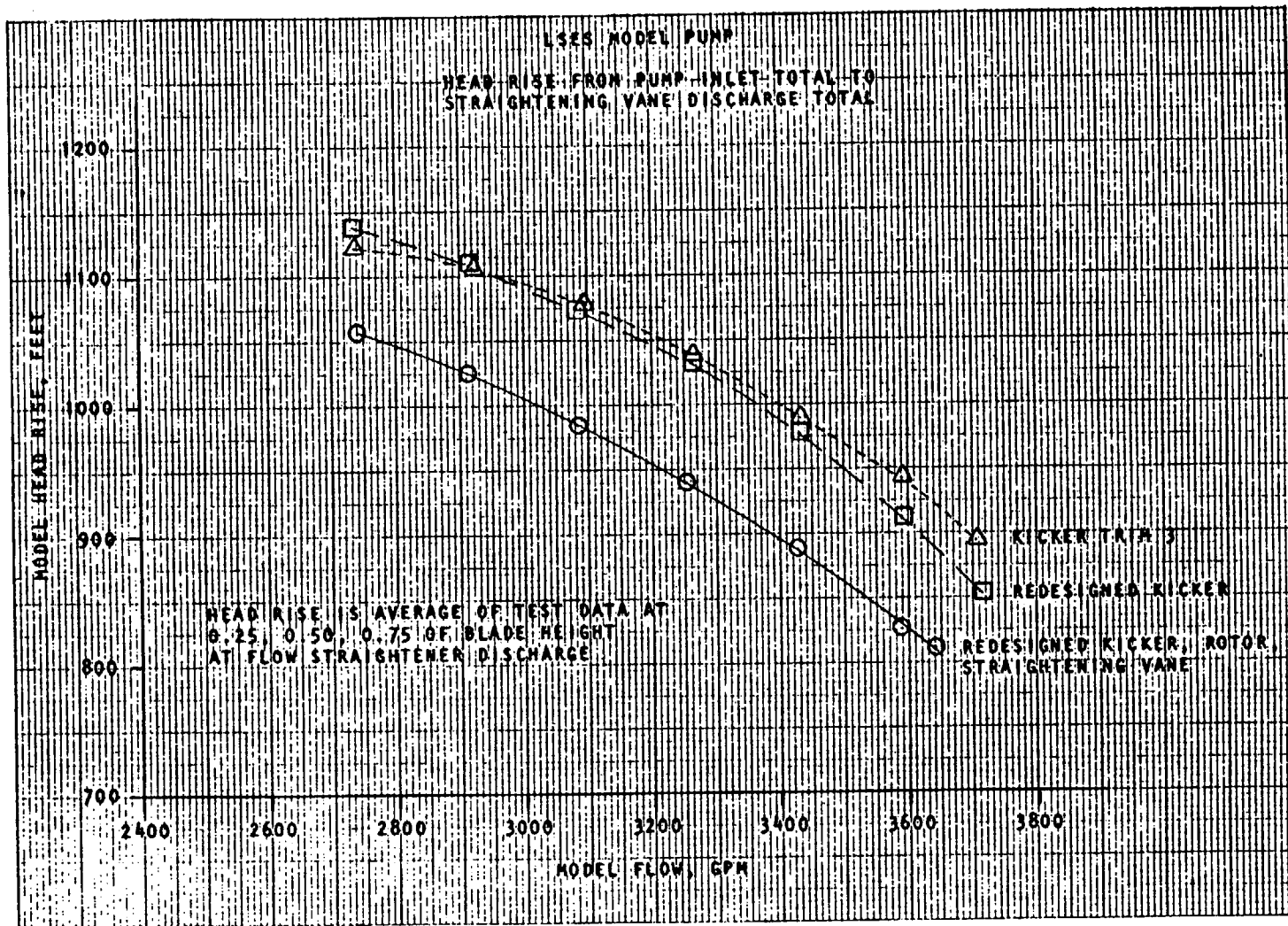


Figure 121. Head Rise Versus Flowrate

from the redesigned kicker configuration (with original rotor) to the final configuration was 90 feet. This change was approximately equal to the head change from the original to redesigned rotor.

The average overall efficiency versus flowrate is shown in Fig. 122 for the three configurations. The lowest efficiency is shown for the trim-three kicker with the trimmed straightening vane. Redesigning the kicker improved the average efficiency significantly. The efficiency for the final configuration was 81.6% at design flow.

A total of 42 hours of life testing was accumulated at hump flow conditions on the redesigned straightening vane. Figure 123 shows the leading edge section of the vanes after 29 hours. No cavitation erosion was observed on the vanes or on the hub and tip walls after 42 hours of testing.

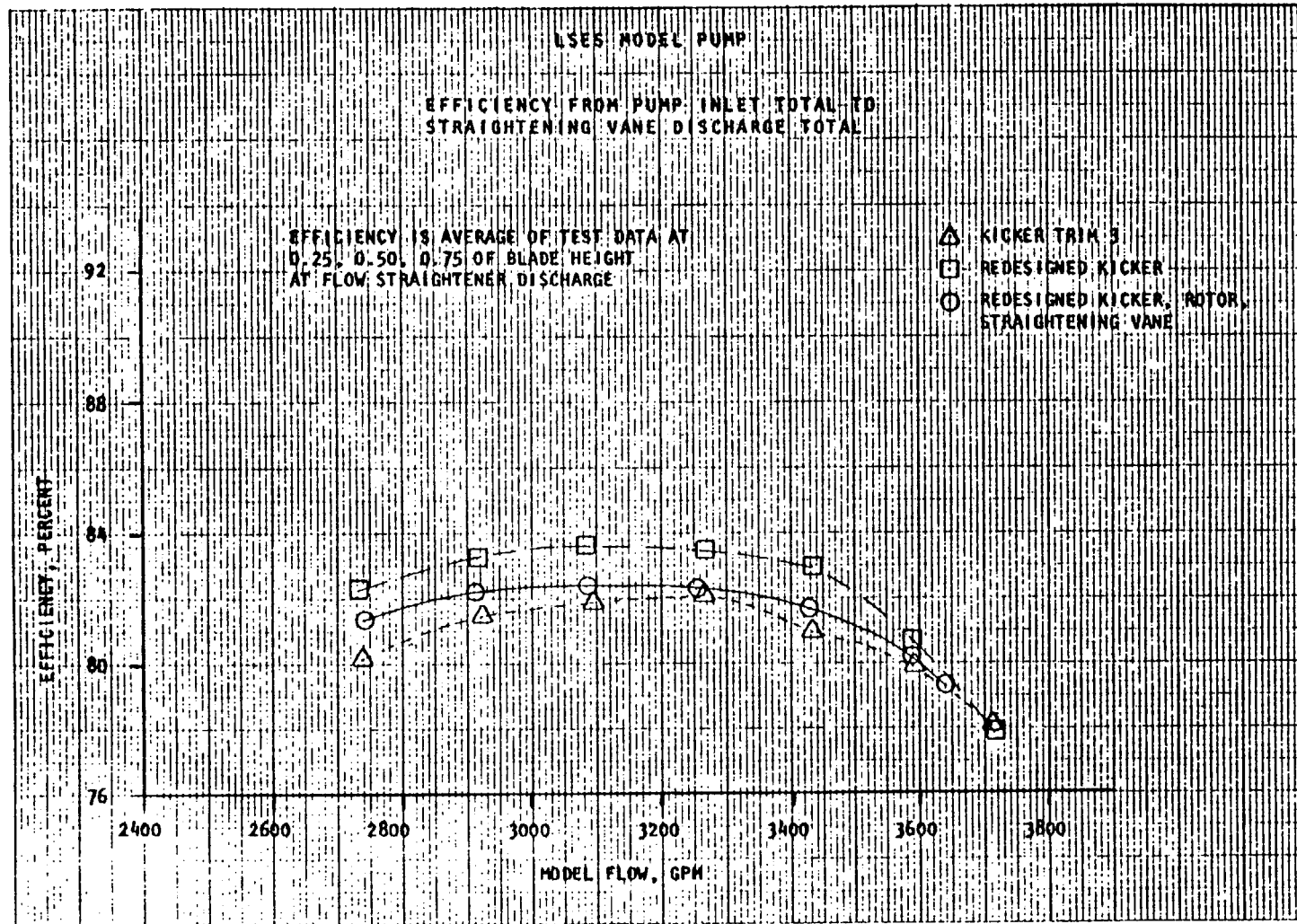
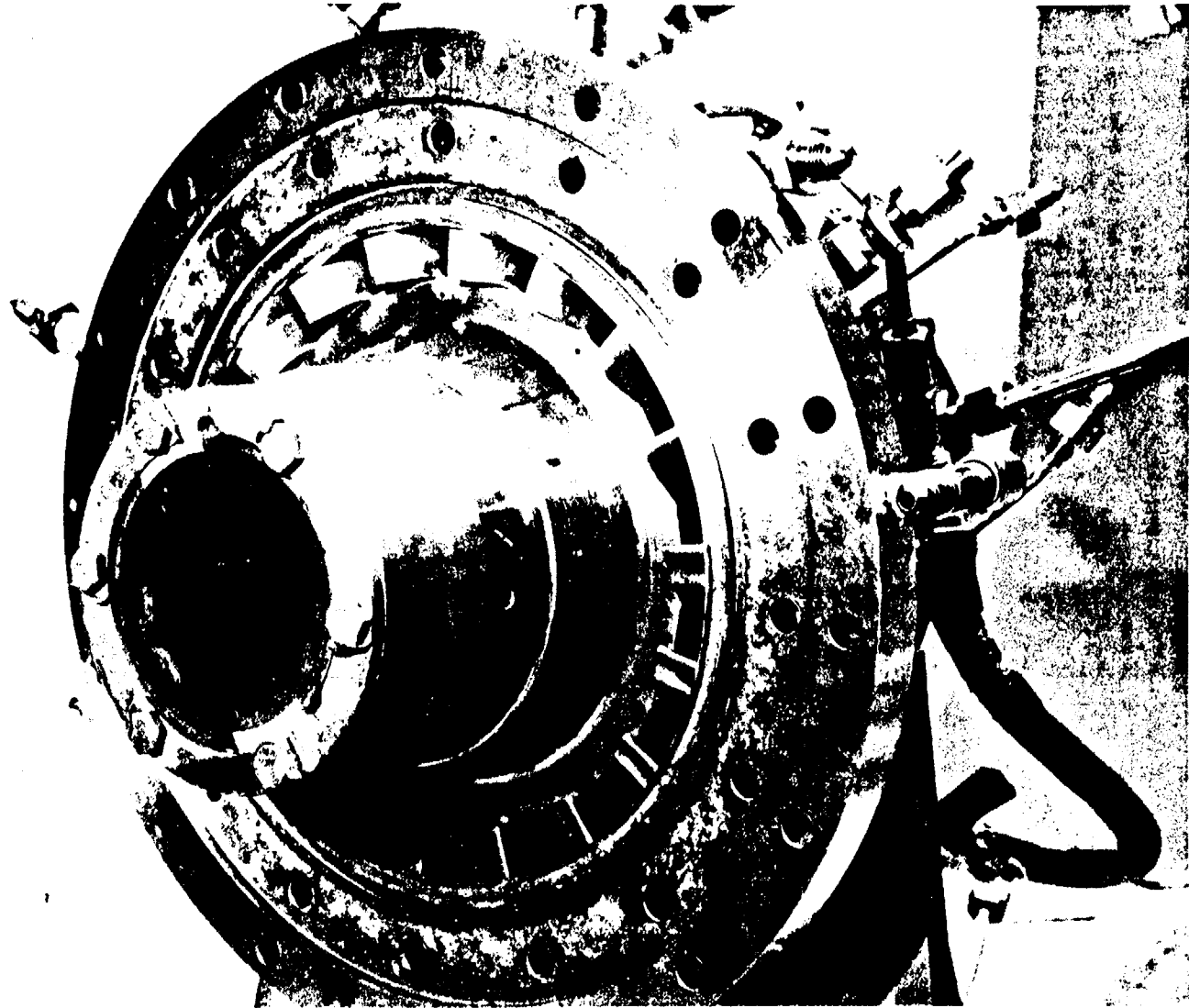


Figure 122. Efficiency Versus Flowrate



4MS45-9/10/79-C1B

Figure 123. Straightening Vanes, Leading Edge

COMPARISON OF RESULTS TO REQUIRED PERFORMANCE

The current performance of the model pump is used as the basis for projecting the following operating points for the 3K SES propulsion system:

	<u>HUMP</u>	<u>CRUISE</u>
Shaft Power, hp	40,000	40,000
Inlet Head (TIH), feet	40.8	200
Turbine Speed, rpm	4073	4065
Pump Flow, gpm	132,700	139,286
Gross Thrust, pounds	149,830	165,040

The suction performance is expected to be as good as that shown in Fig. 74, which is much better than the requirement. Figure 124 shows the thrust versus total inlet head at various powers for the 3K SES propulsion system.

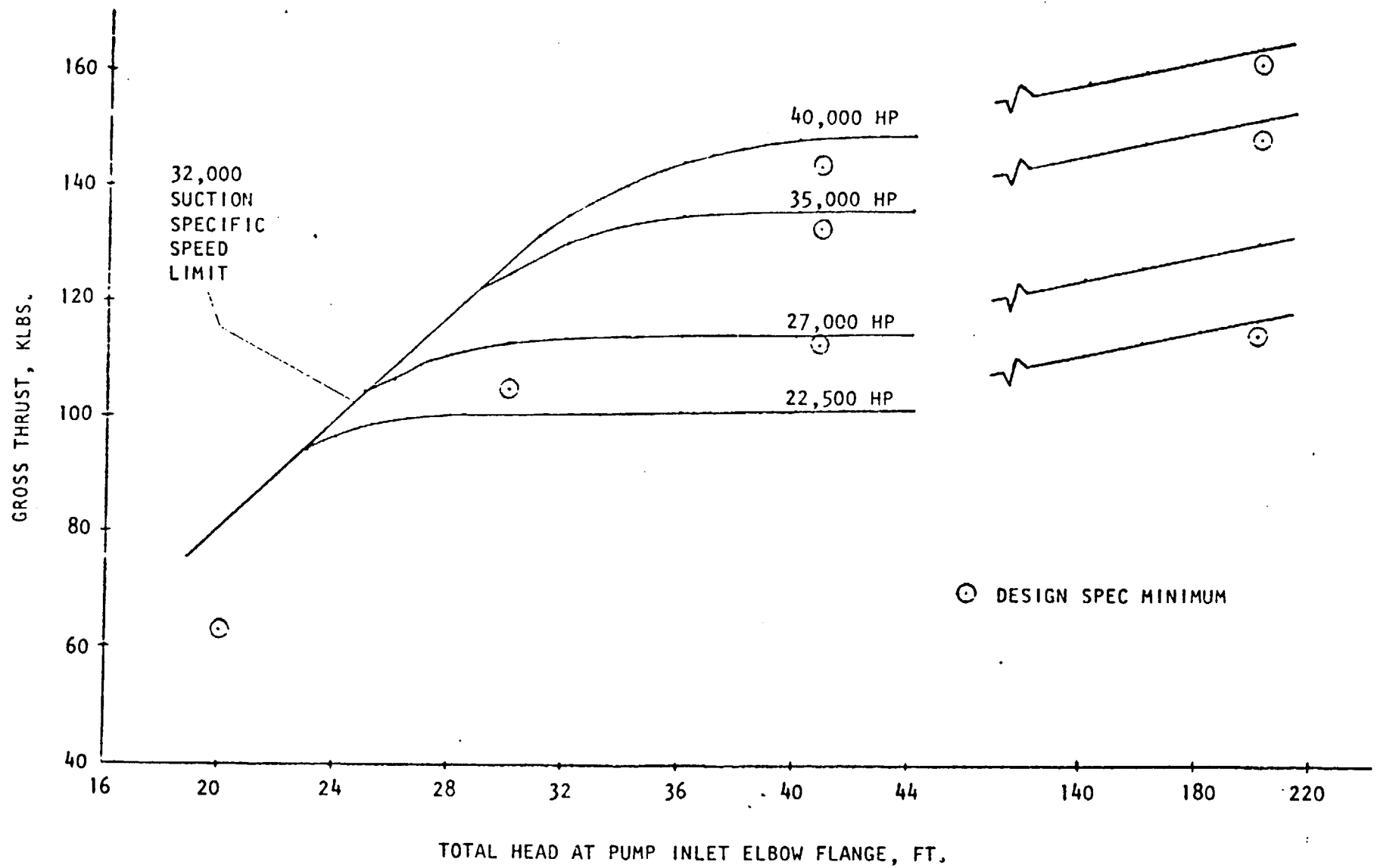


Figure 124. SES Waterjet Propulsor Performance Based on Model Pump Performance as Updated 11/15/79

## LIST OF ILLUSTRATIONS

1.	3K SES Program Schedule . . . . .	2
2.	3K SES Propulsor Assembly . . . . .	4
3.	Thrust Versus Total Inlet Head . . . . .	5
4.	LSES Model Pump Assembly Drawing . . . . .	13
5.	LSES Model Pump Drive Train Drawing . . . . .	15
6.	LSES Model Pump Parts List . . . . .	17
7.	LSES Model Inlet Housing . . . . .	21
8.	LSES Model Inlet Elbow . . . . .	23
9.	LSES Model Inducer Assembly . . . . .	25
10.	Inducer (Front Row) . . . . .	27
11.	Kicker -005 . . . . .	28
12.	LSES Stator Housing . . . . .	31
13.	Stator . . . . .	33
14.	LSES Model Rotor . . . . .	35
15.	Rotor -007 . . . . .	37
16.	Discharge Housing Assembly . . . . .	39
17.	Discharge Housing Instrumentation Locations . . . . .	41
18.	Discharge Housing . . . . .	43
19.	3K SES Inducer Profile . . . . .	48
20.	Blade Centerline Profile at Tip . . . . .	50
21.	Kicker Cavitation Margin at Tip . . . . .	55
22.	Inducer Front Row Static Pressure Rise Vs. Axial Length . . . . .	57
23.	Inducer Head Rise Vs Radius . . . . .	58
24.	Inducer Discharge Flow Angle . . . . .	60
25.	Axial Rotor Inlet Absolute Flow Angle . . . . .	61
26.	Axial Rotor Inlet Total Head . . . . .	62
27.	Rotor Discharge Relative Flow Angle . . . . .	65
28.	Rotor Vector Diagrams . . . . .	67
29.	Axial Rotor Efficiency . . . . .	68
30.	Rotor Discharge Flow Angles . . . . .	70
31.	Rotor Discharge Flow Velocities . . . . .	71
32.	Total Head Rise, Pump Inlet to Rotor Discharge . . . . .	72
33.	Axial Rotor Tip Cavitation Performance . . . . .	74

34.	Axial Rotor Mean Radius Cavitation Performance . . . . .	75
35.	Rotor Hub Cavitation Performance . . . . .	76
36.	Axial Rotor Redesign Blade Loading Profiles	
	From Douglas Neumann, Scaled From R3DAP . . . . .	78
37.	Axial Rotor Discharge Total Head . . . . .	79
38.	Axial Rotor Discharge Absolute Flow Angle . . . . .	81
39.	Axial Rotor Discharge Flow Velocities . . . . .	82
40.	Straightening Vanes Defining Surface Definitions . . . . .	85
41.	Straightening Vanes Typical Vane Contour . . . . .	86
42.	Straightening Vane Boundary Layer Separation Prediction . . . . .	90
43.	Straightening Vane Cavitation Performance	
	With Hub at Cruise Conditions . . . . .	93
44.	Straightening Vane Cavitation Performance	
	With Hub at Hump Conditions . . . . .	94
45.	Straightening Vane Cavitation Performance	
	With Mean at Run 1 Inlet Conditions . . . . .	95
46.	Straightening Vane Cavitation Performance	
	With Tip at Run 1 Inlet Conditions . . . . .	96
47.	Straightening Vanes Blade Load With Run 1 Inlet Conditions . . . . .	97
48.	Straightening Vanes Total Head Survey	
	Near Tip at Design Flow Conditions . . . . .	98
49.	Straightening Vane Total Head Survey	
	at Mean at Design Flow Conditions . . . . .	99
50.	Straightening Vane Total Head Survey	
	Near Hub at Design Flow Conditions . . . . .	100
51.	Kiel Probe Locations Relative to Flow Straightener . . . . .	101
52.	Straightening Vane Performance at Design Flow . . . . .	103
53.	Yaw Probe Surveys at Discharge of Straightening Vanes . . . . .	105
54.	Inducer-Only Test Setup . . . . .	107
55.	Pump Test Facility Modification Details . . . . .	108
56.	Initial Facility Modification . . . . .	110
57.	Modified Test Facility Inlet	
	With Welded Elbow Support and Diffuser Angles . . . . .	113
58.	Model Pump Configuration A; Inducer only, Plastic Tunnel . . . . .	116

59.	Model Pump Configuration B; Inducer Only, Steel Tunnel . . . . .	117
60.	Model Pump Configuration C; Surveys at Stator Discharge . . . . .	118
61.	Model Pump Configuration D; Surveys at Rotor Discharge . . . . .	119
62.	Model Pump Configuration E; Plastic Tunnel . . . . .	120
63.	Model Pump Configuration F; All Titanium . . . . .	121
64.	Model Pump Configuration G; Surveys at Kicker Discharge . . . . .	122
65.	Model Pump Instrumentation Locations . . . . .	124
66.	Model Pump Test Facility Schematic . . . . .	125
67.	Test Facility, Inducer-Only Test . . . . .	127
68.	Model Pump Test Facility for Complete Pump Test . . . . .	128
69.	Flexible Coupling Section . . . . .	131
70.	Failed Shaft, End View . . . . .	132
71.	Pump Head Rise Versus Flowrate . . . . .	141
72.	Pump Efficiency Versus Flowrate . . . . .	142
73.	Static Pressure Distribution . . . . .	145
74.	Current Model Suction Performance . . . . .	147
75.	Projected Full-Scale Suction Performance . . . . .	148
76.	Stator Modifications . . . . .	150
77.	Inducer Only - Plastic Housing . . . . .	151
78.	Inducer Performance . . . . .	153
79.	Inducer Suction Performance . . . . .	154
80.	Inducer Head Rise Survey . . . . .	155
81.	Inducer Discharge Angle Survey . . . . .	157
82.	Inducer Post-Test, 25-Hour Life Test . . . . .	158
83.	Pump With Plastic Housings . . . . .	159
84.	Kicker Discharge Pressure Survey . . . . .	161
85.	Kicker Discharge Angle Survey . . . . .	162
86.	Kicker Head Rise Survey . . . . .	163
87.	Inducer Post-Test, 25-Hour LVT . . . . .	164
88.	Kicker Post-Test, 25-Hour LVT . . . . .	165
89.	Stator Discharge Pressure Versus Flow . . . . .	167
90.	Stator Discharge Pressure Survey . . . . .	169
91.	Yaw Probe Survey; Stator Discharge . . . . .	170
92.	Kiel Probe Survey; Stator Discharge . . . . .	171

93.	Stator Discharge Angle Survey . . . . .	173
94.	Rotor Head Rise Survey . . . . .	174
95.	Rotor Discharge Angle Survey . . . . .	176
96.	Rotor Head Rise Versus Flow . . . . .	177
97.	Rotor Discharge Efficiency Versus Flow . . . . .	178
98.	Rotor Discharge Head Rise Survey . . . . .	179
99.	Rotor Discharge Angle Survey . . . . .	180
100.	Rotor . . . . .	181
101.	Rotor Blades 13 and 14 . . . . .	182
102.	Pump Performance . . . . .	185
103.	Pump Head Rise Survey . . . . .	186
104.	Pump Discharge Angle Survey . . . . .	187
105.	Pump Head Rise Survey . . . . .	188
106.	Pump Discharge Angle Survey . . . . .	189
107.	Pump Head Rise Survey (Test 79A01C) . . . . .	191
108.	Pump Discharge Angle Survey (Test A01C) . . . . .	192
109.	Pump Head Rise Survey (Test A01D) . . . . .	193
110.	Pump Discharge Angle Survey (Test A01D) . . . . .	194
111.	Pump Head Rise Survey (Test 79A16 and 79A17) . . . . .	195
112.	Pump Head Rise Survey (Test 79A40 and 79A41) . . . . .	196
113.	Vane-to-Vane Head Rise Survey . . . . .	198
114.	Head Rise Versus Radius . . . . .	199
115.	Flow Angle at Discharge . . . . .	200
116.	Head Rise Versus Radius . . . . .	201
117.	Flow Angle at Discharge . . . . .	202
118.	Discharge Pintle . . . . .	203
119.	Discharge Pintle . . . . .	204
120.	Discharge Outer Housing . . . . .	205
121.	Head Rise Versus Flowrate . . . . .	206
122.	Efficiency Versus Flowrate . . . . .	208
123.	Straightening Vanes, Leading Edge . . . . .	209
124.	SES Waterjet Propulsor Performance	
	Based on Model Pump Performance as Updated 11/15/79 . . . . .	211

## LIST OF TABLES

1.	Design Point for SES Inducer . . . . .	46
2.	Inducer First Blade Row Discharge Design Vectors . . . . .	51
3.	Inducer Discharge Design Vectors . . . . .	52
4.	Kicker Profile Shape . . . . .	54
5.	Axial Rotor Design Characteristics . . . . .	64
6.	Rocketdyne Three-Dimensional Analysis Programs Input for Axial Rotor . . . . .	69
7.	Predicted Axial Rotor Discharge Head . . . . .	73
8.	Comparison of Predicted and Model Test Rotor Head Rise Performance . . . . .	80
9.	Straightening Vane Characteristics . . . . .	84
10.	Axial Thrust Predictions . . . . .	88
11.	Predicted Boundary Layer Separation Locations On Straightening Vanes . . . . .	91
12.	Comparison of Predicted/Measured Model Performance . . . . .	102
13.	Projected Full-Size Pump Performance . . . . .	102
14.	LSES Model Pump Test Program Test Log . . . . .	134
15.	Projected Full-Size 3K SES Performance . . . . .	143
16.	LSES Model Pump Overall Performance at Design Flow, 3435 GPM . . . . .	183